Encapsulation of Tetrahedral Anions in Nickel Mesocate Cages

A thesis presented in partial fulfilment of the requirements for the degree of

Master of Science

In

Chemistry

At Massey University, Manawatu, New Zealand

Chong Yon Nicole Park

2022

Abstract

Finding ways to isolate anions and metals is a modern problem as concerns over pollution of anions have become popular in the scientific community. The applications of supramolecular structures are endless, ranging from drug delivery to refining metals at an industrial scale.

In this thesis, three variations of a di-salicylaldimine linked ligands were designed to form anion encapsulating mesocates. Each ligand differs by the spacer linking the salicylaldimine units. **L1** has a six-carbon spacer, **L2** has a *p*-xylylic spacer and **L3** has a *m*-xylylic spacer. After the synthesis and characterisation of these ligands, complexation was achieved with various nickel salts resulting in the formation of dinuclear triple-stranded mesocate complexes; $[BF_4{\subset}Ni_2(\mathbf{L1})_3](BF_4)_3$ (**C1**), $[ClO_4{\subset}Ni_2(\mathbf{L1})_3](ClO_4)_3$ (**C2**) and two dinuclear di-stranded mesocate complexes; $[SO_4{\subset}Ni_2(\mathbf{L3})_2][Ni(SO_4)_2(EtOH)_4]$ (**C3**), $[ClO_4{\subset}Ni_2(\mathbf{L3})_2](ClO_4)_2$ (**C4**). The crystals have been characterised with IR spectroscopy, UV-Vis spectroscopy, mass spectrometry, atomic absorption spectroscopy, conductivity measurements and single crystal X-ray diffraction. An uncommon mesocate structure was observed from the X-ray diffraction data collected whereby the anion in the centre of the cage forms covalent bonds with the two Ni^{2+} metal ions.

In addition, metal salt extraction experiments were attempted in a two-phase solvent system with **L3**, nickel sulfate to assess how much nickel and sulfate could be extracted from the aqueous mixture to the organic solution. Although a reliable measurement of sulfate could not be obtained, the highest percentage of the nickel extracted measured in hexane was 89%. However, there is potential to gather a higher value using the optimal conditions found in these experiments.

Acknowledgements

For the progress I have made this year, I would like to thank my supervisor Professor Paul Plieger for his guidance and support and my co-supervisor Assoc. Professor Gareth Rowlands for his advice on my synthesis procedures.

I am grateful for the extensive help I received from Tyson Dais for the collection of crystal structures via X-ray crystallography, Graham Freeman with FAAS and Dr. Pat Edwards with NMR spectroscopy.

In addition, I could not have completed this thesis without the support of the Plieger group; Sidney Woodhouse, Tyson Dais, Marryllyn Donaldson, and Brodie Matheson who have answered my many questions with invaluable advice and help.

Finally, I am grateful for the continual support and love from my family and friends.

Contents

Table of Figures

List of Tables

Abbreviations

⊂	Indicates encapsulation of an anion within a host complex
1a	5-*tert*-butyl-3-(bromomethyl)-2-hydroxybenzaldehyde
1b	*N,N'*-dimethyl-*N,N'*-hexamethylene-di(5-*tert*-butyl-2-hydroxybenzyaldehyde
1c	*N,N'*-dimethyl-*N,N'*-hexamethylenedi(2-hydroxy-5-tert-butylbenzyaldehyde)
L1	*N,N'*-dimethyl-*N,N'*-hexamethylene-di(3-(propylimino)-5-*tert*-butylphenol
C1	$[BF_4 \subset Ni_2(\mathbf{L1})_3](BF_4)_3$
C2	$[ClO_4 \subset Ni_2(\mathbf{L1})_3](ClO_4)_3$
C3	$[SO_4 \subset Ni_2(\mathbf{L3})_3][Ni(SO_4)_2(EtOH)_4]$
C4	$[ClO_4 \subset Ni_2(\mathbf{L3})_2](ClO_4)_2$
C5	$[SO_4 \subset Ni_2(\mathbf{L3})_2](ClO_4)_2$
C6	$[ClO_4 \subset Ni_2(\mathbf{L1})_2](BF_4)_3$
2b	*N, N'*-dimethyl-*p*-xylylenediamine-di(5-*tert*-butyl-2-hydroxybenzyaldehyde
L2	*N, N'*-dimethyl-*p*-xylylenediamine-di(3-(propylimino)-5-*tert*-butylphenol
3b	*N, N'*-dimethyl-*m*-xylylenediamine-di(5-*tert*-butyl-2-hydroxybenzaldehyde
L3	*N, N'*-dimethyl-*m*-xylylenediamine-di(3-(propylimino)-5-*tert*-butylphenol
L4	*N, N'*-dimethyl-*m*-xylylenediamine-di(3-(octylimino)-5-*tert*-butylphenol
R1	*N, N'*-dimethyl-*N, N'*-hexanediamine
R2	*N, N'*-dimethyl-*p*-xylylenediamine
R3	*N, N'*-dimethyl-*m*-xylylenediamine

CCDC	Cambridge Crystallographic Data Center
DMSO-d6	Deuterated dimethyl sulfoxide
MS	Mass spectrometry
IR-ATR	Infrared
MeOH	Methanol
EtOH	Ethanol
MeCN	Acetonitrile
TEA	Triethylamine
NMR	Nuclear magnetic resonance
t-Bu	tertiary butyl group or 1,1-dimethylethyl group ($(CH_3)_3C–$)
UV-Vis	Ultraviolet-Visible
AAS	Atomic absorption spectroscopy
SX	Solvent extraction
Conc.	Concentration
Cndct.	Conductivity
Mol. Abs.	Molar Absorbance
RT	Room temperature

1.0 Introduction

1.1 Supramolecules

Supramolecules are molecules held together with covalent and noncovalent bonds. They are stabilised by numerous weak intramolecular bonds which gives them the special name ‘supermolecule’. Jean-Marie Lehn—a pioneer in the field of supramolecular chemistry—contributed to our current understanding of molecular recognition towards molecular information processing and self-organisation.

To explore how metallosupramolecules form by spontaneous self-assembly following the most favourable Gibbs free energy pathway, Lehn and his team performed spectrophotometric kinetic studies of a tricopper double-stranded helicate (Cu_3L_2) to explore this idea which resulted in a stepwise mechanism with many kinetic intermediates.[1]

1.2 Helicates and Mesocates

Helicates are a type of supramolecular structure classified by their metal-ligand (M_xL_y) composition and derive their name from the Greek word *helix* meaning 'spiral' and the suffix *-ate* denoting the host-guest relationship between the receptor and metal ion.[2] Helicates are commonly comprised of two metal ions and three ligands. They are also distinguished by other factors. Right-handed (P) helicates have ligands that turn clockwise while left-handed (M) helicates have ligands that turn anti-clockwise.[3]

Ligands form the helix shape they are named after by wrapping around a central axis. In order to form the helicate, ligands must feature binding domains for the coordination with metal ions.[4] They must have spacers between the binding domains to guarantee that a ligand will not bind twice to the same metal and be flexible enough to twist around into a helical structure.[5] In order to form a dinuclear triple-helical arrangement, a metal capable of octahedral geometry and the homochirality of the two coordination sites are required.[6]

There is also a lot of variation under the helicate category. Helicates can be categorised by differences such as the direction of ligand rotation (clockwise/anti-clockwise), number of ligands, same or odd ligands (homostrand/heterostrand), or whether they have the same binding domains on ligands or different binding domains (homotopic/heterotopic).[4] The strands can adopt different positions such as head-to-head (a mesocate) or head-to-tail (a helicate) as shown below in Figure 1.

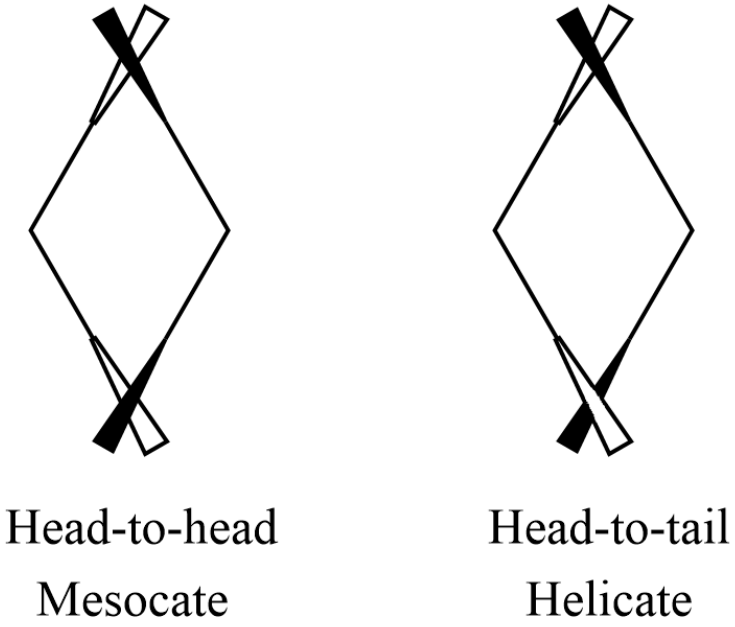

Figure 1. The difference between a mesocate (head-to-head) and helicate (head-to tail) configuration.

It is important to note the differences between a mesocate and a helicate (as shown in Figure 1). M_2L_3 helicates have ligands that rotate around the centre and produce a racemic mixture of chiral M (ΛΛ) and P (ΔΔ) isomers. A third isomer exists and this is called a mesocate for its achiral structure *meso* (ΛΔ).

Forming a helicate is slightly different from a mesocate as a helicate cannot be deemed a helicate without the trademark helix shape. As shown in Figure 2, the two structures are not alike. To form these isomers, different conditions are required. Mayans *et al*., characterised new $[M_2L_2X_2]^{n+}$ complexes and analysed the transition from the mesocate to helicate by varying the flexibility of the central spacers of the Schiff bases and size of substituents.[7] The research presents the ability to control the design of the helicate or mesocate configuration by changing the size of the ligand, metal ion, anions, and by introducing less or more points of rotation.

The two configurations also have different properties such as cavity size, stability and flexibility.[4] The helicate structure generally has a smaller cavity size and the two isomers have different packing patterns, the mesocate exhibiting smaller solvent and anion filled pores. An analysis of the two isomers in a 1D/2D NMR study also revealed more rigidity

in the mesocate structure via a split -CH_2CH_2- signal which appeared as a singlet for the helicate.[5]

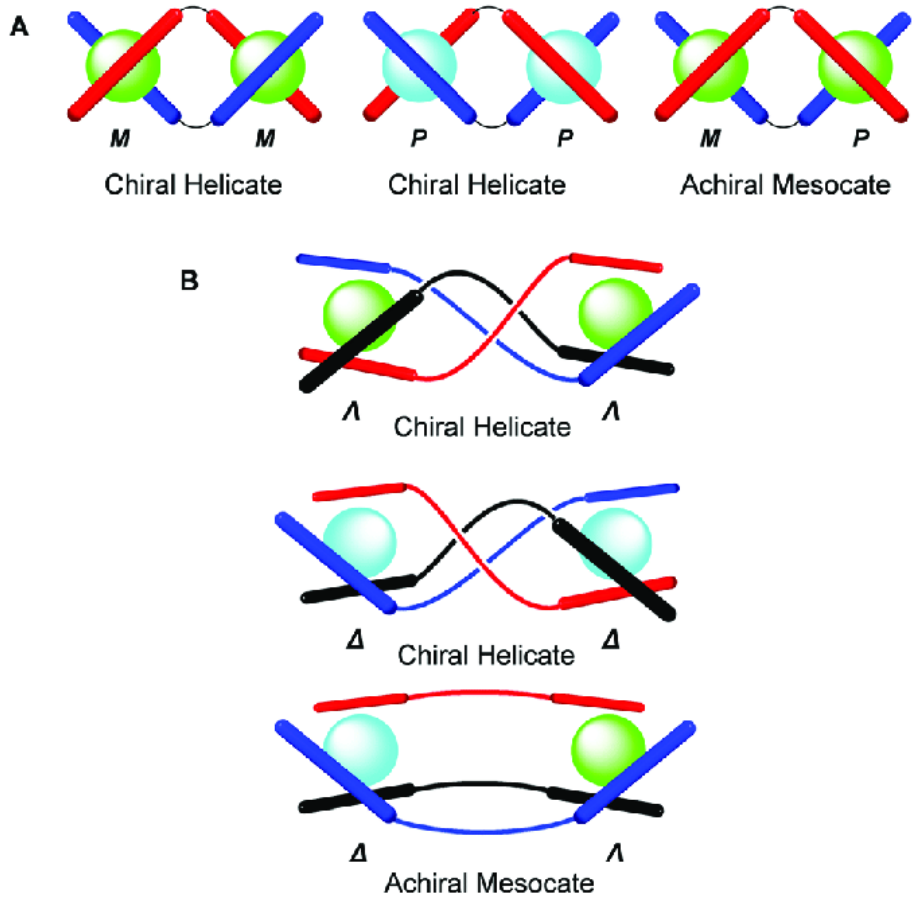

Figure 2. Differences between a mesocate and helicate.

1.3 Anions

The importance of trapping or releasing anions have increased in recent years due to highlighted public concerns of pollution and popularity in various research fields such as medicine, medical technology and chemical synthesis.[8–13] This research project seeks to explore the capture of anions by helicates derived from salicylaldimine based ligands. Whether an anion can be encapsulated depends on the size of the cavity, the anion, and interactions such as hydrogen bonding or Van der Waals forces.

Supramolecular cages can separate or clean up unwanted anions in the environment. Anions that pollute the environment include chlorides, nitrates, sulfates, phosphates, or bicarbonates. Anions can also be useful in scientific research that requires a switch or catalyst.

The perchlorate anion ClO_4^- is used as an oxidiser in flares, pyrotechnics, explosives, rocket propellants and missile motors.[14] It is recommended in the US to maintain 1-18 μgL^{-1} concentration of ClO_4^- in drinking water.[14] The concern with the level of ClO_4^- is due to its ability to inhibit the uptake of iodine and thereby leading to an imbalance of thyroid hormones and hypothyroidism. Current methods of decreasing ClO_4^- concentration in ground water include ion exchange and the use of bioreactors which involves ClO_4^- digesting bacteria and in-situ bioremediation. This takes advantage of naturally existing bacteria that can break down ClO_4^- with nutrients such as ethanol, lactate, acetate, citrate, sugars and edible oils.[14] Due to ClO_4^- pollution, methods of decreasing the concentration of ClO_4^- in water or soil are important in scientific research.

Both BF_4^- and sulfate are better alternatives to ClO_4^- for use in the chemistry lab and industries, as ClO_4^- can form explosive derivatives. Sulfate is also an important anion in the chemistry laboratory as it has numerous uses and is present in all sorts of consumer products from batteries, plaster building materials to shampoo and mineral supplements.[15] Sulfate is involved in the sulfur cycle which regulates sulfur concentration in the environment, forms molecules, releases elements and gives nutrients to plants and animals. It is formed in the atmosphere and in the combustion of sulfur-containing fuels.[15] As a pollutant, it contributes to the acidification of water and soil but has a cooling effect on climate change.[16]

1.4 Solvent Extraction

Solvent extraction is a method of separating a solute from two immiscible solutions by solubility. To successfully extract a solute, the solute needs to be solubilised in both solvents. Typically, this requires an extractant that has a higher affinity with the solute than the other solution to pull the solute from one solvent to another. However, unwanted solutes can also be co-extracted if they are also soluble.

Applications of solvent extraction vary from environmental, medical, scientific research and industrial use. It is useful for effluent treatment as it provides a cheap and safe method of recovering a wide range of products that meets the statutory requirements.[3] It is easily automated, requires little supervision and provides an easy method of separating a compound without having to handle solids unlike extraction methods such as coprecipitation and solid phase extraction.[2] Solvent extraction provides more flexibility as different types of solvents with different solubilities can be chosen.[17]

The solvent extraction of metals became prolific during the Manhattan project in the 1940s to provide pure uranium.[18] Since then, it has become adapted for industrial use in refining other metals. For example, solvent extraction was the first method used by the nickel industry and today it is favoured due to its success in copper refining processes, the ongoing research and developments that have led to improved extraction solvents and equipment.[17]

Extractive metallurgy is forever evolving to meet the needs of industries. The basic steps of the process are concentration, separation, reduction and refining as shown in Table 1.[19] Leaching, refers to the separation of a metal ion from a metal ore using an appropriate solvent.[18] Extraction provides purification via separation of the desired product between an aqueous and organic layer using a binding molecule such as an extractant. Stripping displaces the binding molecule and electrowinning is the purification of the metal ion from the anion it is bound to.[19] These steps in Table 1 below outlines the overall base-metal recovery process that is used for 25% of worldwide copper production.[20] In this thesis we will focus on step 2, the extraction part of the process to see if our ligand can act as an extractant with $NiSO_4$ due to the successful formation of **C3**.

Table 1. Basic steps of a base-metal recovery process.[20]

	Overall	**$NiS + H_2O + 1/2O_2$**	⟷	**$Ni + H_2SO_4$**
Step 1	Leach	$NiS + 2O_2$	⟷	$NiSO_4$
Step 2	Extraction	$NiSO_4 + L_{(org)}$	⟷	$NiLSO_{4\,(org)}$
Step 3	Strip	$NiLSO_{4\,(org)}$	⟷	$NiSO_4 + L_{(org)}$
Step 4	Electrowinning	$NiSO_4 + H_2O$	⟷	$Ni + 1/2O_2 + H_2SO_4$

1.5 Introduction to the Salicylaldimine Ligand

The salicylaldimines (Figure 3, right), are used as caps on the ligands for metal binding as they provide useful nitrogen and oxygen donor groups for coordination. Since the 1930s, salicylaldimine and salicylaldehyde containing ligands have successfully formed metallo-supramolecular complexes such as discrete macrocycles, helicates and polymers due to their flexibility in steric and electronic modifications.[21] Applications of these complexes include molecular magnets, and industrial use hydrometallurgy, in the area of extraction of metals from the ore. They have also formed various metal complexes with interesting structures and applications such as the photocatalytic ability to enhance the degradation of a dye in hydrogen peroxide and daylight.[22]

Salicylaldimine ligands are also popular in the chemical research literature as they provide an ideal cap for supramolecular structures. The addition of a bulky group such as a *tert*-butyl group improves solubility and increases the efficiency of the synthesis by blocking the *para* site of the salicylaldimine. The R_1 group represents the amine of the spacer group that will join two salicylaldimine caps together and R_2 represents the propyl arm that stabilises the complex. This thesis will attempt to complex helicates using ligands with these features.

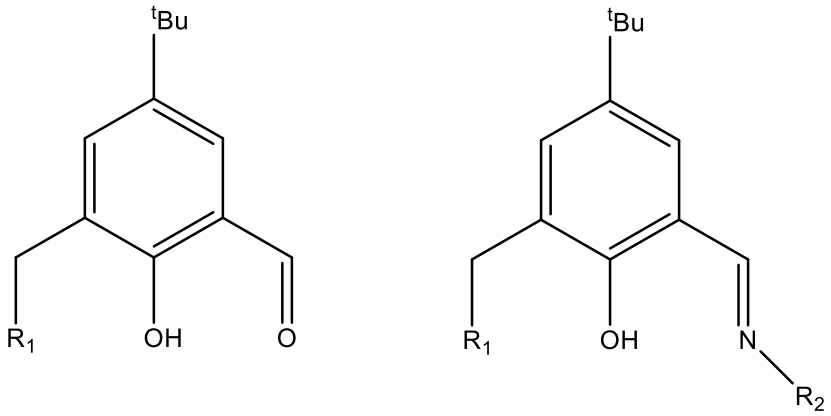

Figure 3. Structure of Salicylaldehyde (left), Salicylaldimine (right).

Tasker and coworkers have produced extensive research with salicylaldimine ligands for Cu^{2+} and Ni^{2+} extraction.[19,23–25] These projects have been centred around mononuclear

and dinuclear complexes. For example, Plieger *et al*., studied dicopper helicates complexed with two salicylaldimine ligands, similar to **L1** (Figure 4) but with phenyl rings instead of propyl groups.[24] They found that long chain secondary diamines can easily attach to the salicylaldehyde via a Mannich condensation to gain high yields >80% of diimines in the product.[24] Knapp used this ligand to crystallise a helicate using Cu^{2+} and iodine.[26] Next, McGarry built his project on these findings by synthesising a similar ligand with propyl groups.[27]

McGarry, was successful in his synthesis and characterisation of a new salicylaldimine ligand, and obtained mesocate structures of $[BF_4{\subset}Ni_2(\mathbf{L1})_3](BF_4)_3$ and $[I{\subset}Ni_2(\mathbf{L1})_3](BF_4)_3$.[27] The structural analysis of his $[BF_4{\subset}Ni_2(\mathbf{L1})_3](BF_4)_3$ mesocate revealed both a significant amount of additional space present inside the cage despite the BF_4^-.[27] Structural cage distortion was possible due to the significant flexibility of the C6 spacer as seen by X-ray crystallography analysis. The modelling data suggested that a larger anion could be bound within the mesocate.[27]

Anion coordination chemistry suggests that the type of anion introduced into the complexation affects the final structure of an isolated helicate and can cause a transformation into a mesocate structure. For example, Cui *et al*., found that their M_2L_3 complexes with bipyridylimidazolium ligands became mesocates with large anions such as (BF_4^-, ClO_4^-, and SO_4^{2-}), while helicates formed with small Br^- and NO_3^- anions.[28] Although Wenzel *et al*., found that the introduction of a BF_4^- anion to a dicopper double helicate caused a major reduction of the cavity and increase in helicity, McGarry formed a $[BF_4{\subset}Ni_2(\mathbf{L1})_3](BF_4)_3$ mesocate with a large cavity.[25,27] In consideration of Cui *et al*., findings, it is possible that mesocates formed because the anions were too large for the cage, or because the length of the ligands were too short and unable to twist around the structure. These perspectives will be considered in this project.

2.0 Aim of Research

Helicates are an intriguing supramolecular structure. The aim in this thesis is to synthesise salicylaldimine-based metal coordinated helicates. Once formed, the anion binding properties of these helicates will be explored using a series of characterisation methods such as X-ray crystallography to prove the formation of salicylaldimine complexes and solvent extraction experiments to research the potential using a salicylaldimine ligand as the extractant to transfer Ni^{2+} ions to the organic phase.

The formation of a variety of salicylaldimine complexes requires the synthesis of various ligands. Three ligands **L1**-**L3** (Figure 4) will be synthesised and characterised by NMR, mass, UV-Vis and IR spectroscopy. Next, a series of complexation reactions will be carried out with different metal salts and anions. The complexes will be characterised by AAS, UV-Vis, mass and IR spectroscopies, X-ray diffraction and CHN analysis where possible. The **L1** ligand and complexes **C1** and **C2** were previously formed by McGarry However, due to poor crystallographic analyses with high R values, the goals of repeating his work were to obtain better crystal data, suitable for publication and to continue the analysis of the crystals that McGarry could not do due to a lack of crystal product.[27]

In addition, the synthesis of ligands with different linkages between the salicylaldimine groups will be carried out in the attempt to form other helicates or mesocates. Finally, a solvent extraction experiment will be carried out to test the effectiveness of **L4** for the solvent extraction of Ni^{2+}. **L4** is simply **L3** with octyl amine arms instead of propyl amine for solubility in decanol and to mimic other popular extractants such as LIX 84-I. **L3** was chosen as the extractant due to the successful crystallisation of **C3** (Chapter 4), which confirms the affinity of Ni^{2+} binding to **L3** in the presence of SO_4^{2-}. Various solvents and aqueous: organic (A:O) ratios will be attempted to find the optimal conditions for nickel extraction. For the organic solvent, decanol and hexane will be attempted due to ease of access and handling.

2.1 Discussion and Synthesis of L1-L3

The salicylaldimine ligand and its variants have been a key point of research for the Plieger group. Salicylaldimines are a sub-class of Schiff-base compounds. The dedication to salicylaldimine based ligands in the research community exists because of its interactions with transition metals that provide interesting magnet, spectral, catalytic, redox and bioinorganic properties.[29,30]

The aim of the design is to create bis(tridentate) triple dinuclear nickel complexes. All **L1-L3** ligands have the structure below, differing only by the type of spacer labelled **R1**, **R2**, **R3** respectively (in Figure 4). The **R1** spacer was obtained commercially but **R2** and **R3** were synthesised from terephthalaldehyde and isophthalaldehyde.

Although the design of **L1** allowed for the formation of BF_4^- and ClO_4^- complexes, **L3** formed bidentate dinuclear nickel complexes with SO_4^{2-} and ClO_4^- as the metal formed covalent bonds with the oxygen donor groups of the central anion.

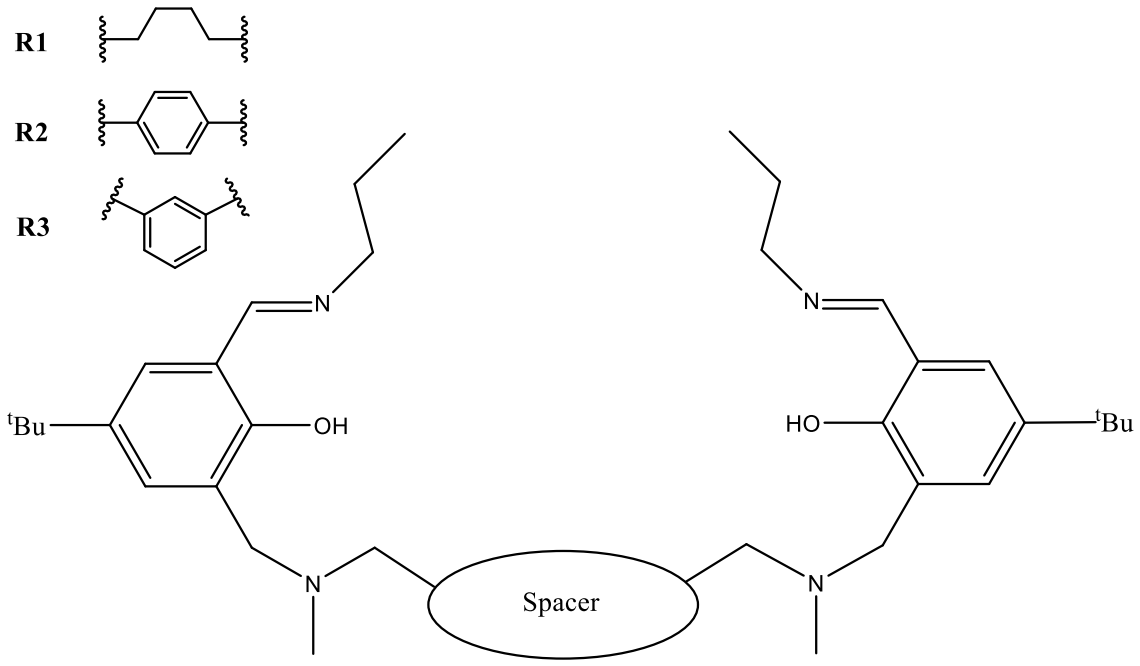

Figure 4. Structure of ligand design.

All ligands in this project required an initial synthesis of 5-*tert*-butyl-3-bromomethyl-2-hydroxybenzaldehyde. This product was synthesised in bulk following the established procedure by Aldred *et al*., where a 4-*tert*-butylphenol went through a formylation reaction.[31] The product was purified via column chromatography and the final product was collected from the crude material as a golden oil with a total yield of 43%.

Next, a methylbromination reaction according to Meier *et al*., was followed and the product was purified by hot recrystallisation.[32] Beige crystals of the 5-*tert*-butyl bromosalicylaldehyde were afforded at a yield of 87.8% (**1a** in Figure 5).

Using **1a** and the spacer group **R1/R2/R3**, a coupling reaction from Stevens and Plieger was carried out.[33,34] Their amine alkylation reaction was simple and reliable with a reported yield of 97%.[33] As shown below, the propyl amine was added to the aldehyde of **1b** via a Mannich condensation reaction from Wenzel *et al*., to afford **L1** in a 92.2% yield as a golden oil (last step in Figure 5).[23] The propyl arms help with solubility and stability. The success of the addition of these propyl groups to form **L1**/**L2**/**L3** was determined by the disappearance of an aldehyde peak around 10.35 ppm in the ^{1}H NMR spectra. To form **L4** for the solvent extractions, this last step with propyl amine and **L3** was replaced with octyl amine for better solubility in decanol.

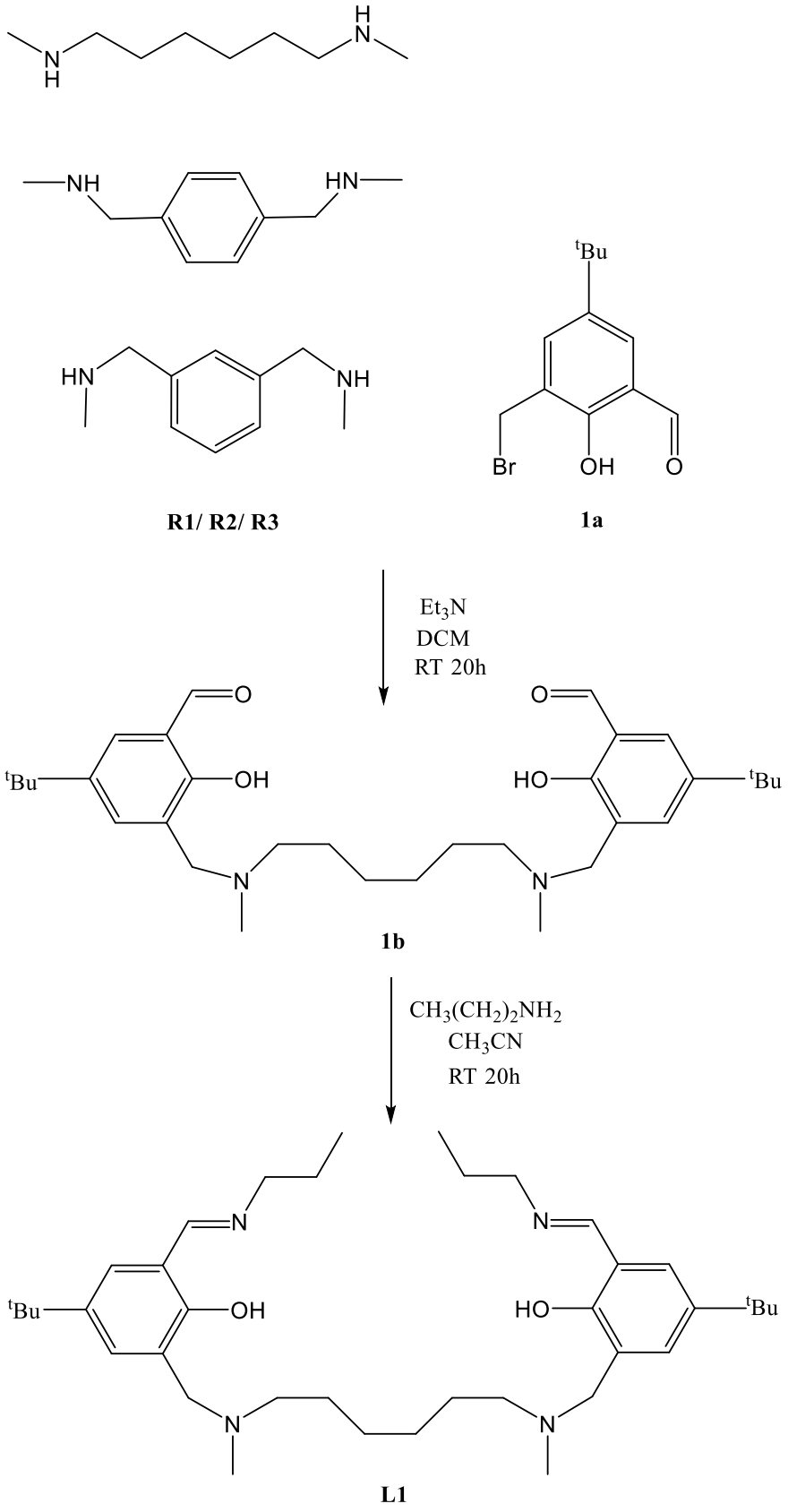

Figure 5. Example reaction scheme for **L1/L2/L3**.

The synthesis of **L2** requires the addition of methylamine groups on the terephthalaldehyde to produce **R2** in a 80.4% yield before it can be attached to the salicylaldehyde groups (Figure 6).[24]

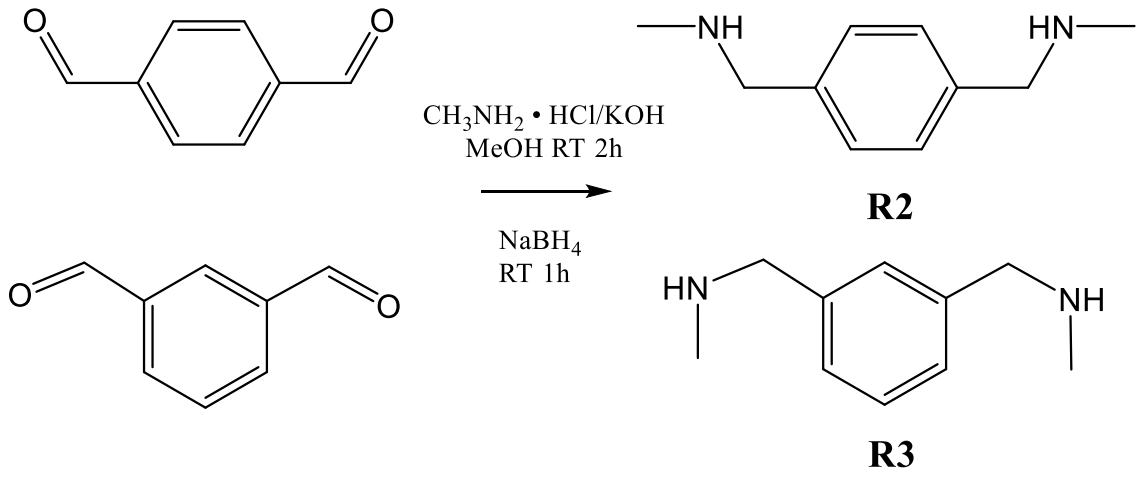

Figure 6. Reaction scheme of **R2** and **R3**.

2.2 Characterisation of L1-3.

2.2.1 Mass Spectrometry of L1-3

The mass spectrometry of the charged species was carried out in methanol. The molecular weight of **L1** is 606.94 g mol^{-1} and the estimated m/z is 606.49 (100%), 607.49 (41.1%) and 608.49 (8.2%) m/z. For **L2** and **L3**, the molecular weight is 626.91 g mol^{-1} and the estimated m/z for both are 626.49 (100%), 627.49 (43.3%) and 628.49 (9.1%) m/z.

As shown in Appendix F1.1, the mass spectra of **L1** show peaks at 607.40 (41%) and 232.22 (100%) m/z. The peak at 607.40 m/z confirms the presence of the correct ligand. The mass spectra for **L2** and **L3** also confirms the presence of the correct ligand with peaks at 627.37 (45%) and 627.35 (90%) m/z respectively. The base peak at 232.22 m/z in all the **L1-3** spectra represents the salicylaldimine-propyl group shown below in Figure 7.

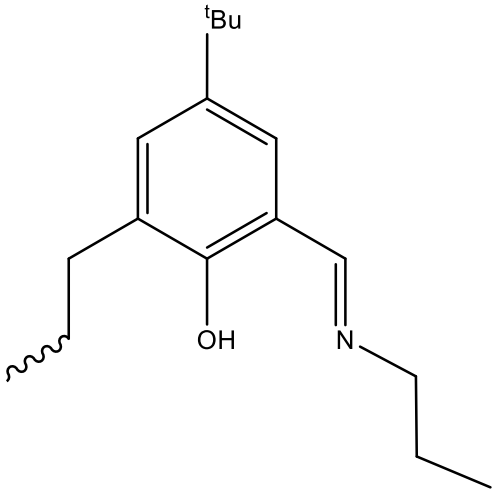

Figure 7. The *tert*-butyl salicylaldimine group with a propyl arm.

2.2.2 ^{1}H NMR Spectroscopy of L1-3.

The purity and identity of the ligand synthesised was checked via NMR. In particular, the most important peaks to distinguish the product from the reagent are imine formation at 8.35 ppm (**a),** and the disappearance of the aldehyde peak (Figure 8). The peaks (**e**) 3.57 ppm, (**f**) 2.25 ppm, (**j**) 2.4 ppm, (**k**) 1.69 ppm, (**l**) 1.30 ppm confirm the successful attachment of the **R1** spacer group. For **R2** and **R3**, the aromatic ring in the spacer causes the chemical shift downfield as a result of the deshielding effect of the ring. For both spacer groups, the attachment of the correct spacer is shown by (**e**) 3.66 ppm, (**f**) 2.25 ppm, (**j**) 3.55-7 ppm, (**k**) 7.31-37 ppm, (**l**) 7.15 ppm, and (m) 7.15 ppm. The difference between **R1** and **R2** can be seen by the extra peaks (**l**), and (**m**). The peaks at (**g**) 3.57 ppm, (**h**) 1.70 ppm, and (**i**) 0.97 ppm are consistent in the tables for **L1**-**3** which represent the propyl group. Finally, the 18 protons peak of the *tert*-butyl group (**c**) at 1.30 ppm and the aromatic protons (**b**), (**d**) around 7.00 ppm show the presence of the salicylaldimine group.

The comparison of **L1-3** can be seen between Table 2-4. Only the assignments between the tables on the spacer group j-m change significantly. The assignment for all peaks are in accordance with the assignments from McGarry and Stevens.[27,33]

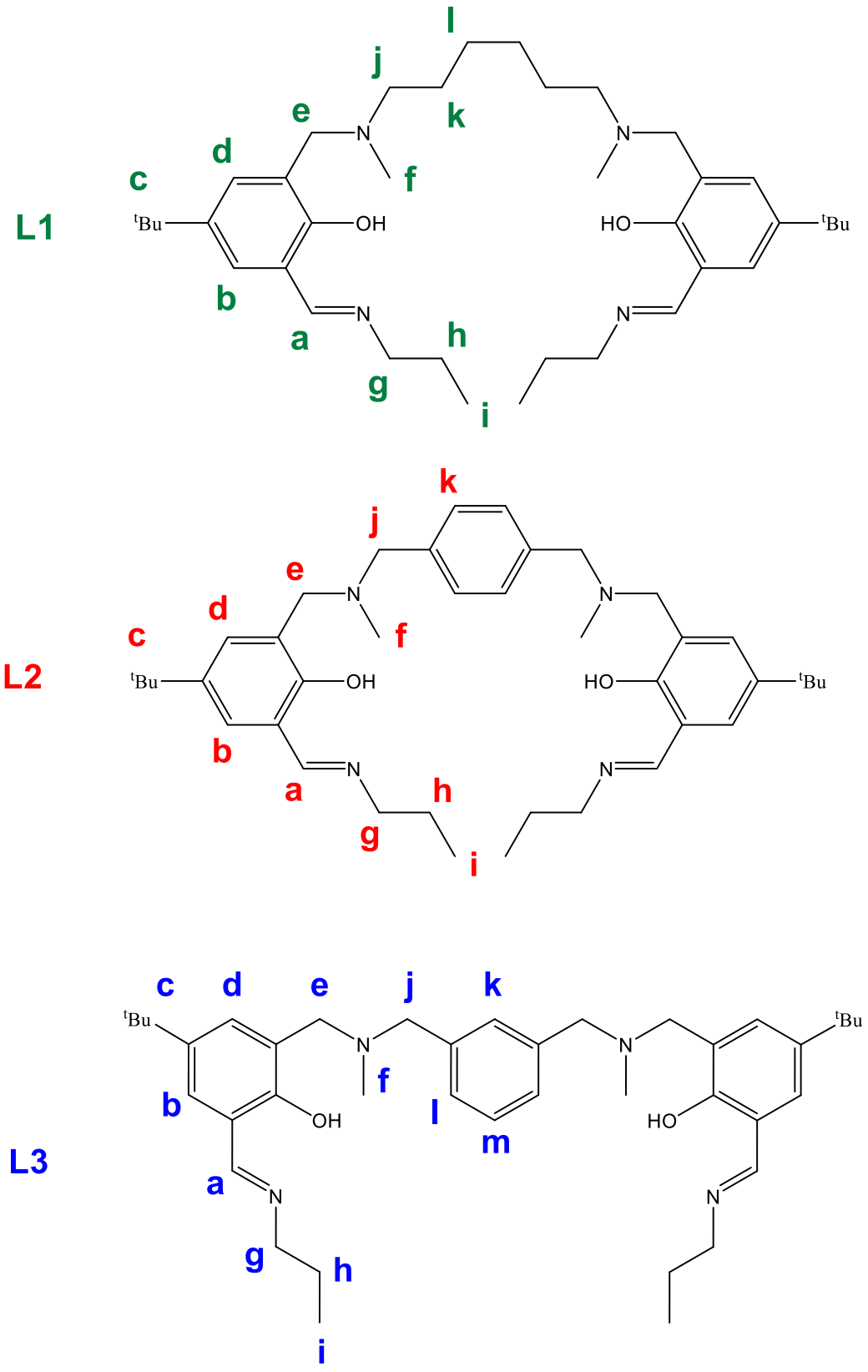

Figure 8. The NMR numbering system of the ligands L1-L3.

Table 2. ^{1}H NMR characterisation of **L1**.

	a	b	c	d	e	f	g	h	i	j	k	l
^{1}H NMR (δppm)	8.35	7.39	1.30	7.16	3.57	2.25	3.57	1.70	0.97	2.4	1.69	1.30
	s 2H	d 2H	s 18H	d 2H	s 4H	s 6H	td 4H	h 4H	t 6H	t 4H	m 4H	m 4H
J (Hz)		2.0		2.0								

Table 3. ^{1}H NMR characterisation of **L2**.

	a	b	c	d	e	f	g	h	i	J	k
^{1}H NMR (δppm)	8.35	7.53	1.30	7.16	3.66	2.24	3.55	1.71	0.97	3.55	7.31
	s 2H	d 2H	s 18H	d 2H	s 4H	s 6H	td 4H	h 4H	t 6H	t 4H	td 4H
J (Hz)		2.0		2.0							7.0

Table 4. ^{1}H NMR characterisation of **L3**.

	a	b	c	d	e	F	g	h	i	j	k	l	m
^{1}H NMR (δppm)	8.35	7.54	1.31	7.15	3.66	2.25	3.55	1.71	0.98	3.57	7.37	7.37	7.37
	s 2H	d 2H	s 18H	d 2H	s 4H	s 6H	td 4H	h 4H	t 6H	t 4H	s 1H	d 2H	t 1H
J (Hz)		2.0		2.0							7.0	7.0	2.0

2.2.3 ATR-FTIR Spectroscopy of L1-3.

The IR spectra for **L1, L2** and **L3** are almost identical, except for the appearance of more peaks in the 700-800 cm^{-1} region as the addition of different spacer groups does not introduce any new functional groups that are not already existing in the structure. The recorded spectrum in Table 5-7 agrees with that previously obtained from McGarry, confirming successful synthesis.[27]

The strongest, broadest peak at 2961 cm^{-1} represents the stretch from the CH group of the aromatic ring from the *tert*-butyl cap. The other strong-medium peaks show the stretch of C=N and C=C at 1634, 1468 cm^{-1}. In the fingerprint region, the medium-weak peaks C-O, C-N, and C=C correlate to 1394, 1039, 980 cm^{-1} respectively. The expected stretch for N-H was not observed in our data nor in the data provided by McGarry.

Table 5. Selected IR peaks of **L1**.

	C-H s, b	**C=N S**	**C=C s**	**C-O m**	**C-N m**	**C=C w**
Absorption cm^{-1}	2961	1634	1469	1394	1050	980

Table 6. Selected IR peaks of **L2**.

	C-H s, b	**C=N S**	**C=C s**	**C-O m**	**C-N m**	**C=C w**
Absorption cm^{-1}	2962	1634	1469	1394	1039	980

Table 7. Selected IR peaks of **L3**.

	C-H s, b	**C=N s**	**C-H s**	**C-O m**	**C-N m**	**C=C w**
Absorption cm^{-1}	2961	1634	1470	1394	1039	980

2.2.4 UV-Vis Spectroscopy of L1-3

The UV-Vis spectrum for **L1** presented 5 defined peaks while 4 peaks were recognised in the **L2** spectrum and 3 peaks in the **L3** spectrum (Table 8-10). The shape of the peaks and patterns match with similar reported compounds found in the literature.[27,33] For example McGarry found that his analysis of **L1** in methanol presented UV-Vis peaks at 415, 325, 280, 255, 222 nm with absorbances 0.07, 0.09, 0.13, 0.29, 0.61 respectively.[27] The peaks are from the phenol structure of the salicylaldimine.

In particular, the broad 400 nm peak is related to *n* to π^* electron transfer which is responsible for the yellow colour of the ligand.[33] The shoulder peaks between 250-350 nm represent the π to π^* transitions of the phenolate while the large peak near 200 nm was considered an inconsistent, unreliable peak as it was very close to the cuvette absorption.[33]

Table 8. UV-Vis peak absorbances and wavelengths of **L1**.

	Wavelength (nm)	**Absorbance**	**Mol. abs. (M^{-1} cm^{-1})**
1	403	0.158	2,787
2	316	0.146	2,575
3	270	0.259	4,568
4	247	0.458	8,078
5	213	1.086	19,153

Table 9. UV-Vis peak absorbances and wavelengths of **L2**.

	Wavelength	**Absorbance**	**Mol. abs. (M^{-1} cm^{-1})**
1	402	0.086	1,968
2	317	0.112	2,563
3	246	0.355	8,124
4	212	0.989	22,632

Table 10. UV-Vis peak absorbances and wavelengths of **L3**.

	Wavelength	**Absorbance**	**Mol. abs. (M^{-1} cm^{-1})**
1	402	0.115	2,693
2	317	0.186	4,356
3	248	0.585	13,700

3.0 Metal Complexes with L1-L3

3.1 Metal Complexation Reactions with L1

The aim to synthesise cages suitable for anion encapsulation using bis-salicylaldimine ligands was carried on from where McGarry finished his honours project.[27] The complexations were repeated to obtain better X-ray crystallography data suitable for publication.

The complexes **C1** and **C2** were formed easily in ethanol as shown in Table 11 below. Attempts to form variations of the complexes using other metal salts (with different anions) were attempted but only salt crystals were isolated in crystallisation attempts. The complexes that were formed with **L1** were analysed using various methods and compared with results from McGarry where possible to confirm the same complex was made.

Complexations with dysprosium were also attempted due to the availability of the metal salt, however the complex did not form because the conditions of complexation were not right. Metal ion size is also a factor, nickel has an empirical radius of 135 pm and a covalent radius of 110 pm while dysprosium has an empirical radius of 175 pm and a covalent radius of 167 pm.[12]

Table 11. Successful metal complexations with **L1**.

Crystal name	RT solvent	Ratio M:L	Colour change	Crystal
C1 **$[BF_4 \subset Ni_2(L1)_3](BF_4)_3$**	Methanol	2:3	Green to yellow	Green blocks
C2 **$[ClO_4 \subset Ni_2(L1)_3](ClO_4)_3$**	Ethanol	2:3	Green to yellow	Dark green blocks

3.2 Characterisation of L1-Containing Metal Complexes

3.2.1 Mass Spectrometry of L1 Complexes

Samples of **C1 (**0.0008 g) and **C2** (0.0005 g) crystals were dissolved in methanol and run for mass spectrometry analysis.

The mass spectra of both compounds showed five similar peaks. The most prominent ones are listed in Table 12. The three peaks most likely correspond to the groups listed on the left.

Table 12. Experimentally obtained mass spectrometry peaks for **L1** complexes

	C1	**Expected mass C1**	**C2**	**Expected mass C2**
L1 + Ni	663.31	663.18	663.32	663.18
L1	607.37	607.49	607.29	607.49
L1 + Ni + BF_4^-/ClO_4^-	751.23	751.00	763.20	764.63

3.2.2 ATR-FTIR Spectroscopy of L1 Complexes

ATR-FTIR spectra were recorded for the complexes on crushed powders (Table 13). The peak at 1625 cm^{-1} of the ligand which is assigned to the C=N imine functional group is retained in the complexes which indicates the complex was formed with no hydrolysis occurring at this bond. A strong new peak around 1080-1050 cm^{-1} in the complex spectra is assigned to either the BF_4^- or ClO_4^- stretching mode of the central atom with that of its peripheral atom[35,36] The data and interpretation below is identical to the data found by McGarry.[27] Lutz *et al*., studied $TiClO_4$, $TiBF_4$ and $NHBF_4$ single crystals in their polarised IR reflection spectra and found peaks within the range stretching modes 1036-1040 cm^{-1} for $TiBF_4$, 1067-1090 cm^{-1} for $NHBF_4$, and 1059-82 cm^{-1} for $TiClO_4$.[35] A different research group, Zafiu *et al*., analysed the bonding of their protein on electrodes which contained $NaClO_4$ with FTIR and found a strong stretch at 1107 cm^{-1}.[36] Therefore, both assignments of BF_4^- at 1052 cm^{-1} and ClO_4^- at 1081 cm^{-1} appear plausible. Another change is the appearance of peaks which were not present in the IR spectra of the ligands at 621-650 cm^{-1} and 650-850 cm^{-1} which represents the Ni-O and Ni-N respectively.[29]

Table 13. Selected IR absorption peaks of washed crystal products.

	C-H	**C=N**	**C=C**	**C-O**	**B-F or Cl-O**	**Ni-N**	**Ni-O**
C1 (cm^{-1})	2968 *m, b*	1625 *s*	1471 *m*	1394 *w*	1077 *s*	765 *w*	622 *m*
C2 (cm^{-1})	2959 *w*	1625 *m*	1472 *m*	1383 *w*	1081 *s*	764 *w*	622 *m*

As shown (Figure 9) below in the comparison of **L1** and **C2**, there are many differences between the spectra of the ligand and complex. For all complexes, a medium peak appears at 620-640 cm^{-1} and a strong peak appears at 1080 cm^{-1} while the peaks present in the ligand spectra become less prominent.

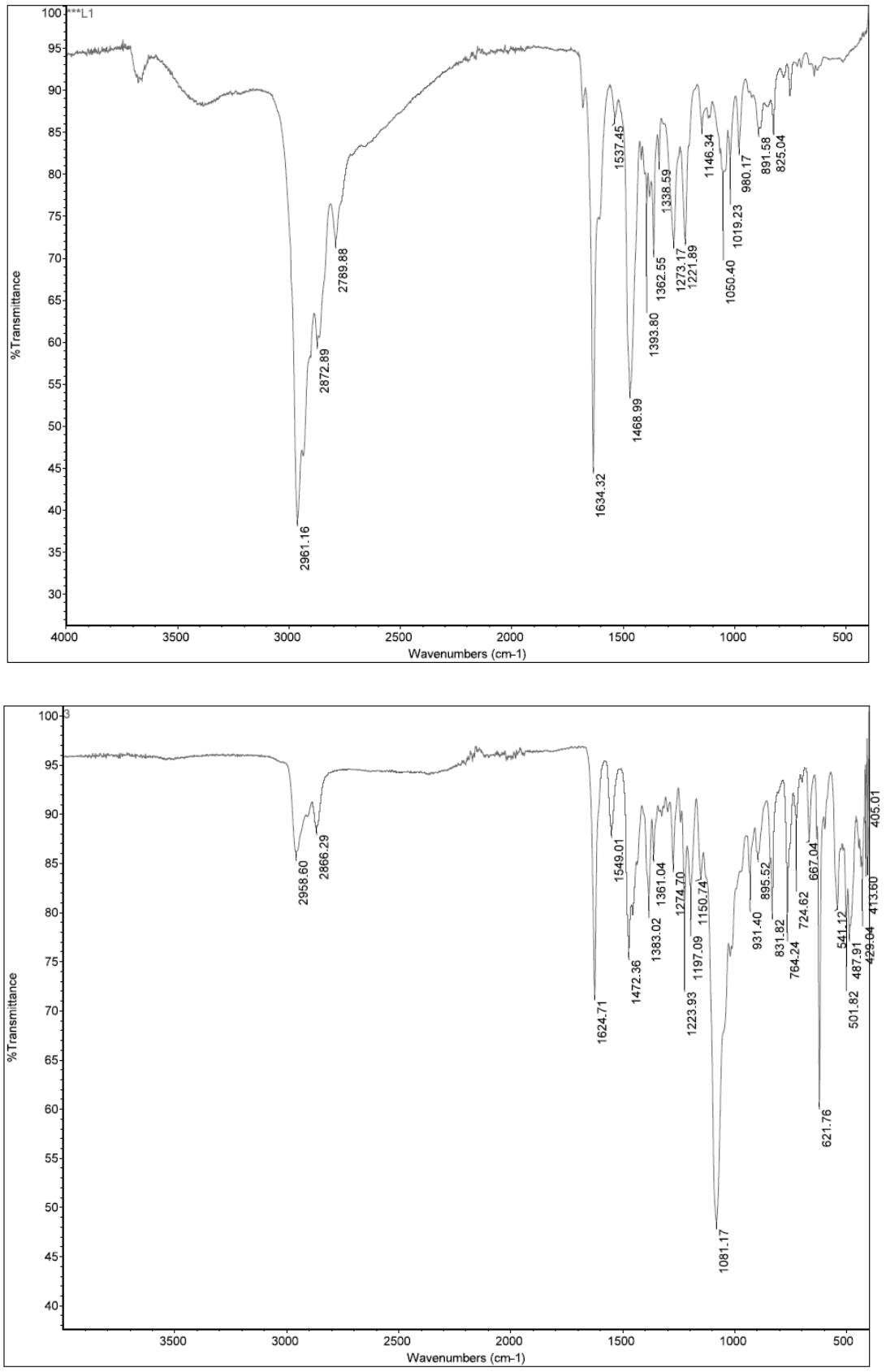

Figure 9. IR spectra of **L1** (top) and **C2** (bottom) for comparison.

3.2.3 UV-Vis Spectroscopy of L1 Complexes

McGarry, presented absorbance results that showed four peaks at 365 nm, 266 nm, 245 nm, and 224 nm at absorbances 0.17, 0.40, 0.75 and 0.85 respectively from 1.72 $x10^{-5}$ M of C1 in acetonitrile.[27] Although the shape of the UV-Vis spectra from our crystal with looks similar, the shoulder peak at 245 nm from our complex was not recognised by program UV Probe and there was no shoulder peak at 266 nm (Figure 10). In Stevens' analysis, the UV-Vis spectra had the same shape as ours however, due to a slight difference in ligand structure, the wavenumbers recorded were slightly higher.[33] Table 14 below does not include the small shoulder peak around 243 nm.

The UV-Vis spectra for the complexes are different from that of the ligand. The most obvious differences are the appearance of a shoulder peak and the disappearance of three peaks at 247, 270, 316 nm. It appears that the 403 peak also shifted to absorb at a lower wavelength. According to Stevens' analysis, the peak at 228 is related to the π-π_1*, the peak at 366 nm shows the phenolate n-π_2* electronic transition, and the latter is the reason for the dark green colour of the crystals.[33] Stevens reported that below 230 nm, the peaks are inconsistent, and the absorbance line drops rapidly.[33]

Due to the interaction of the ligand to the metal ion, the UV-Vis spectra of the complex on the right of Figure 10, is different from the spectra of the ligand **L1** on the left. The broad peak at 400 nm of the ligand shifted to 366 nm in the spectra of the complex due to the coordination of the Ni^{2+} to the ligand which lowers the π* orbital of the ligand and the energy of the transition. These changes were observed by other researchers who also complexed salicylaldimine ligands with metal ions.[29,30,37]

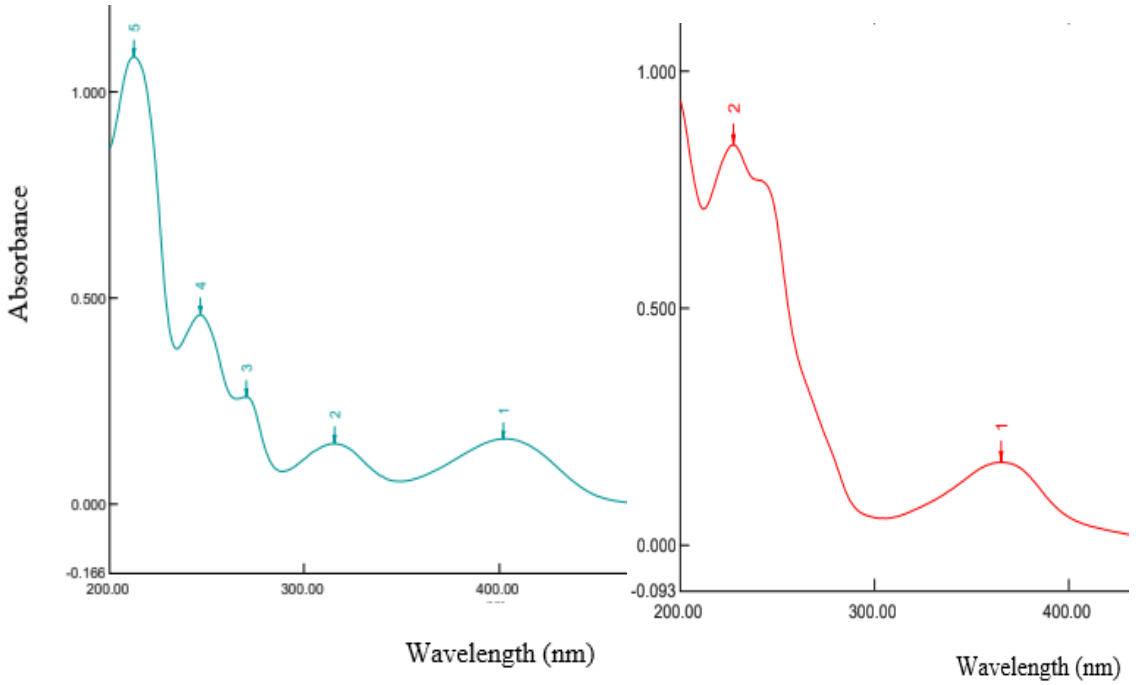

Figure 10. UV-Vis absorption spectra comparison of **L1** (left) and **C1** (right).

Table 14. UV-Vis data of **L1** and **C1**.

	Wavelength (nm)	**Absorbance**	**Conc. ($1x10^{-6}$ M)**	**Mol. abs. (M^{-1} cm^{-1})**
L1				
1	402.50	0.158	56.7	2,787
2	315.50	0.146	56.7	2,575
3	270.00	0.259	56.7	4,568
4	246.50	0.458	56.7	8,078
5	212.50	1.086	56.7	19,153
C2				
1	364	0.343	29.6	11,588
2	228	1.620	29.6	54,730

3.2.4 Atomic Absorption Spectroscopy of L1 Complexes.

Atomic absorption spectroscopy was carried out for the two complexes with **L1**. Six standards were made up using a standard nickel solution (Ni^{2+} 1.00 g L^{-1}) and 2 M HCl within the optimum working range 6-25 μg mL^{-1} for 341.5 nm. After the standards were measured, the complexes diluted with 2 M HCl within the concentration range 9-17 μg mL^{-1} were also measured. The six standards gave a linear line in Figure 11.

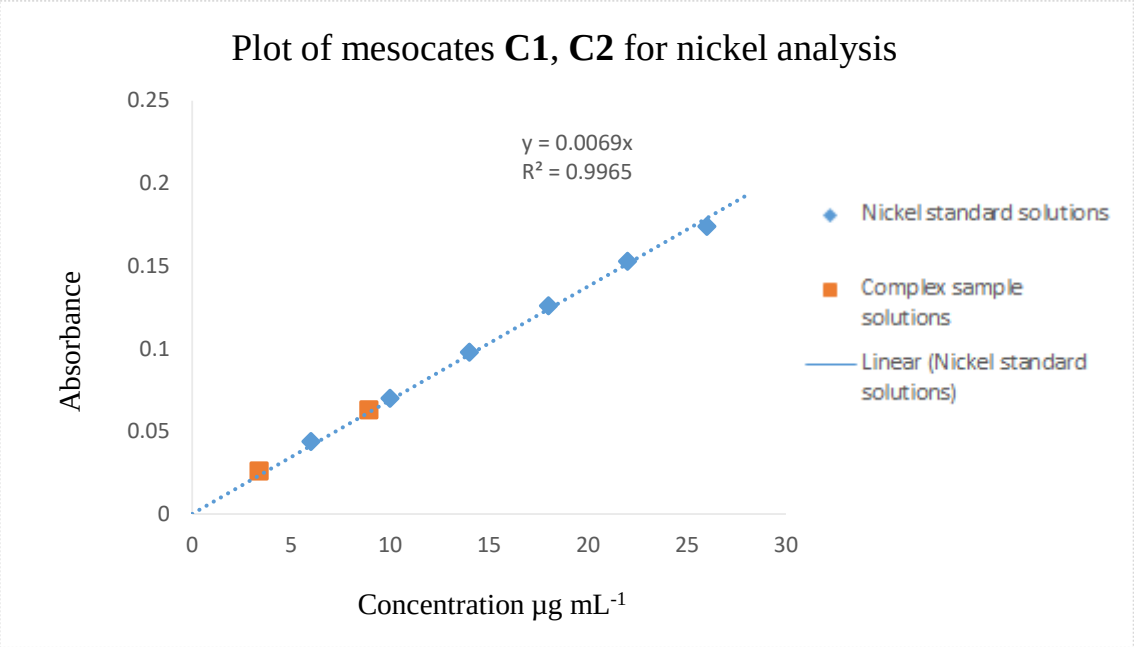

Figure 11. Plot of mesocates **C1** and **C2** for nickel analysis.

Table 15. Table of nickel standards solutions.

Concentration (μg mL^{-1})	**Absorbance**
6	0.044
10	0.070
14	0.098
18	0.126
22	0.153

26	0.174

For **C1** and **C2**, the experimental and theoretical values were close enough to confirm the complex has two nickel ions (Table 16). **C2** was repeated as the first run showed a high percentage of nickel. Using a higher concentration of crystal fixed the problem and gave more accurate values.

Table 16. AAS analysis of **L1** complexes.

Sample	**Amount (μg)**	**Conc. (μg mL^{-1})**	**Abs**	**Calculated Theoretical % Ni**	**% Ni from (FAAS)**
C1 **[BF_4⊂Ni_2($L1$)$_3$](BF_4)$_3$**	1700	8.93	0.063	5.16 (0.2)	5.25 (0.9)
C2 **[ClO_4⊂Ni_2($L1$)$_3$](ClO_4)$_3$**	3100	3.38	0.262	4.97 (0.2)	4.91 (0.8)

3.2.5 Conductivity of L1-L3 Complexes.

The molar conductivity (ʌ) is defined by the conductivity divided by its molar concentration. It is determined by the ion ratio of the products. The ion ratio of a complex gives us an idea of how many ions there are and if they are stable in the centre of a mesocate structure or transient. The ratio of the complex: counterion can be found using the relationship between molar conductance, molar conductivity, and the number of counterions present in a particular solvent.

Table 17. Relationship between molar conductivity and complex: counterion ratio in methanol.

Molar conductivity (S cm^2 mol^{-1})	**Ion ratio**
100-130	1:1
210-250	2:1
340-380	3:1
450-490	4:1

The conductivity of $[BF_4{\subset}Ni_2(\mathbf{L1})_3](BF_4)_3$ (**C1**), $[ClO_4{\subset}Ni_2(\mathbf{L1})_3](ClO_4)_3$ (**C2**), $[SO_4{\subset}Ni_2(\mathbf{L3})_2][Ni(SO_4)_2(EtOH)_4]$ (**C3**), $[ClO_4{\subset}Ni_2(\mathbf{L3})_2](ClO_4)_2$ (**C4**) was conducted over concentrations of 0.0563, 0.0628 µmol mL^{-1} in methanol. As discussed in the following chapters, **L1** complexes have one anion encapsulated inside via weak bonds with three anions weakly interacting outside of the cage. The **L3** complexes have two peripheral anions, and a centre anion with covalent bonds to the metal ion.

Conductivity measurements were carried out on **C1**-**C4** to determine how the complexes behave in solution. We would expect for **C1**, a ratio of 4:1 as we know that there are four anions that are not covalently bound and can dissociate in MeOH. However, the result we got was 2:1 which suggests that perhaps the centre anion and one peripheral could not dissociate. For **C2** we would also expect 4:1 however we measured 1:1 showing that the complex is a 1:1 electrolyte in MeOH. **C3** presented a ratio of 1:1 as we would expect as there is only one peripheral anion. **C4** achieved the expected ratio and because the

complex has two peripheral anions, it suggests that the MeOH was able to dissociate the central anion as well.

Table 18. Conductivity results for **C1**, **C2**, **C3** and **C4** in methanol.

	Ion ratio	**Expected Ratio**
C1 $[BF_4 \subset Ni_2(L1)_3](BF_4)_3$	2:1	4:1
C2 $[ClO_4 \subset Ni_2(L1)_3](ClO_4)_3$	1:1	4:1
C3 $[SO_4 \subset Ni_2(L3)_3][Ni(SO_4)_2(EtOH)_4]$	1:1	1:1
C4 $[ClO_4 \subset Ni_2(L3)_2](ClO_4)_2$	3:1	3:1

The analysis of **C3** and **C4** provided a conductivity measurement that agrees with expected values according to our X-ray crystallisation analysis, however **C1** and **C2** presented a lower ion ratio than expected. The experiment was repeated but the same ion ratios were obtained. It was noticed that the due to the amount of complex used, it was difficult to dissolve in methanol, ethanol, or acetone. Knapp suggests that performing single conductivity measurements on systems with both strong and weakly bound electrolytes is not ideal.[26] He found that his conductivity measurements did not match the known counteranion: cation structure.[26] Due to the large size of our complex, it is understandable that the electrolyte movement would be much slower and may not match the ideal data created from simple salts.

3.2.6 X-Ray Crystallography Analysis of L1 Complexes

3.2.6.1 X-Ray Diffraction Structure for $[BF_4 \subset Ni_2(L1)_3](BF_4)_3$ (C1).

A mixture of $Ni(BF_4)_2 \cdot 6H_2O$ and **L1** in a M:L 2:3 molar ratio was dissolved in ethanol. The green solution was kept at room temperature and the product was isolated using vapour diffusion with Et_2O as the precipitant. After a few weeks, small blocks of dark green crystals of **C1** resulted. The complex was confirmed with FTIR, UV-Vis spectroscopy, and X-ray crystallography.

The complex **C1** is crystallised in an orthorhombic space group $P2_12_12_1$. The complex shows disorder as the ligands do not wrap tightly around the anion but hang loosely in a C shape. Due to the disorder of the anion and the complex, the overall refinement *R*-factor was rather large at 13.58% and wR_2 was 0.3512.

Three ligands are bound to the nickel in a Ni_1-ʌ Ni_2-**Δ** chirality which classifies it as a mesocate. Both Ni_1 and Ni_2 are in a slightly distorted octahedral arrangement as shown in Figure 12 below. Each Ni^{2+} ion has 3 oxygen donors and 3 nitrogen donors. We can see the octahedral nickel ion bonds slightly tilted towards the oxygen groups of the centre anion. The oxygen and nitrogen groups bonded to the nickel is coordinated in a facial conformation.

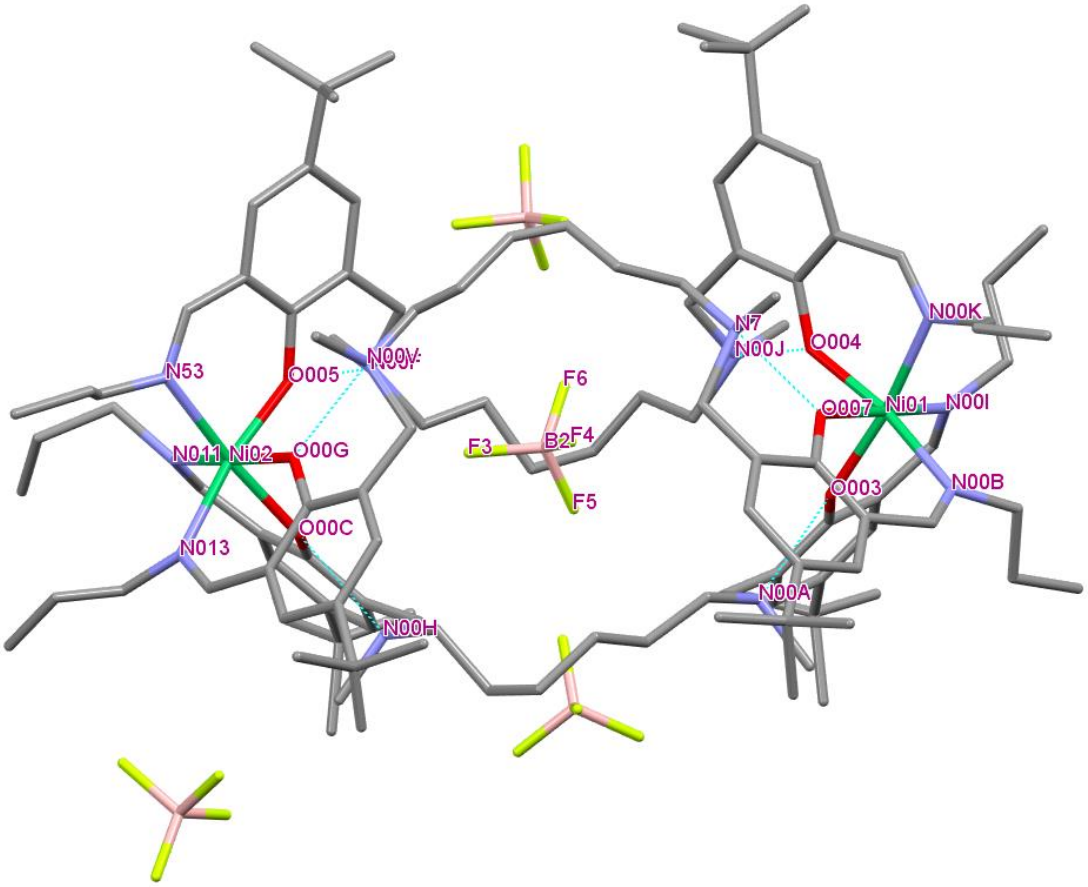

Figure 12. X-ray crystal structure of $[BF_4 \subset Ni_2(\mathbf{L1})_3](BF_4)_3$. Labels for non carbon atoms, and blue dotted lines for the hydrogen bonds between the amines next to the spacer of the ligands with the oxygen groups bonded to the nickel ion. Colour code: grey (C), red (O), blue (N), green (Ni), pink (B), yellow (F). Hydrogens omitted for clarity.

Considering the structure above, it is likely that most of the disorder exists due to the large hexyl spacer used and the resulting amount of empty space in the centre of the mesocate. Although the aim of this experiment was to gain X-ray crystallography structures with better data, **C1** had a high final *R*-factor 0.1358 compared to McGarry's 0.0909. The bond distance values for **C1** are similar to **C2** and the bond distances and angles found by McGarry agree with the values in Table 19 below. The angle of O^{003}-Ni^{01}-O^{004} is 85.5 º instead of 90.0 º and N^{00K}-Ni^{01}-O^{004} is 88.1 º. Since a perfectly symmetrical octahedral structure would have a linear angle of 180 º the data suggests that the octahedral coordination of the nickel is not perfectly symmetrical and that the distortion in the molecule is from the rigidity of the donor groups. The O^{003} is pulled

towards the centre anion, 8.10º away from the opposing nitrogen. On the other hand, there is distortion shown by the <N-Ni-N angle as the angle 95.0 º is bigger than the expected 90.0 º. The average distortion (Δd) for the axial and equatorial sections can be calculated by dividing the sum of distortions from expected angles by the number of distortions summed up as shown in the equation below.

The equation derived by Buron-Le Cointe is as follows:[38]

$$\Delta d = \left(\frac{1}{n}\right) \sum_{i=1}^{n} [\pm(\Phi_i - A)]$$

The calculated Δd values give us an indication of the distortion around the octahedral metal centre. The values 2.55 º, 5.53 º and 3.18 º show that there is some distortion with lower values approaching an ideal octahedral geometry.

Table 19. Bond lengths of nickel in **C1**.

Bond	**Length in Å**
Ni^{01}-O^{003}	2.037(9)
$Ni^{\mathbf{01}}$-N^{00B}	2.140(1)
B^{02}-F^{6}	1.430(2)
B^{02}-F^{3}	1.390(2)

Table 20. Angles and average distortion values of nickel in **C1**.

Angles perpendicular to O^{003}	**Angle (º)**	**Angles perpendicular to N^{00K}**	**Angle (º)**	**Angle in the planar square arrangement**	**Angle (º)**
O^{003}-Ni^{01}-O^{004}	85.5 (3)	N^{00K}-Ni^{01}-O^{004}	88.1 (4)	O^{004}-Ni^{01}-O^{007}	85.5 (3)
O^{003}-Ni^{01}-N^{00B}	86.9 (4)	N^{00K}-Ni^{01}-O^{007}	85.5 (4)	O^{004}-Ni^{01}-N^{00I}	89.2 (4)
O^{003}-Ni^{01}-O^{007}	89.1 (3)	N^{00K}-Ni^{01}-N^{00B}	99.0 (4)	O^{007}-Ni^{01}-N^{00B}	88.0 (4)
O^{003}-Ni^{01}-N^{00I}	88.3 (4)	N^{00K}-Ni^{01}-N^{00I}	96.7 (4)	N^{00I}-Ni^{01}-N^{00B}	95.4 (4)
Average	87.5 ± 1		92.0 ± 6		89.5 ± 4
Δd	2.55		5.53		3.18

Linear bond angles	
O^{003}-Ni^{01}-N^{00K}	171.9 (4)
O^{007}-Ni^{01}-N^{00I}	175.6 (4)
O^{004}-Ni^{01}-N^{00B}	171.0 (4)
Bond angles of BF_4^-	
F^6-B^2-F^4	108.0 (1)
F^3-B^2-F^5	114.0 (1)

There are six hydrogen bonds in **C1**, two on each ligand. As we can see in Figures 12 and 13, the hydrogen on the amine next to the spacer acts a donor group to the oxygen of the salicylaldimine group, the acceptor. The distances and angles of these hydrogen bonds are listed in Table 21. The distance of the donor to hydrogen (D-H) was calculated by Olex based on their ideal positions. Measurements via Mercury gave 1.0 Å. While the difference may seem significant, it does not affect the categorisation of the hydrogen bond in this case as the distance from the anion to the hydrogen (H-A) is double the value of (D-H).

Table 21. Distance and angle of hydrogen bonds in **C1**.

DHA	**d(D-H)/Å**	**d(H-A)/Å**	**d(D-A)/Å**	**D-H-A/°**
N^{00A} H^{00A} O^{003}	0.930(1)	1.650(8)	2.507(9)	142.7(3)
N^{00F} H^{00F} O^{005}	0.930(1)	1.674(9)	2.521(10)	141.5(4)
N^{00H} H^{00H} O^{00C}	0.930(1)	1.753(8)	2.599(9)	141.0(3)
N^{00J} H^{00J} O^{004}	0.930(1)	1.731(10)	2.543(10)	138.0(3)
N^{00V} H^{00V} O^{00G}	0.930(1)	1.697(11)	2.587(11)	146.2(3)
N^7 H^7 O^{007}	0.930(1)	1.715(10)	2.556(10)	140.6(4)

The structure is supported by the weak interactions between the oxygen group on the salicylaldimine cap and the neighbouring imine. The average distance of this interaction

is 2.553(10) Å. This emphasises the role each N and O donor atoms have in the ligand and how each group in the ligand functions to stabilise the complex.

Although the definition of strong, moderate or weak hydrogen bonds are considered guidelines, Table 22 provides a general classification of hydrogen bonds.[39] According to the values in Table 22, the hydrogen bonding in complex **C1** can be assigned as moderate and mostly electrostatic. The distance for (H-A) of a moderate hydrogen bond ranges between 1.5-2.2 Å and the distance from donor to acceptor (D-A) are considered between 2.5-3.2 Å.[40] As discussed above, the (H-A) distance is double the (D-H) distance and the bond angles are larger than 130 °.

As we can see, all of the values agree with the ranges specified for a moderate hydrogen bond so we can assume that their bond energies would also fall within 4-15 k cal mol^{-1}. An aspect of this classification that is not shown in the table is that the gap between a strong and moderate hydrogen bond is much larger than the moderate and weak.
Although one hydrogen bond may seem weak, the presence of six hydrogen bonds is much stronger and supports the structure despite any disorder present.

Table 22. Classification of strong, moderate and weak hydrogen bonds.[40]

	Strong	**Moderate**	**Weak**
Interaction type	Strongly covalent	Mostly electrostatic	Electrostatic/ dispersive
Bond length H···A (Å)	1.2-1.5	1.5-2.2	>2.2
Lengthening of D-H (Å)	0.08-0.25	0.02-0.08	<0.02
D-H vs H···A	D-H ≈ H···A	D-H < H···A	D-H << H···A
D···A (Å)	2.2-2.5	2.5-3.2	>3.2
Directionality	Strong	Moderate	Weak
Bond angles	170-180	>130	>90
Bond energy (kcal mol^{-1})	15-40	4-15	<4

The X-ray structure shows 3 BF_4^- anions around the periphery of the complex while one BF_4^- anion is free floating in the centre. The central BF_4^- anion is disordered over two sites in a 50:50 ratio. McGarry attributed the disorder of the BF_4^- as possibly arising due to the extra space in the cavity.[27] As shown below, if we view the complex along the Ni_1-Ni_2 axis, the BF_4^-, atoms around the Ni^{2+} and the ligands are aligned almost perfectly with each other. Although from this view it seems there might be π-π stacking, the aromatic rings are facing the same direction along a plane so there are no π-π interactions.

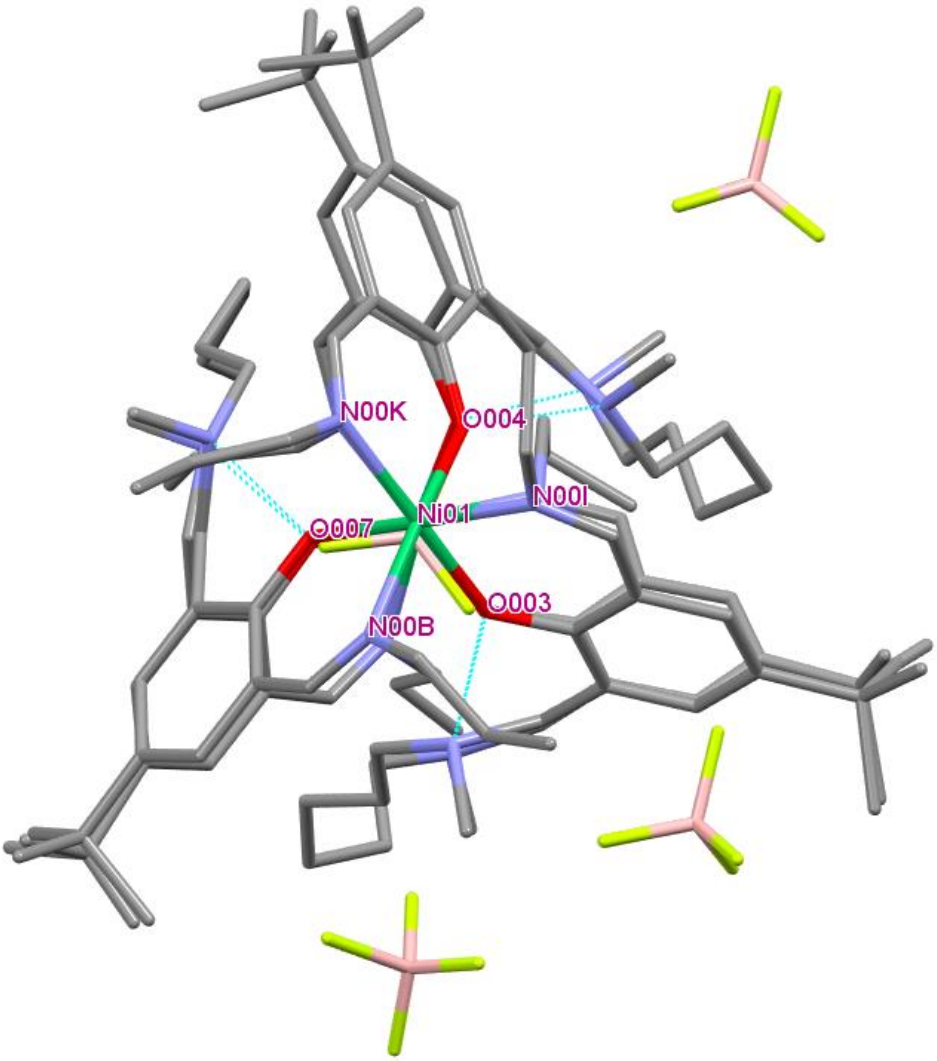

Figure 13. X-ray crystal structure of $[BF_4{\subset}Ni_2(\mathbf{L1})_3](BF_4)_3]$. View along Ni_1-Ni_2 axis with labels for non carbon atoms, and blue dotted lines for the hydrogen bonds between the amines next to the spacer of the ligands with the oxygen groups bonded to the nickel ion. Colour code: grey (C), red (O), blue (N), green (Ni), pink (B), yellow

(F). Distortion shown by the differences in the overlay. Hydrogens omitted for clarity.

3.2.6.2 X-Ray Diffraction Structure for $[ClO_4 \subset Ni_2(L1)_3](ClO_4)_3$ (C2).

A mixture of $Ni(ClO_4)_2 \cdot 6H_2O$ and **L1** in a M:L 2:3 molar ratio was dissolved in ethanol. The green solution was kept at room temperature and the product was isolated using vapour diffusion with Et_2O as the precipitant. After 1-2 weeks small blocks of dark green crystals of **C2** resulted. The complex was confirmed with FTIR, UV-Vis spectroscopy, and X-ray crystallography.

The data for **C2** has the same ligand and metal but different anion. It resulted in an isomorphous structure as **C1**, and the orthorhombic space group $P2_12_12_1$. From the X-ray crystallography data, the refinement *R*-factor was 6.80% and wR_2 was 0.2472. Our goal was met as McGarry deemed their identical crystal data to be unusable and did not provide a *R*-factor in their report. The larger scale synthesis allowed additional conductivity and elemental analysis to be performed on the sample.

Similar to **C1**, the ligands are bound to the nickel in a mesocate Ni_1-Λ Ni_2- **Δ** chirality and coordinated in a facial conformation. Both Ni_1 and Ni_2 are in a slightly distorted octahedral arrangement as shown in Figure 14 below. Each Ni^{2+} ion has 3 oxygen donors and 3 nitrogen donors.

The complex has the same weak interactions as **C1** and the average distance between the N and O of the interaction is 2.553 Å, the same as **C1**. These interactions help stabilise the complex and decrease the disorder of the alkane spacer group.

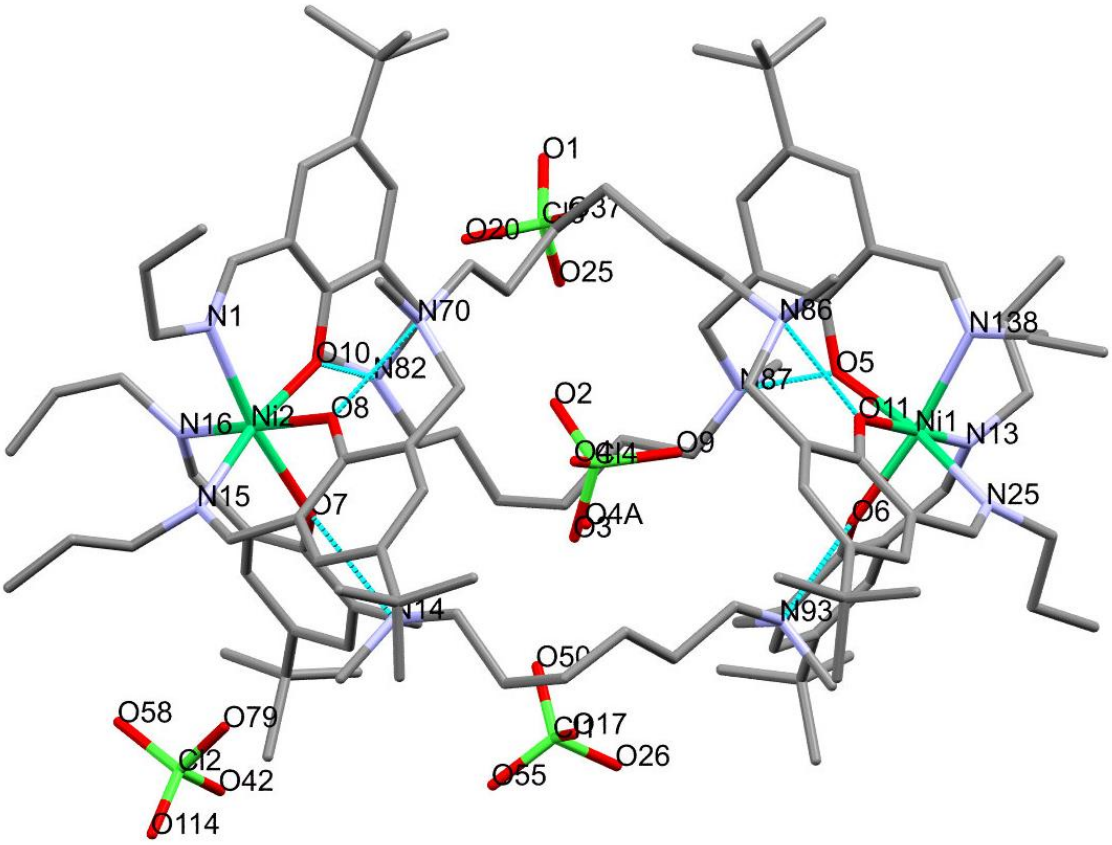

Figure 14. X-ray crystal structure of $[ClO_4 \subset Ni_2(\mathbf{L1})_3](ClO_4)_3$ with labels for non carbon atoms, and blue dotted lines for the hydrogen bonds between the amines next to the spacer of the ligands with the oxygen groups bonded to the nickel ion. Colour code: grey (C), red (O), blue (N), dark green (Ni), green (Cl). Hydrogens omitted for clarity.

As seen in Table 23 below, the bond distances of Ni-O or Ni-N are similar to **C1** and are longer than the Cl-O bonds. The distance between Ni_1 and Ni_2, 12.104(1) Å, of **C2** is shorter than the Ni_1-Ni_2 distance of the **C1** which measured 12.297(3) Å. In **C2**, the oxygen groups are also drawn to the centre anion while the nitrogen face outwards causing distortion in the molecule.

Table 23. Bond lengths of nickel in **C2**.

Bond	**Length in Å**

Ni^{01}-O^{5}	2.022(4)
Ni^{01}-N^{13}	2.093(4)
Cl^{1}-O^{17}	1.434(6)
Cl^{1}-O^{50}	1.404(7)

As detailed in Table 24, all O-Ni-O and O-Ni-N angles are smaller than 90.0º, while the linear O-Ni-N angles are 171.5º instead of the expected 180º. To compensate for the distortion towards the centre, all the N-Ni-N angles are 96.8º. The Δ*d* values are lower than the ones found for **C1** suggesting that there is less distortion in **C2**.

Table 24. Angles of nickel in **C2**.

Angles ⊥ to O^{11}	**Angle (º)**	**Angles ⊥ to N^{13}**	**Angle (º)**	**Angle in the square planar arrangement**	**Angle (º)**
O^{11}-Ni^{01}-N^{138}	86.2 (2)	O^{6}-Ni^{01}-N^{13}	89.3 (2)	O^{5}-Ni^{01}-N^{138}	89.3 (2)
N^{25}-Ni^{01}-O^{11}	88.3 (2)	O^{5}-Ni^{1}-N^{13}	88.1 (2)	N^{25}-Ni^{01}-O^{6}	87.0 (2)
O^{5}-Ni^{1}-O^{11}	87.0 (2)	N^{25}-Ni^{01}-N^{13}	96.2 (2)	O^{5}-Ni^{1}-O^{6}	85.6 (2)
O^{6}-Ni^{01}-O^{11}	88.0 (2)	N^{13}-Ni^{01}-N^{138}	96.0 (2)	N^{25}-Ni^{01}-N^{138}	97.7 (2)
Average	87.4 ± 1		92.4 ± 7		89.9 ± 5
Δ*d*	2.63		3.7		3.95

Linear bond angles	
O^{5}-Ni^{1}-N^{25}	171.3 (2)
O^{6}-Ni^{01}-N^{138}	172.5 (2)
O^{11}-Ni^{01}-N^{13}	174.6 (2)
Bond angles of ClO_4^-	
Cl^{1}-O^{17}	1.434 (6)
Cl^{1}-O^{50}	1.404 (7)

There are six hydrogen bonds in **C2**, two on each ligand. In Figures 14 and 16, the placements of the hydrogen bonds are the same as **C1**. The hydrogen of the amine next

to the spacer acts a donor group to the oxygen of the salicylaldimine group. According to the classification from Jeffrey, the hydrogen bonds in **C2** can also be assigned as moderate.[39] The distance for H-acceptor of a moderate hydrogen bond is 1.5-2.2 Å and the values in Table 25 are around 1.7-8 Å.[40] The distance of a moderate hydrogen bond from donor to acceptor is 2.5-3.2 Å and **C2** has strong moderate values of 2.5 Å. The H-acceptor bond is longer than the H-donor bond which also indicate a moderate hydrogen bond as well as an angle that is between 130-170 º although on the stronger side 130-145 º. This means the hydrogen bonds are mostly electrostatic and their bond energies would fall within 4-15 k cal mol^{-1}.

Table 25. Distance and angle of hydrogen bonds in **C2**.

D H A	**d(D-H)/Å**	**d(H···A)/Å**	**d(D···A)/Å**	**D-H···A/°**
N^{93} H^{93} O^{6}	0.930(1)	1.681(5)	2.539(5)	142.8(15)
N^{14} H^{14} O^{7}	0.930(1)	1.753(5)	2.581(5)	139.3(18)
N^{86} H^{86} O^{11}	0.930(1)	1.679(5)	2.544(5)	143.4(18)
N^{82} H^{82} O^{10}	0.930(1)	1.711(6)	2.549(6)	140.1(2)
N^{87} H^{87} O^{5}	0.930(1)	1.712(5)	2.550(5)	140.3(16)
N^{70} H^{70} O^{8}	0.930(1)	1.715(7)	2.523(7)	136.8(2)

When we view the mesocate along the Ni_1-Ni_2 axis in Figure 15 below, it is apparent that the ligands are better aligned than **C1**. Like **C1**, there are no π-π stacking interactions present in the mesocate.

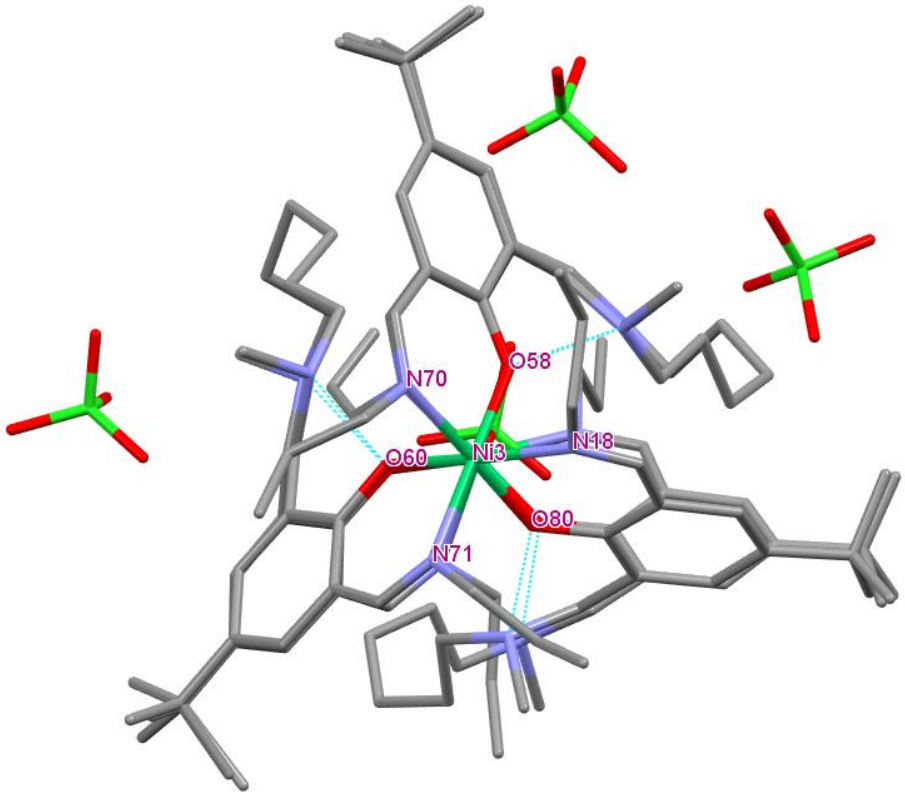

Figure 15. X-ray crystal structure of $[ClO_4 \subset Ni_2(\mathbf{L1})_3](ClO_4)_3$ viewed along the Ni-Ni axis with labels for non carbon atoms, and blue dotted lines for the hydrogen bonds between the amines next to the spacer of the ligands with the oxygen groups bonded to the nickel ion. Colour code: grey (C), red (O), blue (N), dark green (Ni), green (Cl). Hydrogens omitted for clarity.

4.0 Metal Complexes with L3

4.1 Metal Complexation Reactions with L3

Complexation reactions were carried out with **L3**, nickel, various anions, solvents and ratios. Out of all the complexations, two afforded green crystals. **C3** was formed overnight while **C4** took just over two weeks.

Table 26. Successful metal complexations with **L3**.

Crystal name	**RT solvent**	**Ratio M:L**	**Colour change**	**Crystal**
C3 **$[SO_4 \subset Ni_2(L3)_3][Ni(SO_4)_2(EtOH)_4]$**	Ethanol	1:1	Green to yellow	Dark green blocks
C4 **$[ClO_4 \subset Ni_2(L3)_2](ClO_4)_3$**	Ethanol	2:3	Green to yellow	Dark green blocks

4.2 Characterisation of L3-Containing Metal Complexes

4.2.1 Mass Spectrometry of L3 Complexes

The mass spectra of **C1** and **C2** showed similar peaks. The main groups are listed in Table 27.

As we can see below, the fragmentation pattern between the two **L3** complexes with SO_4^{2-} and ClO_4^- are the same for the major peaks. This confirms that both complexes have the same functional groups that get ionised and separated by their m/z.

Table 27. Main mass spectrometry peaks.

	C3 **$[SO_4 \subset Ni_2(L3)_3][Ni(SO_4)_2(EtOH)_4]$**	**C4** **$[ClO_4 \subset Ni_2(L3)_2](ClO_4)_3$**
L3 + Ni^{2+}	683.24	683.26
L3	627.29	627.34
L3 + $2Ni^{2+}$ + $C_1H_9N_2O_3$	837.09	837.14

In the comparisons below, the m/z values obtained from the mass spectra matches the values from the simulated patterns. Although the number of peaks is also the same, there are slight differences in the height of the peaks for 685 m/z and 841 m/z in Figures 17 and 18 respectively. However, the general pattern is the same and there may be some overlay in the mass spectrometry peaks.

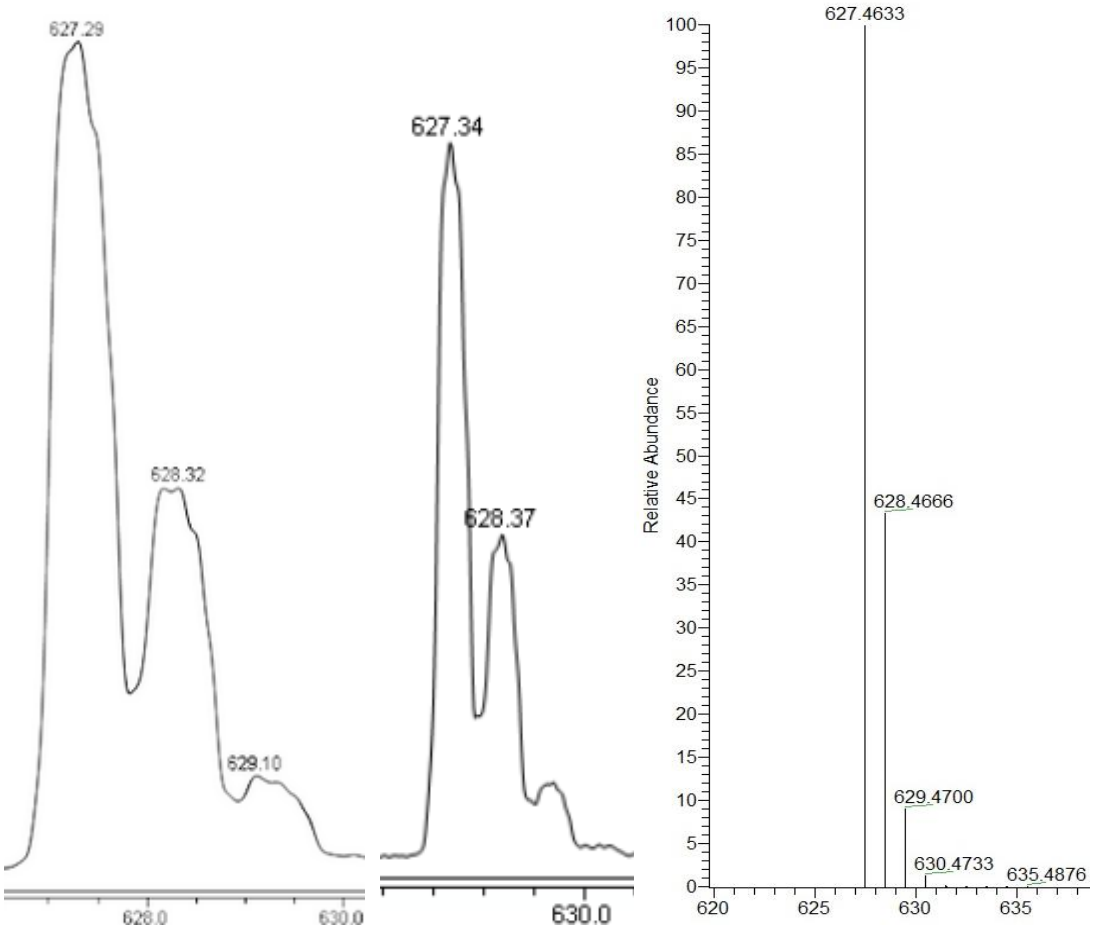

Figure 16. MS peak of **L3** from **C3** (left) and **C4** (middle) in comparison with the calculated peak pattern (right).

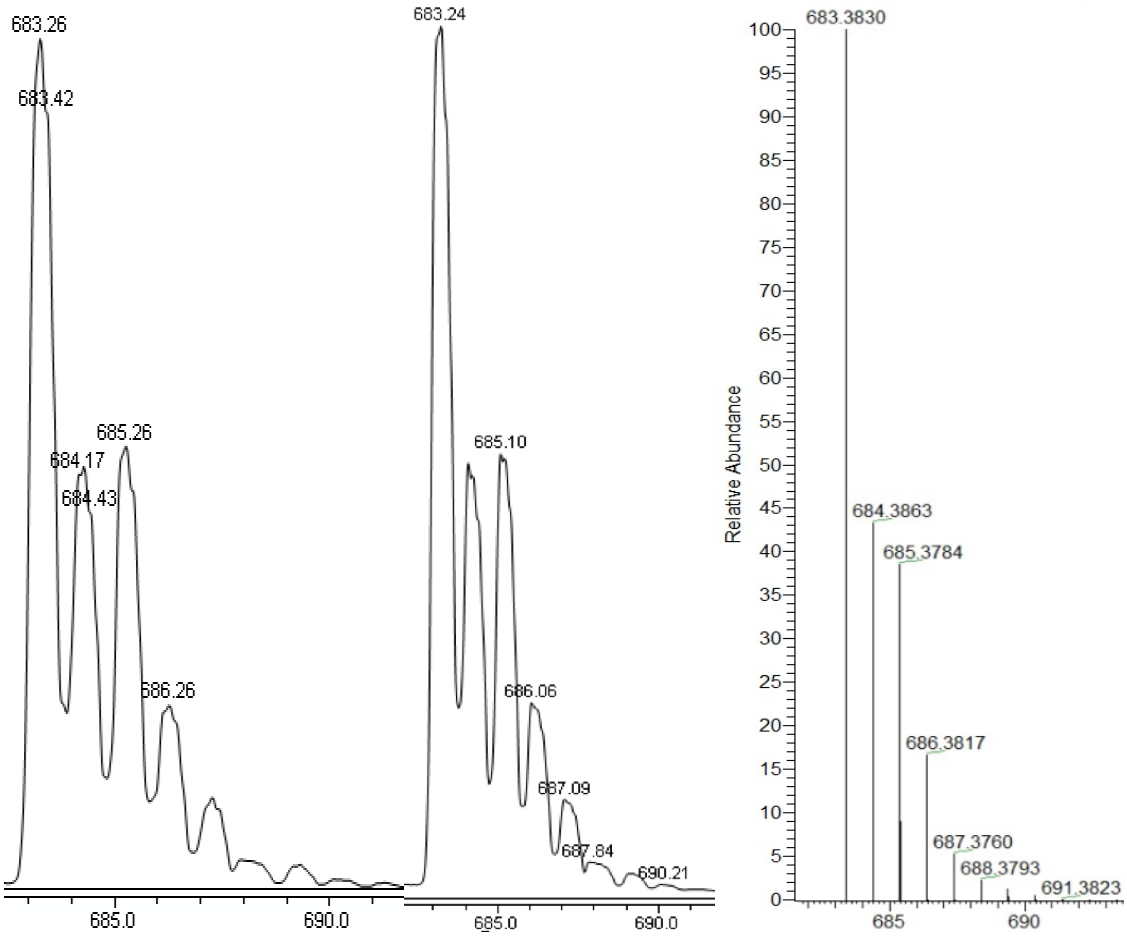

Figure 17. MS peak of **L3** +Ni^{2+} from **C3** (left) and **C4** (middle), in comparison with the calculated peak pattern (right).

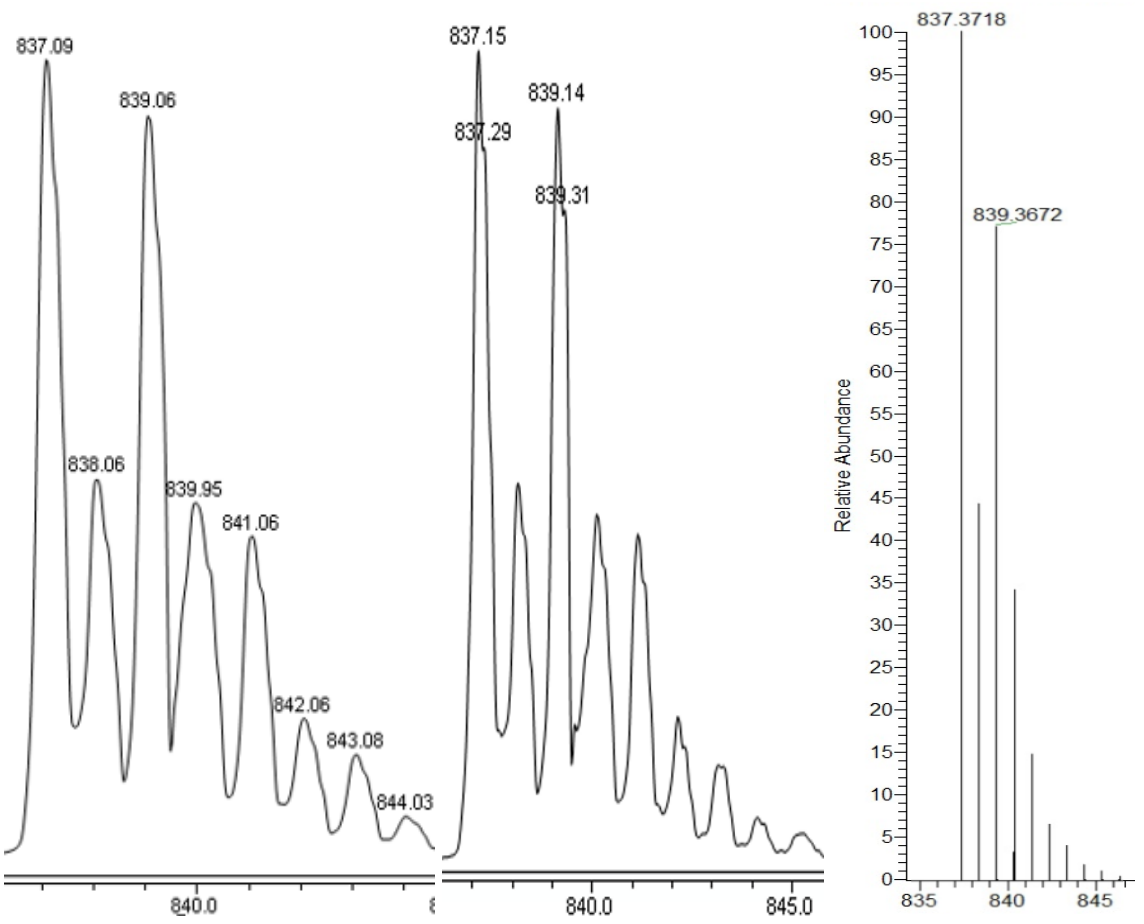

Figure 18. MS peak of **L3**+2Ni^{2+}+$(OH)_3$+NH_2+$NHCH_3$ from **C3** (left) and **C4** (middle), in comparison with the calculated peak pattern (right).

4.2.2 ATR-FTIR Spectroscopy of L3 Complexes

ATR-FTIR spectra were recorded for the complexes on crushed powders (Table 13). The peak at 1625 cm^{-1} of the ligand which is assigned to the C=N imine functional group is retained in the complexes which indicates the complex was formed with no hydrolysis occurring at this bond. As explained for **C1** and **C2**, new peaks arise at 621-650 cm^{-1} and 650-850 cm^{-1} for the bonds Ni-O and Ni-N respectively. The vibrational frequencies for SO_4^{2-} of T_d symmetry can be found around 1104 cm^{-1} and 613 cm^{-1} while for SO_4^{2-} with reduced symmetry vibrations at 1070-1090 cm^{-1} and 613-648 cm^{-1} can be found.[41]

As previously discussed, there are a couple of differences between the ligands and complexes. In addition to the new peaks mentioned above, many peaks occurring in the analysis of **L1** and **L3** appear much weaker in the spectra of the complexes.

Table 28. Selected IR peaks of washed crystal products.

	C-H	**C=C**	**C=N**	**C=C**	**C-O**	**S-O or Cl-O**	**Ni-N**	**Ni-O**
C3 (cm^{-1})	2962 *s*	2870 *m*	1627 *s*	1463 *m*	1394 *w*	1083 *s*	836 *W*	647 *m*
C4 (cm^{-1})	2958 *s*	2869 *m*	1627 *s*	1466 *m*	1362 *w*	1084 *s*	836 *W*	646 *m*

4.2.3 UV-Vis spectroscopy of L3 Complexes

The peak wavelengths in the UV-Vis spectra for the **L3** complexes have slightly higher values than the complexes with **L1** (Table 29). Otherwise, the shape of the spectrum is the same as the spectra gathered for **C1** and **C2** complexes and are different from the UV-Vis spectra of the **L3** ligand. The peak at 227.5 nm is related to the π-π_1*, the peak at 378 nm shows the phenolate n-π_2* electronic transition. The 378 nm peak is the reason for the dark green colour of the crystals.[33] Due to the interaction of the ligand to the metal ion, the UV-Vis spectra of the complexes are different from the spectrum of the ligand. The broad peak at 400 nm of the ligand shifted to 378 nm in the spectra of the complex due to the coordination of the Ni^{2+} to the ligand which lowers the π* orbital of the ligand and the energy of the transition.

Table 29. UV-Vis data of **L3** complexes.

	Wavelength (nm)	**Absorbance**	**Conc. ($1x10^{-3}$ M)**	**Mol. abs. (M^{-1} cm^{-1})**
C3-peak 1	378.00	0.253	0.667	379
C3-peak 2	230.50	0.958	0.667	1,436
C4-peak 1	378.50	0.262	0.044	5,982
C4-peak 2	230.00	1.083	0.044	24,726

4.2.4 Atomic Absorption Spectroscopy of L3 Complexes

Atomic absorption spectroscopy was carried out for the two complexes with **L3** at 341.5 nm. Six standards were made up using a standard nickel solution (Ni 1.00 g L^{-1}) and 2 M HCl within the optimum working range 6-25 μg mL^{-1} for 341.5 nm. After the standards were measured, the complexes were diluted with 2 M HCl within the concentration range 9-17 μg mL^{-1} and were also measured for a quantitative nickel analysis. The percentage of nickel recorded from the AAS was within the error values for **C3** and **C4** (Table 30). **C4** was repeated as the first run showed a high percentage of nickel. Using an initial higher concentration of the crystalline sample fixed the problem and gave more accurate values. Unfortunately, there was not enough of the **C3** crystal to perform a repeat run on the AAS. However, the result below for **C3** is not too far from the calculated values. Considering the amount of material used, the uncertainty of the measurement was rather high which may affect the accuracy of the results.

Table 30. Table of nickel complex solutions.

Sample	Amount of crystal (mg)	Concentration (μg mL^{-1})	Absorbance	Theory% Ni	% Ni (FAAS)
C3	4.00	19.08	0.760	5.34 (0.3)	4.77 (0.6)
C4	3.00	3.60	0.246	5.03 (0.3)	5.40 (0.8)

4.2.5 X-Ray Crystallography Analysis of L3 Complexes

4.2.5.1 X-Ray Diffraction Structure for $[SO_4 \subset Ni_2(L3)_3][Ni(SO_4)_2(EtOH)_4]$ (C3)

A mixture of $NiSO_4 \cdot 6H_2O$ and **L3** in a M:L 2:2 molar ratio was dissolved in ethanol. The green solution was kept at room temperature and kept in vials for vapour diffusion with Et_2O. After a few weeks small blocks of green crystals of **C3** resulted. The complex was confirmed with FTIR, UV-Vis spectroscopy, and X-ray crystallography.

The **C3** complex crystallised in a triclinic space group P-1. The central SO_4^{2-} has unique bonds to the nickel allowing the formation of a M_2L_2 mesocate. The overall refinement *R*-factor is 9.30% and wR_2 was 0.2582. In a different set of complexations, (**C5**), $[SO_4 \subset Ni_2(\mathbf{L3})_2](ClO_4)_2$ was formed with the same structure but in the presence of peripheral SO_4^{2-} anions. This collection had an overall refinement *R*-factor of 5.90% suggesting SO_4^{2-} provides better stabilisation of the mesocate.

From Figure 19 below, it is apparent that the only bonds that are able to rotate are between the *m*-xylene and the salicylaldimine groups. The steric hindrance in the complex may contribute to the stability of the mesocate and it suggests that a much larger or smaller anion would not be able to form this type of mesocate where all the oxygen groups of the centre anion bind directly to the nickel.

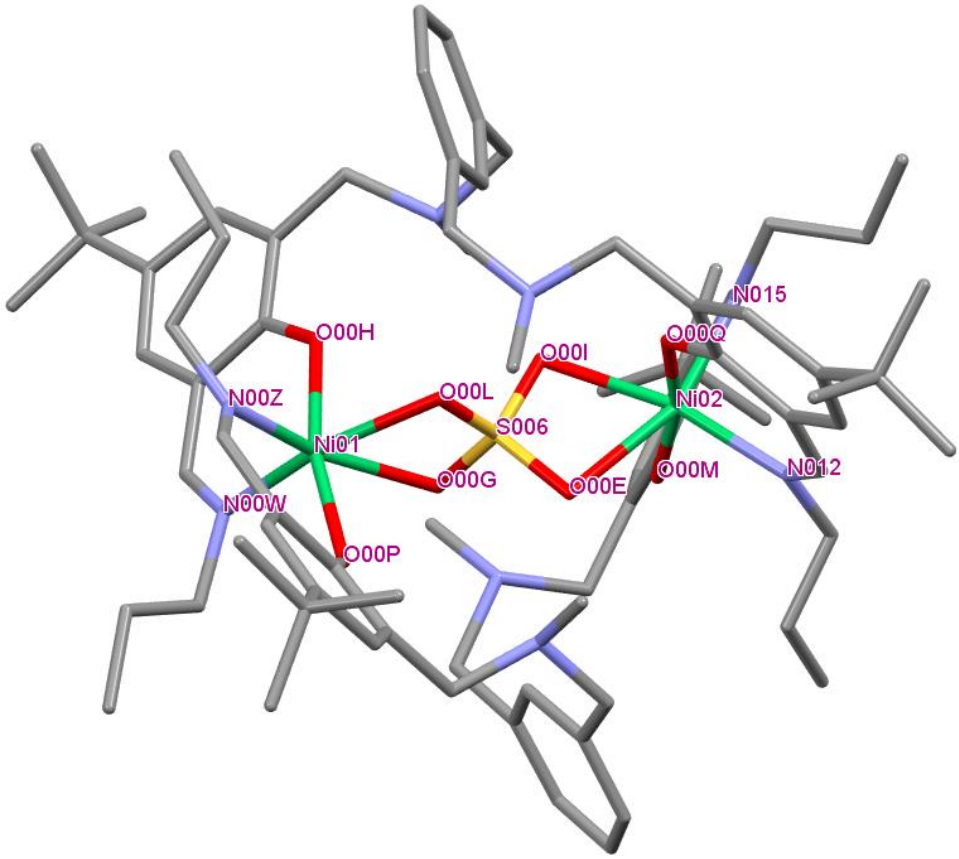

Figure 19. X-ray crystal structure of $[SO_4 \subset Ni_2(\mathbf{L3})_3][Ni(SO_4)_2(EtOH)_4]$ (**C3**) minus peripheral anions with labels for non carbon atoms. Colour code: grey (C), red (O), blue (N), green (Ni), yellow (S). Hydrogens and peripheral anions omitted for clarity.

Unlike the other complexes, the peripheral anions in this X-ray crystallography study showed a structure of a nickel ion bound to ethanol and sulfate groups as shown in Figure 20 below. Through the program Olex2, we were able to conclude that there is one anion group per complex. This suggests that the charge balance 4^+ from the 2 Ni^{2+} anions is achieved by one centre SO_4^{2-} anion and 2^- from the peripheral $[Ni(SO_4)_2(EtOH)_4]$ group.

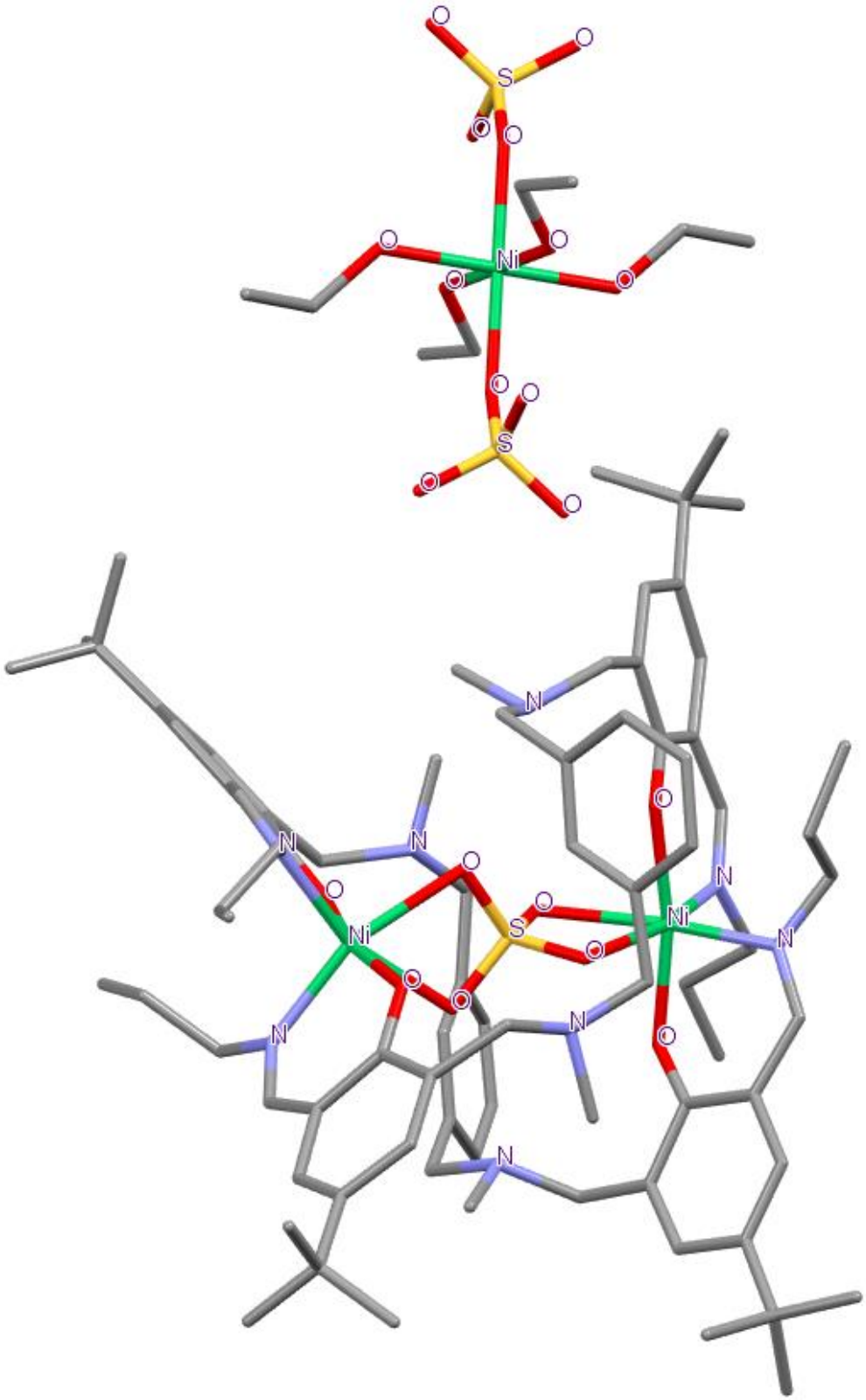

Figure 20. X-ray crystal structure of $[SO_4 \subset Ni_2(\mathbf{L3})_3][Ni(SO_4)_2(EtOH)_4]$ (**C3**) with labels for non carbon atoms. Colour code: grey (C), red (O), blue (N), green (Ni), yellow (S). Hydrogens omitted for clarity.

Table 31 shows the bond distances of Ni-O and S-O. The first two rows have values of the bonds between the nickel and the central SO_4^{2-} which are longer than the Ni-O bonds connected to the ligands. This suggests the Ni-O bond must stretch to bond to the centre sulfate. This also suggests that the Ni-O bond connected to the ligands is stronger than the Ni-N and Ni-O bonds to the SO_4^{2-}. The effect on the SO_4^{2-} is shown by the comparison of the S-O bonds of the free-floating sulfate molecule which ranges from 1.331-1.502 Å, and the more uniform bond lengths of the S-O bond in **C3** 1.484-1.480 Å.

Table 31. Bond distances of Ni-O, Ni-N and S-O bonds in **C3**.

Around the centre anion		**Ligand/peripheral anions**	
Bond	**Length in Å**	**Bond**	**Length in Å**
Ni^{01}-O^{00G}	2.189(2)	Ni^{01}-O^{00H}	2.010(3)
Ni^{01}-O^{00L}	2.203(2)	Ni^{01}-O^{00P}	2.010(3)
Ni^{02}-O^{00I}	2.164(2)	Ni^{02}-O^{00Q}	2.003(3)
Ni^{02}-O^{00E}	2.244(3)	Ni^{02}-O^{00M}	1.999(2)
S^{006}-O^{00L}	1.481(2)	S^{00C}-O^{04U}	1.479(6)
S^{006}-O^{00G}	1.480(2)	S^{00C}-O^{05W}	1.502(9)
S^{006}-O^{00I}	1.480(2)	S^{00C}-O^{05X}	1.331(6)
S^{006}-O^{00E}	1.484(2)	S^{00C}-O^{02D}	1.467(5)
		Ni^{02}-N^{0015}	2.029(3)
		Ni^{02}-N^{0012}	2.016(3)
		Ni^{01}-N^{00Z}	2.023(3)
		Ni^{01}-N^{00W}	2.018(3)

From the analysis of the angles, the O-Ni-O angle 84.25 º is smaller than the expected 90 º. Instead, there is a wider angle for O-Ni-N and N-Ni-N which are 98.2 º and 99.0 º. However, the O-Ni-N angle 162.7 º is much smaller than the expected 180 º. The angle of the two oxygens connected to the same nickel and sulfur have a smaller angle of 107.9 º than the angle of two oxygens connected to different nickel atoms. The highest value of Δd for the **C1** was 5.53 º which is nearly half of the average distortion calculated for **C3**. The main reason for this high value is due to the angle between the two oxygen atoms bound to both nickel and sulfur. The rest of the angles show an average distortion value

around 5 º (Table 32). The average angle values around Ni^{01} and Ni^{02} are similar and the Δ*d* does not differ by more than 1.5.

Table 32. Angles of nickel in **C3**.

Angles perpendicular to O^{00P}/ O^{00E}	**Angle (º)**	**Angles perpendicular to O^{00H}/ N^{0015}**	**Angle (º)**	**Angle in the planar square arrangement**	**Angle (º)**
N^{00Z}-Ni^{01}-O^{00P}	91.5 (1)	N^{00Z}-Ni^{01}-O^{00H}	97.6(1)	N^{00Z}-Ni^{01}-N^{00W}	99.0(1)
O^{00L}-Ni^{01}-O^{00P}	83.3(9)	O^{00H}-Ni^{01}-N^{00W}	91.2(1)	N^{00Z}-Ni^{01}-O^{00L}	96.8(1)
O^{00P}-Ni^{01}-N^{00W}	96.6(1)	O^{00G}-Ni^{01}-O^{00H}	84.3(9)	O^{00G}-Ni^{01}-N^{00W}	98.2(1)
O^{00G}-Ni^{01}-N^{00P}	84.3(9)	O^{00H}-Ni^{01}-O^{00L}	86.3(9)	O^{00G}-Ni^{01}-O^{00L}	66.1(9)
Average	88.9 ± 5		89.8 ± 5		90 ± 14
Δ*d*	5.11		4.56		11.98
O^{00M}-Ni^{02}-N^{0012}	95.8(1)	N^{0012}-Ni^{02}-O^{00Q}	92.3(1)	O^{00E}-Ni^{02}-O^{00I}	65.64(9)
O^{00M}-Ni^{02}-O^{00I}	83.7(1)	O^{00I}-Ni^{02}-O^{00Q}	85.9(1)	N^{0015}-Ni^{02}-N^{012}	101.4(1)
N^{0015}-Ni^{02}-O^{00M}	92.4(1)	N^{0015}-Ni^{02}-O^{00Q}	84.34(9)	O^{00E}-Ni^{02}-N^{0012}	99.4(1)
O^{00E}-Ni^{02}-O^{00M}	85.9(1)	O^{00E}-Ni^{02}-O^{00Q}	82.6(1)	N^{0015}-Ni^{02}-O^{00I}	93.6(1)
Average	89.5 ± 1		86.3 ± 3		90.0 ± 3
Δ*d*	6.2		3.02		12.19

Linear bond angles	
O^{00G}-Ni^{01}-N^{00Z}	162.7(1)
O^{00H}-Ni^{01}-N^{00P}	167.0(1)
O^{00L}-Ni^{01}-N^{00W}	164.2(1)
Angles of centre SO_4^{2-}	
O^{00E}-S^{006}-O^{00G}	110.1(1)
O^{00G}-S^{006}-O^{00L}	107.9(1)

S^{006}-O^{00I} -Ni^{02}	95.1(1)
S^{006}-O^{00E} -Ni^{02}	91.8(1)
S^{006}-O^{00L} -Ni^{01}	92.6(1)
S^{006}-O^{00G} -Ni^{01}	93.2(1)

There are seven hydrogen bonds in **C3**, two from each amine donor group connected to the C6 spacer. Each of these amines has one hydrogen bond to oxygen of the centre anion it is above, and three out of four amines have a hydrogen bond with the oxygen of the salicylaldimine. In Figure 21, the placements of the hydrogen bonds are different from **C1** and **C2**. There is an odd number of hydrogen bonds as one of the donor amines is too far from the acceptor oxygen of the salicylaldimine group.

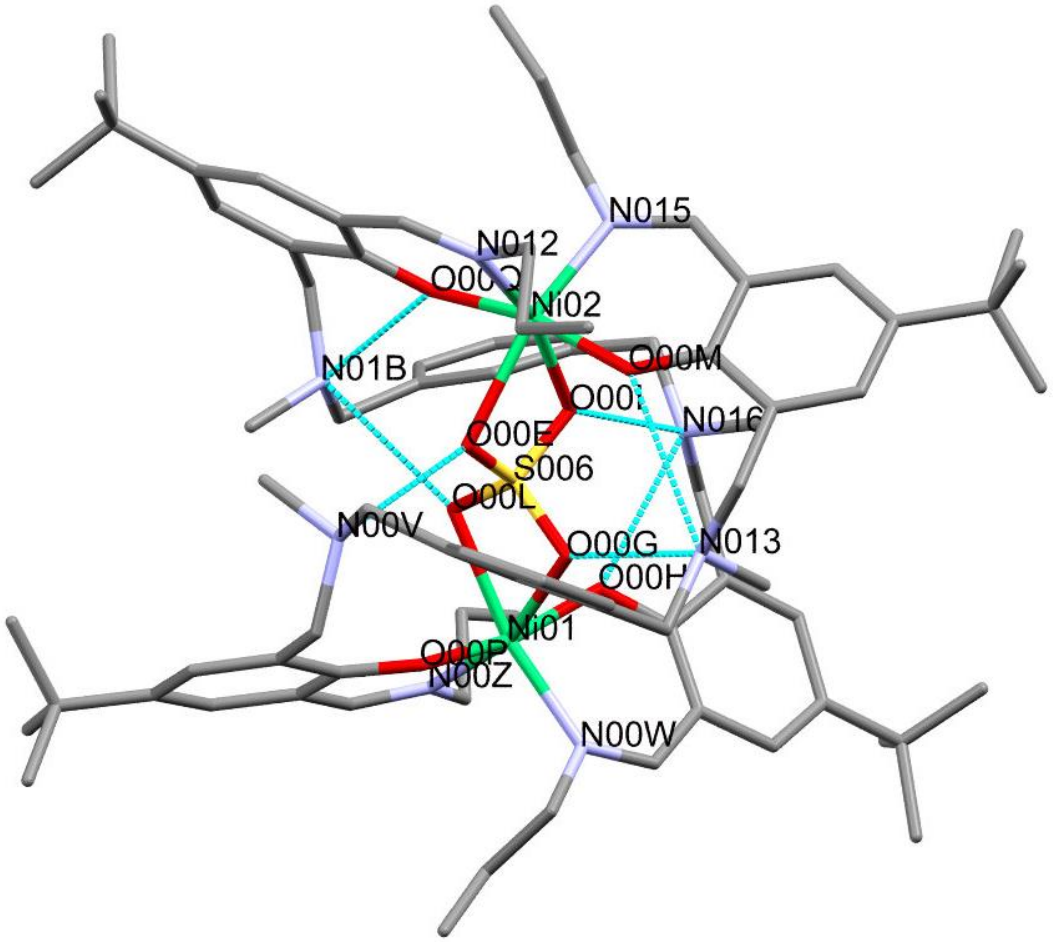

Figure 21. X-ray crystal structure of $[SO_4{\subset}Ni_2(\mathbf{L3})_3][Ni(SO_4)_2(EtOH)_4]$ (**C3**) with labels for non carbon atoms, and blue dotted lines for the hydrogen bonds between the

amines next to the spacer of the ligands with the oxygen groups bonded to the nickel ion. Colour code: grey (C), red (O), blue (N), green (Ni), yellow (S). Hydrogens omitted for clarity.

According to the classification from Jeffrey in Table 33, the hydrogen bonds in **C3** can be thought of as moderate.[39] The distance for H-acceptor of a moderate hydrogen bond is 1.5-2.2 Å. Although the data below shows that most of the (H···A) lengths are greater than 2.2 Å, the (D···A) distance is less than 3.2 Å and the bond angles are for the most part, larger than 130 º. All the N-H-O angles except for two, fall under moderate as they are on average larger than 130˚. Angle N^{01B} H^{01B} O^{00Q} and N^{013} H^{013} O^{00M} between the ligand and salicylaldimine group, have bond angles of 126 º and 127 º which is close to 130 º.

The values for **C3** are approximately 0.3 Å longer than the 1.7-8 Å range of **C1** and **C2** suggesting that compared to the **C1**-**C2** complexes, the hydrogen bonds are weaker. Although some of the hydrogen bonds for the O···H interaction classify as weak, the other values suggest they are moderate-weak, electrostatic, hydrogen bonds.

Table 33. Distance and angle values of hydrogen bonds in **C3**.

D H A	**d(D-H)/Å**	**d(H···A)/Å**	**d(D···A)/Å**	**D-H···A/°**
N^{00V} H^{00V} O^{00E}	0.790(4)	2.080(4)	2.804(4)	154.6(4)
N^{016} H^{016} O^{00H}	0.840(5)	2.190(4)	2.805(4)	130.4(4)
N^{016} H^{016} O^{00I}	0.840(4)	2.300(5)	2.940(4)	132.9(4)
N^{013} H^{013} O^{00G}	0.700(4)	2.260(5)	2.850(4)	142.8(4)
N^{013} H^{013} O^{00M}	0.700(4)	2.590(4)	3.052(4)	125.6(4)
N^{01B} H^{01B} O^{00L}	0.730(5)	2.420(4)	3.013(4)	139.5(4)
N^{01B} H^{01B} O^{00Q}	0.730(5)	2.390(5)	2.891(5)	126.8(4)

4.2.5.2 X-Ray Diffraction Structure for $[ClO_4 \subset Ni_2(L3)_2](ClO_4)_2$ (C4)

A mixture of $Ni(ClO_4)_2 \cdot 6H_2O$ and **L1** in a M:L 2:2 molar ratio was dissolved in ethanol. The green solution was kept at room temperature and kept in vials for vapour diffusion with Et_2O. After a few weeks small blocks of dark green crystals of **C4** resulted. The complex was confirmed with FTIR, UV-Vis spectroscopy, and X-ray crystallography.

The structure of this crystal is monoclinic $P2_1/n$. The structure has appropriate shift, minimum peak and GooF. The final *R*-factor is 4.01% and wR_2 is 11.25%.

Unlike **C3** and **C5**, the X-ray crystallography data of **C4** and **C6** presents structures that have unbalanced charges. For example, in Figure 22, instead of $4ClO_4^-$ to balance the 4^+ charge from the $2Ni^{2+}$ ions, there are only $3ClO_4^-$. Likewise, **C6** presents a complex that has 3 anions that cannot balance the 4^+ of the Ni^{2+}. Without a sulfate analysis, it is hard to determine how the charges of the complex has been balanced. It is possible that either there is an additional anion, a different anion, or a loss of a hydrogen on one of the amines.

Appendix I1.0 and I1.1 contains CHN analysis data for **C2** and **C4**. For both complexes, the CHN percentages are not within 0.3% of the expected values. The expected values for **C2** CHN analysis are C: 58.32-92%, H: 7.73-8.33% and N: 6.90-7.50%. The closest values from the duplicate run are C: 56.53%, H: 8.25% and N: 5.11%. The percentage of H is within the error range however, both C and N are lower by 2%. Unfortunately, there was a lack of crystal material for **C4** for a duplicate analysis. The expected values for **C4** CHN analysis are C: 57.25-57.85%, H: 6.70-7.3% and N: 6.41-7.01%. The values from the single run are C: 57.87%, H: 7.08% and N: 6.19%. The percentage of H is within the error range however the value for C is over by 0.02% and N is under the expected range by 0.12%. Although the crystals were washed with diethyl ether, it is possible that the values are affected by residual solvent impurity as even a minuscule amount can affect the analysis results.

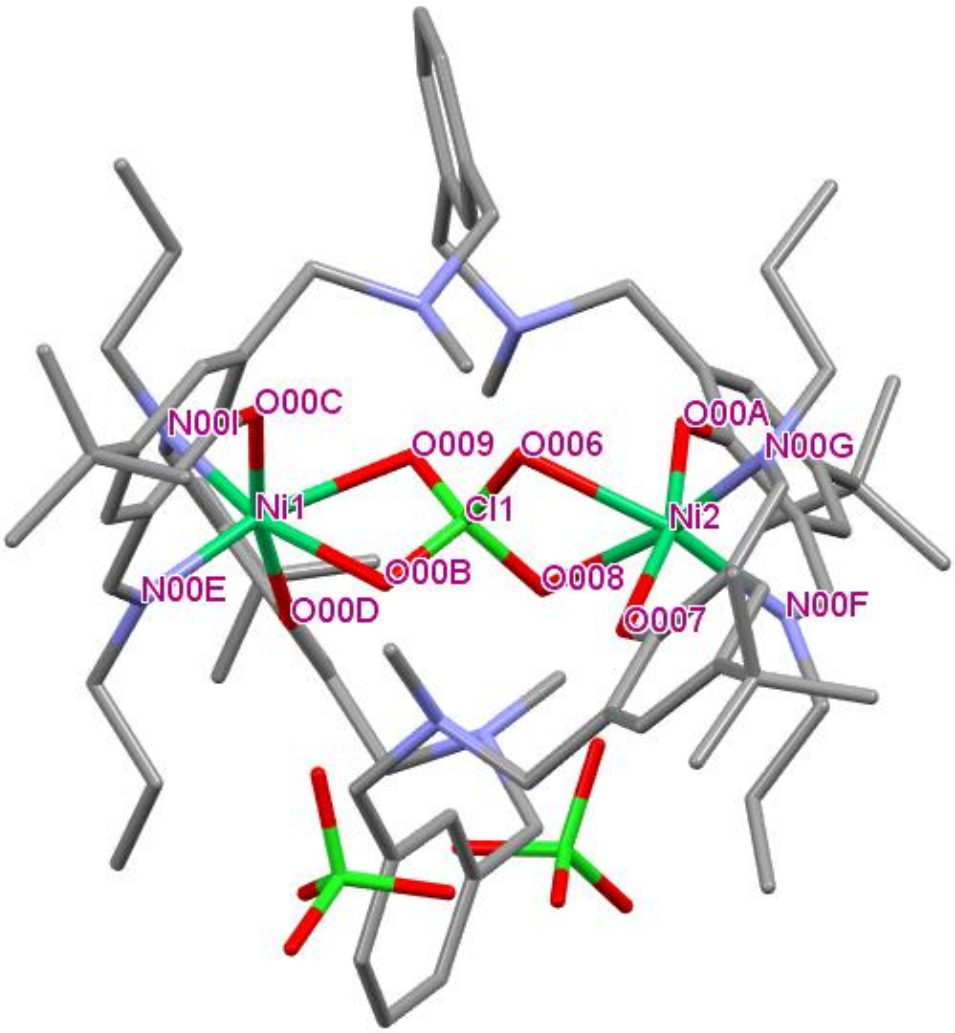

Figure 22. X-ray crystal structure of $[ClO_4 \subset Ni_2(\mathbf{L3})_3](ClO_4)_2$ (**C4**) with labels for non carbon atoms. Colour code: grey (C), red (O), blue (N), dark green (Ni), light green (Cl). Hydrogens omitted for clarity.

The bond lengths between the nickel, oxygen and chloride in **C4** are all similar to the bond lengths in **C3** despite the difference in anion. However, the sulfate anions on the periphery of **C3** have an average S-O bond distance of around 1.445 Å while the free-floating Cl-O of **C4** has an average Cl-O distance of 1.424 Å. The bond lengths are within literature values. The bond lengths of a free-floating ClO_4^- ranges between 1.405-1.432(13) Å while the ClO_4^- bound within a mesocate has bond distances ranging 1.479-1.484(11) Å. A group of researchers found that a Cl-O bond of a perchlorate bound to their complex has a distance of 1.50(1) Å. Although the bond distances of S-O and Cl-O

in the complex are the same, this is because the bonds of the anion is adjusted when inside the complex. The distance between Ni_1-Ni_2 is 5.4323(8) Å for **C3** and 5.4453(4) Å for **C4**.

Table 34. Bond lengths of Ni-O and Cl-O in **C4**.

Around the centre anion		**Peripheral anions**	
Bond	(Å)	Bond	(Å)
Ni^{01}-O^{006}	2.197(1)	Cl^{05}-O^{00O}	1.416(2)
Ni^{01}-O^{008}	2.202(1)	Cl^{05}-O^{00N}	1.420(1)
Ni^{01}-O^{007}	2.005(1)	Cl^{05}-O^{01Y}	1.466(2)
Ni^{01}-O^{00A}	2.000(1)	Cl^{05}-O^{00S}	1.411(2)
Ni^{02}-O^{00C}	2.008(1)	Cl^{04}-O^{00S}	1.415(2)
Ni^{02}-O^{00D}	2.009(1)	Cl^{04}-O^{02F}	1.405(2)
Ni^{02}-O^{009}	2.221(1)	Cl^{04}-O^{00H}	1.430(1)
Ni^{02}-O^{00B}	2.185(1)	Cl^{04}-O^{00P}	1.432(2)
Cl^{03}-O^{006}	1.482(11)		
Cl^{03}-O^{008}	1.481(11)		
$Cl^{0\,3}$-O^{009}	1.484(11)		
Cl^{03}-O^{00B}	1.479(11)		

The average distortion values are the same and slightly higher than the values found for **C3**. As we can see in Figure 23, extra distortion is created by the direct bonds between the two Ni^{2+} and the ClO_4^- oxygen groups.

Like **C3**, the angles of **C4** in Table 35 show that the oxygen atoms of the nickel are pulled closer to the centre anion so that the angles of the octahedral corners around the nickel are not equal.

Table 35. Angles of nickel in **C4**.

Angles perpendicular to O^{007}	**Angle (°)**	**Angles perpendicular to O^{00A}**	**Angle (°)**	**Angle in the planar square arrangement**	**Angle (°)**
O^{006}-Ni^{01}-O^{007}	83.77(4)	O^{006}-Ni^{01}-O^{00A}	84.65(5)	O^{006}-Ni^{01}-O^{008}	65.77(4)
O^{007}-Ni^{01}-O^{00G}	91.71(5)	O^{008}-Ni^{01}-O^{00A}	83.88(5)	N^{00F}-Ni^{01}-O^{008}	98.40(5)
N^{00F}-Ni^{01}-O^{007}	97.37(5)	N^{00F}-Ni^{01}-O^{00A}	92.06(5)	O^{006}-Ni^{01}-N^{00G}	102.24(5)
O^{007}-Ni^{01}-O^{008}	85.64(4)	O^{00A}-Ni^{01}-N^{00G}	96.89(5)	N^{00F}-Ni^{01}-N^{00G}	93.63(6)
Average	89.6 ± 5		89.4 ± 5		90.0 ± 14
Δ*d*	4.92		5.11		12.13

Linear bond angles	
O^{006}-Ni^{01}-N^{00F}	164.6(5)
O^{008}-Ni^{01}-N^{00G}	167.9(5)
O^{007}-Ni^{01}-O^{00A}	166.8(5)
Bond angles of ClO_4^-	
O^{008}-Cl^{006}-O^{006}	107.4(6)
O^{00B}-Cl^{001}-O^{006}	110.8(6)
O^{006}-Cl^{001}-Ni^{02}	93.46(5)
O^{008}-Cl^{001}-Ni^{02}	93.27(5)
O^{009}-Cl^{001}-Ni^{01}	92.45(5)
O^{00B}-Cl^{001}-Ni^{01}	94.06(5)

In Figure 23 below, there are seven hydrogen bonds in **C4**, two from each amine donor group next to the spacer. Each of these amines have one hydrogen bond to the oxygen of the centre anion and three out of four amines have a hydrogen bond with the oxygen of the salicylaldimine. The placements of the hydrogen bonds are the same as **C3**. There is an odd number of hydrogen bonds as one of the donor amines is too far from the acceptor oxygen of the salicylaldimine group suggesting slight distortion.

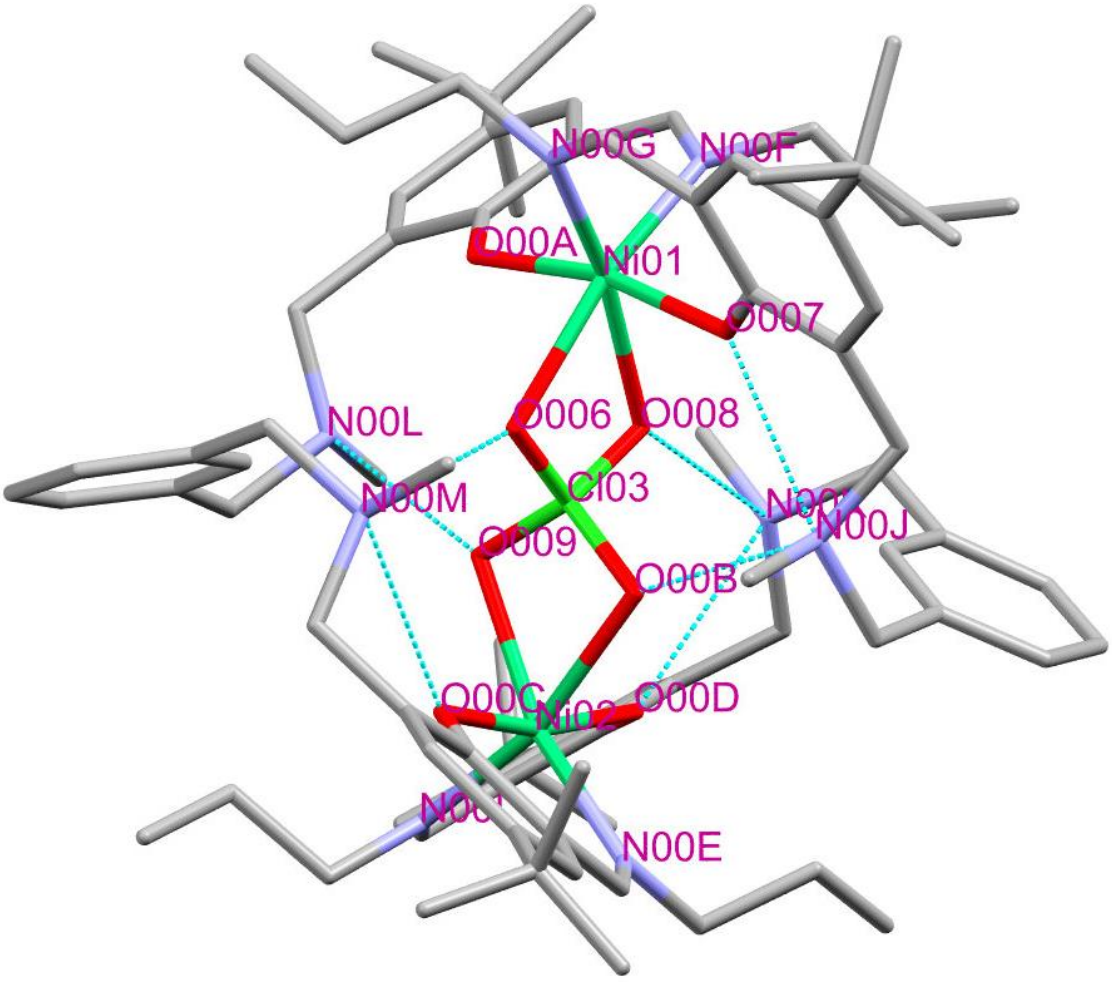

Figure 23. X-ray crystal structure of $[ClO_4 \subset Ni_2(\mathbf{L3})_3](ClO_4)_2$ (**C4**) with labels for non carbon atoms, and blue dotted lines for the hydrogen bonds between the amines next to the spacer of the ligands with the oxygen groups bonded to the nickel ion. Colour code: grey (C), red (O), blue (N), dark green (Ni), light green (Cl). Hydrogens omitted for clarity.

According to the classification from Jeffrey in Table 36, the hydrogen bonds in **C4** can also be assigned as moderate-weak.[39] The distance for H-acceptor of a moderate hydrogen bond is 1.5-2.2 Å. The values for **C4** shows that the $H^{00M}\cdots O^{00C}$, $H^{00J}\cdots O^{00B}$, $H^{00K}\cdots O^{00D}$ interactions are longer and weaker than the others, two of which are related to the oxygen on the salicylaldimine group. The angles of some of these interactions $< N^{00M}\ H^{00M}\ O^{00C}$, $< N^{00J}\ H^{00J}\ O^{007}$, $< N^{00K}\ H^{00K}\ O^{00D}$ are less than 130 º suggesting they are weaker. This is different from **C3** which had higher angle values and only one angle that was less than

130˚. The values for the distance between the donor N and acceptor O are all within the moderate range 2.5-3.2. Overall, the hydrogen bonds classify as moderate-weak, mostly electrostatic, and the data suggests that the hydrogen bonds are weaker than **C3.**

Table 36. Hydrogen Bonds for **C4**.

D H A	**d(D-H)/Å**	**d(H-A)/Å**	**d(D-A)/Å**	**D-H-A/°**
N^{00M} H^{00M} O^{006}	0.930(2)	2.105(17)	2.843(17)	135.4(5)
N^{00J} H^{00J} O^{007}	0.930(2)	2.158(17)	2.813(17)	126.5(5)
N^{00L} H^{00L} O^{009}	0.930(2)	2.001(18)	2.805(18)	143.6(5)

4.2.5.3 X-Ray Diffraction Structure for $[SO_4 \subset Ni_2(L3)_2](ClO_4)_2$ (C5)

Two other complexations worth mentioning have a centre anion that is different from the spectator anions. A mixture of $NiSO_4 \cdot 6H_2O$, **L3** and $NaClO_4$ was added in a M:L:anion 2:2:1 molar ratio respectively in ethanol. The green solution was kept at room temperature and kept in vials for vapour diffusion with Et_2O. After one or two days, small blocks of dark green crystals of **C5** resulted. The complex was confirmed with X-ray crystallography as shown in Figure 24. The structure of this crystal is monoclinic $P2_1/n$. The final *R*-factor is 5.90% and wR_2 is 16.70%.

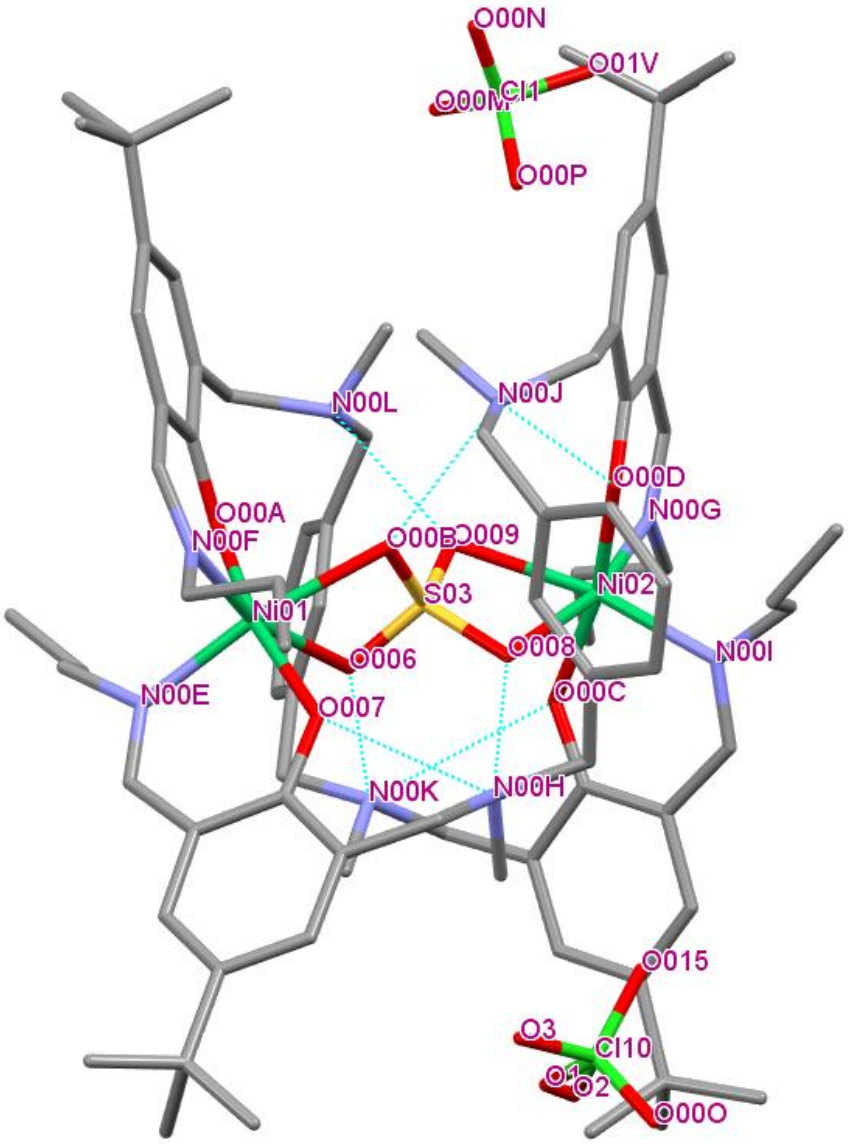

Figure 24. X-ray crystal structure of $[SO_4 \subset Ni_2(\mathbf{L3})_3](ClO_4)_2$ (**C5**) with labels for non carbon atoms, and blue dotted lines for the hydrogen bonds between the amines next

to the spacer of the ligands with the oxygen groups bonded to the nickel ion. Colour code: grey (C), red (O), blue (N), dark green (Ni), light green (Cl), yellow (S). Hydrogens omitted for clarity.

The complexation of **C5** was inspired by an accidental formation of **C6**. In a crystallisation attempt with **L3**, $NiBF_4$ in ethanol, a vial that had been cleaned but retained traces of ClO_4^- yielded the complex (**C6**) with a ClO_4^- bound in the centre as shown in Figure 25. The structure of this crystal is orthorhombic $P2_1/n$. The final *R*-factor is 5.69% and wR_2 is 16.18%.

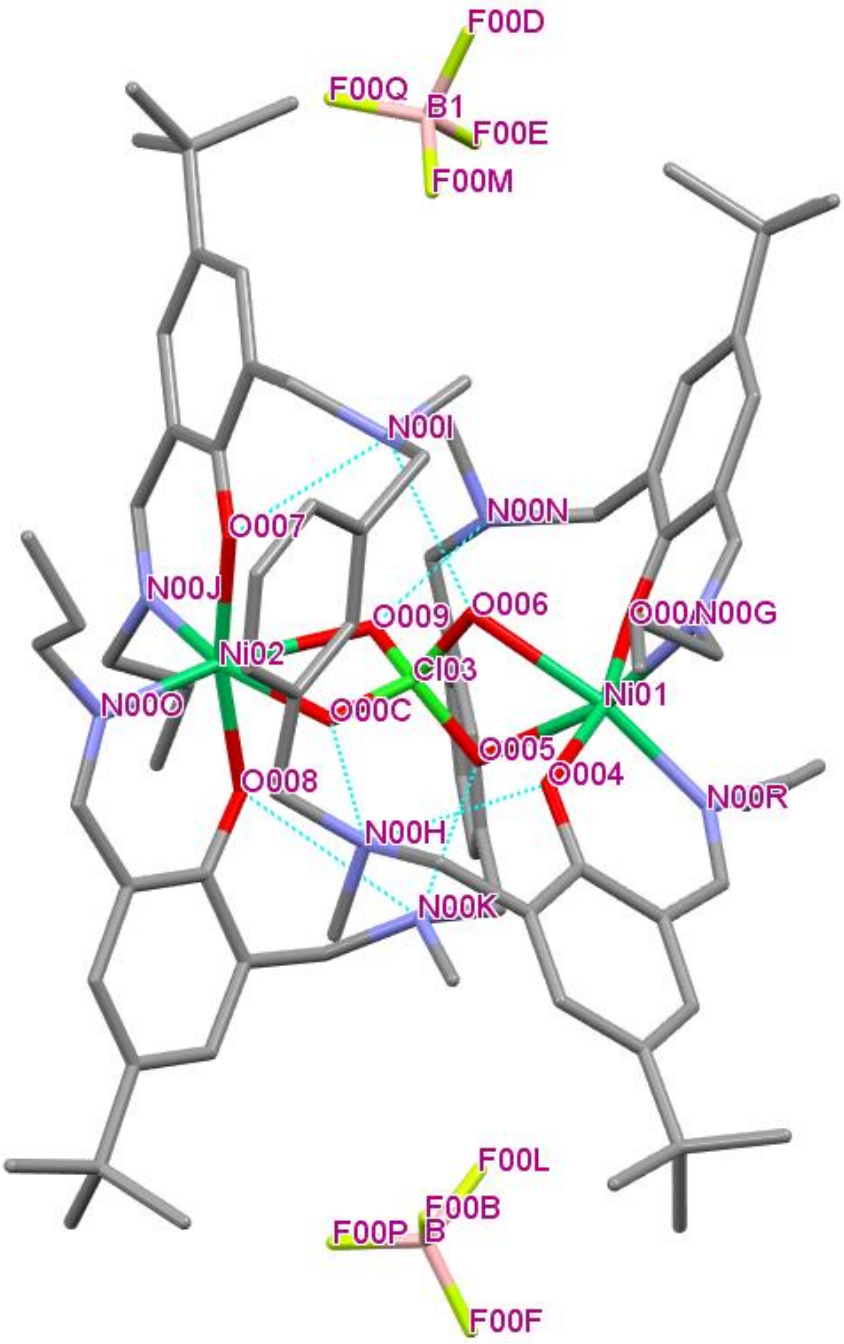

Figure 25. X-ray crystal structure of $[ClO_4 \subset Ni_2(\mathbf{L3})_3](BF_4)_2$ (**C6**) with labels for non carbon atoms, and blue dotted lines for the hydrogen bonds between the amines next to the spacer of the ligands with the oxygen groups bonded to the nickel ion. Colour code: grey (C), red (O), blue (N), dark green (Ni), light green (Cl), yellow (F), pink (B). Hydrogens omitted for clarity.

In Table 37 below a comparison is made between the complexes analysed in this thesis with ClO_4^- or SO_4^{2-} anions. **C5** shares the crystal system (monoclinic with primitive

Bravais lattice) of the complexes with tetrahedral periphery anions such as **C4** and **C6**, while **C3** has a triclinic system. The structures for **C4**, **C5** and **C6** are isomorphous with space group $P2_1/n$ while the space group for **C3** is P-1. From experimental records, we are certain of the **C3**, **C4** and **C6** which leaves **C5** to be determined.

The bond distances Ni-O, Cl/S-O and the angle <O-Ni-O of the centre of the complex provides data that does not present large differences between the different complexes. There are slight differences in the Ni-Ni, Ni-Cl/s distances. The values for **C5** is closer to **C4** and **C6** than **C3** which may be influenced by the peripheral anion. Although the bond lengths and distortion values are very similar, the crystal system, space group and dimensions all resemble **C4** and **C6** as they have tetrahedral anions on the periphery of the complex.

However, we can determine the bond distances of the peripheral anions. Because of the accumulated 4^- charge from the oxygens and 4^+ from the nitrogens on the ligand, the 4^+ charge from the two Ni^{2+} must be balanced. If there are two ClO_4^- anions on the periphery, then it follows that the central anion must be a SO_4^{2-}.

In consideration of all factors, the centre anion of **C5** appears to be SO_4^{2-}. To confirm this hypothesis, it would be ideal to check the complex with mass spectrometry or other characterisation methods used for **C3** and **C4** for comparison.

Table 37. Comparison of structural data.

Complex	**C6**	**C4**	**C3**		**C5**
Centre anion	ClO_4^-	ClO_4^-	SO_4^{2-}	SO_4^{2-} fragment 2	SO_4^{2-}
Crystal system	Mono P	Mono P	Triclinic P		Mono P
Peripheral anion	$2BF_4^-$	2 ClO_4^-	$1.5[Ni(SO_4)_2(EtOH)_4]$		2 ClO_4^-
Charge balance	0	0	0		0
Space group	$P2_1/n$	$P2_1/n$	P-1		$P2_1/n$
a	25.1	25.3	19.4		25.4
b	16	16	22.2		15.9
c	25.5	25.3	27.6		25.4
A	90	90	86		90
B	102.9	102.9	80.4		102.7
Γ	90	90	85.7		90
Ni-Ni	5.440(7)	5.445(4)	5.432(8)	5.410(9)	5.457(5)
Ni_1-Cl/S	2.723(7)	2.724(4)	2.710(9)	2.698(1)	2.729(6)
Ni_1-O (anion)	2.189-2.209(2)	2.198-2.199(1)	2.189-2.203(2)	2.184-2.204(3)	2.200-2.203(1)
Ni_2-O (anion)	2.186-2.218(2)	2.198-2.220(1)	2.164-2.244(3)	2.180-2.182(3)	2.195-2.219(1)
Cl/S-O	1.479-1.485(2)	1.476-1.481(1)	1.480-1.484(2)	1.471-1.485(2)	1.477-1.483(1)
Periphery Cl/S-O, B-F	1.373-1.392(4)	1.405-1.432(2)	1.4445-1.502(4)	1.471-1.485(3)	1.406-1.454(2)
O-Cl-O **O-S-O angles°**	107.42(9) 107.96(9)	107.71(6) 107.44(6)	107.49(1) 107.90(1)	106.80(1) 108.60(1)	107.18(8) 107.74(8)
O-Ni-O° connected to (Cl/S)	65.81(6) 65.87(6)	65.76(4) 65.78(4)	65.64(9) 66.08(9)	66.18(9) 66.23(9)	65.55(5) 65.63(5)

5.0 Results and Discussion

L3 is a ligand that has been studied and used to make various complexes by the Plieger group. As we can see in the Figure 26, the complex formed with **L3** in this thesis creates an interesting mesocate where the oxyanions bind directly to the metal. This creates more stability and decreases the disorder in the complex. Unlike **C1** and **C2** that had an even number of N and O atoms around the Ni^{2+} octahedral centre, the Ni^{2+} ions in **C3** and **C4** is bonded to 4 oxygen and 2 nitrogen atoms.

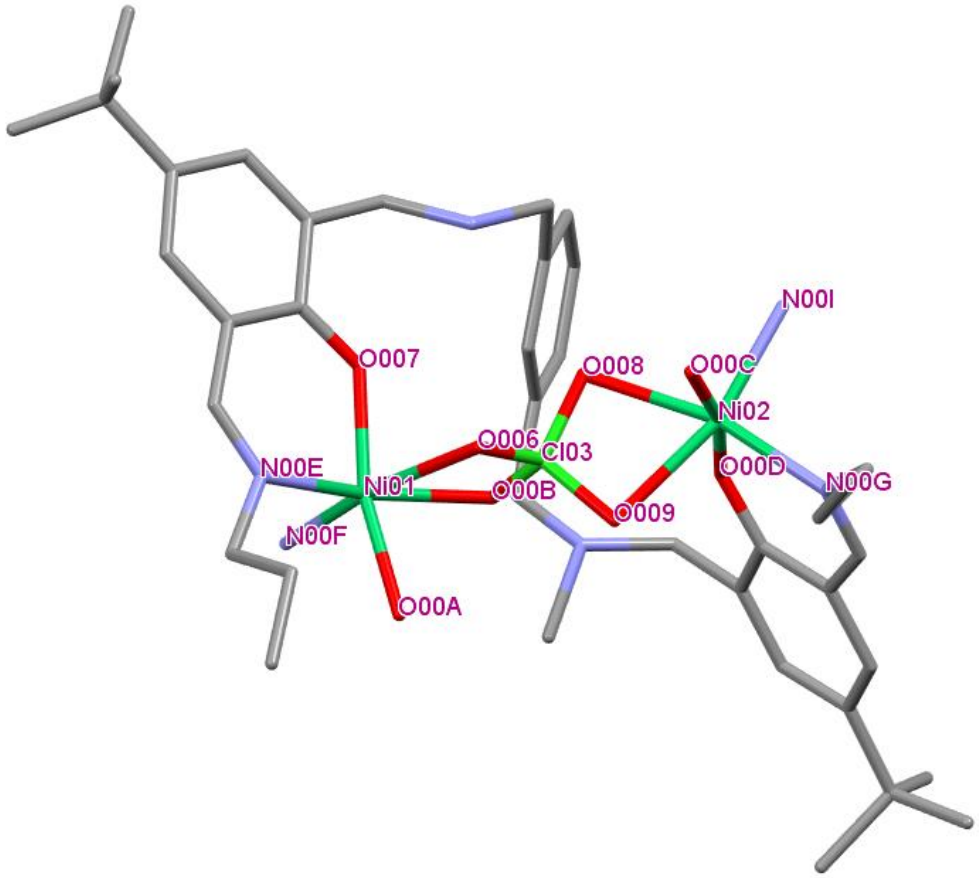

Figure 26. X-ray crystal structure of $[ClO_4 \subset Ni_2(\mathbf{L3})_3](ClO_4)_2$ (**C4**) with labels for non carbon atoms. Colour code: grey (C), red (O), blue (N), dark green (Ni), light green (Cl). Hydrogens and one ligand omitted for clarity.

The addition of aromatic spacers into ligand was a strategy that improves rigidity, increase sites for additional π-π stacking interactions, provide more possibilities for electrostatic, hydrophobic and hydrogen bond interactions.[42]

This component is an example of pre-organisation. Studies on cryptands reveals this phenomenon. For example, ligand B shown in Figure 27 below can crowd an anion with hydrogen and ion interactions.[43,44]

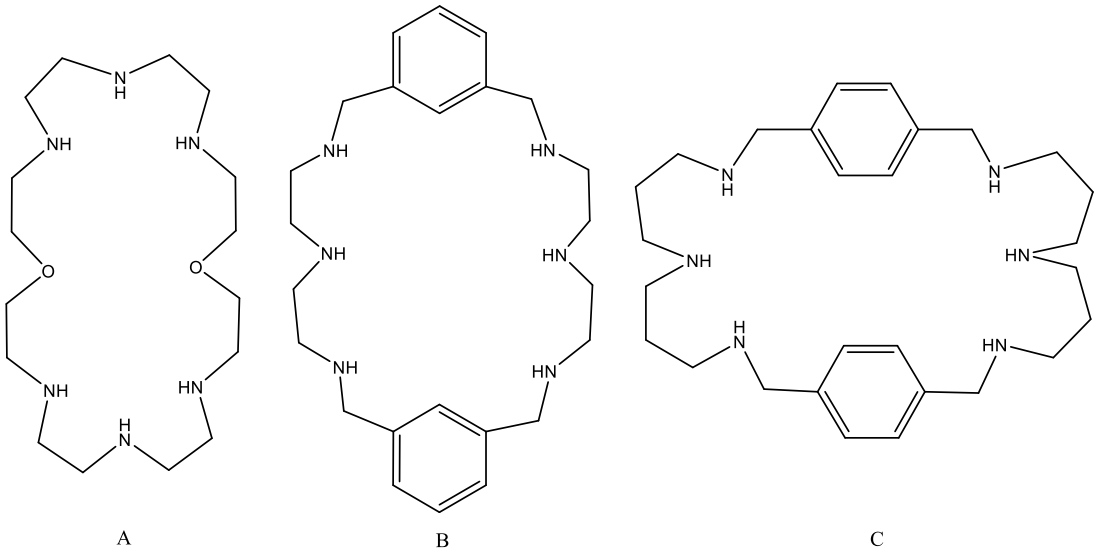

Figure 27. Ligand A, B, C from literature. [42]

However, the addition of an aryl ligand does not always lead to improved binding of anions. Similar cryptands such as ligand A above shows higher log K binding constant values.[42] The increased binding strength of these non-aryl cryptands may be due to the increased flexibility of the alkyl ligands and the diminished size of the cavity.[42] Between ligands B and C however it was found that a diphosphate anion binds better to the *m*-xylylic ligand rather than the *p*-xylylic ligand in the 4-6 pH range.[45]

This finding is supported in this thesis by the fact that no crystals were formed with **L2** while crystals were formed with **L3** with the same method. An explanation for the **L3** crystal formation may be because a smaller cavity space is possible with the increased flexibility generated by a *m*-xylylic linker. From the X-ray crystallography we found that the *m*-xylylic linker does not wrap around the anion in a flat/straight manner but is bunched so that the nickel ions can be squeezed closer together and have a stronger interaction with the centre anion.

The structure of the complex is uncommon for the metal, ligand and anion combination although similar complexes have been formed. With similar xylylic ligands, Stevens extended Knapp's research.[46] With these ligands and Cu^{2+} ions, X-ray crystal structures of Cu_2L_2 with the anions ClO_4^-, BF_4^-, NO_3^- and Br^- were collected. Stevens was successful in forming helicates with the *p*-xylylic linker and suggested that tetrahedral anions larger than ClO_4^- such as $H_2PO_4^-$ are unable to pass the aryl arms due to size.[33] He found that the sulfate anion bound the strongest with a log K value of ~5.5 while ClO_4^- had a log K value 3.86 ± 0.22 and Br^- and NO_3^- weakly bound at log K value ~3.7.[34] On the other hand, the mesocate with the *m*-xylylic linker increased the binding affinity of ClO_4^- over sulfate and bromide over BF_4^-.[34]
Overall, Stevens found that the addition of a *p*-xylylic linker and *m*-xylylic linker boosted the affinity of sulfate and perchlorate respectively.[33] Although increased flexibility is a favourable aspect of a ligand, the xylylic group provides a constraint on conformational flexibility which increases the stability of the complex.

In addition, Warzeska and Kramer complexed copper cages with ligands that are similar to **L1** with a pyridine cap rather than a salicylaldimine.[47] Their complex has the copper directly bonded to an acetonitrile group.[47] Also, Amendola *et al*., conducted a more in-depth study of similar complexes such as dicopper(II) bistren cryptates and used them to capture ambidentate anions.[48] By changing the length of the spacers they adjusted the size of the ellipsoidal cavity so that an anion could sit in the middle and share a covalent bond with both copper atoms. The anions they studied were halides, polyatomic anions, aromatic and aliphatic dicarboxylates.

Amendola *et al*., found that urea behaves as a bifurcate H-bond donor towards oxoanions. The high tendency of urea to function as a H-bond donor is related to the acidity of the receptor and the basicity of the anion.[36] The study on urea explains the advantage of using salicylaldimine ligands which functions in a similar manner to form hydrogen bonds between the imine group and oxygen from the centre anion. Further complexations with copper may be of interest as octahedral Cu^{2+}-O has a larger mean distance, standard deviation and range than an octahedral Ni^{2+}-O.[49] However other factors must be considered. Because copper is more electronegative, it may increase the length of ligand

but decrease the M-O bond strength, and the likelihood of forming bonds with tetrahedral oxyanions.

6.0 Solvent Extraction (SX)

The solvent extraction of a metal requires an aqueous layer with the metal of interest and an organic layer with an extractant. The metal is expected to move from the aqueous layer to the organic layer via sufficient contact from mixing. After extraction, the aqueous layer is called a barren or raffinate.

The efficiency of solvent extraction is dependent on various factors such as the type of extractant, extractant concentration, diluent, phase ratio, the concentration of salt in the aqueous layer, strength of mixing, pH, and temperature.

There are many extractant solutions commonly used for nickel extractions. Popular ones include di(2-ethylhexyl)phosphoric acid (DEHPA) and the Cyanex series. However DEHPA requires a specific pH range and tends to form emulsions.[50] The Cyanex series 272, 301 and 302 from Cytec Industries Ltd., have been very successful and have for the most part, replaced other solvents. The most popular one, Cyanex 272 contains 76% bis(2,4,4-trimethylpentyl) phosphinic acid. Although Cyanex 272 requires pH control, it presents high extraction efficiency of metal such as cobalt from a cobalt-nickel mixture.[50] Cyanex 272 was used as it has proven in various studies to be an efficient and selective extractant in the separation of metals Ni^{2+}, Cu^{2+}, Zn^{2+}, Co^{2+}, Fe^{2+} in leach liquor solutions from crude $NiSO_4$, especially in comparison to other techniques such as precipitation.[51–54] In the experiments below, **L4** was used as an extractant instead of these commercially available types.

Extraction concentration is known to have a positive relationship with metal extraction at a constant pH. This is calculated by finding the distribution ratio and comparing it to the change in extraction concentration.[55–57] The distribution ratio (D) provides a reliable representation of the efficiency of the extraction, as well as the effect of pH, and the extractant concentration.[58]

The extraction equilibrium of nickel from the extractant is presented by the equation:[58]

$$Ni^{2+}_{(aq)} + 2HA_{(org)} \xrightarrow{K_{ex}} NiA_{2(org)} + 2H^{+}_{(aq)}, \qquad (1)$$

Where K_{ex} is the equilibrium constant,

$$K_{ex} = \frac{[NiA_2][H^+]^2}{[Ni^{2+}][(HA)\}^2} \quad (2)$$

$$K_{ex} = \frac{D[H^+]^2}{[(HA)\}^2} \quad (3)$$

$$D = \frac{[NiA^2]}{[Ni^{2+}]} \quad (4)$$

Rearranged logarithm:[58]

$$\log D = \log K_{ex} + 2\log[HA] + 2pH. \quad (5)$$

Diluents with an aromatic component can increase the distribution ratio and solubility in the organic phase of the metal complex. They perform as an equilibrium modifier and affects selectivity.[50] More specifically, aromatic diluents can enhance the extraction of nickel. Although Singh *et al*., reported little differences between diluents, Preston noted that aromatic diluents improved nickel extraction.[55,58,59] Reddy and Priya compared different diluents using LIX84-I at pH 7.5 and rated the diluents by the distribution ratios found via experimentation: kerosene (D=233.3) > n-hexane (D=47.8) > cyclohexane (D=32) > benzene (D=17.3) > carbon tetrachloride (D=10.32) > chloroform (D=3.61) > xylene (D=1.15).[58] Due to ease of access, decanol and hexane were chosen instead of kerosene for the extraction trials.

Phase ratio refers to the volume of aqueous solution versus volume of organic solution (A:O). Reddy *et al*., carried out counter-current batch simulation studies for nickel extraction and found that the best extraction 95.8% occurred with 65% reagent neutralisation, 1:3 phase ratio and pH 5.8.[14] The authors found that when the ratio is 1:2, >99% of nickel could be extracted after three stage extraction tests while with a ratio of 1:3, only two stage extraction tests were needed for the same percentage.[60] For nickel extractions in hexane conducted by Jung *et al*., it was found that the best phase ratio A:O is 5:1.[73]

The efficiency of solvent extraction can also be increased by adding certain salts to the aqueous solution. Using LIX 841, the addition of $NaNO_3$ was found to decrease the extraction efficiency of nickel from 100% to 88.6% while other salts such as NaCl,

Na_2SO_4, NaSCN only showed a marginal decrease (100-95%).[58] However the effect is also dependent on the extractant. For extractants such as DEHPA, no changes to nickel extraction was observed on the addition of salts.[61]

The strength of mixing determines whether the metal of interest in the aqueous solution is given enough contact with the organic solution to be extracted efficiently. For an experiment with 5 mL in 30 minutes on a magnetic stirring plate, 750 rpm was found to be the most efficient speed.[58] Because our extractions were carried out for 24 hours, the rpm was set around 150-300 rpm.

The effect of pH is also a huge determining factor of solvent extraction. The optimum pH is dependent on the type of extractant. For example, Table 39 shows the pH of a few common extractants when 50% of nickel is extracted with decanol/kerosene.

Table 39. Table of common extractants.

Extractants 0.2 M	**Salt concentration mol/dm^3**	**Ni $pH_{50\%}$**
Cyanex 272	0.10	6.7
Cyanex 302	0.02	4.2
Cyanex 301	0.10	1.4
DEHPA	0.10	4.2

Temperature studies on the extraction of nickel showed that there was no effect when carboxylic acid or oxime based extractants were used.[62] Yet, an increase in nickel extraction was seen with increased temperature when organophosphorus acid based extractants were used.[63,64]

6.1 Method for SX

The ligand used for the solvent extraction was based on **L3** but instead of propyl arms, octyl arms were attached as shown in Figure 28.

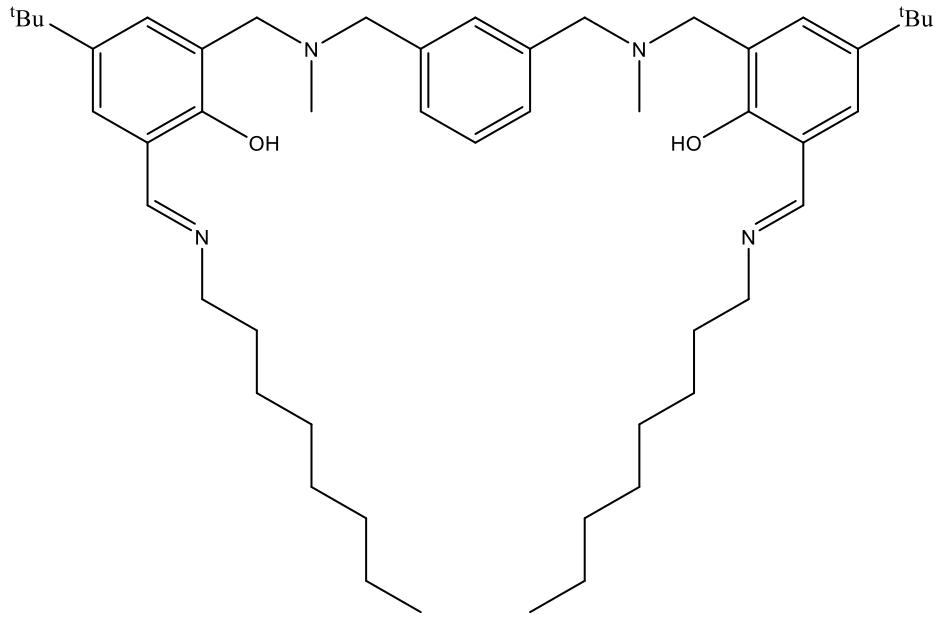

Figure 28. Structure of **L4** used for solvent extraction.

$NiSO_4$ (3.4410 g) and Na_2SO_4 (35.34 g) were dissolved in deionised water (160 mL). The solution was separated into 5 vials and the pH was adjusted for each vial to pH 0, 2, 4, 6 and 8 with H_2SO_4 and NaOH 0.1465 M. The amount of H_2SO_4 added for the pH adjustment was measured and included in the calculations. 1.5 mL of each pH was then distributed among 8 vials. For the organic solution, **L4** (8.0052 g) was dissolved in decanol (128 mL) to form a 0.1 M solution of ligand. Then the vials were set up via the Table 39 below with duplicates for each.

Table 39. Groups for extraction.

pH 0, 2, 4, 6, 8	**A**	**B**	**C**	**D**
	DeOH	**L4**	**L4**	**L4**
		DeOH	DeOH	DeOH
			THF 0.2909 g per vial	TBAH 0.6632 g per vial

For an efficient solvent extraction, it is recommended to have less aqueous solvent than the organic.[50] For this reason, each vial contained the organic solution (2 mL) and the aqueous solution (1.5 mL). For the vials with THF, ligand (17 mL) and THF (3 mL) were mixed and then separated into individual vials.

The vials were mixed on a shaking plate for 24 hours at 150 rpm in a 25 ºC room. After aliquots for analysis were taken, they were left on a shaking plate for 70 hours at 150 rpm in a 37 ºC room.

6.2 Sulfate Analysis

For the analysis of SO_4^{2-}, the protocol from Roy *et al.*, was loosely followed.[65] Although there are other methods such as ICP-AES for SO_4^{2-} determination, there was no access to this equipment. Also, ICP-AES can have interference from calcium and hydrochloric acid.[66]

An alternative method to measure SO_4^{2-} is ion chromatography but this method is inadvisable for low SO_4^{2-} concentrations.[67] Other methods such as the gravimetric technique and turbidimetric method require the precipitation of barium sulfate. The gravimetric method is time consuming and subject to errors while the turbidimetric has a strict quantification range and is prone to interference from metal and anions.[68]

For the analysis of SO_4^{2-}, the spectrophotometric method was chosen. This method relies on the reaction between SO_4^{2-} and barium chloranilate which releases chloranilic acid which can be measured via UV-Vis spectroscopy at the wavelength 350 nm. This method is useful for solutions with a SO_4^{2-} concentration between 10-1000 mg L^{-1}. An ion exchange column was not set up for AsO_4^{3-} and PO_4^{3-} as impurities were not a concern in this experiment. A possible source of error may have derived from insoluble amounts of barium chloranilate as it creates a stock solution with an inconsistent concentration that cannot interact with sulfate.

6.3 Method for Sulfate Analysis

The barium sulfate stock solution was made with barium choranilate (3.603 g), ethanol (133.2 mL) and was made up to the 400 mL mark with deionised water. The acetate buffer solution was made with sodium acetate (2.72 g), acetic acid (1.28 mL) and made up to the 200 mL mark with deionised water. This created a buffer that was pH 4.5.

The preparation of samples was carried out in 15 mL Falcon tubes by taking out the aqueous sample (0.2 mL), after 24 or 70 hours of mixing and adding the aliquot to ethanol (0.8 mL), acetate buffer (1 mL) and the barium chloranilate stock solution (2.1 mL). The tubes were shaken for 10 minutes for thorough mixing and then spun in a centrifuge at 5000 rpm for 10 minutes.

Approximately 0.05-0.1 mL of the sample was diluted in a glass cuvette for analysis and adjusted for an appropriate absorbance value. Standards were made up in a similar manner but using a nickel stock solution dissolved in water.

6.4 Method for Nickel analysis

For the analysis of nickel, the decanol sample (0.4 mL) for each vial was diluted with ethanol (4.6 mL). The solution was mixed for 10 minutes before running on the AAS instrument at 232 nm. The wavelength 232 nm was chosen because 232 nm is suitable for samples with lower nickel concentrations of 1.8-8 μg mL^{-1} with a sensitivity of 0.04 μg mL^{-1} compared to the sensitivity of 341.5 nm, 0.12 μg mL^{-1}.

6.5 Results and Discussion

From the UV-Vis analysis of the SO_4^{2-}, a small amount of SO_4^{2-} was detected in the aqueous layer suggesting a large amount had been extracted in the organic layer. However, we would expect SO_4^{2-} to remain in the aqueous layer. In the repeat of this experiment, an extra step in preparing barium chloranilate might be helpful as it was noticed that the barium chloranilate used was not sufficiently soluble in the current mixture. Another potential step could be the addition of acid or other reagent that can separate $NiSO_4$ and prevent interference so that all the sulfate in the solution is free to interact with the barium chloranilate. The results collected require more repeats for confirmation of the optimal conditions.

The solvent extraction experiment was based on the method in Akkus *et al*. They added various metal salts and anions to the aqueous phase and used a mixture of Orform SX7/decyl alcohol in the organic phase.[19]

Our first experiment used the **L4** and decanol with no other extractants in the organic phase and no competing metal or anions in the aqueous phase. Akkus *et al*., found that the transfer of Ni^{2+} was low when the A:O (<2) was used and noticed a colour change in the aqueous phase from green to blue.[19] They concluded that impurities in the extractant were forming stable water-soluble Ni^{2+}-amine complexes and found that removing the impurities in the extractant via a load/strip cycle improved the data.[19] After our extraction, the colour change of the aqueous phase changed from blue/green to a transparent blue/green while the organic phase changed from yellow to a dark gold. The A:O 3:4 was used, however the analysis of the amount of nickel transferred appears unreliable. If the extraction with decanol is to be repeated, it would be best to analyse the aqueous phase on the AAS to calculate how much nickel was extracted as the analysis of the organic phase with the current method appears to present unreliable results.

Finally, a solvent extraction was set up using an adapted protocol from Jung *et al*. Because it was not clear if the optimal pH was dependent on the extractant, or diluent, a range of pH values and A:O ratios were trialled.

6.5.1 Result from the SX of Sulfate

The measurement of the standards was very difficult due to the sensitivity of the UV-spectrometer with the slightest changes in concentration. As shown in Table 40, only four concentrations provided reliable values.

Table 40. Standards for SO_4^{2-} analysis.

Concentration (mg mL^{-1})	Absorbance
0.127	0.496
0.0959	0.268
0.084	0.12
0.108	0.432

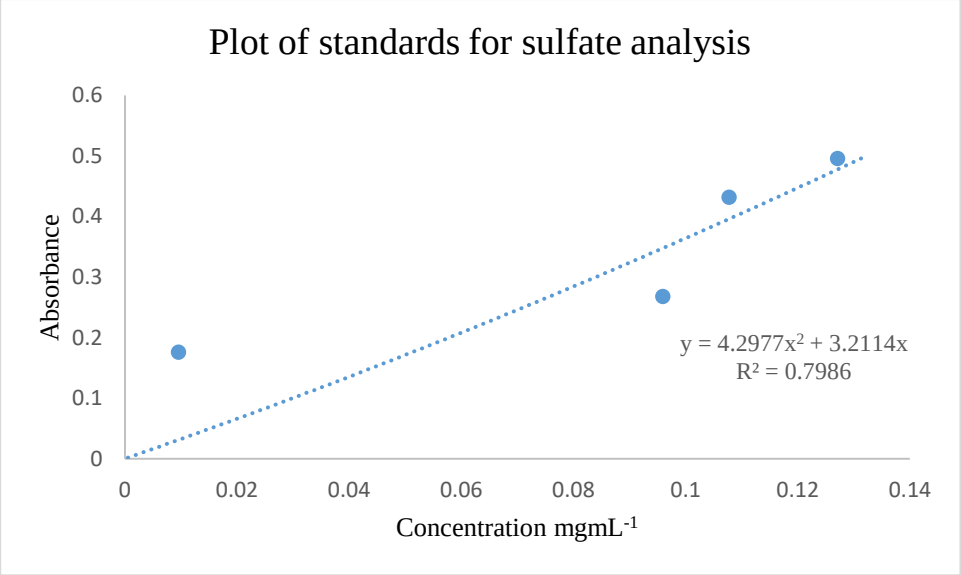

Figure 29. Plot of standards for SO_4^{2-} analysis.

For the analysis of SO_4^{2-}, the aqueous solution from the solvent extraction was measured, and to estimate the amount of SO_4^{2-} in the organic phase, the amount of SO_4^{2-} in the aqueous phase was taken away from the total amount of SO_4^{2-}. As a result, Figures 30-33 below present the percentage of SO_4^{2-} extracted into the organic solution.

Because the hydration energy of SO_4^{2-} is high (ΔG= -1103 $kJmol^{-1}$) it is difficult to extract but can aid the extraction of metal cations to the hydrophobic organic phase via

the salting out, electronic repulsion and hydrophobic effect. However, in our results, we can see a high extraction efficiency of SO_4^{2-}. The values are higher than expected but this may be due to interference from the nickel ions, binding to the SO_4^{2-} or the insoluble amounts of barium chloranilate.

Typically before the barium chloranilate is introduced, the aqueous solution is run through an ion exchange column to get rid of interfering cations. Cations can interfere by forming insoluble chloranilates at even low concentrations because of their high optical density. Hence, it is possible that the prescence of the nickel ions interfered with the measurement, or that there was a different experimental error. Further studies regarding the interference from nickel may be beneficial to understanding how it changes the results.

From Figure 30 and 31 below, it appears that the addition of ligand does not show any significant changes at the various pH values tested.

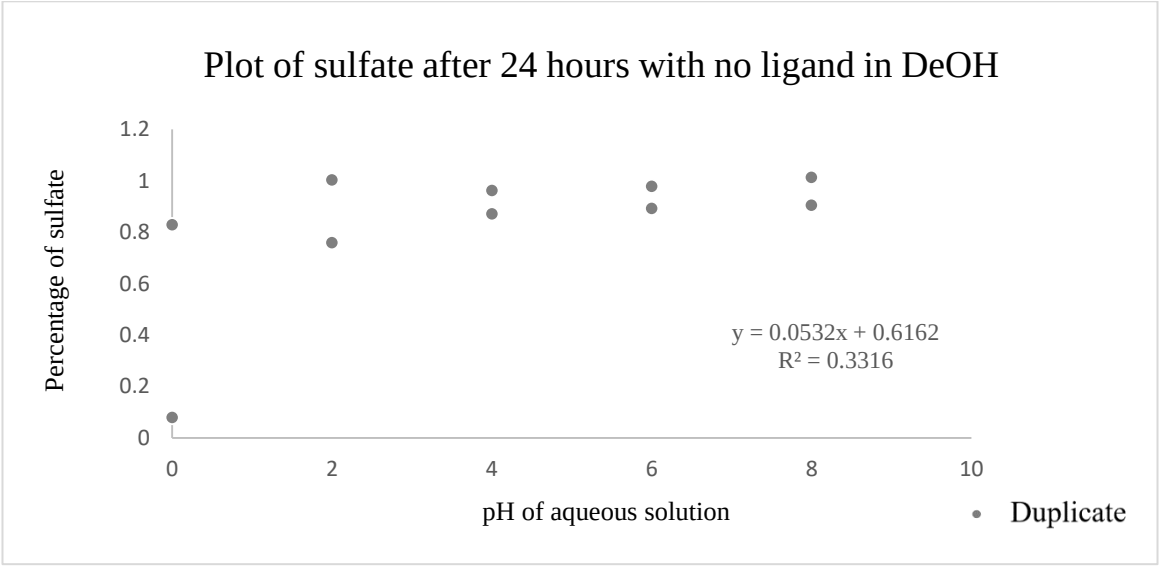

Figure 30. Plot of SO_4^{2-} after 24 hours with no ligand in DeOH.

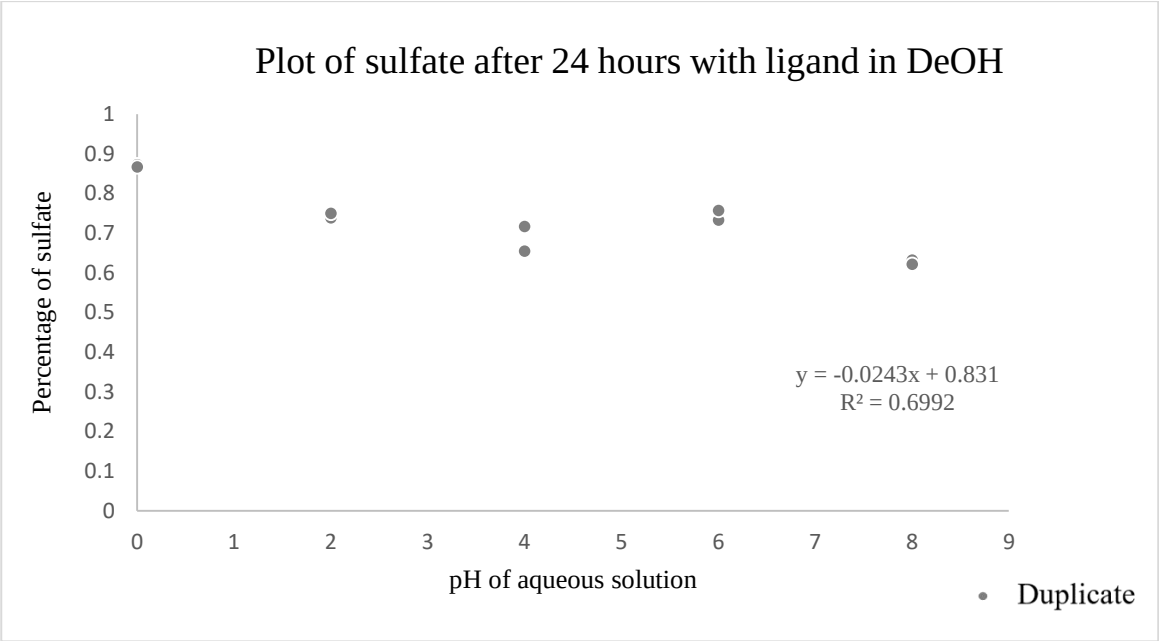

Figure 31. Plot of SO_4^{2-} after 24 hours with ligand in DeOH.

Below in Figure 32, the curve of the plots show that the addition of THF provide slight changes. Although the addition of TBAH in Figure 33 was also trialled, the experiment presented unreliable results due to precipitation during the solvent extraction.

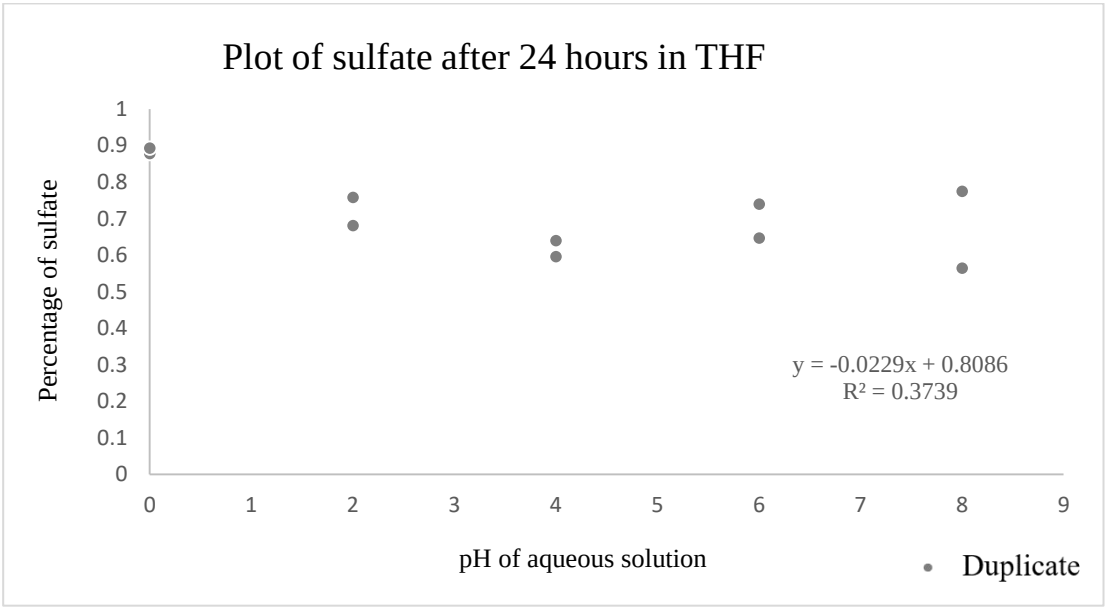

Figure 32. Plot of SO_4^{2-} after 24 hours in THF.

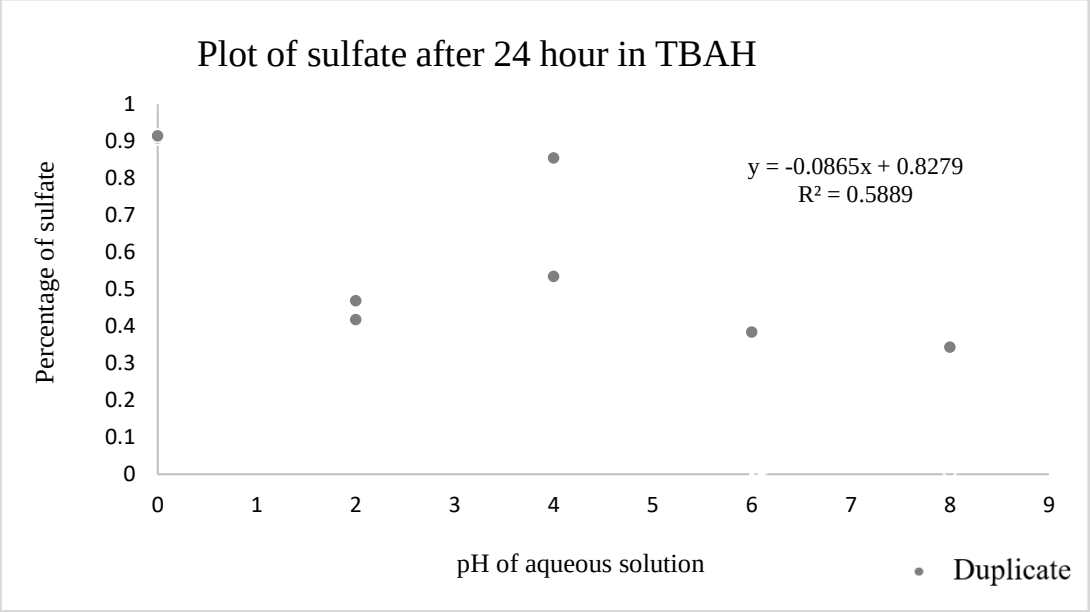

Figure 33. Plot of SO_4^{2-} after 24 hours in TBAH.

6.5.2 Result from the SX of Nickel in 1-Decanol

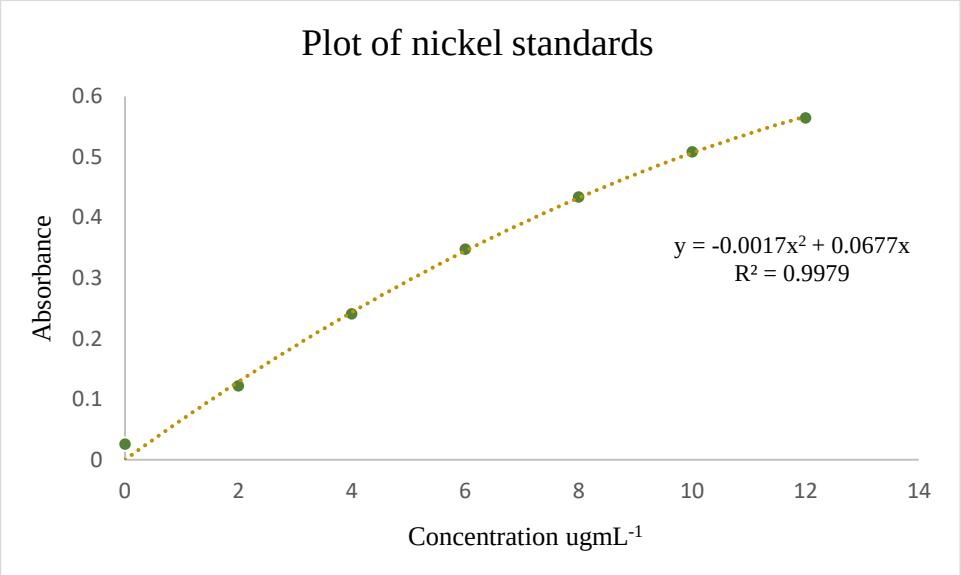

Figure 34. Plot of nickel standards.

For the analysis of nickel in the organic layer, decanol was diluted with ethanol. For the two experiments with no ligand or addition of TBAH with ligand, both showed results with 0% extraction. A summary of the experiment can be seen in Table 41. The highest extraction occurred at pH 8 without THF.

Table 41. Vials set up for SX with decanol as organic phase.

Extractant	pH pre-extraction	Time (hours)	% Nickel extracted
L4	0	24	0
L4	2	24	0.5
L4	4	24	0.97
L4	6	24	1.13
L4	8	24	1.39
L4	0	70	0
L4	2	70	0.29
L4	4	70	0.53
L4	6	70	0.62
L4	8	70	1.53
L4 + THF	0	24	0.02
L4 + THF	2	24	0.14
L4 + THF	4	24	0.47
L4 + THF	6	24	0.49
L4 + THF	8	24	1.01
L4 + THF	0	70	0.03
L4 + THF	2	70	0.11
L4 + THF	4	70	0.33
L4 + THF	6	70	0.36
L4 + THF	8	70	1.16

As we can see in Figure 35 and 36, the percentage of nickel extracted is very low. In the following experiment with hexane, it was found that the AAS analysis of nickel in the aqueous phase achieved results above 30% while the analysis of the organic solvent dissolved in methanol afforded values around 1%. It may be interesting to see the effects of different diluents on the extraction of nickel with **L4** such as aromatic diluents such as kerosene.

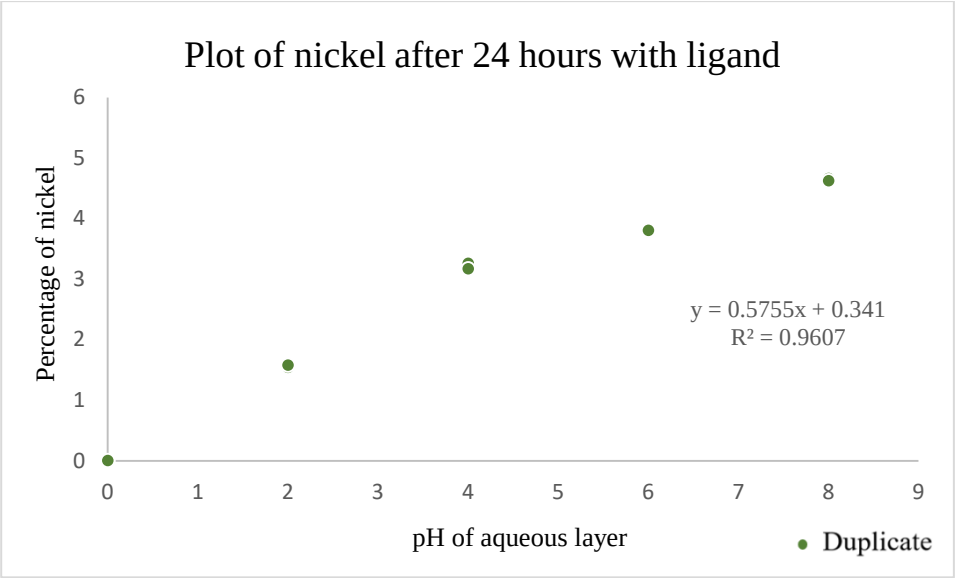

Figure 35. Plot of nickel after 24 hours with ligand.

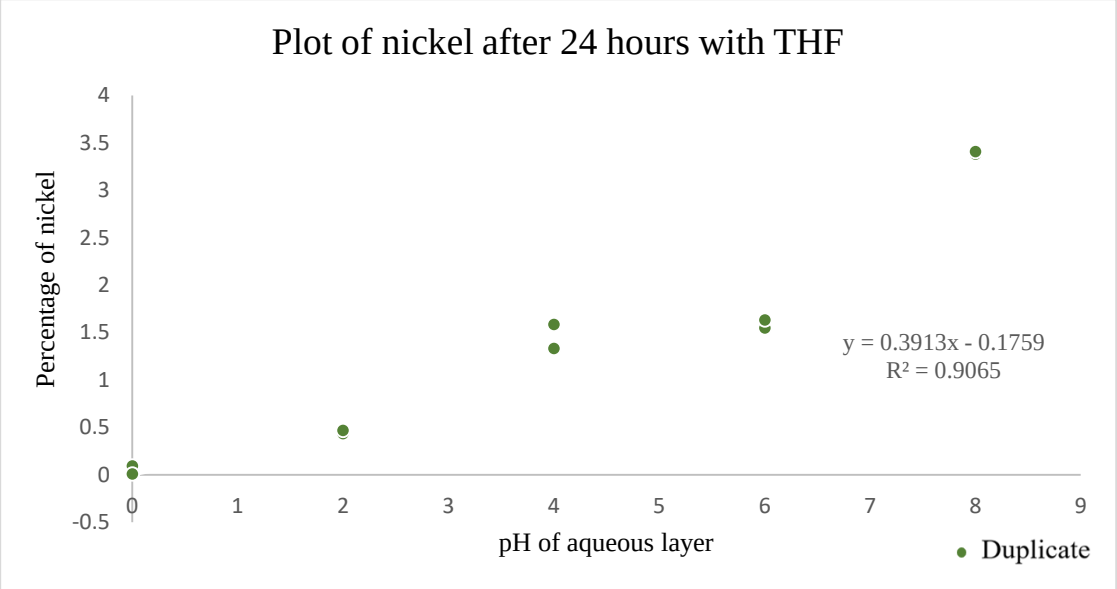

Figure 36. Plot of nickel after 24 hours with THF.

In Figures 37 and 38 below, the amount of nickel that is extracted between 24-70 hours is shown. As we can see, the extraction appears to have slowed past the 24 hours mark as the percentage extracted after 70 hours is not too different than the values after 24 hours of mixing. In some cases, the values measured after 70 hours is lower than the 24 hours. From the results, pH 8 is most favoured although a higher pH may be of interest to see if the percentage of nickel extracted continues to increase.

A repeat of the nickel extraction in DeOH including higher pH may be of interest, but more importantly, the AAS analysis should be run with the aqueous samples as the following experiment with hexane has shown that the AAS analysis with the organic solution is unreliable.

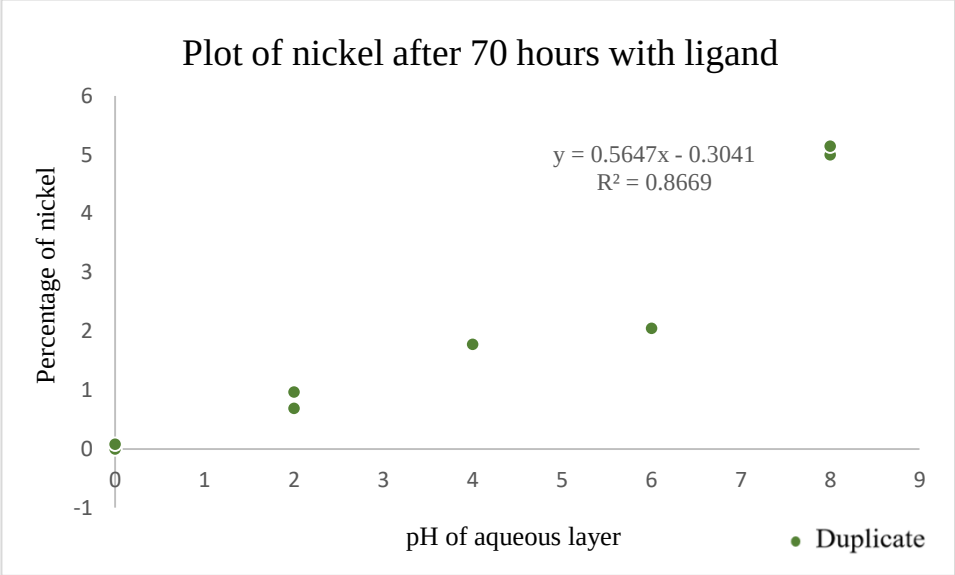

Figure 37. Plot of nickel after 70 hours with ligand.

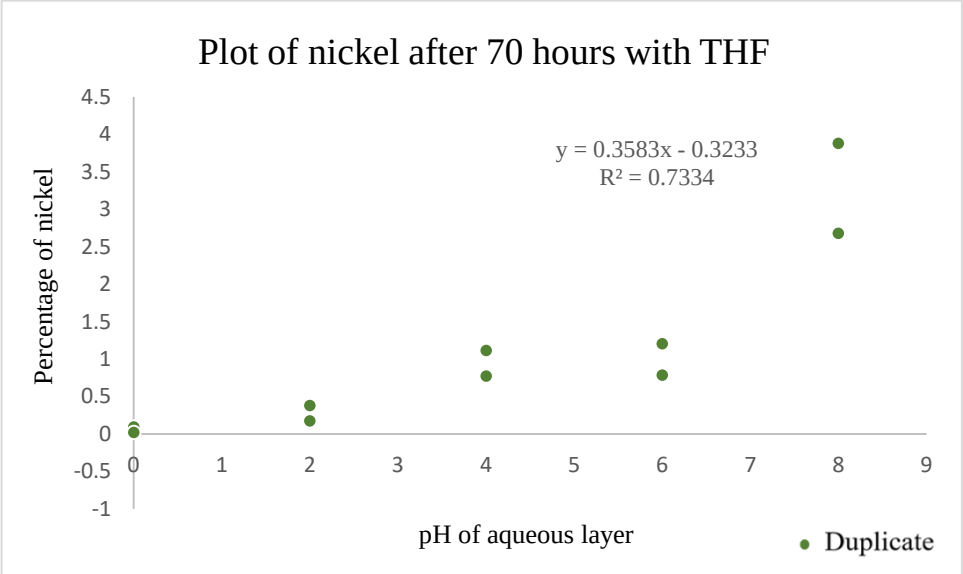

Figure 38. Plot of nickel after 70 hours with THF.

Another experiment in literature regarding the extraction of nickel include the challenge of separating Co^{2+} and Ni^{2+} from SO_4^{2-}, two metal ions with chemical and physical similarities.[69] In order to extract cobalt, Stefaniak *et al*., used 0.6 M of Cyanex 272 in 1-decanol with $NiSO_4$, $CoSO_4$, $NaSO_4$. 10 M NaOH and 1 M H_2SO_4 was used for pH control. It was found that at a pH higher than 3, a high concentration of SO_4^{2-} ion improved the extraction of the cobalt and nickel.[69] The experiment was carried out at pH 5.2 and it was found that the nickel extraction decreased with increasing metal ion concentrations.[51] The final amount of nickel extracted was a third of Co^{2+}. This selective extraction is possible because different metals react differently to ionic strength depending on the changes in free ion activity and presence of other metal ions.[70] From their experiment, it was found that unlike Co^{2+}, a high ionic strength reduced the extraction of nickel to the organic solution.[69]

Despite their low extraction efficiency of nickel, the authors found that they could increase the rate by increasing the concentration of the extractant.[69] As we can see in Figure 39 below, the extraction efficiency improves from around 10% to almost 40%. Considering these results, a trial of different extractant concentrations may be of interest for future studies.

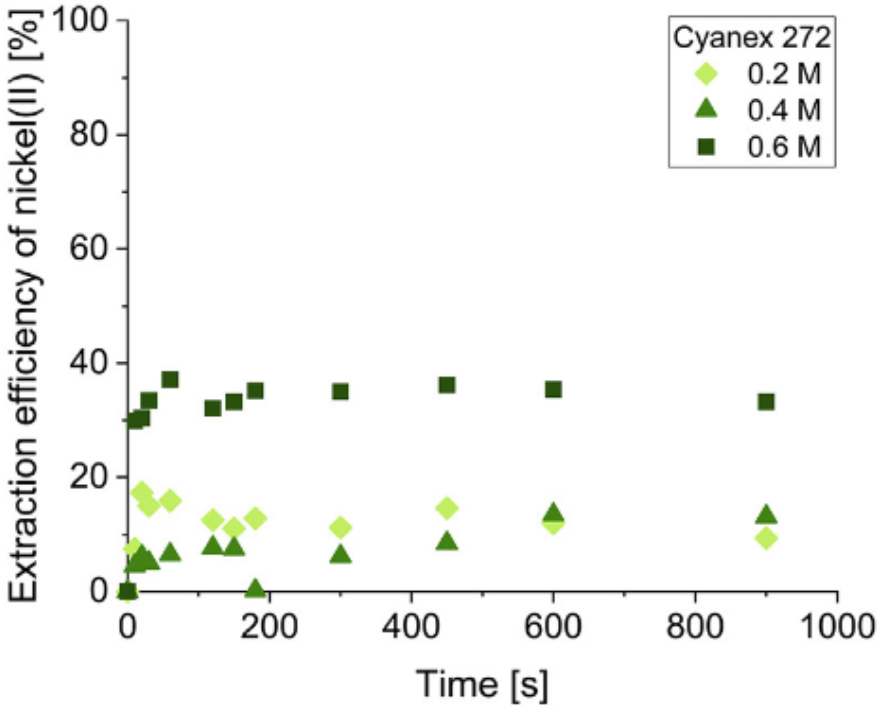

Figure 39. Comparison of different extractant concentrations.[69]

6.5.3 Result from the SX of Nickel in n-Hexane

The extraction with nickel was repeated using hexane as the solvent. The procedure was inspired by a successful nickel extraction from Jung *et al.*[71] The authors performed their nickel extraction using 5% triethylamine (TEA) as the extractant in hexane. At pH 4.5 and an A:O ratio 5:1, a maximum extraction of 99.6% was achieved.

The use of a high pH for the extraction of nickel was carried out by Nippon Mining's Hitachi refinery in 1975. They extracted Ni^{2+} from a SO_4^{2-} solution (30 gL^{-1} Ni) at pH 9–10 using ammonia for pH control and the extractant LIX® 64N in kerosene. To find out if the optimal pH is dependent on the extractant or solvent, a wide range of pH values were trialled.

Hexane was chosen for the repeated experiment as it was more easily accessible than kerosene but still had a high distribution ratio. Instead of TEA, **L4** was used although one duplicated extraction was carried out with TEA and no ligand to compare their extractant capabilities. To find the best pH and A:O ratio for **L4** extraction capabilities in hexane, various conditions were trialled as we can see in Table 42 below.

Table 42. Vials set up for SX with hexane as organic phase.

Extractant	pH pre-extraction	A:O	% Nickel extracted
TEA	4.95	1:5	94.5
L4	1.36	1:2	43.1
L4	3.52	1:2	46.4
L4	6.6	1:2	63.9
L4	8	1:2	70.0
L4	10.53	1:2	89.0
L4	7.95	1:5	71.5
L4	7.95	1:3	61.4
L4	7.95	1:2	54.4
L4	7.95	1:1	52.7

In Figure 40 below, the standard curve portrays how the curve plateaus around concentration 15 µg mL^{-1} according to the Beer-Lambert law.

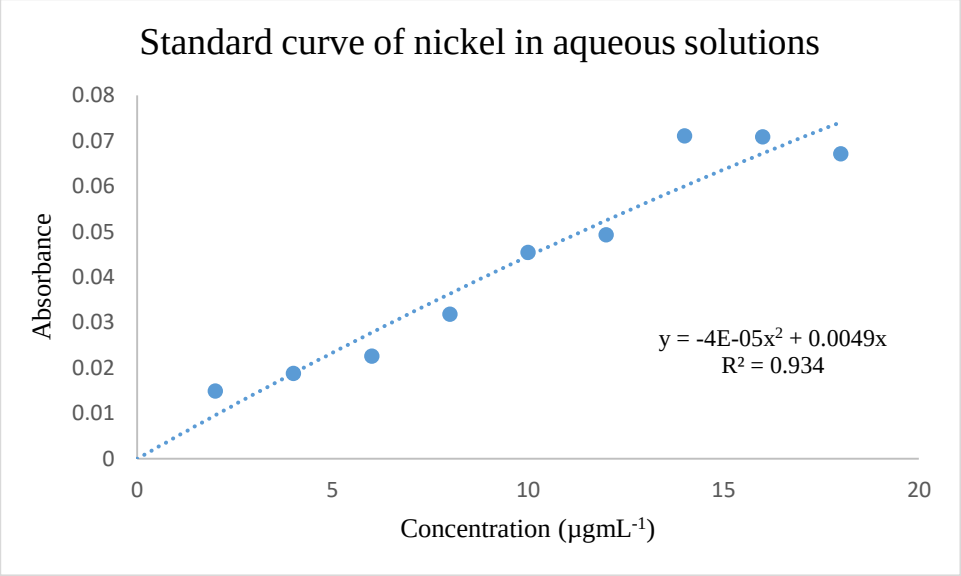

Figure 40. Standard curve of nickel in aqueous solutions.

From the extraction of nickel at different pH levels (Figure 41) it appears that the extraction was most efficient around pH 10. This is different from the optimal pH found by Jung *et al*., suggesting that the optimal pH is dependent on the type of extractant.[71]

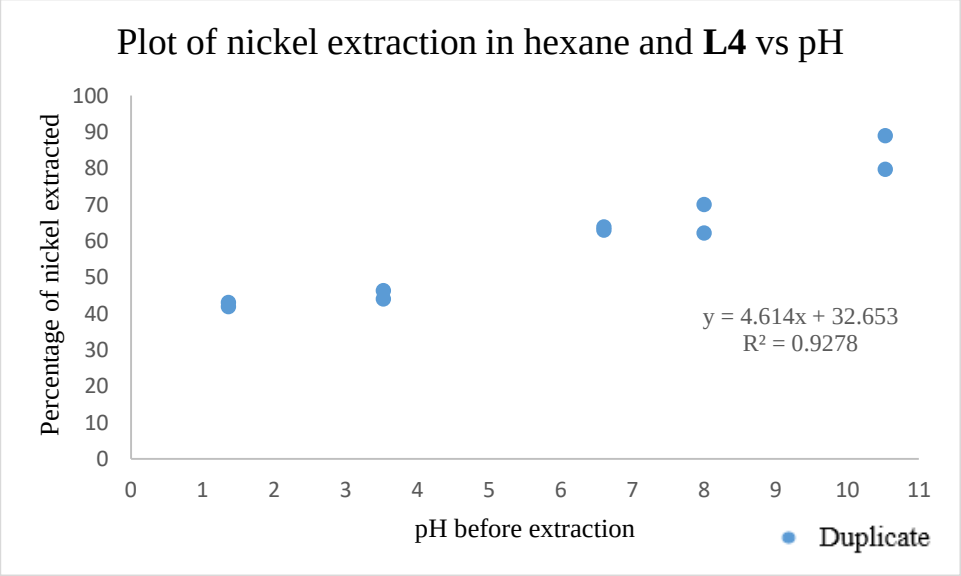

Figure 41. Plot of nickel extraction in hexane and **L4** vs pH.

The A:O ratios in Figure 42 produced nickel extraction percentages ranging from 52-71%. The most successful ratio was A:O 1:5 with nickel extraction of 71.5% in pH 7.95. A comparison of an extraction carried out at A:O 5:1 may be useful as Jung *et al*., found

that their most efficient A:O ratio was 5:1.[71] Although the A:O ratio was accidentally set up as 1:5 instead of 5:1, it resulted in the highest extraction value out of the ratios trialled. In consideration of the best extraction result of 89% from A:O 1:2 and pH 10.53, another extraction carried out at A:O 1:5 at pH 10 may be of interest to see if it would produce even better results.

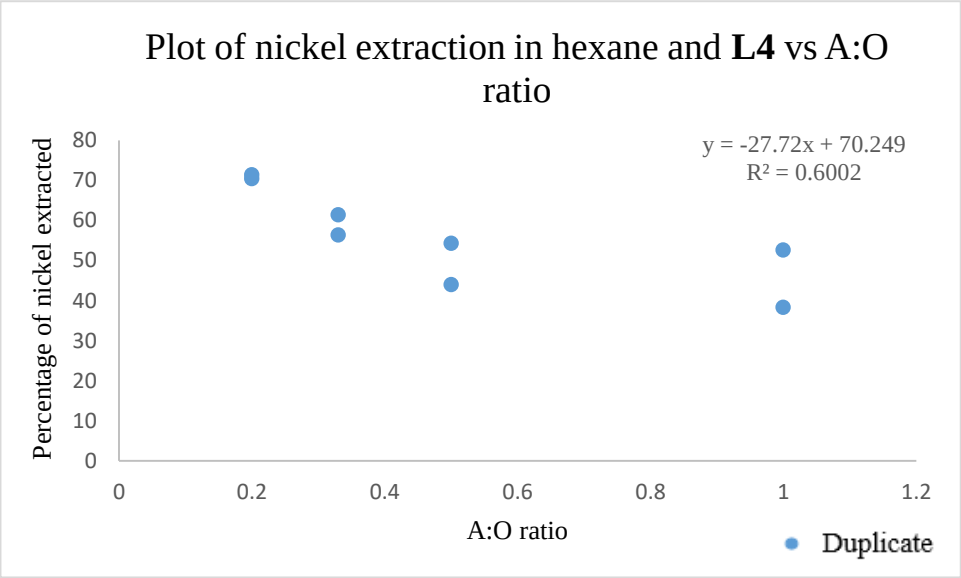

Figure 42. Plot of nickel extraction in hexane and **L4** vs A:O ratio.

Using the phase-ratio data, an extraction isotherm was determined by plotting the McCabe-Thiele diagram. Although the diagram is commonly used to determine the number of stages required for a binary distillation, this graphical method can also be applied to solvent extraction. The method assumes that the mixture has two components, 100% tray efficiency, that thermodynamic effects are negligible, and the heat of vaporization is the same.[72] For the analysis of solvent extractions, it is recommended to use the McCabe-Thiele diagram with experiments with the same pH.[18] Hence, one part of the experiment was organised so that the only variable was the A:O ratio. The use of this method is favoured as there is only one metal ion present in the experiment. However, the heat of vaporisation of water is 40.8 kJ mol^{-1} while it is 28.85 kJ mol^{-1} for hexane.[73,74] Despite this factor, the graphical method may portray an estimate of how many stages are required to obtain the maximum extraction.

Figures 43 and 44 below confirms that the maximum efficiency of A:O volume of 1:1 is achieved in three stages and the maximum efficiency of A:O volume of 1:5 is achieved in one stage. Hence, the 1:5 ratio can be seen as more efficient.

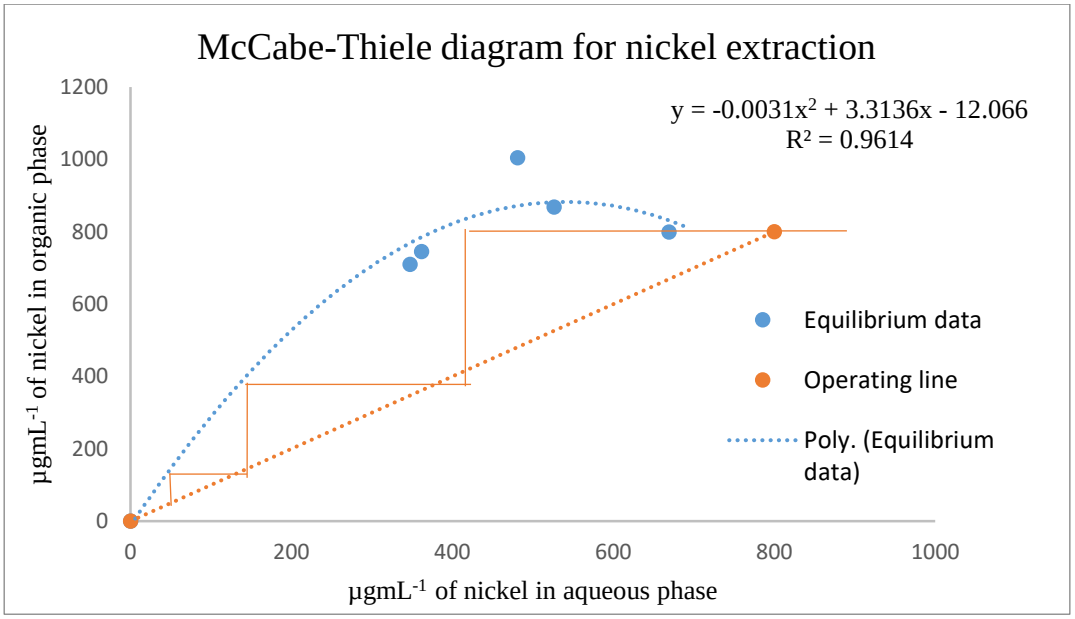

Figure 43. McCabe-Thiele diagram for nickel extraction at A:O 1:1.

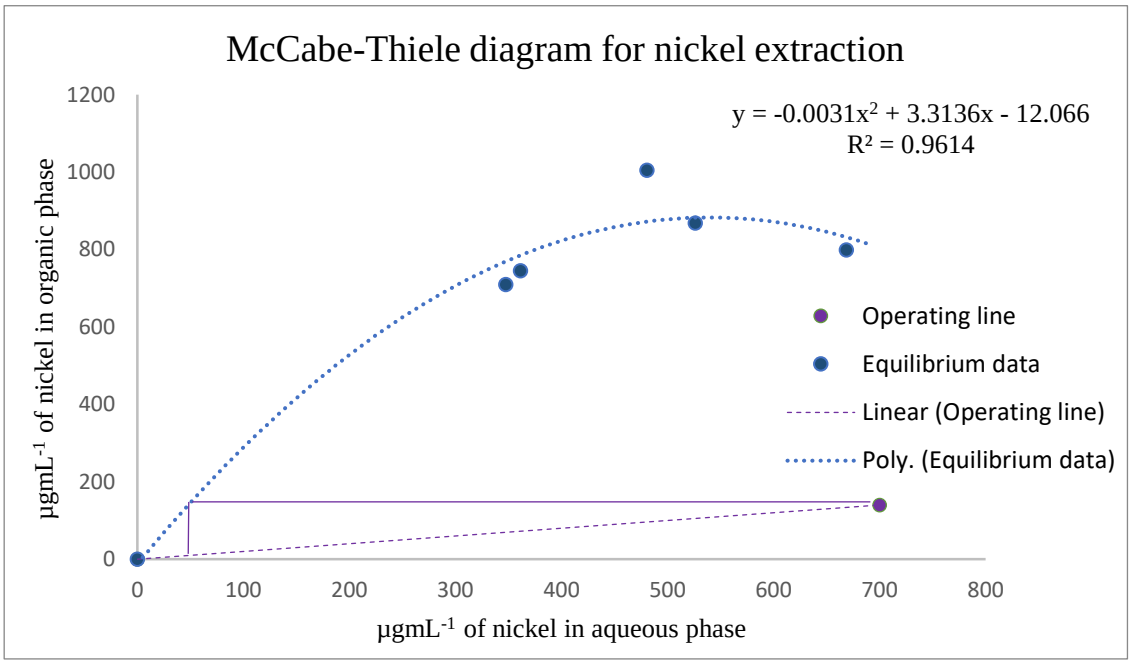

Figure 44. McCabe-Thiele diagram for nickel extraction at A:O 1:5.

A different method carried out in the literature takes advantage of the tendency for reduced nickel transfer in the presence of other metal ions.[75] By getting other metal ions to extract into the organic layer, the nickel can be purified in the aqueous phase. The method purifies $NiSO_4$ from an impure solution.[75] The steps includes; sulfurisation, adding sulfur to an acidic impure solution and precipitating nickel sulfide, redissolution which requires adding an oxidising agent to the solution, and then, a neutralising agent is added after to get rid of a bulk of impurities via precipitation, leaving behind a concentrated solution of nickel.[75] The following purification of $NiSO_4$ includes adding an organic solvent so that the A:O is 1:3.5. A phosphoric acid ester extractant is diluted with a diluent at a volume ratio of 20:80 and the pH is adjusted to 4.5.[75] Next, a solvent extraction is carried out so that the metal impurities such as Co and Mg will transfer to the organic solvent, leaving the stripped nickel solution in the aqueous phase. Finally, a sulfurising agent is added to precipitate impurities such as Cu^{2+} and Zn^{2+}.[75]

7.0 General Experimental Methods

7.1 General Procedures

All reagents obtained from standard chemical suppliers did not require further purification. Analytical grade solvents were used for reactions and the metal salts used were stored in desiccators.

All reactions were carried out in acetone washed, oven dried glassware, and stored in room temperature. Crystallisation vials were used straight from purchase.

Column chromatography required the use of silica gel (grade 60, mesh size 230-400), Scharlau, and Celite 545. Drying tubes used calcium chloride with 8-16 mesh granular size.

All ligands have been characterised by UV-Vis, NMR, and ATR-FTIR spectroscopy. All complexes have been characterised by X-ray, UV-Vis, ATR-FTIR, ESI-MS, and AAS spectroscopy. Conductivity measurements were carried out for all complexes and for the ClO_4^- complexes $[ClO_4 \subset Ni_2(\mathbf{L1})_3](ClO_4)_3$ and $[ClO_4 \subset Ni_2(\mathbf{L3})_2](ClO_4)_2$, CH-N analysis was carried out by the Campbell Microanalytical Laboratory in Otago.

^{1}H NMR was run in $CDCl_3$ on a Bruker Advanced 500 MHz spectrometer using the software TopSpin version 2.1. The ATR-FIR spectroscopy was carried out on Thermo Scientific Nicolet 5700 FT-IR, ESI-MS was run in positive mode on a Dionex Ultimate 3000 in MeOH, UV-Vis spectroscopy was Shimadzu UV 3101PC spectrophotometer, and conductivity measurements were run on a Philips PW 5909 conductivity meter. The settings for the measurements run on the conductivity meter are: 2000 Hz frequency, MTC depression, cell constant = 3, coefficient % = 2.5 $^oC^{-1}$, and 20 ^{o}C temperature.

The AAS spectroscopy was run on SavantAA Atomic Absorption spectrometer from GBC Scientific Equipment. The absorbance was measured at 341.5 nm using a slit width of 0.2 nm with the sensitivity of 0.12 μg mL^{-1} for all ligands and complexes. The wavelength 341.5 nm was chosen because 232.0 nm tends to show an exaggerated curve due to an unresolved non-resonance line at 232.14 nm. However, for the solvent extraction, the measurements were carried out at 232 nm due to the low concentration of Ni^{2+}.

Structural characterisation was achieved by X-ray crystallography on a Bruker D8 Venture diffractometer via Cu radiation with a IμS Diamond, microfocus X-ray source. Crystals were mounted on Mitigen loops using Fombin (R) and moved into the cold gas stream of the detector. The crystal was kept at 100 K during data collection. Finally, using Olex2, the structure was solved with the ShelXT structure solution program using intrinsic phasing and refined with the ShelXL refinement package using least squares minimisation.

7.2 Experimental Procedures and Characterisation of L1

The method for the synthesis of the **L1** and mesocate was the same as McGarry but carried out in bulk of around 5x.[27]

7.2.1 Synthesis of 5-*tert*-butyl-2-hydroxybenzaldehyde (0a)

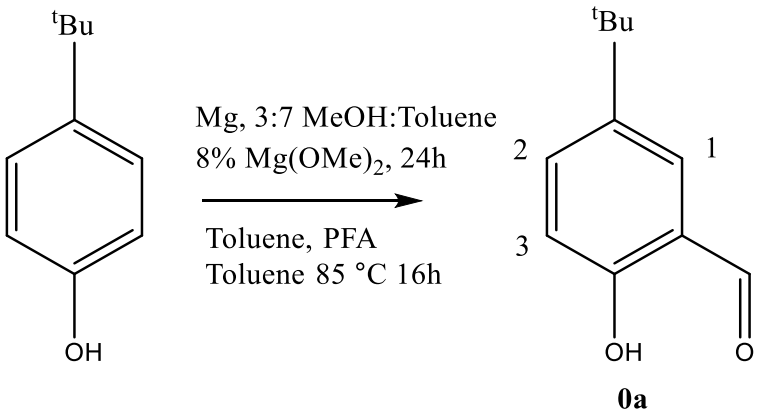

Figure 45. Schematic of **0a** from *tert*-butyl phenol.

The procedure for this synthesis was derived from Aldred *et al*.[31]

Mg turnings (19.8 g. 0.816 mol) were put in a dry oven for 1-2 days before being added to a stirred solution of 3:7 dry MeOH/toluene (260 mL) and 8% $Mg(OMe)_2$ solution (130 mL) and refluxed under argon overnight until all the Mg had dissolved. Pure crystalline *tert*-butyl phenol (203.59 g, 1.35 mol) was dissolved in toluene (135 mL) and mixed with the Mg mixture to create a grey slurry that was refluxed for three hours. Toluene (130 mL) was added prior to fractionally distilling a MeOH/toluene azeotrope until the reaction mixture had a thick consistency. More toluene (130 mL) was added along with a paraformaldehyde mixture (92.33 g, 3.07 mol) in toluene (100 mL), in small amounts over an hour while volatile by products was removed by vacuum distillation. Toluene (200 mL) was added to the reaction mixture and the solution was stirred overnight at 85 ºC under argon. To the thick yellow/brown mixture a solution of 30% H_2SO_4 (500 mL) was added dropwise over an hour and stirred for three hours at 50 ºC until two yellow layers were formed. The aqueous layer was extracted with toluene (3 x 150 mL), the combined organic layers were washed with 10% H_2SO_4 (2 x 200 mL), and deionised H_2O. The product was dried over anhydrous $MgSO_4$, filtered and concentrated in *vacuo* to

produce a dark orange oil. Small quantities of the oil (5.63 g) were purified via column chromatography with 4:1 n-hexane : EtOAc, (R_f = 0.75) to afford an orange oil (4.45 g, 79%).

^{1}H NMR spectrum agreed with literature values: (500 MHz, $CDCl_3$) δ 10.90 (1H, s, *Ar-OH*), 9.92 (1H, s, *CH=O*), 7.61 (1H, dd, J1 = 8.8 Hz, Jz = 2.5 Hz, *C3*), 7.54 (1H, d, J = 2.5 Hz, *C2*), 6.97 (1H, d, J = 8.8 Hz, *C1*), 1.36 (9H, s, ^{t}*Bu*).

7.2.2 Synthesis of 5-*tert*-butyl-3-(bromomethyl)-2-hydroxy benzaldehyde (1a)

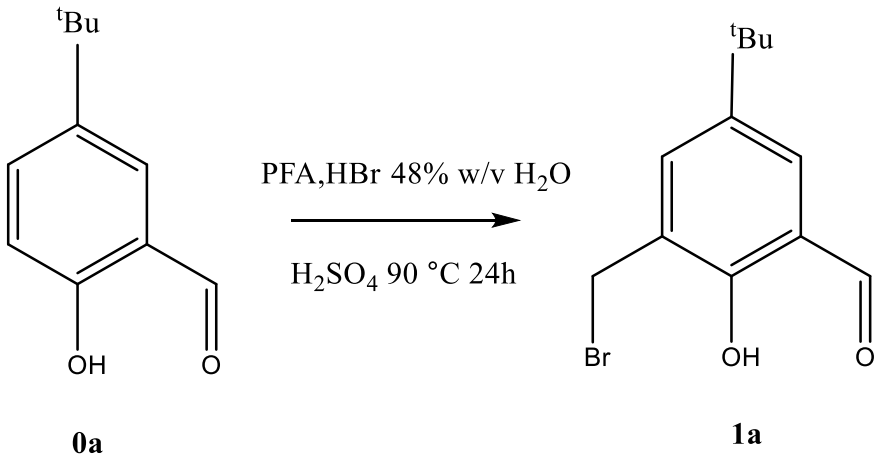

0a **1a**

Figure 46. Structure of **1a**.

Prepared as per the method of Meier *et al*.[32]

5-*tert*-butyl salicylaldehyde (20.0 g, 0.112 mol), paraformaldehyde (5.00 g, 0.167 mol) and HBr (48% w/v in H_2O, 95.6 mL, 0.846 mol) were combined and stirred at 0 °C. To the continually stirred mixture kept at 0 °C, concentrated H_2SO_4 (1.50 mL) was added slowly dropwise to avoid the formation of any dark brown/black product in the translucent yellow mixture. The resulting mixture was refluxed at 90 °C for 24 hours. The reaction mixture was cooled to RT and deionised water (100 mL) was added. The product was separated with DCM (62.5 mL) with (4 x 100 mL deionised water) until the water remained clear. The organic layer was dried over anhydrous Na_2SO_4, filtered, and concentrated in vacuo, to leave a brown oil. The crude product was recrystallised from hot pentane (10% w/v) to give light yellow/brown block shaped crystals (26.7 g, 87.8%).

^{1}H NMR spectrum agreed with literature values: (500 MHz, $CDCl_3$) δ 11.32 (1H, s, *OH*), 9.90 (1H, s, *C3*), 7.64 (1H, d, J = 2 Hz, *C1*), 7.51 (1H, d, J = 2 Hz, *C2*), 4.59 (2H, s, *C4*), 1.34 (9H, s, *C5*).

7.2.3 Synthesis of *N,N'*-dimethyl-*N,N'*-hexamethylene-di(5-*tert*-butyl-2-hydroxy benzyaldehyde) (1b)

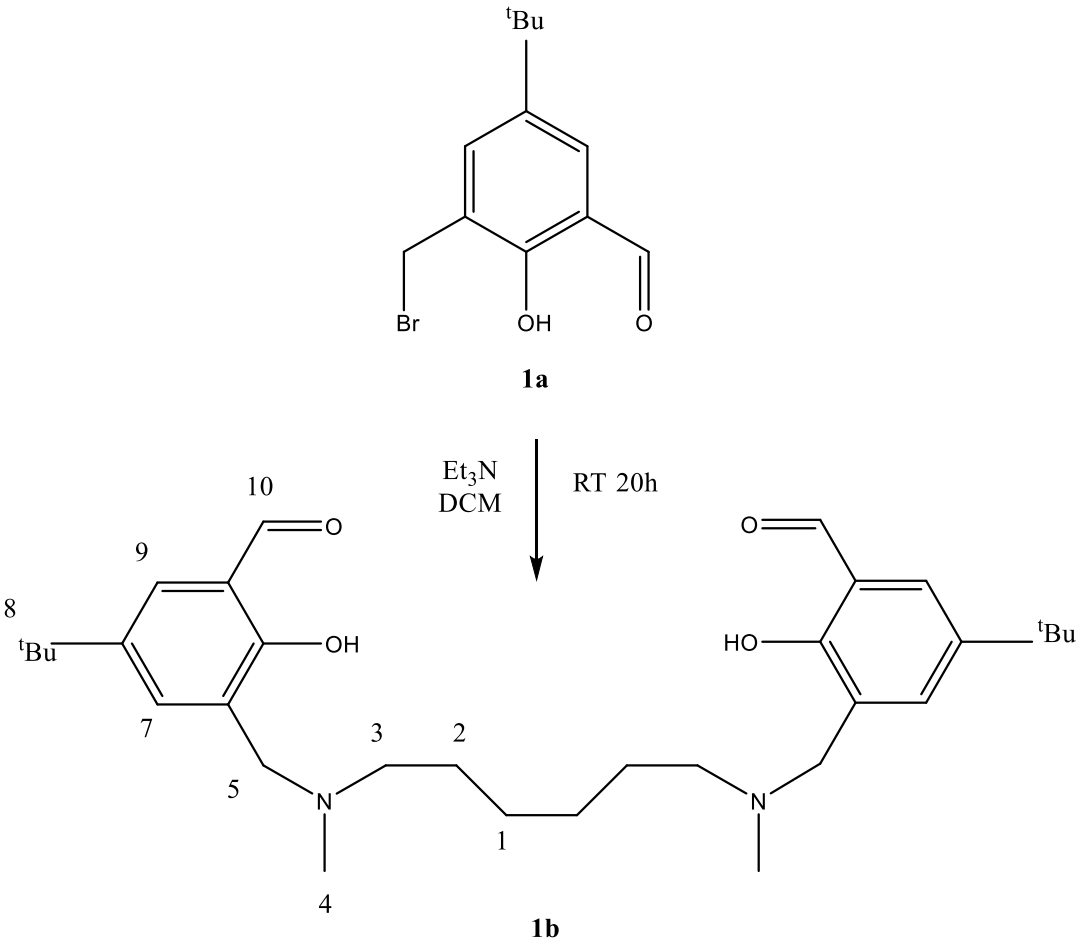

Figure 47. Structure of **1b**. change label

Preparation was guided by Chang *et al*.[34]

5-*tert*-butyl-3-(bromomethyl)-2-hydroxybenzaldehyde (1.10 g, 4.06 mmol) in chloroform (20.0 mL) and *N,N'*-dimethyl-*N,N'*-hexanediamine (0.343 g, 1.84 mmol) in chloroform (20.0 mL) were both added dropwise to a stirred solution of Et_3N (0.346 mL, 2.35 mmol) in chloroform (30.0 mL) in a round bottom flask.[24] The reaction was stirred overnight at RT. The product was washed with water (70 mL x4), and the organic layer was dried over Na_2SO_4, filtered and evaporated in vacuo to obtain an orange/yellow oil (1.23 g, 116%).

^{1}H NMR spectrum agreed with literature values: (500 MHz; $CDCl_3$) δ 10.36 (2H, s, *C10*), 7.63 (2H, d, J = 2.5 Hz, *C9*), 7.26 (2H, s, *C7*), 3.72 (4H, s, *C5*), 2.50 (4H, t, J = 7 Hz, *C3*), 2.30 (6H, s, *C4*) 1.59 (4H, m, *C2*), 1.36 (4H, m, *C1*), 1.29 (18H, s, *C8*).

7.2.4 Synthesis of *N,N'*-dimethyl-*N,N'*-hexamethylene-di(3-(propyl imino)-5-*tert*-butylphenol) (L1)

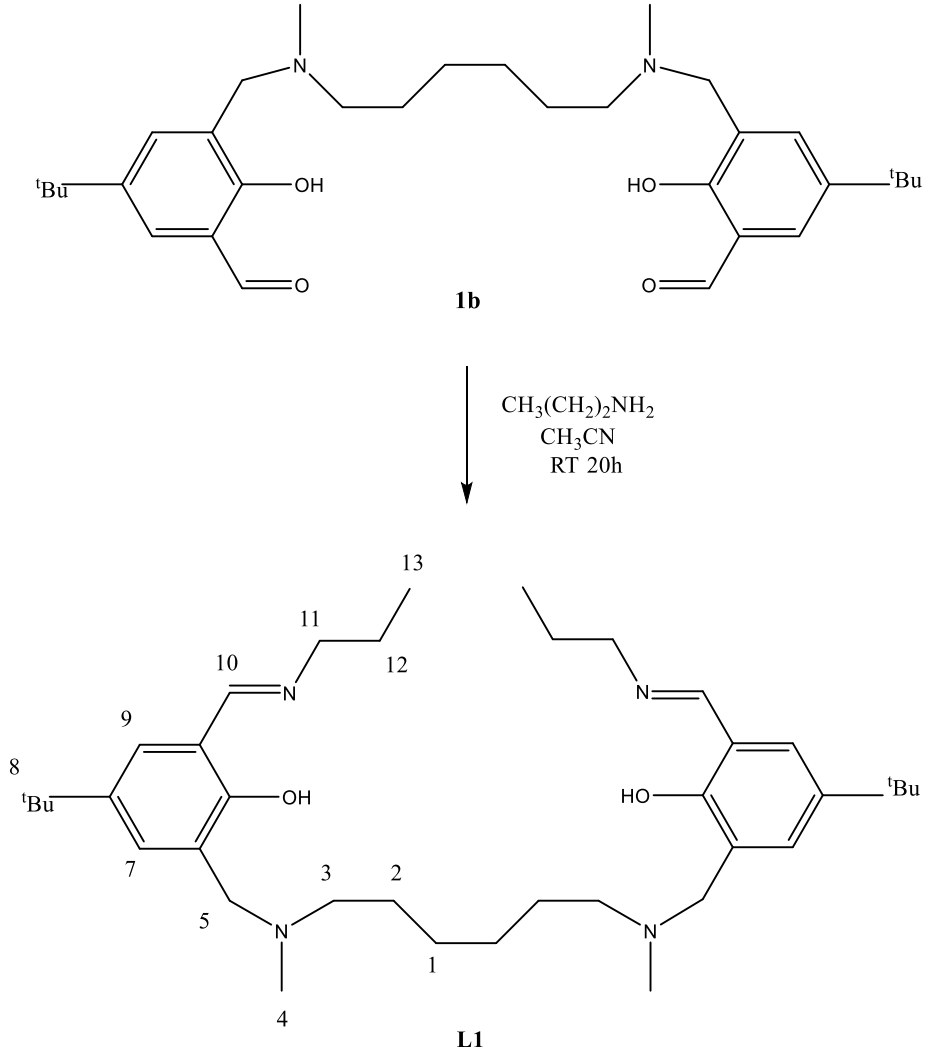

Figure 48. Structure of **L1**.

The procedure was followed from McGarry.[27]

N,N'-dimethyl-N,N'-hexamethylenedi(5-*tert*-butyl-2-hydroxybenzyaldehyde) (1.31 g 2.50 mmol) was added dropwise to propylamine (0.409 ml, 6.92 mmol) in acetonitrile (30.0 mL) under argon and left to stir at RT for a minimum of 12 hours. The solvent was evaporated in vacuo and the product was collected as a yellow/orange oil (1.40 g, 92.2%).

^{1}H NMR spectrum agreed with literature values: (500 MHz; $CDCl_3$) δ 8.35 (2H, s, *C12*), 7.39 (2H, d, J = 2 Hz, *C7*), 7.16 (2H, d, J = 2 Hz, *C11*), 3.57 (4H, s, *C5*), 3.57 (4H, td, *C13*), 2.40 (4H, t, J = 7.5 Hz, *C3*), 2.25 (6H, s, *C4*), 1.70 (4H, h, J = 7.25, *C14*), 1.55 (4H, m, *C2*), 1.30 (18H, s, *C10*), 1.30 (4H, m, *C1*), 0.97 (6H, t, J = 7.50, *C15*).

m/z (ESI) calculated $[M^{+}H]^{+}$= 606.49, found: 607.40. FT-IR (ATR): *ν*max(cm^{-1}) = 2961 vs (C-H stretch), 1634 s (C=N), 1469 m (C=C), 1222 w (C-N), 1050 w (C-O stretch). UV-Vis (MeOH: 56.7 x 10^{-6} M, λMax 402.5, 315.5, 270,246.5, 212.5; ε 2787, 2575, 4568, 8078, 19153 mol^{-1} L cm^{-1}).

7.3 Experimental Procedures and Characterisation of L2

7.3.1 Synthesis of *N, N'*-dimethyl-*p*-xylylenediamine (R2)

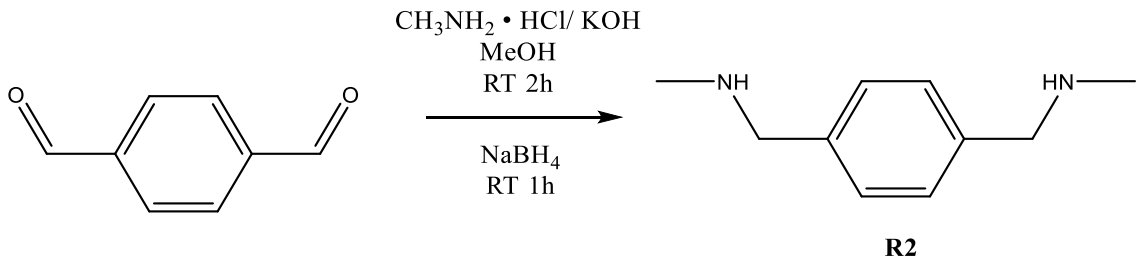

R2

Figure 49. Structure of **R2** precursor of **L2**.

The procedure was followed from Knapp.[26]

A dissolved solution of methylamine hydrochloride (3.12 g, 46.2 mmol) in methanol (60 ml) was added to a dissolved solution of potassium hydroxide (2.74 g, 49.7 mmol) in methanol (60 ml). Once the reaction seemed complete, it was filtered to get rid of the white powder. The filtered solution was added dropwise to a mixture of terephthalaldehyde (2.53 g, 18.2 mmol) in methanol (80 ml). The champagne-coloured solution was stirred at RT for 2 hours. Sodium borohydride (1.22 g, 33.9 mmol) was slowly added to the stirred solution to not lose any product and then stirred for 1 hour. The solvent was removed under reduced pressure and the resulting white powder was dissolved in chloroform (70 ml) and washed with water (50 ml x 4). The organic layer was separated and dried over anhydrous $MgSO_4$. The solvent was evaporated in vacuo to obtain a pale beige oil (2.49 g, 80.4%).

^{1}H NMR spectrum agreed with literature values: (500 MHz; $CDCl_3$) δ 7.20 (4H, s, *C1*), 3.66 (4H, s, *C2*), 2.37 (6H, s, *C4*), 1.32 (2H, s, *C3*).

7.3.2 Synthesis of *N, N'*-dimethyl-*p*-xylylenediamine-di(5-*tert*-butyl-2-hydroxy benzyaldehyde) (2b)

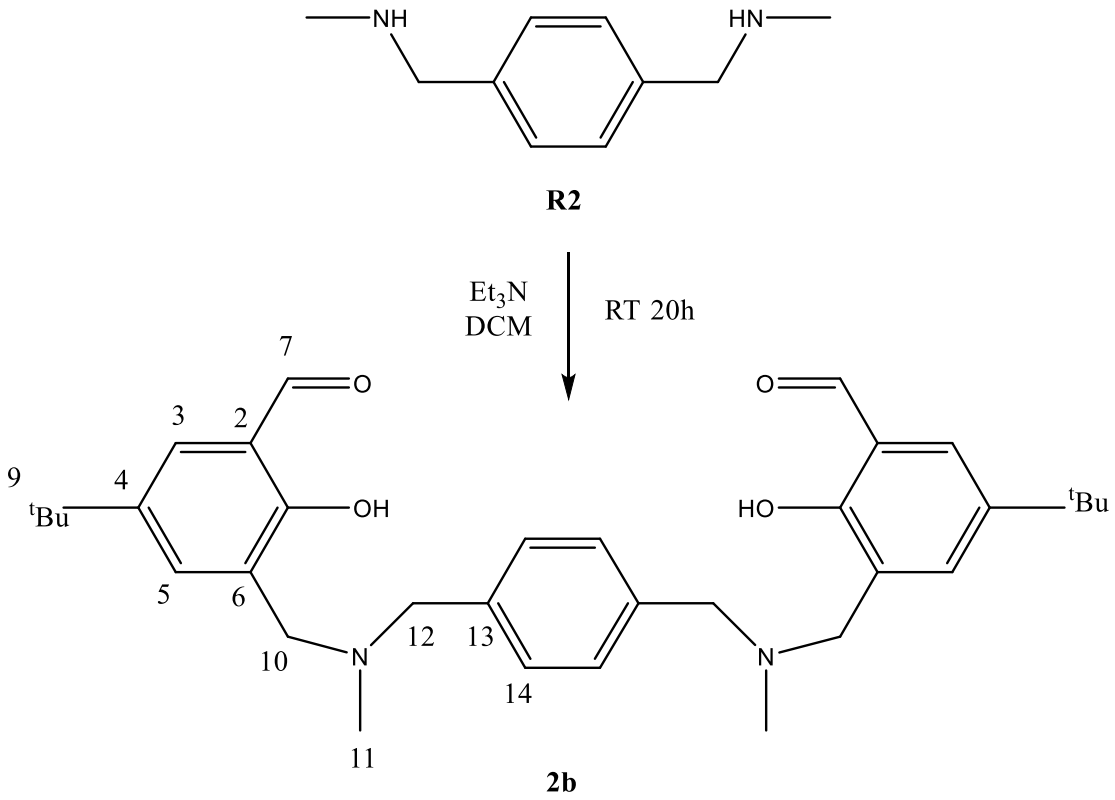

Figure 50. Structure of **2b**, the precursor to the **L2** ligand.

The procedure was followed from Knapp.[26]

Mixtures of 3-(bromomethyl)-5-*tert*-butyl-2-hydroxybenzaldehyde (6.78 g, 12.3 mmol) in dichloromethane (50 ml) and *N, N'*-dimethyl-*p*-xylylenediamine (2.016 g, 6.5 mmol) in methanol/dichloromethane (1:20, 50 ml) were added slowly dropwise to a stirred solution of triethylamine (2.93 g, 13.0 mmol) in dichloromethane (50 ml). The solution was left to stir in RT overnight. Once the reaction was checked for completion via 1H-NMR, the solvent was evaporated in vacuo. The yellow solid was redissolved in chloroform (80 ml) then filtered. The organic layer was washed with water (3 x 30 ml), separated and dried over anhydrous $MgSO_4$. The filtered solution was dried in vacuo to give a yellow oil (10.402 g, 126%).

^{1}H NMR spectrum agreed with literature values: (500 MHz; $CDCl_3$) δ 10.32 (2H, s, *C7*), 7.61 (2H, d, J = 2 Hz, *C3*), 7.38 (2H, d, J = 2 Hz, *C5*), 7.31 (4H, s, *C14*), 3.75 (4H, s, *C10*), 3.61 (4H, s, *C12*), 2.27 (6H, s, *C11*), 1.29 (18H, s, *C9*).

7.3.3 Synthesis of *N, N'*-dimethyl-*p*-xylylenediamine-di(3-(propylimino)-5-*tert*-butylphenol) (L2)

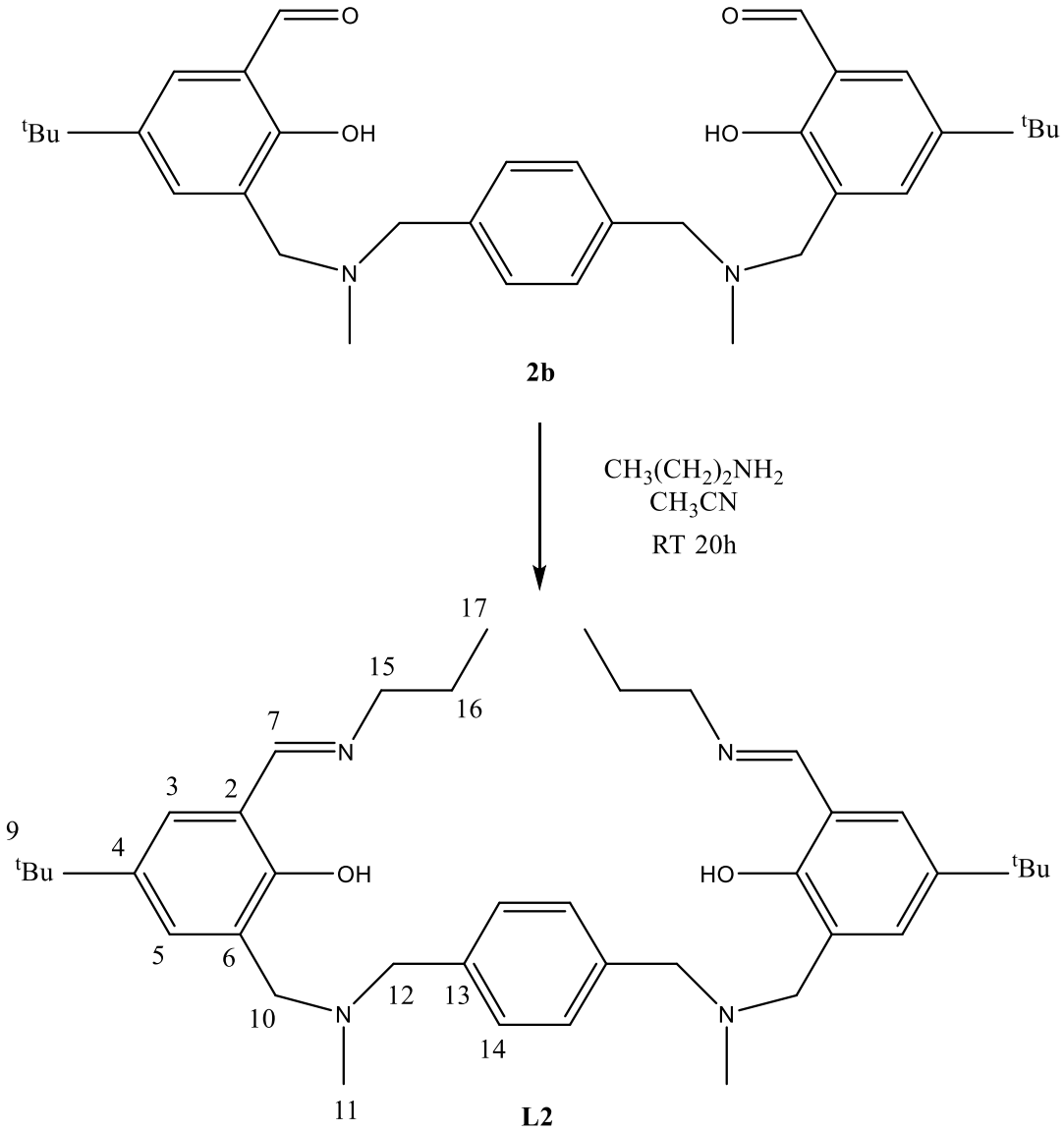

Figure 51. Structure of **L2**.

The procedure was followed from McGarry but using a different spacer to create a new ligand.[27]

N,N'-dimethyl-*N,N'*-hexamethylenedi(5-*tert*-butyl-2-hydroxybenzyaldehyde) (10.4 g 2.50 mmol) was added dropwise to propylamine (3.26 ml, 6.92 mmol) in acetonitrile (234.0 mL) under argon and left to stir at RT for a minimum of 12 hours. The solvent was

evaporated in vacuo and the product was collected as a pale beige oil (4.58 g, 48.3% over reactions **2b** & **c**).

^{1}H NMR spectrum agreed with literature values: (500 MHz; $CDCl_3$) δ 8.35 (2H, s, *C7*), 7.53 (2H, d, J = 2 Hz, *C3*), 7.31 (4H, s, *C14*), 7.15 (2H, d, J = 2 Hz, *C5*), 3.66 (4H, s, *C10*), 3.55 (4H, s, *C12*), 3.54 (4H, td, *C15*), 2.24 (6H, s, *C11*), 1.70 (4H, sx, J = 7, *C16*), 1.31 (18H, s, *C9*), 0.97 (6H, t, *C17*).

m/z (ESI) calculated $[M^+H]^+$= 626.46, found: 627.37. FT-IR (ATR): *ν*max(cm^{-1}) = 2962 vs (C-H stretch), 1634 s (C=N), 1464 m (C=C), 1223 w (C-N), 1039 w (C-O stretch), cm^{-1}. UV-Vis (MeOH: 43.7 x 10^{-6} M, λMax 402, 317, 246, 212; ε 1968, 2563, 8124, 22632 mol^{-1} L cm^{-1}).

7.4 Experimental Procedures and Characterisation of L3

7.4.1 Synthesis of *N, N'*-dimethyl-*m*-xylylenediamine (R3)

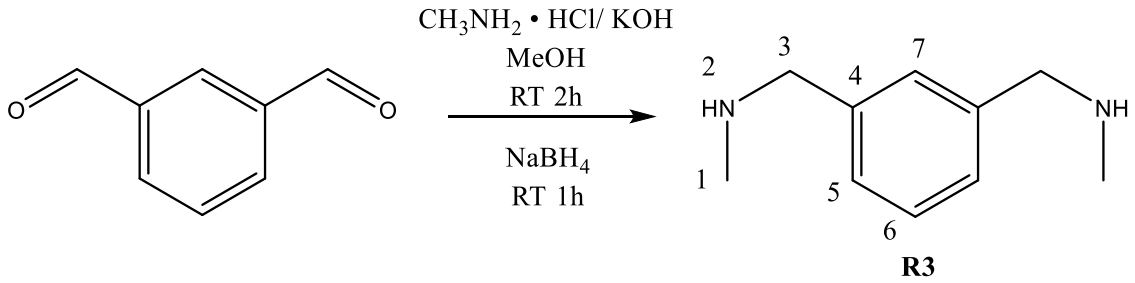

R3

Figure 52. Structure of the precursor **R3**.

The procedure was followed from Knapp.[26]

A dissolved solution of methylamine hydrochloride (0.877 g, 13.0 mmol) in methanol (40 ml) was mixed with a solution of potassium hydroxide (0.808 g, 14.4 mmol) in methanol (40 ml). The filtered solution was filtered to get rid of the white powder. The filtered solution was then slowly added dropwise into a solution of isophthalaldehyde (0.522 g, 3.89 mmol) in methanol (40 ml) over 1 hour. The champagne-coloured solution was stirred at RT for 2 hours. Sodium borohydride (0.314 g, 8.30 mmol) was added in small amounts to the stirred solution so that no product was lost and was left to stir for 1 hour. The solvent was evaporated in vacuo and the remaining white solid was dissolved in chloroform (40 ml) and washed with water (40 ml). The organic layer was separated and dried over anhydrous $MgSO_4$. The product was concentrated in vacuo, resulting in a pale-yellow oil (0.608 g, 95%).

^{1}H NMR spectrum agreed with literature values: (500 MHz; $CDCl_3$) δ 7.23 (2H, m, *C5* & *7*), 7.23 (2H, s, *C6*), 3.68 (4H, d, *C3*), 2.24 (6H, d, *C1*), 1.46 (2H, s, *NH*).

7.4.2 Synthesis of *N, N'*-dimethyl-*m*-xylylenediamine-di(5-*tert*-butyl-2-hydroxy benzaldehyde) (3b)

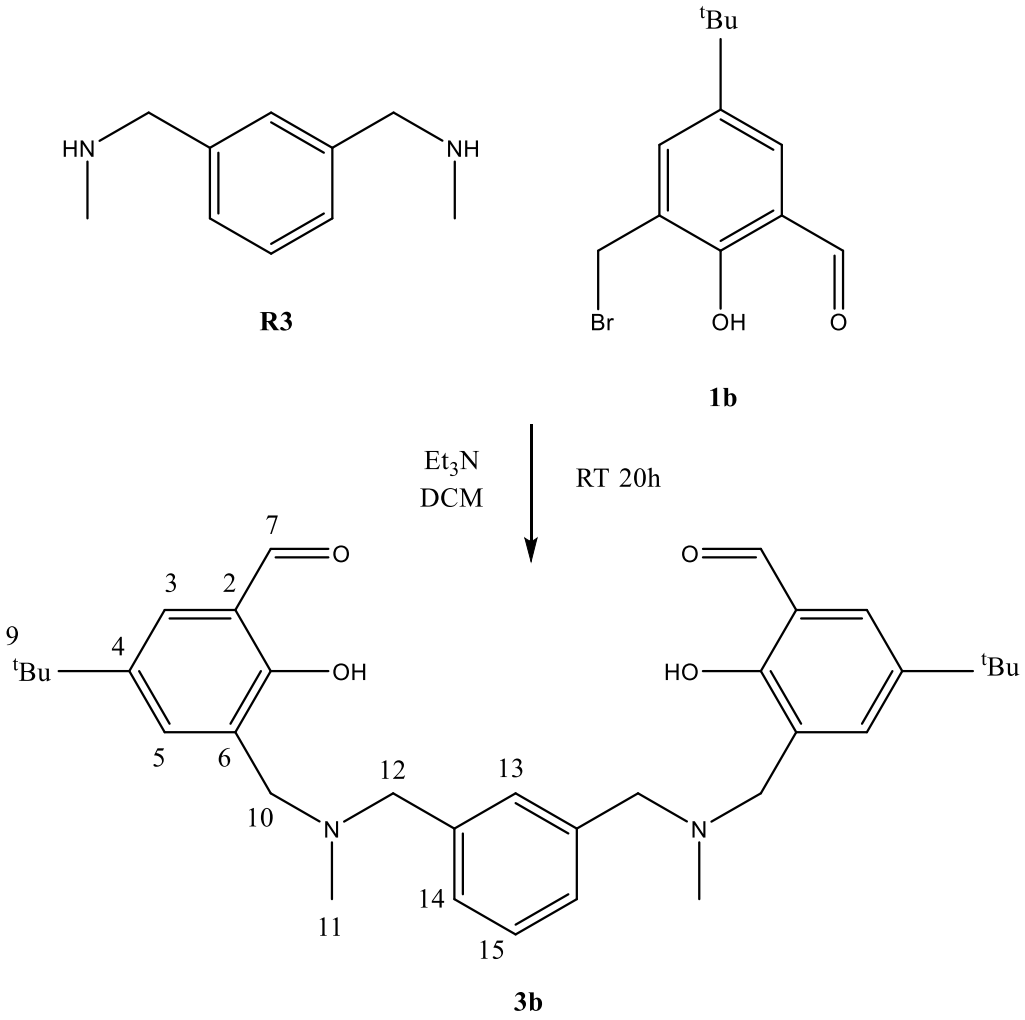

Figure 53. Structure of **3b**, the precursor to **L3**.

The procedure was followed from Knapp.[26]

Solutions of 3-(bromomethyl)-5-*tert*-butyl-2-hydroxybenzaldehyde (2.007 g, 7.42 mmol) in dichloromethane (80 ml) and *N, N'*-dimethyl-*m*-xylylenediamine (0.608 g, 3.75 mmol) in dichloromethane (80 ml) were added dropwise to a stirred solution of triethylamine (0.900 g, 8.89 mmol) in dichloromethane (60 ml). The mixture was left to stir at RT overnight. The reaction was monitored for completion via ^{1}H-NMR. The solvent was reduced to (50 ml) and then the dichloromethane was washed with water (2 x 20 ml),

separated, and dried over anhydrous $MgSO_4$. The solvent was evaporated in vacuo and the product was collected and washed with diethyl ether and dried in vacuo to give a yellow solid (0.807 g, 41%).

^{1}H NMR spectrum agreed with literature values: (500 MHz; $CDCl_3$) δ 10.33 (2H, s, *C7*), 7.62 (2H, d, J= 2 Hz, *C3*), 7.39 (1H, d, *C5*), 7.31 (1H, m, *C16*), 7.31 (1H, s, *H14*), 7.31 (2H, d, *C15*) 3.75 (4H, s, *C10*), 3.62 (4H, s, *C12*), 2.28 (6H, s, *C11*), 1.30 (18H, s, *C9*).

7.4.3 Synthesis of *N, N'*-dimethyl-*m*-xylylenediamine-di(3-(propylimino)-5-*tert*-butylphenol) (L3)

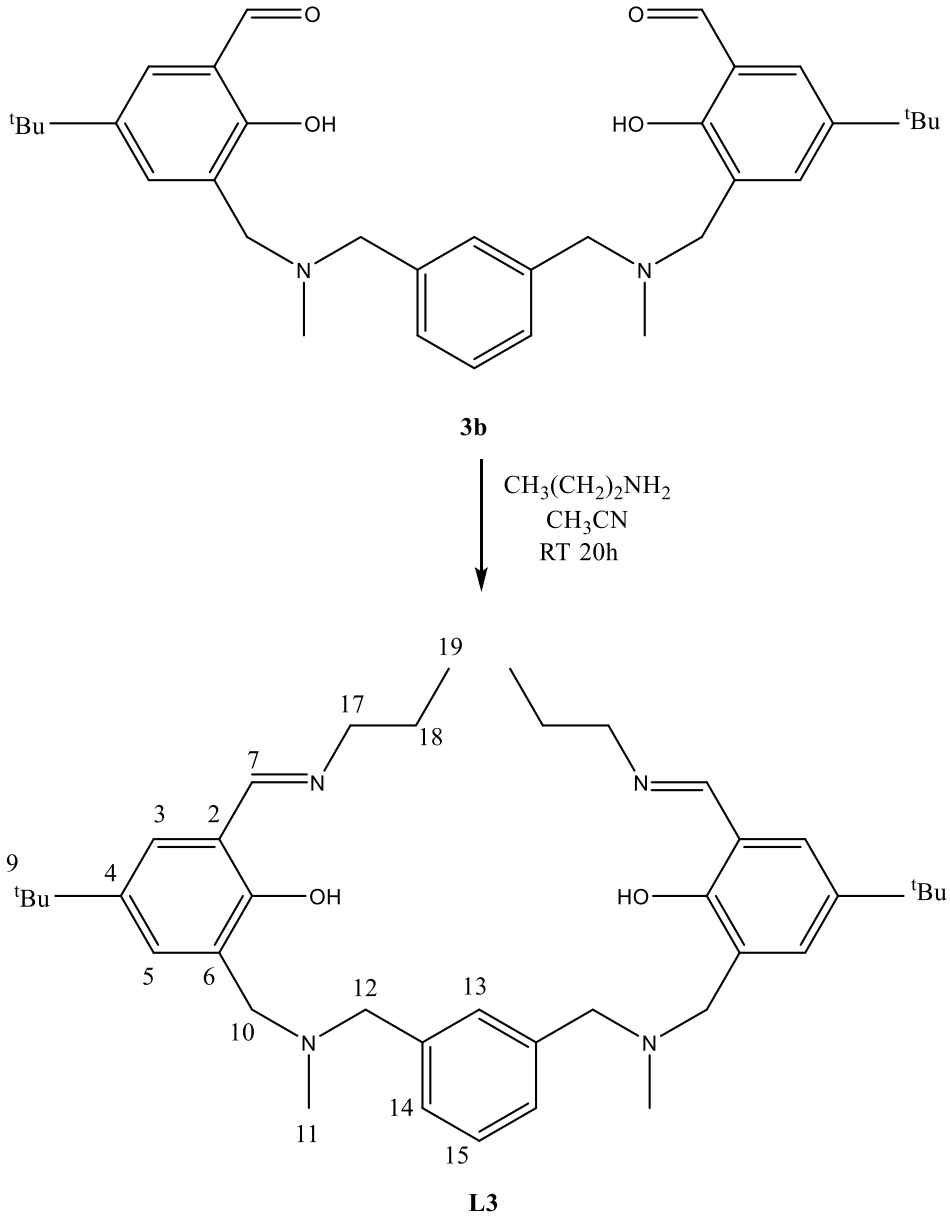

Figure 54. Structure of **L3**.

The procedure was followed from McGarry.[27] This synthesis method was used for **L4** by switching the propylamine with octylamine to make a new ligand for the solvent extraction experiment.

N, N'-Dimethyl-*m*-xylylenediamine-di(5-*tert*-butyl-2-hydroxybenzaldehyde) (10.4 g 2.50 mmol) was added dropwise to propylamine (3.26 ml, 6.92 mmol) in acetonitrile (234.0 mL) under argon and left to stir at RT for a minimum of 12 hours. The solvent was evaporated in vacuo and the product was collected as a pale beige oil (4.58 g, 48.3% overall).

^{1}H NMR spectrum agreed with literature values: (500 MHz; $CDCl_3$) δ 8.35 (2H, s, *C7*), 7.54 (2H, d, J = 2, *C3*), 7.37 (2H, d, *C5*), 7.27 (1H, t, *C16*), 7.15 (2H, s, *C14*), 7.15 (1H, d, J = 2 Hz, *C15*), 3.66 (4H, q, *C10*), 3.56 (4H, td, *C12*), 2.25 (6H, s, *C11*), 1.71 (4H, h, J = 7, *C17*), 1.30 (18H, s, *C18*, *9*), 0.97 (6H, t, J = 7.40, *C19*).

m/z (ESI) calculated $[M^{+}H]^{+}$= 626.46, found: 627.35. FT-IR (ATR): *ν*max(cm^{-1}) = 2961 vs (C-H stretch), 1634 s (C=N), 1470 m (C=C), 1275 (C-N), 1039 (C-O stretch), cm^{-1}. UV-Vis (MeOH: 43.7 x 10^{-6} M, λMax 402, 317, 246, 212; ε 1968, 2563, 8124, 22632 $mol^{-1}Lcm^{-1}$).

7.5 Complexation Methods with L1 and L3

7.5.1 C1: $[BF_4 \subset Ni_2(L1)_3](BF_4)_3$

Using the method from McGarry, a dissolved solution of $Ni(BF_4)_2 \cdot 6H_2O$ (20.6 mg, 0.0605 mmol) in ethanol (3.00 mL) was added to **L1** (60.25 mg, 0.0994 mmol) in ethanol (3.00 mL).[27] Crystals were noted after two months of vapour diffusion with diethyl ether. Yield (0.098 g, 71%).

FT-IR (ATR): *ν*max(cm^{-1}) = 2961 br (C-H stretch), 1626 s (C=C), 1475 m (C-H), 1225 w (C-N), 1052 br (C-O). UV-Vis (MeOH: 8.77 x 10^{-6} M; λMax 365.5, 227.5; ε 20068, 96351 mol^{-1} L cm^{-1}). Conductivity (MeOH): λ = 257.46 S cm^2 mol^{-1}, Ion ratio 1:2.

Crystal Data for $C_{114}H_{186}B_4N_{12}O_6F_{16}Ni_2$ (M = 2266.89 g/mol): orthorhombic, space group $P2_12_12_1$, a = 19.1177(10) Å, b = 23.6421(12) Å, c = 28.6245(14) Å, α = 90°, β = 90°, γ = 90°, V = 12937.8(11) Å3, Z = 4, T = 100 K, μ(CuKα) = 1.00 mm^{-1}, ρcalc = 1.164 g/cm3, 139060 reflections measured (4.848° ≤ 2Θ ≤ 145.54°), 24933 unique (*R*int = 0.0909, *R*sigma = 0.0687) which were used in all calculations. The final R_1 was 0.1358 (I > 2σ(I)) and wR_2 was 0.3512.

7.5.2 C2: $[ClO_4 \subset Ni_2(L1)_3](ClO_4)_3$

Using the method from McGarry, a dissolved solution of $Ni(ClO_4)_2 \cdot 6H_2O$ (23.4 mg, 0.0640 mmol) in ethanol (3.00 mL) was added to **L1** (79.25 mg, 0.1307 mmol) in ethanol (3.00 mL).[27] Crystals were noted after 1 week of vapour diffusion with diethyl ether (0.1047 g, 69.3%).

FT-IR (ATR): *ν*max(cm^{-1}) = 2959 br (C-H stretch), 1625 m (C=C), 1472 m (C-H), 1224 m (C-N), 1081 br (C-O). UV-Vis (MeOH: 29.64 x 10^{-6} M; λMax 364, 227.5; ε 11572, 54588 mol^{-1} L cm^{-1}). Conductivity (MeOH): λ = 134.03 S cm^2 mol^{-1}, Ion ratio 1:1. Elemental analysis calc. (%) for $C_{126}H_{216}Cl_4N_{12}Ni_2O_{26}$: C 58.62, H 8.03, N 7.20; found: C 56.53, H 8.25, N 5.11.

Crystal Data for $C_{114}H_{186}Cl_4N_{12}Ni_2O_{22}$ (M = 2574.32 g/mol): orthorhombic, space group $P2_12_12_1$, a = 19.2749(7) Å, b = 23.4874(8) Å, c = 28.3888(9) Å, α = 90°, β = 90°, γ = 90°, V = 12852.1(8) Å3, Z = 4, T = 100 K, μ(CuKα) = 1.741 mm^{-1}, ρcalc = 1.330 g/cm3, 232146 reflections measured (4.882° ≤ 2Θ ≤ 152.356°), 25424 unique (*R*int = 0.0525, *R*sigma = 0.0265) which were used in all calculations. The final R_1 was 0.0680 (I > 2σ(I)) and wR_2 was 0.2472.

7.5.3 C3: $[SO_4 \subset Ni_2(L3)_2][Ni(SO_4)_2(EtOH)_4]$

A dissolved solution of $NiSO_4 \cdot 6H_2O$ (36.9 mg, 0.131 mmol) in ethanol (3.00 mL) was added to **L3** (62 mg, 0.099 mmol) in ethanol (3.00 mL). Crystals were noted after 1-2 days of vapour diffusion with diethyl ether.

FT-IR (ATR): *ν*max(cm^{-1}) = 2958 br (C-H stretch), 2869 m (C=C), 1627 s (C-H), 1466 m (C-H), 1380 w (C-H), 1039 w (C-N). UV-Vis (MeOH: 666.9 x 10^{-6} M; λMax 378, 230.5; ε 379.39, 1436.58 mol^{-1} L cm^{-1}). Conductivity (MeOH): λ = 100.96 S cm^2 mol^{-1}, Ion ratio 1:1.

Crystal Data for $C_{88}H_{140}N_8Ni_3O_{28}S_3$ (M = 2101.276 g/mol): triclinic, space group *P*-1, a = 19.3807(8) Å, b = 22.2151(59) Å, c = 27.5811(11) Å, α = 85.99°, β = 80.44°, γ = 85.69°, V = 11657(8) Å3, Z = 4, T = 100 K, μ(CuKα) = 1.616 mm^{-1}, ρcalc = 1.208 g/cm3, 302936 reflections measured (3.254° ≤ 2Θ ≤ 140.948°), 44149 unique (*R*int = 0.0378, *R*sigma = 0.0272) which were used in all calculations. The final R_1 was 0.0930 (I > 2σ(I)) and wR_2 was 0.2582.

7.5.4 C4: $[ClO_4 \subset Ni_2(L3)_2](ClO_4)_2$

A dissolved solution of $Ni(ClO_4)_2 \cdot 6H_2O$ (0.539 mg, 0.0640 mmol) in ethanol (3.00 mL) was added to **L3** (0.125 mg, 0.0022 mmol) in ethanol (3.00 mL). Crystals were noted after one month of vapour diffusion with diethyl ether.

FT-IR (ATR): *v*max(cm^{-1}) = 2962 br (C-H stretch), 2871 m (C=C), 1627 s (C-H alkene), 1464 m (C-H alkane), 1394 w (C-H), 1036 m (C-N). UV-Vis (MeOH: 29.64 x 10^{-6} M; λMax 364, 227.5; ε 11572, 54588 $mol^{-1}Lcm^{-1}$). Conductivity (MeOH): λ = 134.03 S cm^2 mol^{-1}, Ion ratio 1:1. Elemental analysis calc. (%) for $C_{126}H_{216}Cl_4N_{12}Ni_2O_{26}$: C 58.62, H 8.03, N 7.20; found: C 56.53, H 8.25, N 5.11.

Crystal Data for $C_{80}H_{116}Cl_3N_8Ni_2O_{16}$ (*M* =1669.601 g/mol): monoclinic, space group $P2_1/n$ (no. 14), *a* = 25.2959(7) Å, *b* = 16.0466(4) Å, *c* = 25.2963(7) Å, β = 102.900(1)°, *V* = 10008.9(5) $Å^3$, *Z* = 4, *T* = 100.0 K, μ(Cu Kα) = 2.034 mm^{-1}, ρ*calc* = 1.108 g/cm^3, 138685 reflections measured (4.46° ≤ 2Θ ≤ 144.48°), 18813 unique (R_{int} = 0.0370, R_{sigma} = 0.0229) which were used in all calculations. The final R_1 was 0.0401 (I>=2u(I)) and wR_2 was 0.1151.

7.5.5 C5: $[SO_4 \subset Ni_2(L3)_2](ClO_4)_2$

A dissolved solution of $NiSO_4 \cdot 6H_2O$ (88.1 mg, 0.314 mmol), $NaClO_4$ (21.1 mg, 0.172 mmol) in ethanol (1.00 mL) was added to **L3** (178 mg 0.284 mmol) in ethanol (3.00 mL). A small amount of dark green crystals were noted after a few weeks of vapour diffusion with diethyl ether.

Crystal Data for $C_{80}H_{116}Cl_2N_8Ni_2O_{16}S$ (M =1666.18 g/mol): monoclinic, space group $P2_1/n$ (no. 14), a = 25.2315(8) Å, b = 15.8548(5) Å, c = 25.4377(8) Å, β = 102.6600(10)°, V = 9928.7(5) Å^3, Z = 4, T = 100.00 K, μ(CuKα) = 1.631 mm^{-1}, ρ$calc$ = 1.115 g/cm^3, 111285 reflections measured (4.468° ≤ 2Θ ≤ 152.028°), 20319 unique (R_{int} = 0.0396, R_{sigma} = 0.0358) which were used in all calculations. The final R_1 was 0.0590 (I > 2σ(I)) and wR_2 was 0.1670.

7.5.6 C6: $[ClO_4 \subset Ni_2(L3)_2](BF_4)_2$

A dissolved solution of $Ni(BF_4)_2 \cdot 6H_2O$ (0.695 mg, 0.0071 mmol) in ethanol (1.00 mL) was added to **L3** (11 mg 0.0181 mmol) in ethanol (3.00 mL). Due to contamination, crystals with ClO_4 inside were noted after two months of vapour diffusion with diethyl ether (0.1365 g 84.1%).

Crystal Data for $C_{80}H_{116}B_2ClF_8N_8Ni_2O_8$ (M = 1644.30 g/mol): monoclinic, space group $P2_1/n$, a = 25.0801(10) Å, b = 15.9707 (6) Å, c = 25.4521 (10) Å, α = 90 °, β = 103 °, γ = 90°, V = 9935.8 (7) Å3, Z = 4, T = 101 K, μ(CuKα) = 1.54178 mm^{-1}, ρcalc = 1.119 g/cm3, 134441 reflections measured (4.47° ≤ 2Θ ≤ 145.028°), 19533 unique (*R*int = 0.0508, *R*sigma = 0.0306) which were used in all calculations. The final R_1 was 0.0569 (I > 2σ(I)) and wR_2 was 0.1618.

8.0 Alternative Investigations

The following experiments were not discussed in the chapters above as they would distract and add little value to the chapters. However, a short overview of the various experiments that were made may be of use for the understanding of the different directions this thesis has taken. The experimental aims were to form helicates that McGarry formed with better x-ray crystallography data, and to create new helicates with available and appropriate anions. Next an anion was added to the mesocate we formed to see if there would be any anion movement. When we failed to see any results, a new aim to synthesise longer ligands were adopted. In hindsight we spent an excess amount of time on the organic chemistry before switching to solvent extraction experiments.

8.1 Doping of L1 Mesocates

The mesocate used for doping experiments is $[ClO_4 \subset Ni_2(\mathbf{L1})_3](ClO_4)_3$. The washed crystal and anion were added together in methanol and left for slow vapour diffusion with diethyl ether. A summary of the experiment is shown in Table 44.

Table 43. The radii of anions.

Theoretical void space	Radii in Å
Br^-	1.96 ± 0.06
BF_4^-	2.11 ± 0.06
I^-	2.20 ± 0.09
ClO_4^-	2.22 ± 0.03
CrO_4^{2-}	2.29 ± 0.03
IO_4^-	2.31 ± 0.08
MnO_4	2.23 ± 0.03
$Fe(CN)_6^{-3}$	3.24 ± 0.17
Maleic hydrazide	2.51 ±0.09
PO_4^{3-}	2.3 ± 0.07
ReO_4^-	2.23 ± 0.04
SO_4^{2-}	2.18 ± 0.13

Table 44. Amount of crystals formed and doped.

Complex	Amount of crystal	Type of anion doped	Amount (g) of anion	Ratio
C1				
	0.0048	ReO_4	0.0018	1:3
	0.0056	Maleic hydrazide	0.0099	1:4
C2				
	0.0047	MnO_4	0.0012	1:4
	0.0046	ZnOtf	0.0189	1:2.7
	0.0248	$K_3[Fe(CN)_6]$	0.0126	1:3
	0.0435	MnO_4	0.0296	1:10
	0.0693	ReO_4	0.0681	1:8
	0.0651	ZnOtf	0.0876	1:8
	0.1047	Maleic hydrazide	0.0432	1:9
	0.0233	MnO_4	0.0121	1:10

8.2 General Ni Complex Synthesis with L1 with Dysprosium

An attempt to complex the ligand with dysprosium was carried out with **L1** and nickel salts.

8.2.1 $[Dy_4{\subset}NO_3(L1)_3](BF_4)_3$

A dissolved solution of **L1** (459 mg, 0.757 mmol) in methanol (1.00 mL) was added to $Dy(NO_3)_3{\cdot}6H_2O$ (346 mg, 0.7556 mmol) with a 1:1, 1:2, 2:3 ratio in DMF (1.00 mL) (459 mg, 0.757 mmol) in methanol (1.00 mL). At the addition of the metal salt, the solvent turned red.

8.2.2 $[Dy_4{\subset}O_3(L1)_3](BF_4)_3$

A dissolved solution of **L1** (459 mg, 0.757 mmol) in methanol (1.00 mL) was added to $Dy(O_3)_3{\cdot}6H_2O$ (346 mg, 0.7556 mmol) with a 1:1, 1:2, 2:3 ratio in DMF (1.00 mL) (459 mg, 0.757 mmol) in methanol (1.00 mL). At the addition of the metal salt, the solution was orange and white precipitate formed at the bottom.

8.2.3 $[Dy_4{\subset}Cl_3(L1)_3](BF_4)_3$

A dissolved solution of **L1** (459 mg, 0.757 mmol) in methanol (1.00 mL)was added to $Dy(Cl_3)_3 \cdot 6H_2O$ (346 mg, 0.7556 mmol) with a 1:1, 1:2, 2:3 ratio in DMF (1.00 mL) (459 mg, 0.757 mmol) in methanol (1.00 mL). At the addition of the metal salt, the solution turned yellow.

8.2.4 $[Dy_4 \subset (C_2O_4)_3(L1)_3](BF_4)_3$

A dissolved solution of **L1** (459 mg, 0.757 mmol) in methanol (1.00 mL)was added to $Dy(C_2O_4)_3 \cdot 6H_2O$ (346 mg, 0.7556 mmol) with a 1:1, 1:2, 2:3 ratio in DMF (1.00 mL) (459 mg, 0.757 mmol) in methanol (1.00 mL). At the addition of the metal salt, the solution turned yellow and formed a white precipitate.

8.3 Complexation Attempts with $NiCl_2$, L3 and Tetrahedral Oxyanions

To complex a dinuclear nickel complex with **L3** and a tetrahedral oxyanion in a structure where the oxyanion is bound to the nickel, various crystallisation attempts were made using the array of anions and solvents in Table 45 below. The solvents used were based off the solvents other researchers used to complex that anion. Some vials such as the CrO_4^- + formic acid, formed dark green metal salts.

Table 45. Complexation attempts with $NiCl_2$ + **L3**.

Solvents	**$KMnO_4$**	**KIO_4^-**	**HIO_4**	**CrO_4^{2-}**	**KPO_4**	**H_3PO_4**	**ReO_4^-**	**$BaMnO_4$**
MeOH	X	X	X	X	X	X	X	X
10% HCl	X	X	X	X	X	X	X	X
DMF	X	X	X	X	X	X	X	X
Acetic acid	X							X
EtOH	X	X	X	X	X	X	X	X
THF	X	X	X	X	X	X		X
$(CH_3)_2CO$	X	X	X	X	X	X	X	X
$CHCl_3$		X						
Formic acid		X	X	X		X	X	
$BnNH_2$		X	X	X		X	X	
MeCN					X		X	
TMA					X			

8.4 Synthesis Pathways of Different Ligands

The synthesis of a longer ligand was attempted. Several pathways were planned with attempts to make the synthesis pathway cheaper, safer and easier without compromising efficiency. The synthesis pathway in Figure 56 was planned with the goal of making a longer ligand and two ether groups for weak interactions with the anion. The final product of the reactions shown above would be the spacer that is reacted with the salicylaldimine group following the procedure in Figure 48 and 49. The first reaction was not attempted because a few of the reagents in the latter stages of the reaction was not available.

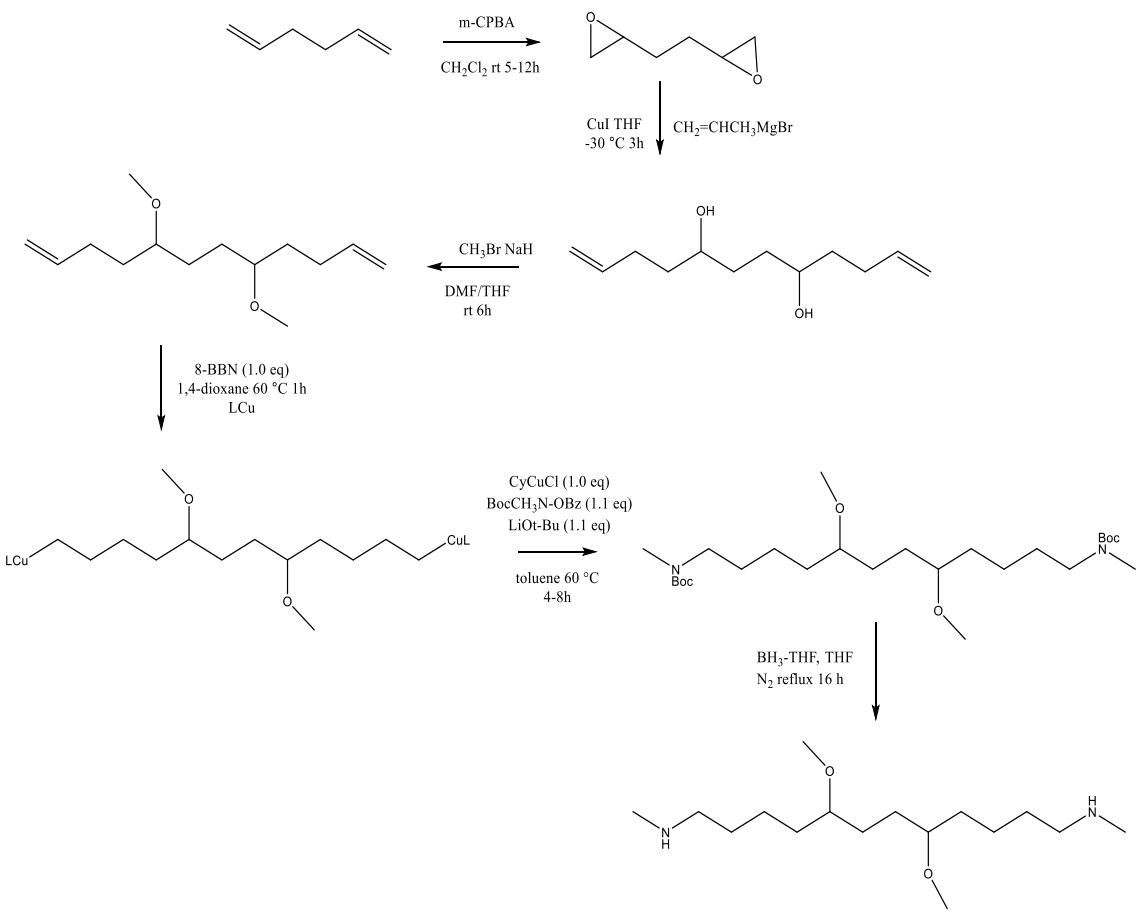

Figure 55. Pathway 1 of potential new ligand.

In the synthesis pathway below (Figure 57), the addition of the protecting group (Appendix B2.1) worked efficiently in many repeated experiments.

However, the Curtius rearrangement procedure outlined in Appendix B2.2 was attempted numerous times with different amounts of reactants, different methods of keeping the reaction dry, and time spent mixing. If another attempt was possible, it may be of interest to heat to room temperature rather than leaving the solution to slowly rise in temperature. Also, a different method of purification such a distillation may lead to better characterisation results.

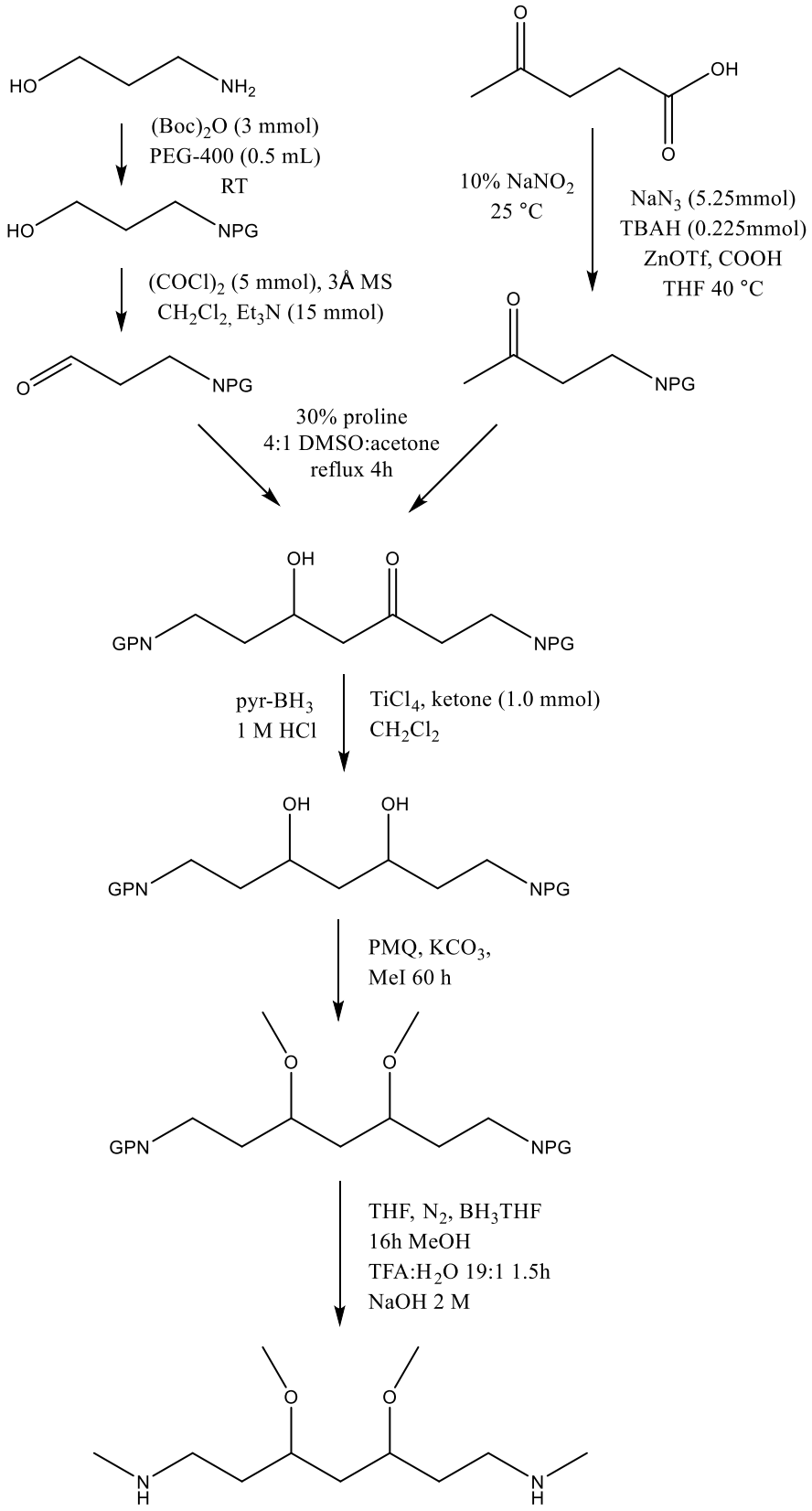

Figure 56. Pathway 2 of potential new ligand.

For pathway 3 in Figure 58, the right side was followed up to the step where Pd/C was required. A favourable aspect of pathways 1 and 3, is that there is no need to add a methyl group onto the Boc-protected amine which is a bonus as this step can be tricky. However due to a lack of time, the synthesis was halted, and the focus was placed on solvent extraction instead.

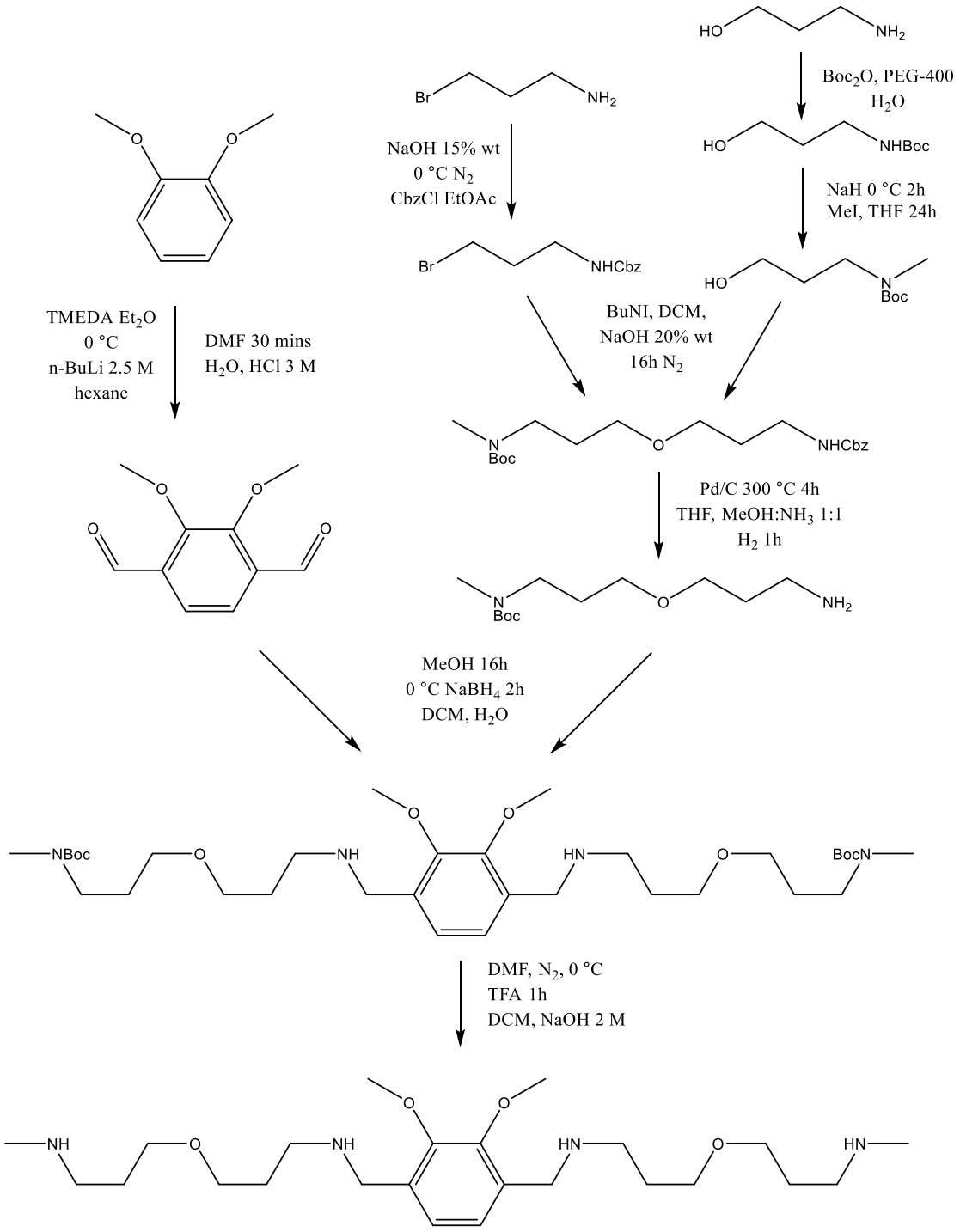

Figure 57. Pathway 3 for a potential new ligand.

Conclusion

The aim of this research was to complex helicates with anions trapped inside its structure. With the two ligands **L1** and **L3**, four different mesocates and an extra two with different spectator anions were complexed and characterised using various methods.

Complexations with **L1** which has a C6 spacer, afforded M_2L_3 mesocates with an anion in the centre bound by only weak hydrogen bonds. **C1** $[BF_4{\subset}Ni_2(\mathbf{L1})_3](BF_4)_3$ provided a structure that showed a lot of disorder in the X-ray crystallography structure. **C2** $[ClO_4{\subset}Ni_2(\mathbf{L1})_3](ClO_4)_3$ had less disorder and was a relatively faster forming mesocate.

Complexations with **L3** which has a *m*-xylylic spacer created interesting M_2L_2 mesocates with a covalent bond between the oxygen groups of the tetrahedral oxyanion and the nickel. From the average distortion values, it was found that the two complexes **C3** $[SO_4{\subset}Ni_2(\mathbf{L3})_2][Ni(SO_4)_2(EtOH)_4]$ and **C4** $[ClO_4{\subset}Ni_2(\mathbf{L3})_2](ClO_4)_2$ had similar levels of distortion.

Complexations with Dy^{3+} was attempted but unsuccessful. With the assumption that the ligands are too short to accommodate any larger anions or metals than ones successfully complexed, new ligands were designed. Although plans for synthesis were made, the execution of them was unsuccessful, especially the Curtius reaction. Due to a lack of time, the focus was placed on solvent extraction.

The solvent extraction procedure was loosely based on an experiment conducted by Akkus *et al.*, and Jung *et al.*[19,71] Using Orform SX7/decyl alcohol, we sought to confirm if **L3** is sufficient to replace a phosphoric acid ester extractant such as Cyanex 272 for nickel extraction. Several repeats of the experiment were required to smoothen problems such as equal mixing and unexplainable data. It was not until the experiment with hexane that the analysis of the aqueous phase on the AAS gave substantial results. The organic phase was giving nickel extraction percentages less than 1% while the aqueous phase results gave values between 40%-95%. The highest nickel percentage measured from the hexane extraction was 89% but with a repeat of this experiment with optimal conditions, better results might be possible.

Future Work

For the continuation of the study on salicylaldimine mesocates, the complexation of mesocates with different tetrahedral oxyanions and metals can be continued. For larger metal ions or oxyanions bigger than ClO_4^- and SO_4^{2-}, it may be helpful to use a longer ligand. Attempts to follow pathway 3 or 4 for a longer ligand may work to help encapsulate larger anions or metals.

Alternatively, a repeat of the crystallisations and more characterisation techniques may be of use to clarify certain aspects of the structures such as the charge balance of **C4** and **C6**. Methods such as sulfate or chloride analysis may provide further insight.

In addition, a repeat of the solvent extraction may be helpful to determine the validity of our results and obtain improved results. The collection of equilibrium data and the plot of a McCabe Thiele diagram shows how many stages are needed to a sufficient extraction and what A:O ratio will optimise the solvent extraction. It may be worthwhile to try the A:O ratios 5:1 and 2:1. From the results in the final experiment, an extraction of nickel with hexane and **L4**, at pH 10 and A:O 1:5 may give a percentage higher than 89% of the nickel extracted.

A similar repeat of the method used for the hexane extraction with decanol may also give better results. If there had been more time, we would have repeated the experiment with extra steps to make sure the barium chloranilate and nickel sulfate was sufficiently dissolved. Also, we would have carried out ion chromatography when preparing for the SO_4^{2-} analysis and repeated the experiment with a higher A:O ratio. It would have been interesting to use different diluents such as kerosene or other aromatic diluents, and a variety of extractant concentrations.

On the other hand, the addition of Co^{2+} or other metals or anions can increase the ionic strength of the solutions and decrease the transfer rate of nickel. It may of interest to use other purification methods to isolate the nickel in the aqueous solution and to extract other metals into the organic phase.

References

(1) Fatin-Rouge, N.; Blanc, S.; Pfeil, A.; Rigault, A.; Albrecht-Gary, A.; Lehn, J. Self-assembly of Tricuprous Double Helicates: Thermodynamics, Kinetics, and Mechanism. *Helv. Chim. Acta* **2001**, *84* (6), 1694–1711.

(2) Piguet, C.; Bernardinelli, G.; Hopfgartner, G. Helicates as Versatile Supramolecular Complexes. *Chem. Rev.* **1997**, *97* (6), 2005–2062. https://doi.org/10.1021/cr960053s.

(3) Wu, N.; Melan, C. F.; Stevenson, K. A.; Fleischel, O.; Guo, H.; Habib, F.; Holmberg, R. J.; Murugesu, M.; Mosey, N. J.; Nierengarten, H. Systematic Study of the Synthesis and Coordination of 2-(1, 2, 3-Triazol-4-Yl)-Pyridine to Fe (II), Ni (II) and Zn (II); Ion-Induced Folding into Helicates, Mesocates and Larger Architectures, and Application to Magnetism and Self-Selection. *Dalton Trans.* **2015**, *44* (33), 14991–15005.

(4) Hannon, M. J.; Childs, L. J. Helices and Helicates: Beautiful Supramolecular Motifs with Emerging Applications. *Supramol. Chem.* **2004**, *16* (1), 7–22.

(5) Flint, K. L.; Collins, J. G.; Bradley, S. J.; Smith, T. A.; Sumby, C. J.; Keene, F. R. Synthesis and Characterisation of Helicate and Mesocate Forms of a Double-Stranded Diruthenium (II) Complex of a Di (Terpyridine) Ligand. *Aust. J. Chem.* **2019**, *72* (10), 762–768.

(6) Lehn, J.; Sanders, J. Supramolecular Chemistry. Concepts and Perspectives. *Angew. Chem.-Engl. Ed.* **1995**, *34* (22), 2563.

(7) Mayans, J.; Font-Bardia, M.; Di Bari, L.; Arrico, L.; Zinna, F.; Pescitelli, G.; Escuer, A. From Mesocates to Helicates: Structural, Magnetic and Chiro-Optical Studies on Nickel (II) Supramolecular Assemblies Derived from Tetradentate Schiff Bases. *Chem. Eur. J.* **2018**, *24* (30), 7653–7663.

(8) Cardo, L.; Nawroth, I.; Cail, P. J.; McKeating, J. A.; Hannon, M. J. Metallo Supramolecular Cylinders Inhibit HIV-1 TAR-TAT Complex Formation and Viral Replication in Cellulo. *Sci. Rep.* **2018**, *8* (1), 1–7.

(9) Kim, M. J.; Lee, H.-W.; Moon, D.; Jeong, K.-S. Helically Foldable Diphenylureas as Anion Receptors: Modulation of the Binding Affinity by the Chain Length. *Org. Lett.* **2012**, *14* (19), 5042–5045.

(10) Malina, J.; Hannon, M. J.; Brabec, V. Recognition of DNA Bulges by Dinuclear Iron (II) Metallosupramolecular Helicates. *FEBS J.* **2014**, *281* (4), 987–997.

(11) Massena, C. J. Triple-Helicate Self-Assembly, Dynamics, and Anion Binding of Halogen-Bonding m-Arylene-Ethynylene Oligomers. **2018**.

(12) Allison, S. J.; Cooke, D.; Davidson, F. S.; Elliott, P. I.; Faulkner, R. A.; Griffiths, H. B.; Harper, O. J.; Hussain, O.; Owen-Lynch, P. J.; Phillips, R. M. Ruthenium-Containing Linear Helicates and Mesocates with Tuneable P53-Selective Cytotoxicity in Colorectal Cancer Cells. *Angew. Chem.* **2018**, *130* (31), 9947–9952.

(13) Gómez-González, J.; Peña, D. G.; Barka, G.; Sciortino, G.; Maréchal, J.-D.; Vázquez López, M.; Vázquez, M. E. Directed Self-Assembly of Trimeric DNA-Bindingchiral Miniprotein Helicates. *Front. Chem.* **2018**, *6*, 520.

(14) Srinivasan, A.; Viraraghavan, T. Perchlorate: Health Effects and Technologies for Its Removal from Water Resources. *Int. J. Environ. Res. Public. Health* **2009**, *6* (4), 1418–1442.

(15) Kontovas, C. A. Integration of Air Quality and Climate Change Policies in Shipping: The Case of Sulphur Emissions Regulation. *Mar. Policy* **2020**, *113*, 103815.

(16) Grennfelt, P.; Engleryd, A.; Forsius, M.; Hov, Ø.; Rodhe, H.; Cowling, E. Acid Rain and Air Pollution: 50 Years of Progress in Environmental Science and Policy. *Ambio* **2020**, *49* (4), 849–864. https://doi.org/10.1007/s13280-019-01244-4.

(17) Bacon, G.; Mihaylov, I. Solvent Extraction as an Enabling Technology in the Nickel Industry. *J. South Afr. Inst. Min. Metall.* **2002**, *102*, 435–443.

(18) Kihlbom, C. Separation of Cobalt and Nickel Using CYANEX 272 for Solvent Extraction. **2021**.
(19) Akkus, N.; Campbell, J. C.; Davidson, J.; Henderson, D. K.; Miller, H. A.; Parkin, A.; Parsons, S.; Plieger, P. G.; Swart, R. M.; Tasker, P. A. Exploiting Supramolecular Chemistry in Metal Recovery: Novel Zwitterionic Extractants for Nickel (II) Salts. *Dalton Trans.* **2003**, No. 10, 1932–1940.
(20) Smolinski, T.; Wawszczak, D.; Deptula, A.; Lada, W.; Olczak, T.; Rogowski, M.; Pyszynska, M.; Chmielewski, A. G. Solvent Extraction of Cu, Mo, V, and U from Leach Solutions of Copper Ore and Flotation Tailings. *J. Radioanal. Nucl. Chem.* **2017**, *314* (1), 69–75. https://doi.org/10.1007/s10967-017-5383-y.
(21) Cox, E.; Sharratt, E.; Wardlaw, W.; Webster, K. 27. The Planar Configuration of Quadricovalent Compounds of Bivalent Copper and Nickel. *J. Chem. Soc. Resumed* **1936**, 129–133.
(22) Tsai, M.-J.; Tsai, C.-J.; Lin, K.; Wu, J.-Y. Anion-Dominated Copper Salicyaldimine Complexes-Structures, Coordination Mode of Nitrate and Decolorization Properties toward Acid Orange 7 Dye. *Polymers* **2020**, *12* (9). https://doi.org/10.3390/polym12091910.
(23) Wenzel, M.; Bruere, S. R.; Knapp, Q. W.; Tasker, P. A.; Plieger, P. G. Zwitterionic Dicopper Helicates: Anion Encapsulation and Binding Studies. *Dalton Trans.* **2010**, *39* (11), 2936–2941.
(24) Plieger, P. G.; Parsons, S.; Parkin, A.; Tasker, P. A. Transport of Metal Salts; Encapsulation of Anions in Dinuclear Cu (Ii) Complexes [Cu 2 L 2 SO 4] SO 4 and [Cu 2 L 2 BF 4](BF 4) 3, Where L= 2, 2'-[1, 6-Hexanediylbis [(Methylimino) Methylene]] Bis [4-Tert-Butyl-6-(Phenylazomethinyl) Phenol]. *J. Chem. Soc. Dalton Trans.* **2002**, No. 21, 3928–3930.
(25) Wenzel, M.; Jameson, G. B.; Ferguson, L. A.; Knapp, Q. W.; Forgan, R. S.; White, F. J.; Parsons, S.; Tasker, P. A.; Plieger, P. G. Anion-Induced Contraction of Helical Receptors. *Chem. Commun.* **2009**, No. 24, 3606–3608.
(26) Knapp, Q. W. The Spectroscopic Analysis of Di-Copper Helicates as Receptors for Encapsulating Anions: A Thesis Presented in Partial Fulfilment of the Requirements for the Degree of Master of Science in Chemistry at Massey University, Palmerston North, New Zealand. **2009**.
(27) McGarry, Liam. Dinuclear Triple-Stranded Anion Binding Capsules with C6 Linkers, IFS Chemistry, Massey University, Palmerston North, New Zealand, 2018.
(28) Cui, F.; Li, S.; Jia, C.; Mathieson, J. S.; Cronin, L.; Yang, X.-J.; Wu, B. Anion-Dependent Formation of Helicates versus Mesocates of Triple-Stranded M2L3 (M= Fe2+, Cu2+) Complexes. *Inorg. Chem.* **2012**, *51* (1), 179–187.
(29) Gonciarz, A.; Żuber, M.; Zwoździak, J. Spectrochemical Properties and Solvatochromism of Tetradentate Schiff Base Complex with Nickel: Calculations and Experiments. *ChemistryOpen* **2018**, *7* (9), 677–687. https://doi.org/10.1002/open.201800100.
(30) Busa, A. V.; Lalancette, R.; Nordlander, E.; Onani, M. New Copper (II) Salicylaldimine Derivatives for Mild Oxidation of Cyclohexane. *J. Chem. Sci.* **2018**, *130* (6), 1–10.
(31) Aldred, R.; Johnston, R.; Levin, D.; Neilan, J. Magnesium-Mediated Ortho-Specific Formylation and Formaldoximation of Phenols. *J. Chem. Soc. Perkin 1* **1994**, No. 13, 1823–1831.
(32) Meier, P.; Broghammer, F.; Latendorf, K.; Rauhut, G.; Peters, R. Cooperative Al (Salen)-Pyridinium Catalysts for the Asymmetric Synthesis of Trans-Configured β-Lactones by [2+2]-Cyclocondensation of Acylbromides and Aldehydes: Investigation of Pyridinium Substituent Effects. *Molecules* **2012**, *17* (6), 7121–7150.
(33) Stevens, J. R. The Solution and Solid State Analysis of Xylylic Di-Copper Complexes as Receptors for Encapsulating Anions: A Thesis Presented in Partial Fulfillment of the Requirements for the Degree of Master of Science in Chemistry at Massey University, Palmerston North, New Zealand. **2011**.

(34) Chang, J. Y.-C.; Parsons, S.; Plieger, P. G.; Tasker, P. A. Anion-Selective Receptors Based on Dinuclear Copper (II) and Nickel (II) Cage Complexes of Bis-Salicylaldimines. *J. Incl. Phenom. Macrocycl. Chem.* **2011**, *71* (3), 529–536.
(35) Lutz, H.; Himmrich, J.; Schmidt, M. Lattice Vibration Spectra. Part LXXXVI. Infrared and Raman Spectra of Baryte-Type TlClO4, TlBF4, and NH4BF4 Single Crystals and Of11B-Enriched NH4BF4. *J. Alloys Compd.* **1996**, *241* (1–2), 1–9.
(36) Zafiu, C.; Trettenhahn, G.; Pum, D.; Sleytr, U. B.; Kautek, W. Structural Control of Surface Layer Proteins at Electrified Interfaces Investigated by in Situ Fourier Transform Infrared Spectroscopy. *Phys. Chem. Chem. Phys.* **2011**, *13* (29), 13232–13237.
(37) Ghann, W.; Sobhi, H.; Kang, H.; Chavez-Gil, T.; Nesbitt, F.; Uddin, J. Synthesis and Characterization of Free and Copper (II) Complex of N, N'-Bis (Salicylidene) Ethylenediamine for Application in Dye Sensitized Solar Cells. *J. Mater. Sci. Chem. Eng.* **2017**, *5* (6), 46–66.
(38) Buron-Le Cointe, M.; Hebert, J.; Baldé, C.; Moisan, N.; Toupet, L.; Guionneau, P.; Letard, J.-F.; Freysz, E.; Cailleau, H.; Collet, E. Intermolecular Control of Thermoswitching and Photoswitching Phenomena in Two Spin-Crossover Polymorphs. *Phys. Rev. B* **2012**, *85* (6), 064114.
(39) Jeffrey, G. A.; Jeffrey, G. A. *An Introduction to Hydrogen Bonding*; Oxford university press New York, 1997; Vol. 12.
(40) Steiner, T. The Hydrogen Bond in the Solid State. *Angew. Chem. Int. Ed.* **2002**, *41* (1), 48–76. https://doi.org/10.1002/1521-3773(20020104)41:1<48::AID-ANIE48>3.0.CO;2-U.
(41) Secco, E. A. Spectroscopic Properties of SO4 (and OH) in Different Molecular and Crystalline Environments. I. Infrared Spectra of Cu4(OH)6SO4, Cu4(OH)4OSO4, and Cu3(OH)4SO4. *Can. J. Chem.* **1988**, *66* (2), 329–336. https://doi.org/10.1139/v88-057.
(42) Bazzicalupi, C.; Bencini, A.; Lippolis, V. Tailoring Cyclic Polyamines for Inorganic/Organic Phosphate Binding. *Chem. Soc. Rev.* **2010**, *39* (10), 3709–3728. https://doi.org/10.1039/B926161N.
(43) Nation, D. A.; Reibenspies, J.; Martell, A. E. Anion Binding of Inorganic Phosphates by the Hexaaza Macrocyclic Ligand 3,6,9,17,20,23-Hexaazatricyclo[23.3.1.111,15]Triaconta-1(29),11(30),12,14,25,27-Hexaene. *Inorg. Chem.* **1996**, *35* (16), 4597–4603. https://doi.org/10.1021/ic9513090.
(44) Lu, Q.; Motekaitis, R. J.; Reibenspies, J. J.; Martell, A. E. Molecular Recognition by the Protonated Hexaaza Macrocyclic Ligand 3,6,9,16,19,22-Hexaaza-27,28-Dioxatricyclo[22.2.1.111,14]Octacosa-1(26),11,13,24-Tetraene. *Inorg. Chem.* **1995**, *34* (20), 4958–4964. https://doi.org/10.1021/ic00124a008.
(45) Anda, C.; Llobet, A.; Martell, A. E.; Donnadieu, B.; Parella, T. Systematic Evaluation of Molecular Recognition Phenomena. 3. Selective Diphosphate Binding to Isomeric Hexaazamacrocyclic Ligands Containing Xylylic Spacers. *Inorg. Chem.* **2003**, *42* (25), 8545–8550. https://doi.org/10.1021/ic034205v.
(46) Pannu, A. P. S.; Stevens, J. R.; Plieger, P. G. Aryl-Linked Salicylaldoxime-Based Copper(II) Helicates and "Boxes": Synthesis, X-Ray Analysis, and Anion Influence on Complex Structure. *Inorg. Chem.* **2013**, *52* (16), 9327–9337. https://doi.org/10.1021/ic400829d.
(47) Warzeska, S.; Krämer, R. A Dicopper (II) Complex of a New Octaaza Macrocycle: A Receptor in the Entatic State. *Chem. Commun.* **1996**, No. 4, 499–500.
(48) Amendola, V.; Bonizzoni, M.; Esteban-Gomez, D.; Fabbrizzi, L.; Licchelli, M.; Sancenon, F.; Taglietti, A. Some Guidelines for the Design of Anion Receptors. *Coord. Chem. Rev.* **2006**, *250* (11–12), 1451–1470.
(49) Gagné, O. C.; Hawthorne, F. C. Bond-Length Distributions for Ions Bonded to Oxygen: Results for the Transition Metals and Quantification of the Factors Underlying Bond-Length Variation in Inorganic Solids. *IUCrJ* **2020**, *7* (4), 581–629.
(50) Chauhan, S.; Patel, T. A Review on Solvent Extraction of Nickel. *Int J Eng Res Technol* **2014**, *3*, 1315–1322.

(51) Janiszewska, M.; Markiewicz, A.; Regel-Rosocka, M. Hydrometallurgical Separation of Co(II) from Ni(II) from Model and Real Waste Solutions. *J. Clean. Prod.* **2019**, *228*, 746–754. https://doi.org/10.1016/j.jclepro.2019.04.285.
(52) Regel-Rosocka, M.; Staszak, K.; Wieszczycka, K.; Masalska, A. Removal of Cobalt(II) and Zinc(II) from Sulphate Solutions by Means of Extraction with Sodium Bis(2,4,4-Trimethylpentyl)Phosphinate (Na-Cyanex 272). *Clean Technol. Environ. Policy* **2016**, *18* (6), 1961–1970. https://doi.org/10.1007/s10098-016-1123-1.
(53) Nayl, A. A.; Hamed, M. M.; Rizk, S. E. Selective Extraction and Separation of Metal Values from Leach Liquor of Mixed Spent Li-Ion Batteries. *J. Taiwan Inst. Chem. Eng.* **2015**, *55*, 119–125. https://doi.org/10.1016/j.jtice.2015.04.006.
(54) Provazi, K.; Campos, B. A.; Espinosa, D. C. R.; Tenório, J. A. S. Metal Separation from Mixed Types of Batteries Using Selective Precipitation and Liquid–Liquid Extraction Techniques. *Waste Manag.* **2011**, *31* (1), 59–64. https://doi.org/10.1016/j.wasman.2010.08.021.
(55) Singh, R.; Kliwaja, A.; Gupta, B.; Tandon, S. Extraction and Separation of Nickel (H) Using Bis (2, 4, 4-Trimethylpentyl) Dithiophosphinic Acid (Cyanex 301) and Its Recovery from Spent Catalyst and Electroplating Bath Residue. *Solvent Extr. Ion Exch.* **1999**, *17* (2), 367–390.
(56) Reddy, B. R.; Priya, D. N. Chloride Leaching and Solvent Extraction of Cadmium, Cobalt and Nickel from Spent Nickel–Cadmium, Batteries Using Cyanex 923 and 272. *J. Power Sources* **2006**, *161* (2), 1428–1434.
(57) Koladkar, D.; Dhadke, P. Cobalt–Nickel Separation: The Extraction of Cobalt (II) and Nickel (II) with Bis (2-Ethylhexyl) Phosphinic Acid (Pia-8) in Toluene. *Solvent Extr. Ion Exch.* **2001**, *19* (6), 1059–1071.
(58) Reddy, B. R.; Priya, D. N. Solvent Extraction of Ni (II) from Sulfate Solutions with LIX 84I: Flow-Sheet for the Separation of Cu (II), Ni (II) and Zn (II). *Anal. Sci.* **2004**, *20* (12), 1737–1740.
(59) Preston, J. S. Solvent Extraction of Cobalt and Nickel by Organophosphorus Acids I. Comparison of Phosphoric, Phosphonic and Phosphonic Acid Systems. *Hydrometallurgy* **1982**, *9* (2), 115–133.
(60) Reddy, B.; Parija, C.; Sarma, P. B. Processing of Solutions Containing Nickel and Ammonium Sulphate through Solvent Extraction Using PC-88A. *Hydrometallurgy* **1999**, *53* (1), 11–17.
(61) Buch, A.; Stambouli, M.; Pareau, D.; Durand, G. Solvent Extraction of Nickel (II) by Mixture of 2-Ethylhexanal Oxime and Bis (2-Ethylhexyl) Phosphoric Acid. *Solvent Extr. Ion Exch.* **2002**, *20* (1), 49–66.
(62) Du Preez, A. & P., JS. Separation of Nickel and Cobalt from Calcium, Magnesium and Manganese by Solvent Extraction with Synergistic Mixtures of Carboxylic Acids. *J. South. Afr. Inst. Min. Metall.* **2004**, *104* (6), 333–338.
(63) Sarangi, K.; Reddy, B.; Das, R. Extraction Studies of Cobalt (II) and Nickel (II) from Chloride Solutions Using Na-Cyanex 272.: Separation of Co (II)/Ni (II) by the Sodium Salts of D2EHPA, PC88A and Cyanex 272 and Their Mixtures. *Hydrometallurgy* **1999**, *52* (3), 253–265.
(64) Darvishi, D.; Haghshenas, D.; Alamdari, E. K.; Sadrnezhaad, S.; Halali, M. Synergistic Effect of Cyanex 272 and Cyanex 302 on Separation of Cobalt and Nickel by D2EHPA. *Hydrometallurgy* **2005**, *77* (3–4), 227–238.
(65) Roy, A.; Das, B. K.; Bhattacharya, J. Development and Validation of a Spectrophotometric Method to Measure Sulfate Concentrations in Mine Water without Interference. *Mine Water Environ.* **2011**, *30* (3), 169–174.
(66) Van Staden, J.; Taljaard, R. Determination of Sulphate in Natural Waters and Industrial Effluents by Sequential Injection Analysis. *Anal. Chim. Acta* **1996**, *331* (3), 271–280.

(67) Singh, R. P.; Abbas, N. M.; Smesko, S. A. Suppressed Ion Chromatographic Analysis of Anions in Environmental Waters Containing High Salt Concentrations. *J. Chromatogr. A* **1996**, *733* (1–2), 73–91.
(68) Burakham, R.; Higuchi, K.; Oshima, M.; Grudpan, K.; Motomizu, S. Flow Injection Spectrophotometry Coupled with a Crushed Barium Sulfate Reactor Column for the Determination of Sulfate Ion in Water Samples. *Talanta* **2004**, *64* (5), 1147–1150.
(69) Stefaniak, J.; Karwacka, S.; Janiszewska, M.; Dutta, A.; Rene, E. R.; Regel-Rosocka, M. Co(II) and Ni(II) Transport from Model and Real Sulfate Solutions by Extraction with Bis(2,4,4-Trimethylpentyl)Phosphinic Acid (Cyanex 272). *Chemosphere* **2020**, *254*, 126869. https://doi.org/10.1016/j.chemosphere.2020.126869.
(70) Soares, M. R.; Casagrande, J. C.; Mouta, E. R. Nickel Adsorption by Variable Charge Soils: Effect of PH and Ionic Strength. *Braz. Arch. Biol. Technol.* **2011**, *54* (1), 207–220.
(71) Jung, M. J.; Venkateswaran, P.; Lee, Y. S. Solvent Extraction of Nickel(II) Ions from Aqueous Solutions Using Triethylamine as Extractant. *J. Ind. Eng. Chem.* **2008**, *14* (1), 110–115. https://doi.org/10.1016/j.jiec.2007.08.004.
(72) Neutrium. Mccabe-Thiele Plot, 2017.
(73) Datt, P. Latent Heat of Vaporization/Condensation. *Encycl. Snow Ice Glaciers* **2011**, 703–703.
(74) Majer, V.; Svoboda, V. Enthalpies of Vaporization of Organic Compounds: A Critical Review and Data Compilation. **1986**.
(75) Idegami, A.; Ozaki, Y.; Heguri, S.; Kudou, K.; Ohara, H.; Matsumoto, S. Method for Producing High-Purity Nickel Sulfate. **2017**.
(76) Baylon, C.; Heck, M.-P.; Mioskowski, C. Bis Ring Closing Olefin Metathesis for the Synthesis of Unsaturated Polycyclic Ethers. O-Membered Ring Cyclization in Favor of C-Membered Ring Cyclization. *J. Org. Chem.* **1999**, *64* (9), 3354–3360. https://doi.org/10.1021/jo982098u.
(77) Rucker, R. P.; Whittaker, A. M.; Dang, H.; Lalic, G. Synthesis of Tertiary Alkyl Amines from Terminal Alkenes: Copper-Catalyzed Amination of Alkyl Boranes. *J. Am. Chem. Soc.* **2012**, *134* (15), 6571–6574.
(78) Siddaiah, V.; Basha, G.; Rao, G. P.; Prasad, U. V.; Rao, R. S. PEG-Mediated Facile Protocol for N-Boc Protection of Amines. *Chem. Lett.* **2010**, *39* (11), 1127–1129.
(79) Kolodyazhnaya, A. O.; Kolodyazhnaya, O. O.; Kolodyazhnyi, O. I. An Efficient Method for the Phosphonation of C=X Compounds. *Russ. J. Gen. Chem.* **2010**, *80* (4), 709–722. https://doi.org/10.1134/S1070363210040055.
(80) Mancuso, A. J.; Swern, D. Activated Dimethyl Sulfoxide: Useful Reagents for Synthesis. *Synthesis* **1981**, *1981* (03), 165–185.
(81) Mancuso, A. J.; Huang, S.-L.; Swern, D. Oxidation of Long-Chain and Related Alcohols to Carbonyls by Dimethyl Sulfoxide" Activated" by Oxalyl Chloride. *J. Org. Chem.* **1978**, *43* (12), 2480–2482.
(82) Lebel, H.; Leogane, O. Boc-Protected Amines via a Mild and Efficient One-Pot Curtius Rearrangement. *Org. Lett.* **2005**, *7* (19), 4107–4110. https://doi.org/10.1021/ol051428b.
(83) Chandrasekhar, S.; Reddy, N. R.; Sultana, S. S.; Narsihmulu, Ch.; Reddy, K. V. L-Proline Catalysed Asymmetric Aldol Reactions in PEG-400 as Recyclable Medium and Transfer Aldol Reactions. *Organocatalysis Org. Synth.* **2006**, *62* (2), 338–345. https://doi.org/10.1016/j.tet.2005.09.122.
(84) Sarko, C. R.; Collibee, S. E.; Knorr, A. L.; DiMare, M. BCl3- and TiCl4-Mediated Reductions of β-Hydroxy Ketones. *J. Org. Chem.* **1996**, *61* (3), 868–873. https://doi.org/10.1021/jo951549x.
(85) Rao, P. S.; Reddy, P. P.; Seshadri, T. Methylation of Hydroxy Flavonols Using Methyl Iodide and Potassium Carbonate; Springer, 1940; Vol. 12, pp 495–497.
(86) Kuhnert, N.; Rossignolo, G. M.; Lopez-Periago, A. The Synthesis of Trianglimines: On the Scope and Limitations of the [3+ 3] Cyclocondensation Reaction between (1R, 2R)-

Diaminocyclohexane and Aromatic Dicarboxaldehydes. *Org. Biomol. Chem.* **2003**, *1* (7), 1157–1170.
(87) Barwell, N.P; Whoberley, (GB); James, T.; Radstock, (GB). Glucose Sensor Molecules. PCT/GB2O12/OOOO18, January 22, 2014.
(88) Malkov, A. V.; Vranková, K.; Černý, M.; Kočovský, P. On the Selective N-Methylation of BOC-Protected Amino Acids. *J. Org. Chem.* **2009**, *74* (21), 8425–8427. https://doi.org/10.1021/jo9016293.

Appendices

A1.0 Method of Pathway 1

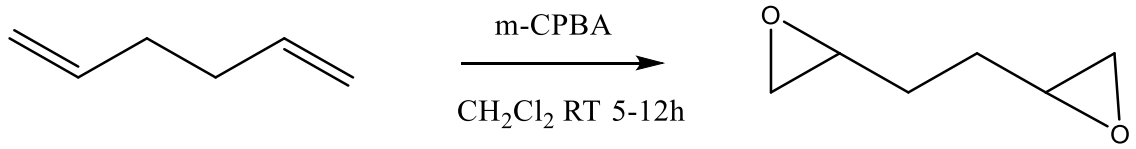

Figure 58. Synthesis of **P1a**.

The plan was to carry out the below method from Baylon *et al*.[76]

To a stirred solution of 1,5- hexadiene (3.6 mL, 30 mmol) in dry CH_2Cl_2 (60 mL) at 0 °C, m-chloroperbenzoic acid (12.95 g, 75 mmol, 57-86% wt) was added in small amounts. After 24 h stirring at room temperature, the product was extracted with CH_2Cl_2 (3 × 10 mL). The product was washed with 1 M KOH (6 × 25 mL), dried over $MgSO_4$, and concentrated. Flash chromatography (hexane:ether 70:30) gave the diepoxide (2.16 g, 63% yield).

^{1}H NMR spectrum literature values: (500 MHz; $CDCl_3$) δ 2.89-2.87 (m, 2H), 2.69 (dd, J) 4.7, 4.7 Hz, 2H), 2.42 (dd, J) 2.5, 4.9 Hz, 2H), 1.73-1.53 (m, 4H).

A1.2 Synthesis of Dodeca-1,11-diene-5,8-diol (P1b).

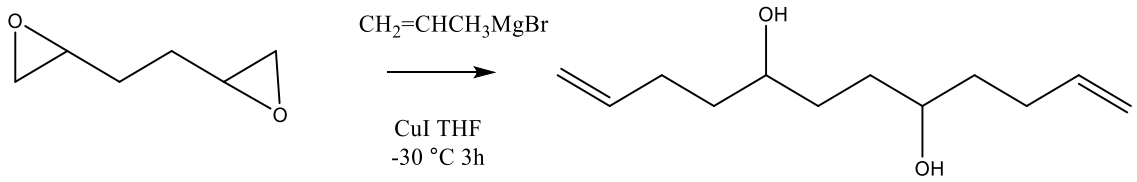

Figure 59. Synthesis of **P1b**.

The plan was to carry out the below method from Baylon *et al.*[76]

To a -30 °C solution of copper(I) iodide (525 mg, 2.6 mmol) in dry Et_2O (5 mL) allylmagnesium bromide (26.3 mL, 26.3 mmol), 1 M in THF was added dropwise, and stirred for 5 minutes. The Grignard reagent (1 g, 8.76 mmol) in dry Et_2O (5 mL) was added, and the mixture was stirred at -30 °C for 2 hours. The mixture was hydrolyzed with saturated NH_4Cl (15 mL) and extracted with Et_2O (3 × 10 mL). The organic layer was separated, dried with $MgSO_4$, and concentrated. The product was purified via column chromatography (hexane:ether 50:50) (1.03 g, 60% yield).

^1H NMR spectrum literature values: (500 MHz; $CDCl_3$) δ 5.86-5.71 (m, 2H, *CHOH*), 5.02-4.68 (m, 4H, *CH_2CHOH*), 3.63-3.34 (m, 4H, *CH_2CHOH*), 2.19-2.02 (m, 4H, *CH_2CHCH_2*), 1.64-1.38 (m, 8H, *CH_2CH*).

A1.3 Synthesis of 5,8-Bis-allyloxy-dodeca-1,11-diene (P1c).

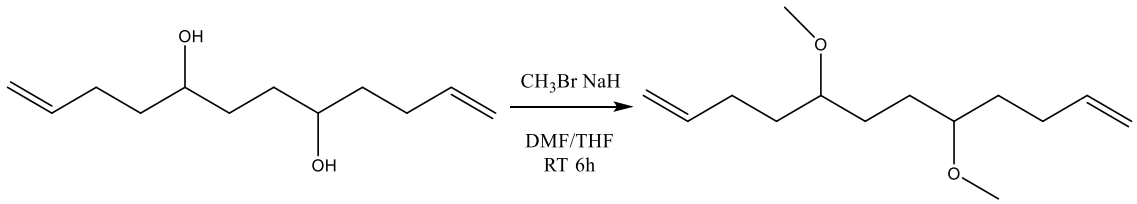

Figure 60. Synthesis of **P1c**.

The plan was to carry out the below method from Baylon *et al*.[76]

To **P1b** (200 mg, 1.01 mmol) in dry THF (3 mL) at 0 °C, was added NaH (80 mg, 2.02 mmol, 60% dispersion in mineral oil), and stirred at room temperature for 15 minutes. The solution was cooled to 0 °C, and allyl bromide (0.18 mL, 2.02 mmol) was added. After 1 hour at room temperature, NaH (80 mg, 2.02 mmol) and allyl bromide (0.18 mL, 2.02 mmol) were added and stirred for 2 hours. The mixture was hydrolyzed with saturated NH_4Cl (5 mL) and extracted with Et_2O (3 × 10 mL). The organic layer was separated and dried ($MgSO_4$). The crude product was purified by column chromatography (hexane:ether 90:10) (170 mg, 65% yield).

^{1}H NMR spectrum literature values: (500 MHz; $CDCl_3$) δ 5.94-5.72 (m, 6H, *CH_3O*), 5.24 (dd, 2H, *CHO*), 3.95 (dd, 4H, *CH_2CHO*), 3.33-3.29 (m, 2H, *CH_2CHO*), 2.15-2.05 (m, 4H, *CH_2CHCH_2*), 1.66-1.45 (m, 8H, *CH_2CH*).

A1.4 Synthesis of 5,8-Bis-allyloxy-dodeca-1,11-Boc-methylamine (P1d)

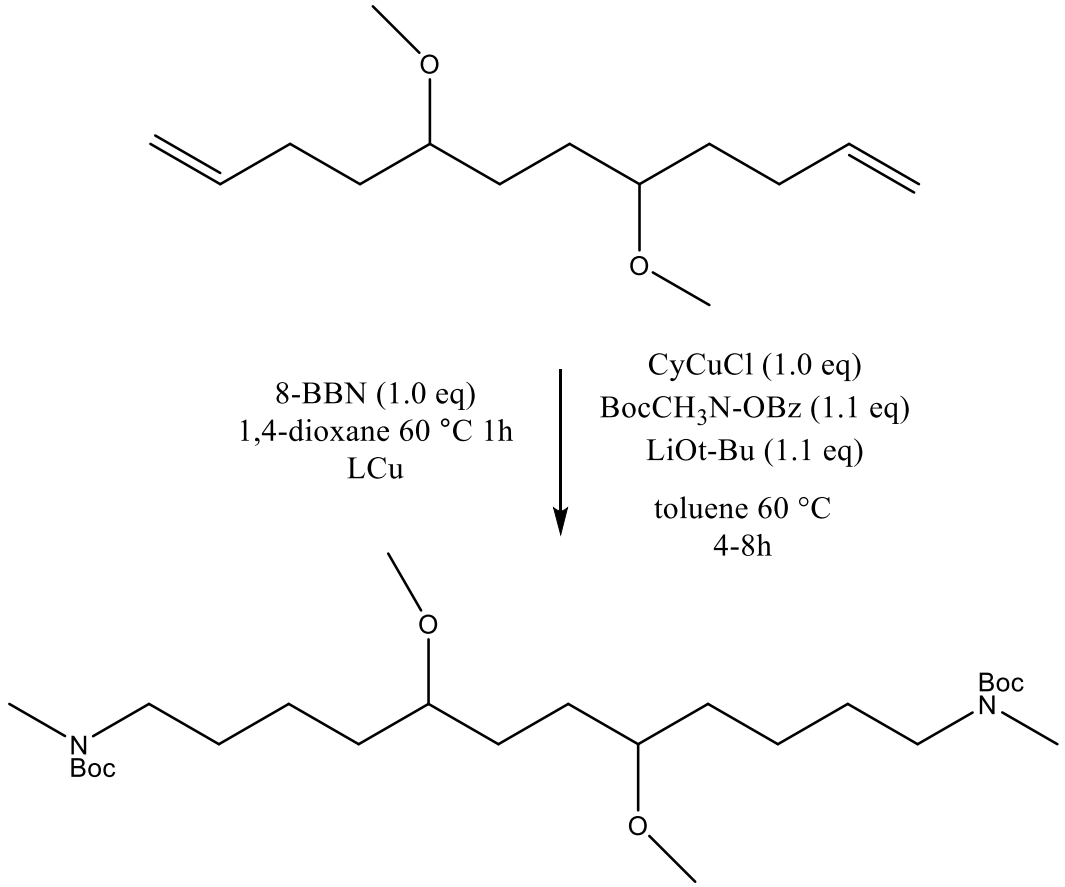

Figure 61. Synthesis of **P1d**.

The plan was to carry out the below method from Rucker *et al*.[77]

In a glove box, 9-BBN dimer (48.8 mg 0.200 mmol), toluene (1.00 mL, 0.40 M), and the alkene (0.400 mmol) was added to a one-dram vial and stirred for 12 hours at 60 °C. Then mixture was cooled to room temperature and placed in a 15 mL Schlenk tube. To the mixture was added lithium *tert*-butoxide (35.2 mg, 0.440 mmol), CyCuCl (6.6 mg, 0.020 mmol), and toluene (6.60 mL, 7.60 mL, 0.05 M). A stock solution of the electrophile was prepared (0.400 mL of reaction co-solvent) and added to the stirred mixture via a gas-tight syringe (500 μL size) over 4 hours at 60 °C. The reaction was monitored over TLC. The product was cooled, and the product was diluted with ether (5 mL) and washed with saturated $NaHCO_3$ solution. The product was extracted with diethyl ether (2 x 10 mL) and dried with Na_2SO_4.

The crude product was concentrated and then purified with diethyl ether (2.5 mL) and hexane (2.5 mL). The organic layer was extracted three times with 3 M aqueous HCl solution (5 mL). The product in the aqueous layer was separated and the pH of the aqueous layer was adjusted by dropwise addition of an aqueous 3 M NaOH solution until pH 10 was measured. The resulting solution was then extracted with dichloromethane (10 mL). The organic layer was washed with saturated brine (5 mL) and then dried with sodium sulfate. The oil product was obtained in vacuo.

B2.0 Method of Pathway 2

B2.1 Synthesis of 3-Boc-aminopropanol (P2a)

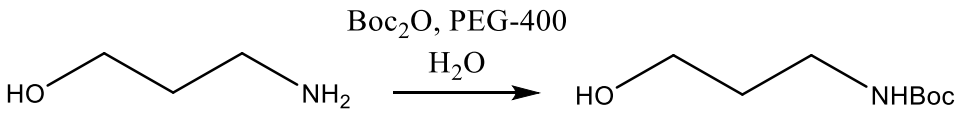

Figure 62. Synthesis of **P2a**.

The procedure was followed using the method from Siddaiah *et al*.[78]

To a stirring mixture of $(Boc)_2O$ (1.309 mL, 3 mmol) and PEG-400 (1 mL), amine (0.5 mL, 3 mmol) was added at room temperature. After stirring the reaction mixture for 5 minutes, water (20 mL) was added to the reaction mixture. After the bubbling stopped in approximately 15 minutes, the product was concentrated in vacuo (0.7825 g, 68.3%).

^{1}H NMR spectrum: (500 MHz; $CDCl_3$) δ 1.4 (s, 9H, $(CH_3)_3C$), 1.7 (t, 2H, CH_2), 3.33 (m, 5H, $NHCH_2$), 6.4 (br, 1H, *OH*).

B2.2 Synthesis of 3-Boc-aminopropanal (P2b)

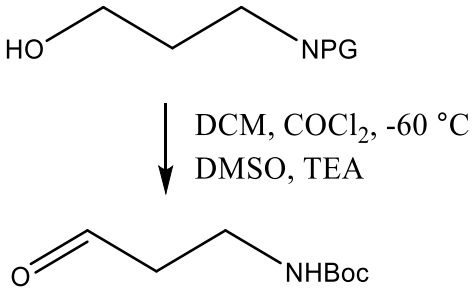

Figure 63. Synthesis of **P2b**.

The procedure was followed using the method from Kolodyazhnaya *et al*.[79] Other methods were also attempted.[80,81]

Anhydrous dichloromethane (6 mL) and oxalyl chloride (0.2833 mL) was bubbled with argon. The solution was cooled with stirring, and at –50 to –60°C was added dropwise dimethyl sulfoxide (0.29 mL) in dichloromethane (10 mL). After 5 minutes, **P2a** (0.28 g) was added dropwise over 10 minutes maintaining the temperature at –50 to –60°C. After 15 minutes, TEA (1.15 mL) was added dropwise, maintaining the temperature below –50°C. The stirring was continued for 5 minutes, then the mixture was left to stabilise to room temperature. (70–80 mL) water with ice was poured into the solution. The product was extracted with (2 × 30 mL) of dichloromethane. The organic layers were washed with (2 × 10 mL) of saturated NaCl and dried with $MgSO_4$ The product was concentrated and extracted with hexane. Then, the purified product was concentrated again (0.435 g, 155%).

^{1}H NMR spectrum literature values: (500 MHz; $CDCl_3$) δ 1.41 (s, 9H, (CH_3)$_3C$), 2.7 (t, 2H, CH_2, J7), 3.45 (m, 2H, CH_2N), 5.05 (br, 1H, *NH*), 9.8 (s, 1H, *CH=O*).

B2.3 Synthesis of 4-Amino-2-pentanone (P2c)

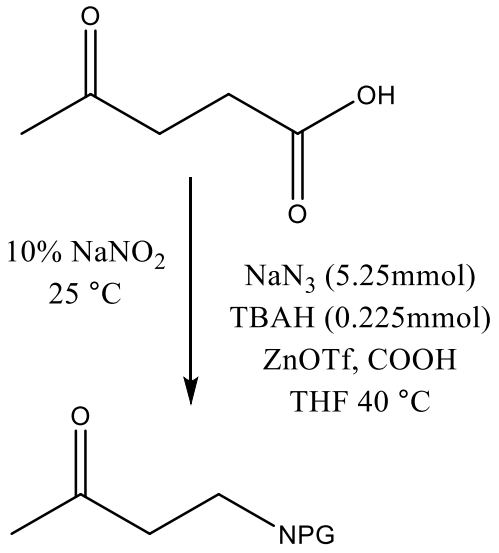

Figure 64. Synthesis of **P2c**.

The procedure was followed using the method from Lebel & Leogane.[82]

To a solution of sodium azide (651 mg), tetrabutylammonium bromide (152.0 mg), zinc triflate (II) (40.3 mg) and carboxylic acid (402.5 mg) in THF (15.0 mL) at 40 °C, was added di-*tert*-butyldicarbonate (750 μL). The resulting mixture was then stirred at 50 °C. After 24 hours a 10% solution of $NaNO_2$ (30 mL) was added. The mixture was stirred with ethyl acetate (30 mL) for 20 minutes at 25 °C. The aqueous layer was extracted with ethyl acetate (3 x 25 mL) and the organic layers were washed with saturated NH_4Cl (2 x 30 mL), with saturated $NaHCO_3$ (2 x 30 mL) and brine (30 mL). The organic layer was dried over Na_2SO_4 and the product was concentrated and by flash chromatography on silica gel with a pre-absorption on silica (6.5 mg, 1.3%).

^{1}H NMR spectrum literature values: (500 MHz; $CDCl_3$) δ 5.05 (br, 1H, *NH*), 2.7 (t, 2H, *CH_2N*), 2.6 (t, 2H, *CH_2CO*), 2.2 (s, 3H, *CH_3CO*), 1.41 (s, 9H, *$(CH_3)_3C$*).

B2.4 Synthesis of (P2d)

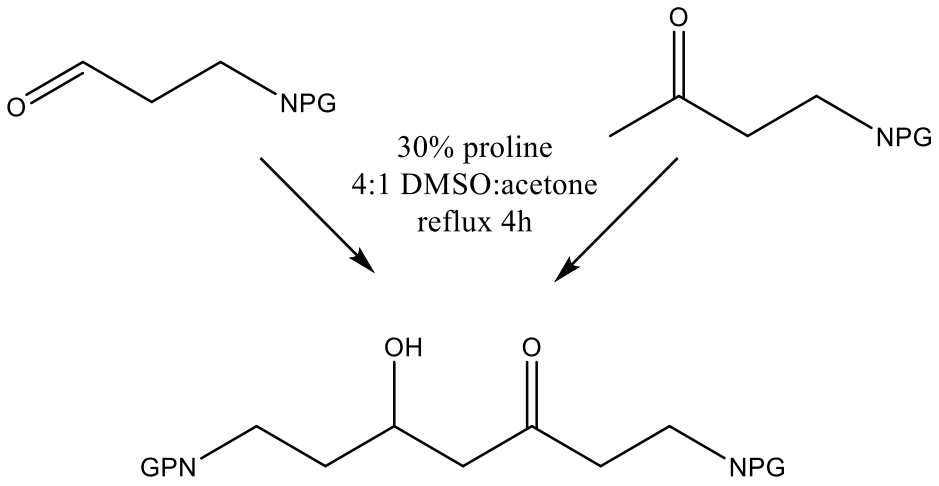

Figure 65. Synthesis of **P2d**.

The plan was to carry out the below method from Chandrasekhar *et al*.[83]

To a stirred solution of l-proline (30 mol%) in DMSO was added diacetone alcohol (4 mmol) at room temperature under argon. After being stirred for 5 minutes **P2c** (2 mmol) was added and stirred for 4 hours. After completion of the reaction (monitored by TLC), water was added and extracted with ethyl acetate twice (2×20 mL). The combined organic layers were washed with brine, dried over anhydrous Na_2SO_4. Solvent was removed under vacuo and purified by silica gel column chromatography to afford the pure product.

B2.5 Synthesis of (P2e)

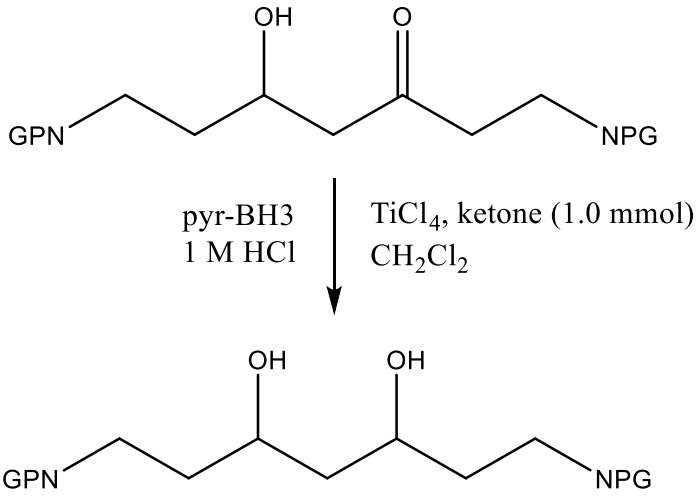

Figure 66. Synthesis of **P2e**.

The plan was to carry out the below method from Sarko *et al*.[84]

To a -78 °C solution of **P2d** (1.0 mmol) in CH_2Cl_2 10 mL was added $TiCl_4$ (1.0 mmol) to give a bright yellow solution, which was stirred 10 minutes. The nucleophile (1.0 mmol) in CH_2Cl_2 (5 mL) was added to the -78 °C solution. After 15 minutes, 1 M HCl (25 mL) was added, and the reaction was warmed to room temperature. The product was extracted with CH_2Cl_2, and the organic layer was concentrated in vacuo. The product was extracted with Et_2O and H_2O. The ether layer was washed with water and brine, dried over anhydrous Na_2SO_4, and concentrated in vacuo. Chromatography gave diastereomeric mixtures of diols in 84-96% yield.

B2.6 Synthesis of (P2f)

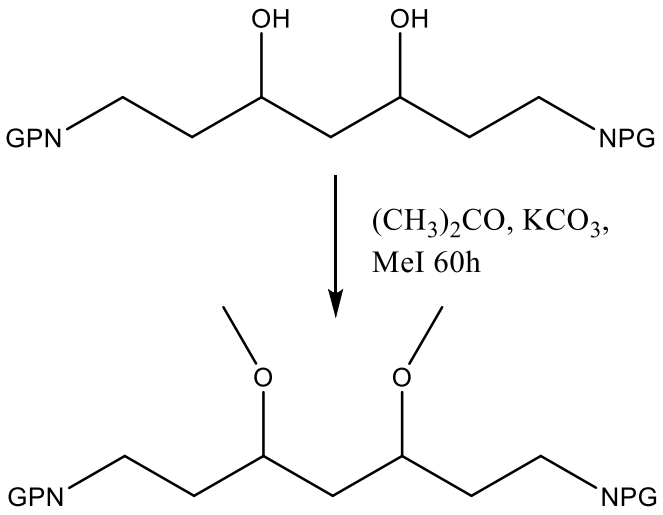

Figure 67. Synthesis of **P2f**.

The plan was to carry out the below method from Rao *et al*.[85]

P2e (1.3 mmol) was dissolved in dry acetone (50 mL) and anhydrous potassium carbonate (2 g), and methyl iodide (5 g) were added. The mixture was refluxed for 60 hours, and a small amount of methyl iodide was added daily to replace the loss of the reagent through evaporation. The mixture was distilled, and water was added to dissolve potassium salts. The product was filtered, washed with water and recrystallised with dilute alcohol. The resulting product were yellow needles in a 45% yield.

B2.7 Synthesis of (P2g)

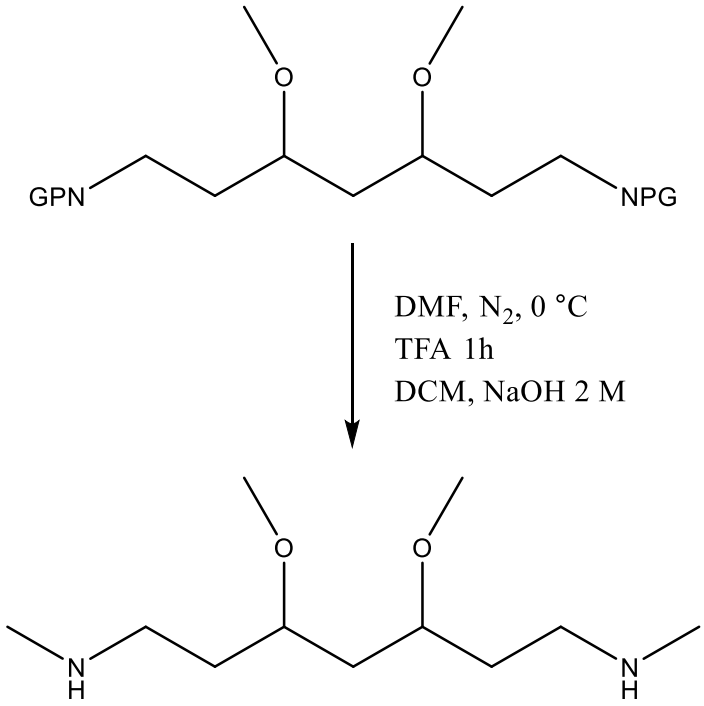

Figure 68. Synthesis of **P2g**.

The Boc protected amine (0.99 mmol) was dissolved in dry DCM (10 ml) under nitrogen and cooled to 0° C. Trifluoroacetic acid (2 ml) was added and the reaction mixture was stirred for 1 hour. The product was extracted in DCM (30 ml) and NaOH (2 M, 50 ml), dried with Na_2SO_4, and concentrated to afford a clear oil (yield 84%).

B3.0 Method for Pathway 3

B3.1 Synthesis of 1,2-Dimethoxy-3,6-diformylbenzene (P3a)

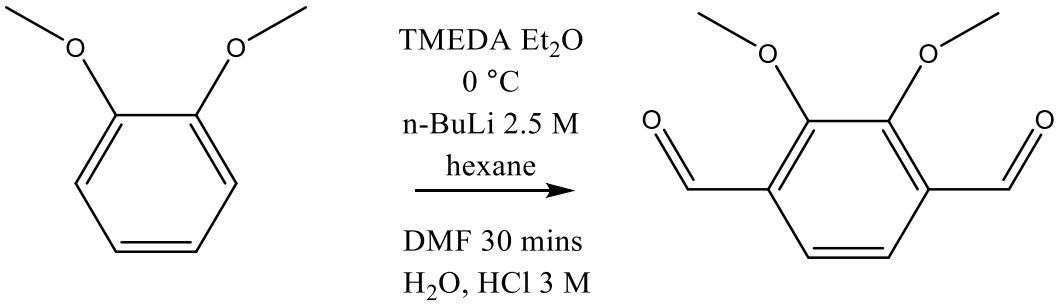

Figure 69. Synthesis of **P3a**.

The procedure was followed using the method from Kuhnert *et al*.[86]

In an oven dried round bottom flask, TMEDA (5 eq., 1.36 mL, 9 mmol) was added to a solution of 1,2-dimethoxybenzene (0.23 mL, 1.8 mmol) in diethyl ether (6 mL). The mixture was cooled in an ice bath (0 °C) under argon. Next, *n*-butyllithium 2.5 M in hexane (3.6 mL, 9 mmol) was added slowly over 1–2 minutes. The mixture refluxed for 10 hours under argon. As predicted, a tannish-yellow precipitate was formed which was assumed to be the intermediate lithium salts.

DMF (0.70 mL, 9 mmol) was added to the mixture, and the reaction was carried out for 30 minutes. Finally, the reaction mixture was allowed to warm to room temperature and hydrolysed with water 10 mL and 3 M hydrochloric acid (2 mL). The organic layer was separated, and the aqueous layer was extracted with 3×15 mL diethyl ether. The extract was dried over Na_2SO_4, and recrystallised from petrol ether, leading to the dicarboxaldehyde (**9**) as a yellow solid (154 mg, 45%).

^{1}H NMR spectrum literature values: (500 MHz; $CDCl_3$) δ 10.44 (2H, s, *CHO*), 7.63 (2H, s, *ArH*), 4.05 (6H, s, *OMe*); δ_C($CDCl_3$) 189.5, 156.9, 134.4, 123.1, 62.9; *m*/*z* (EI) 189.5 (M^+, 100%); CHN (Found: C, 61.6; H, 5.21. $C_{10}H_{10}O_4$ requires: C, 61.8; H, 5.19%).

B3.2 Synthesis of 3-(Benzyloxycarbonylamino)propyl bromide (P3b)

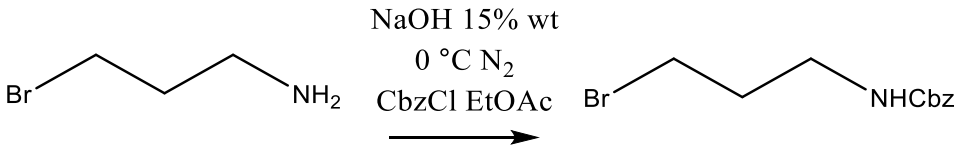

Figure 70. Synthesis of **P3b**.

The plan was to carry out the below method from Barwell *et al*.[87]

3-Bromopropylamine hydrobromide (5.0 g, 22.8 mmol) was dissolved in an aqueous NaOH solution (15 wt %, 80 ml) and cooled to 0° C. under nitrogen before benzyl chloroformate was added dropwise. The reaction was left to stir overnight then ethyl acetate (100 ml) was added, and the phases were separated. The organic phase was further washed with a HCl solution (2 M, 100 ml), a NaOH solution (2 M, 100 ml), brine (100 ml), dried over Na_2SO_4, and evaporated to yield a clear oil (6.22 g, 22.8 mmol, 100%). R_f=0.31 (8:2 Hexane/Ethyl acetate).

^{1}H NMR spectrum literature values: (300 MHz; $CDCl_3$) δ 7.40-7.33 (m, 5H, *ArCH*), 5.11 (s, 2H, *CH_2Ph*), 4.94 (bs, 1H, *NHCbz*), 3.45 (t, ^{3}J(H,H)=6.4 Hz, 2H, *CH_2Br*), 3.36 (q, ^{3}J(H,H)=6.4 Hz, 2H, *CH_2NHCbz*), 2.08 (q, ^{3}J(H,H)=6.4 Hz, 2H, *$CH_2CH_2CH_2$*).

B3.3 Synthesis of 3-Boc-aminopropanol (P3c)

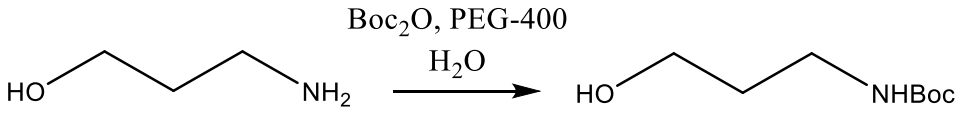

Figure 71. Synthesis of **P3c**.

The procedure was followed using the method from Siddaiah *et al*., in the same way as synthesis of **P2a**.[78]

B3.4 Synthesis of 3-Boc-methylaminopropanol (P3d)

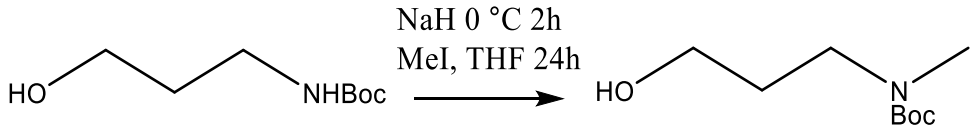

Figure 72. Synthesis of **P3d**.

The plan was to carry out the below method from Malkov *et al*.[88]

Sodium hydride (160 mg, 6.67 mmol, 10 eq.) was added in small quantities over 2 hours to a 0 C solution of 3-Boc-aminopropanol (0.67 mmol) and iodomethane (0.42 mL, 947 mg, 6.67 mmol) in anhydrous THF (2 mL) under argon. The solution was stirred at room temperature for 24 hours and then ether (20 mL) and deionised water (30 mL) was added. The aqueous layer was extracted with ether and acidified to pH 3 with 20% aqueous solution of citric acid and extracted with AcOEt. The organic layer was dried with $MgSO_4$ and concentrated to afford a thick oil with a yield of 98%.

^{1}H NMR spectrum literature values: (300 MHz; $CDCl_3$) δ 1.43 (s, 9H, *Boc-CH_3*), 1.63 (m, 2H, *HO-CH_2-CH_2*), 3.26 (t, J= 6Hz, 2H, *HN-CH_2*), 3.64 (t, J=5.7 Hz, 2H, *HO-CH_2*) 2.90 (s, 3H, *CH_3N*).

B3.5 Synthesis of 2-(*tert*-butoxycarbonylmethylamino)propyl 3-(benzyloxy carbonylamino)propyl ether (P3e)

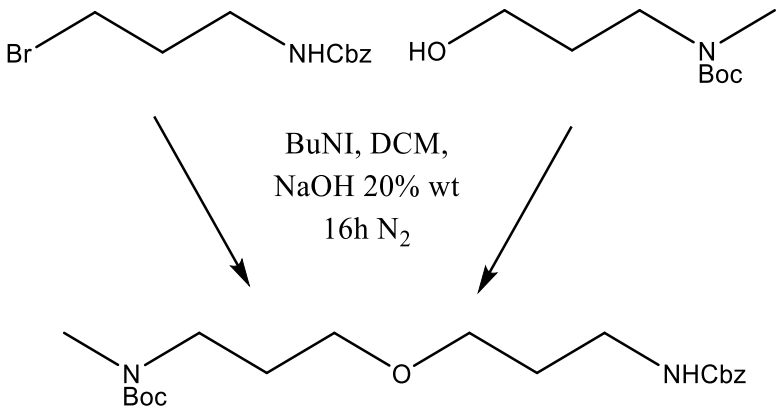

Figure 73. Synthesis of **P3e**.

The plan was to carry out the below method from Barwell *et al*.[87]

P3d (6.20 mmol), **P3b** (8.06 mmol. 1.3 eq.), and BuNI (2.98 g, 8.06 mmol. 1.3 eq.), were dissolved in DCM (50 ml) and an aqueous solution of NaOH (20 wt. %, 50 ml) was added and the reaction was stirred overnight under nitrogen. The phases were separated, and the aqueous phase was washed with DCM (2x50 ml), the organic phases were combined, dried over Na_2SO_4 and evaporated. The residue obtained was purified by flash chromatography (eluent DCM to ethyl acetate) to yield (1.61 mmol, 26%). (R_f = 0.34) (9:1 DCM/MeOH saturated with NH).

^{1}H NMR spectrum literature values: (300 MHz; $CDCl_3$) δ 8–7.38-7.30 (m, 5H, *ArCH*), 5.13 (bs, 1H, *NHX*), 5.10 (s. 2H, *CH_2Ph*), 4.97 (bs, 1H, *NHX*), 3.48 (m, 4H, *CH_2O*), 3.30 (m, 4H, *CH_2N*), 2.90 (s, 3H, *CH_3N*), 1.77 (q, J(H.H)=6.1 Hz, 4H, *$CH_2CH_2CH_2$*), 1.44 (s, 9H, *CH_3*).

B3.6 Synthesis of 2-(*tert*-butoxycarbonylmethylamino)propyl 3-aminopropyl ether (P3f)

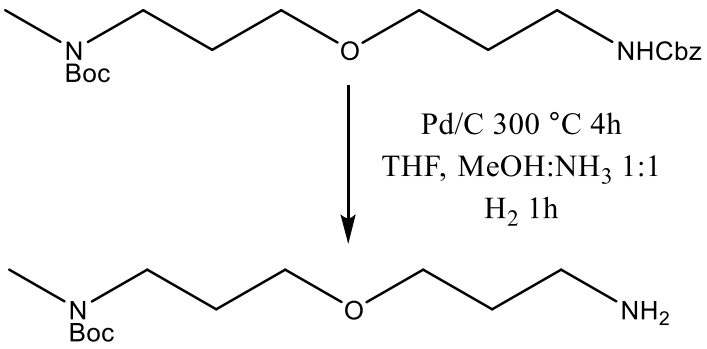

Figure 74. Synthesis of **P3f**.

The plan was to carry out the below method from Barwell *et al*.[87]

Pd/C (200 mg) was activated by heating at 300° C. under vacuum for 4 hours before a solution of **P3e** (1.61 mmol) in THF and MeOH saturated with NH_3 (1:1, 100 ml) was added. The flask was flushed with hydrogen (1 atm) and the reaction was stirred for 1 hour. The reaction mixture was then filtered over celite and washed with ethyl acetate before the filtrate evaporated. The residue obtained was purified by flash chromatography (eluent DCM to DCM/methanol saturated with NH, 19:1) to yield a clear oil (1.57 mmol, 98%). (R_f = 0.65) (17:3 DCM/MeOH saturated with NH).

^{1}H NMR spectrum literature values: (300 MHz; $CDCl_3$) δ 8–5.03 (bs, 1H, *NH_2Boc*), 3.48 (t, J(HH)=5.3 Hz, 2H, *CH_2NH_2*), 3.43 (t, J(HH)=6.2 Hz, 2H, *CH_2NHBoc*), 3.25 (q, J(H.H) =5.3 Hz, 2H, *OCH_2CH_2NHBoc*), 2.75 (t, J(HH)=6.8 Hz, 2H, *CH_2CH_2NH*), 1.67 (quintet, J(H.H)=6.5 Hz, 2H, *$CH_2CH_2NH_2$*), 1.40 (s, 9H, *C(CH_3)$_3$*), 1.27 (bs, 2H, *NH_2*).

B3.7 Synthesis of 1,2-dimethoxy-3,6-((*tert*-butoxycarbonylmethyl amino) propyl-3-N-aminopropyl ether) (P3g)

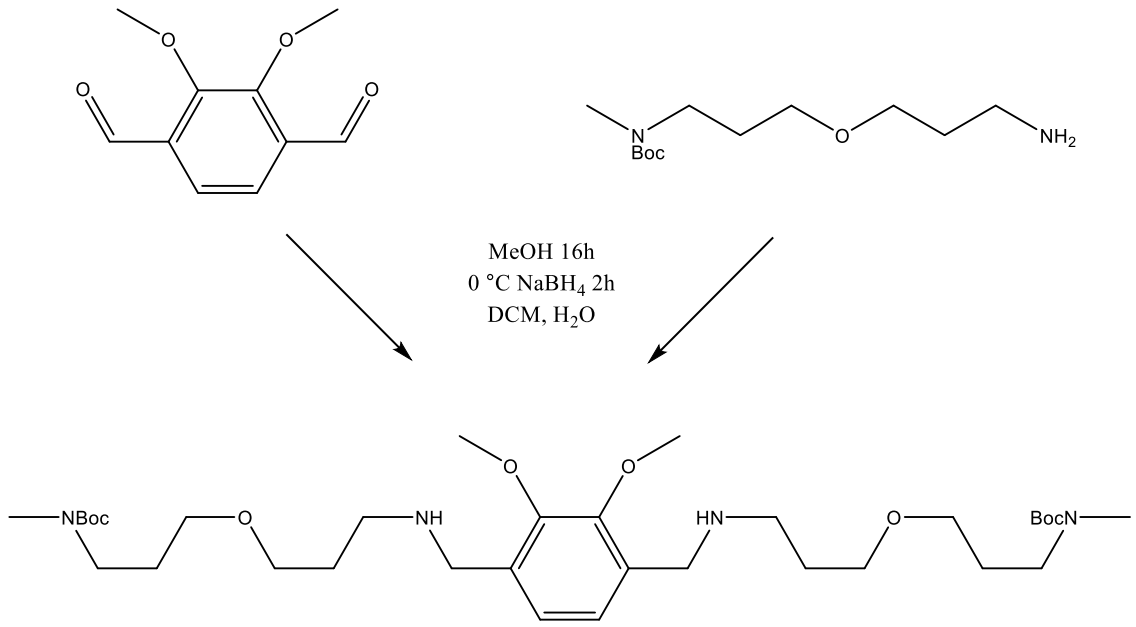

Figure 75. Synthesis of **P3g**.

The plan was to carry out the below method from Barwell *et al*.[87]

P3f (1.24 mmol) and **P3a** (1.36 mmol. 1.1 eq.) were dissolved in methanol (50 ml) and stirred overnight. The reaction mixture was then cooled to 0° C. and $NaBH_4$ (117 mg, 3.1 mmol. 2.5 eq.) was then added slowly and the reaction mixture was stirred for 2 hours, after which the solvent was evaporated. The residue obtained was dissolved in DCM (50 ml) and water (50 ml), the phases were separated, and the aqueous phase was extracted with DCM (2x50 ml), dried over Na_2SO_4, and evaporated. The crude product was purified by flash chromatography (eluent DCM to DCM/methanol saturated with NH, 97:3) yielding **P3g** as an oil (360 mg. 0.99 mmol, 80%). (R_f = 0.63) (97.3 DCM/ MeOH saturated with NH).

B3.8 Synthesis of 1,2-dimethoxy-3,6-((methylamino)propyl-3-N-aminopropylether) (P3h)

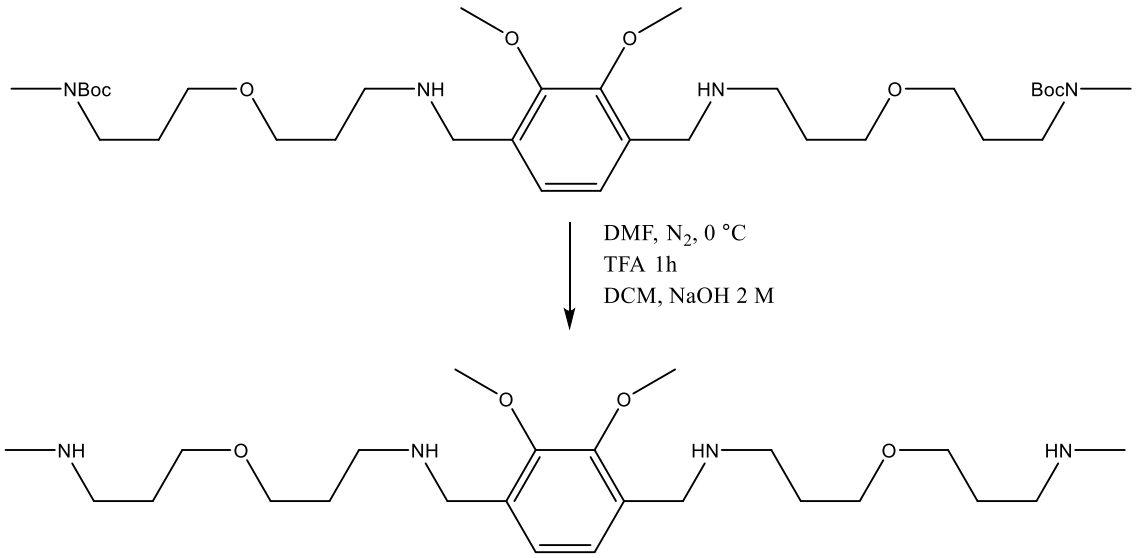

Figure 76. Synthesis of **P3h**.

The plan was to carry out the below method from Barwell *et al*.[87]

Boc protected amine **P3g** (360 mg. 0.99 mmol) was dissolved in dry DCM (10 ml) under nitrogen and cooled to 0° C. Trifluoroacetic acid (2 ml) was added and the reaction mixture was stirred for an hour, after which the solvent was evaporated. The residue obtained was dissolved in DCM (30 ml) and NaOH (2 M, 50 ml), the phases were separated, and the aqueous phase was extracted with DCM (2x30 ml), dried over Na_2SO_4, and evaporated yielding a clear oil (219 mg, 0.83 mmol, 84%). (R_f = 0.40) (9:1 DCM/MeOH saturated with NH).

D1.0 ^{1}H NMR Spectroscopy of Ligands

All the following spectra were run with $CDCl_3$ and have the reference solvent peak at 7.260 ppm.

D1.1 ^{1}H NMR of 1a

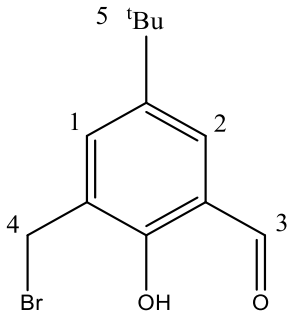

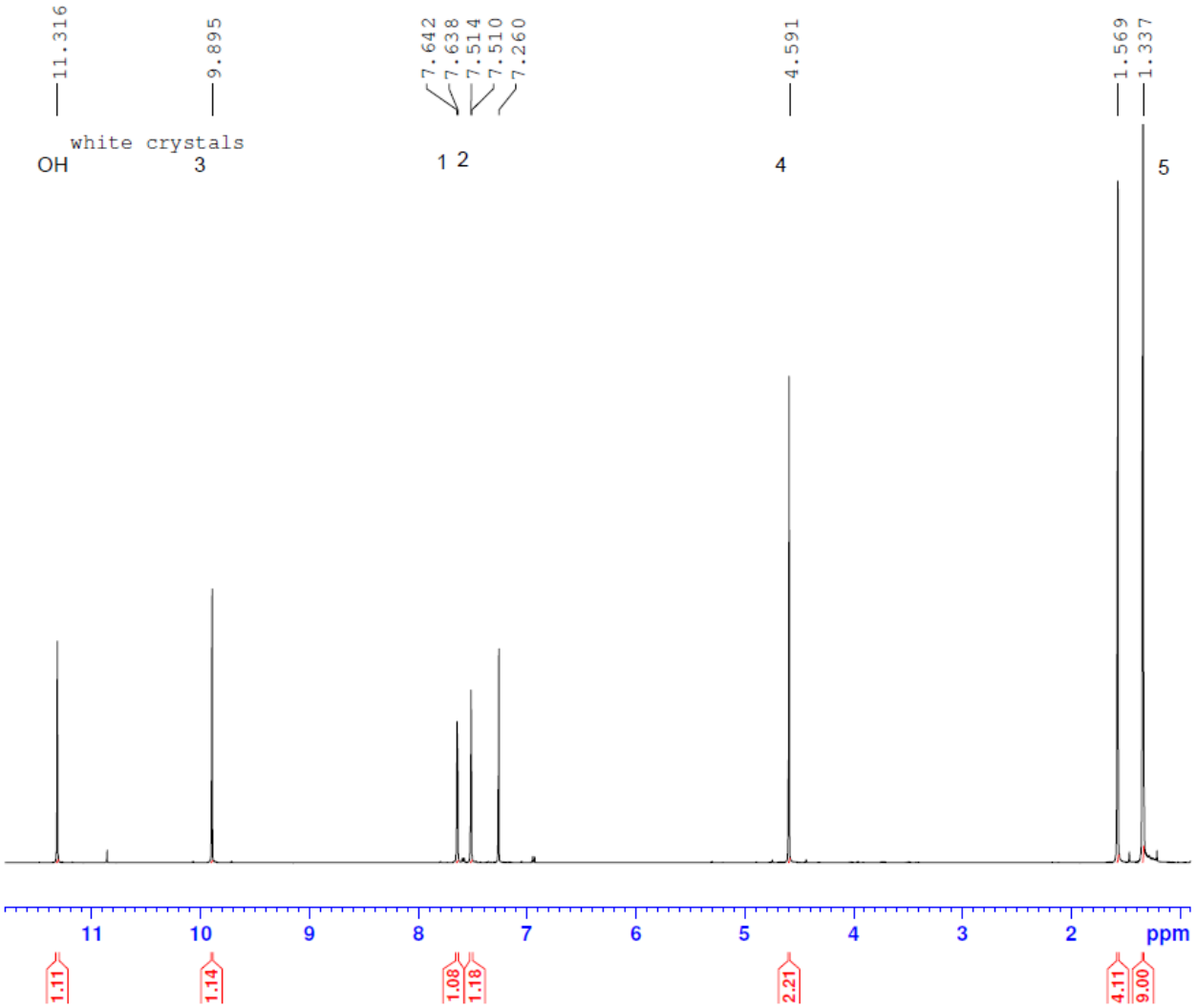

*1.569 ppm: water peak

D1.2 ^{1}H NMR of 1b

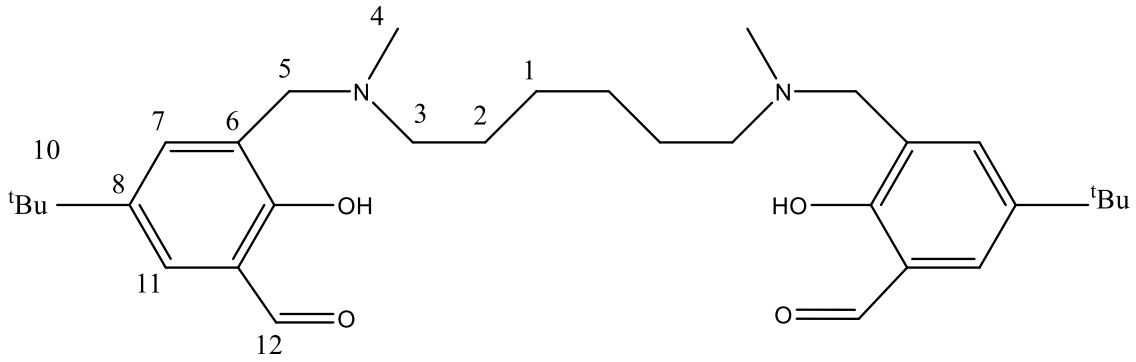

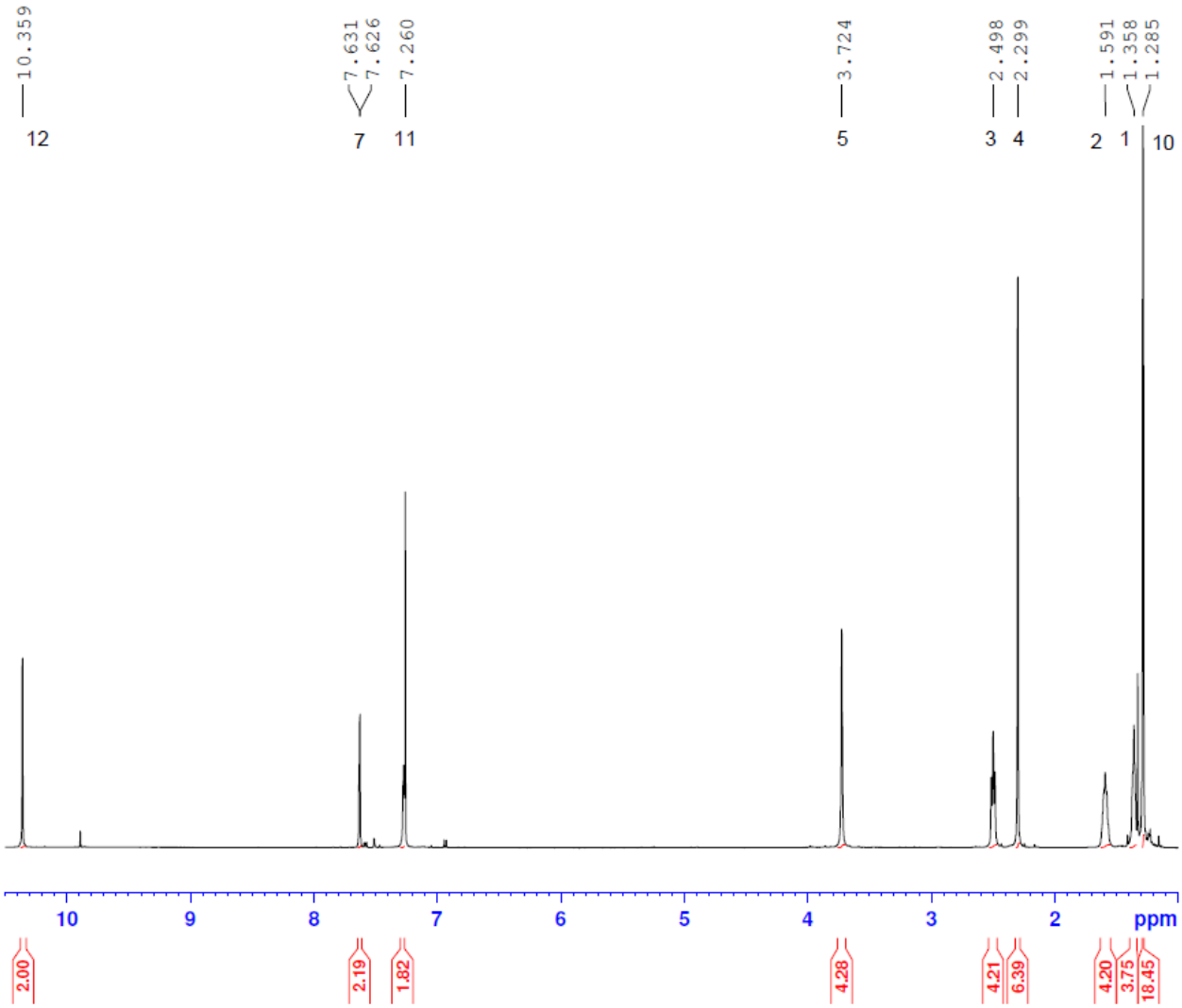

D1.3 ^{1}H NMR of L1

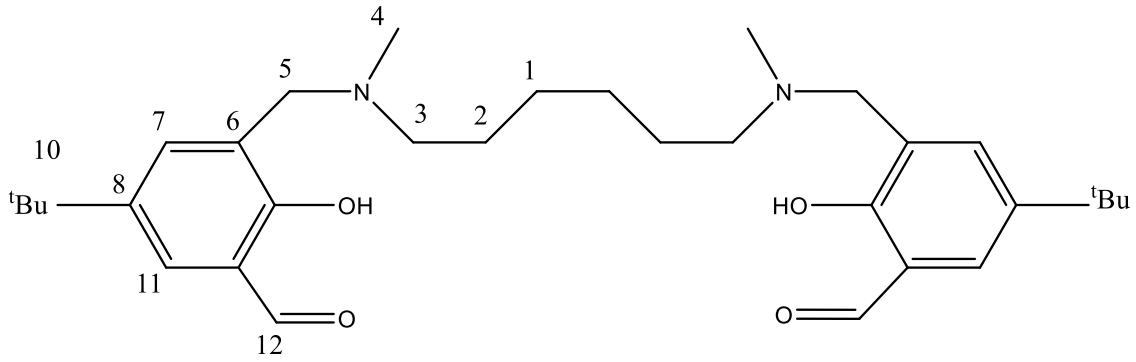

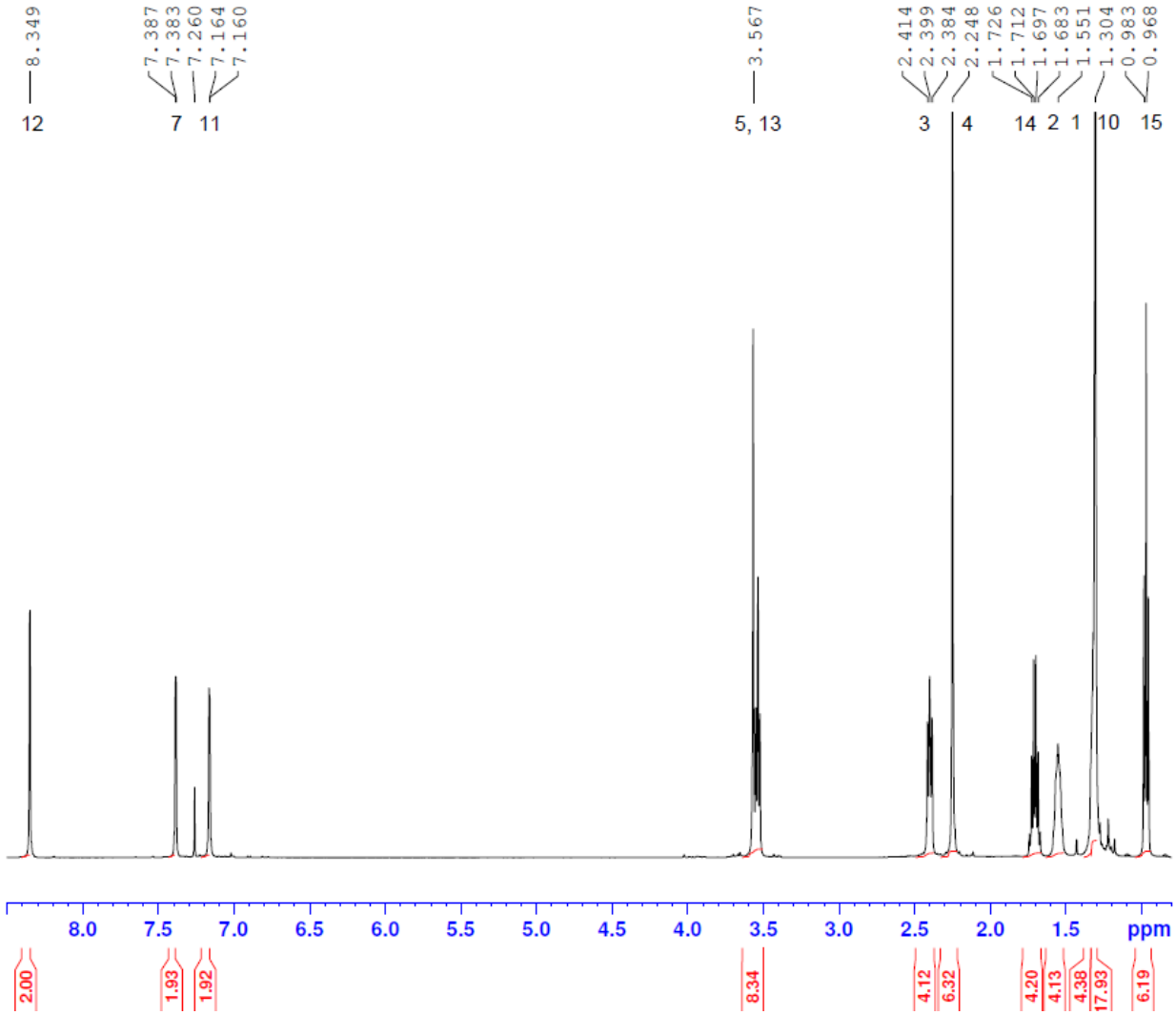

D1.4 ^{1}H NMR of R2

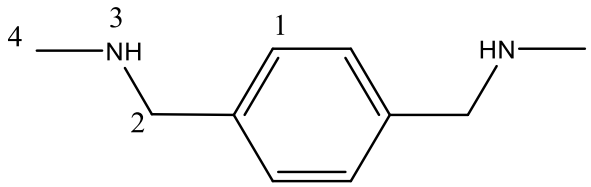

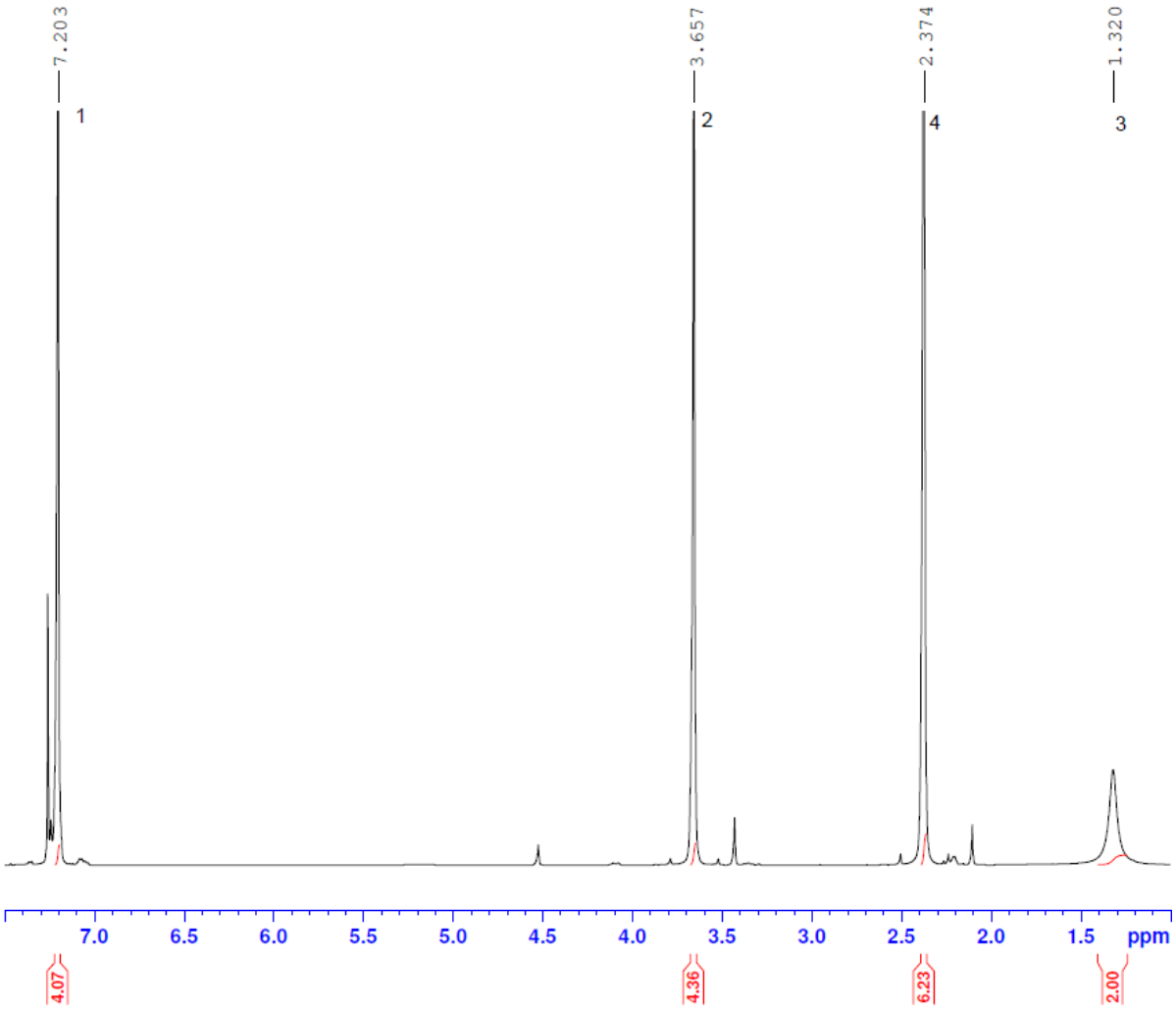

D1.5 ^{1}H NMR of 2b

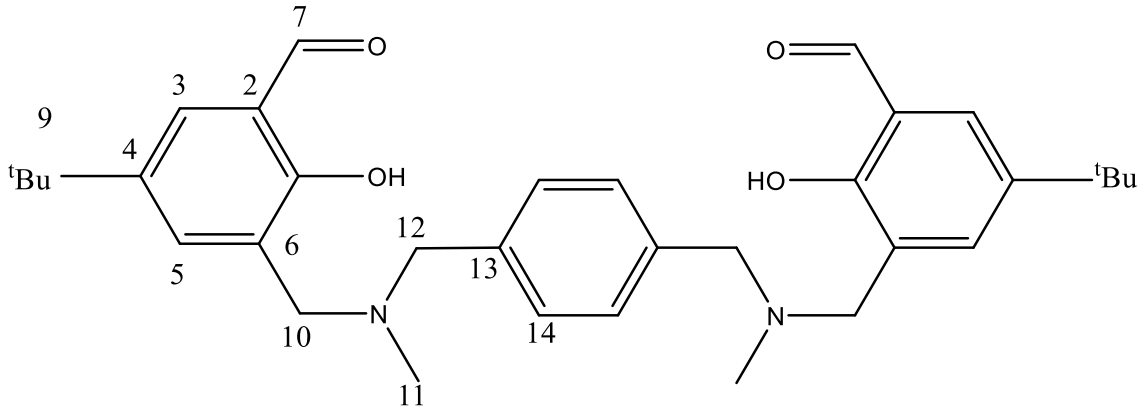

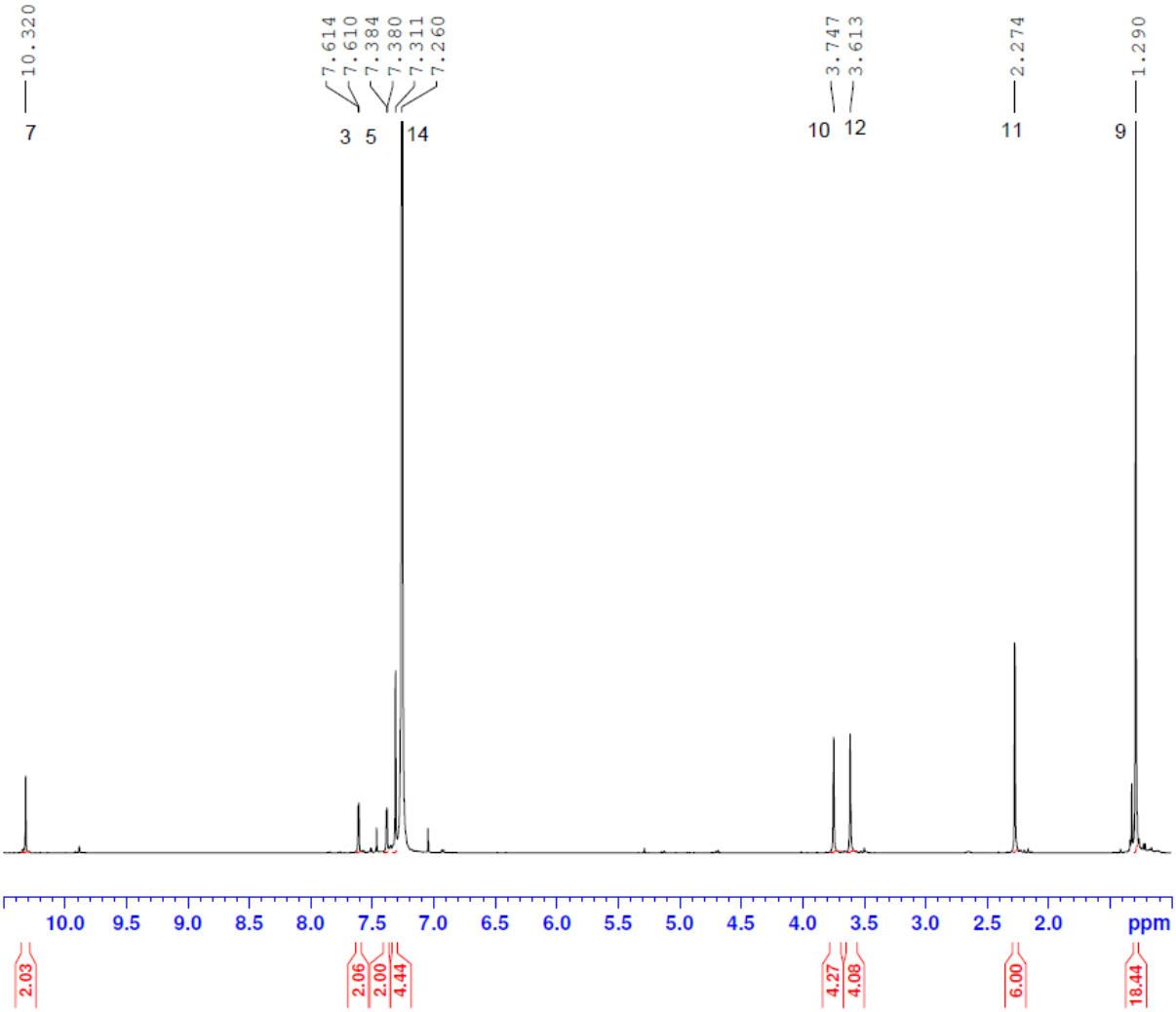

D1.6 ^{1}H NMR of L2

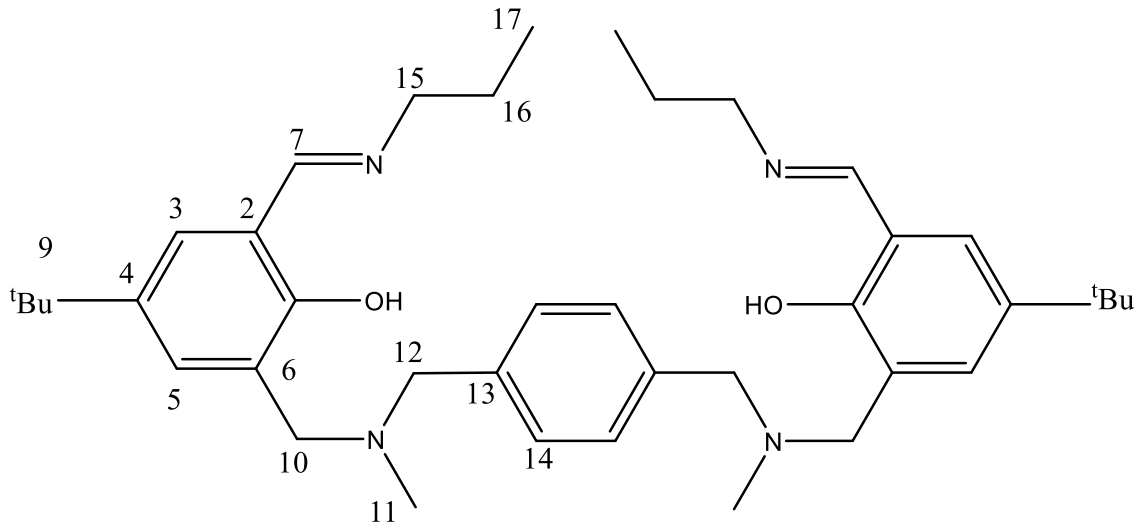

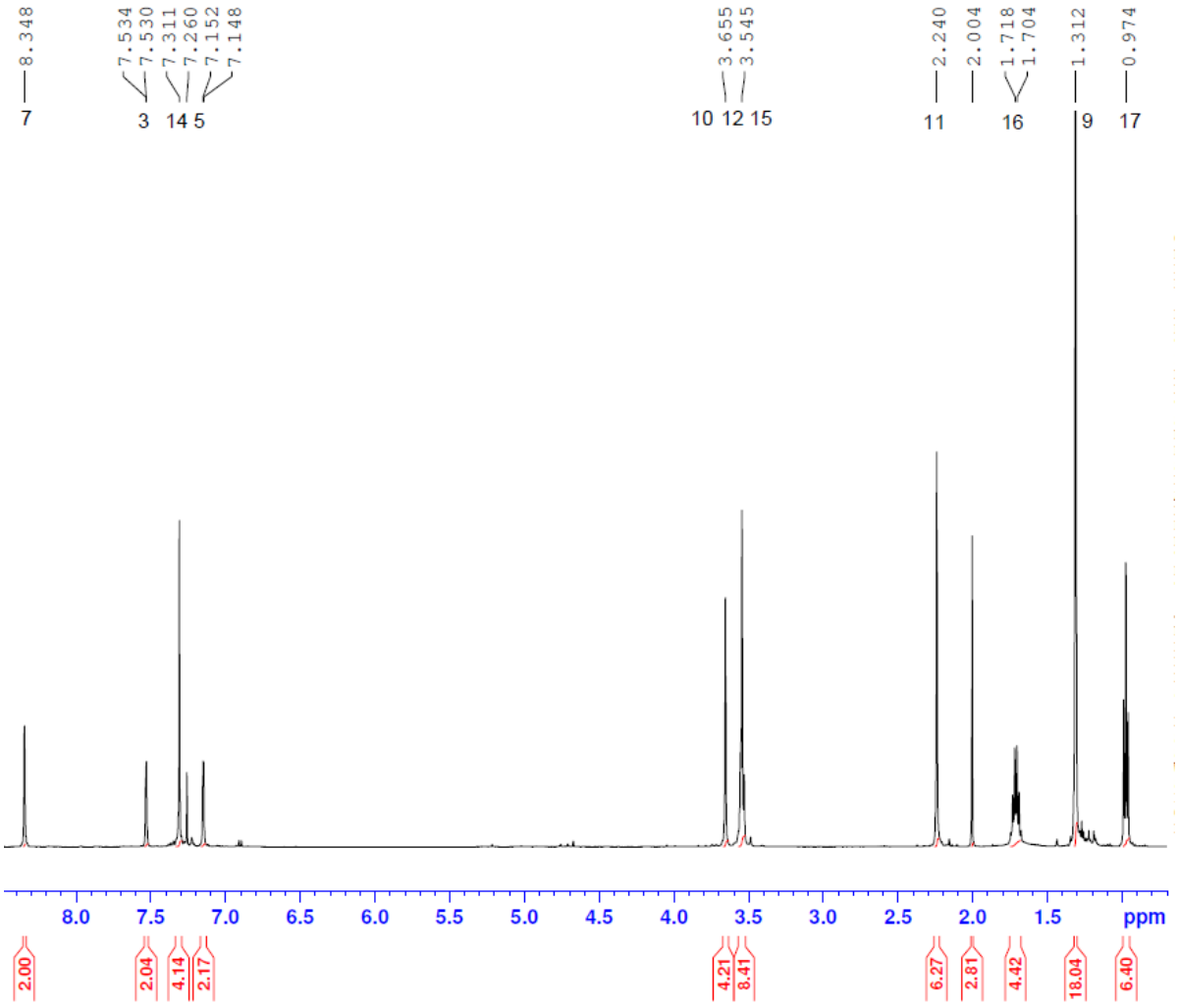

D1.7 ^{1}H NMR of R3

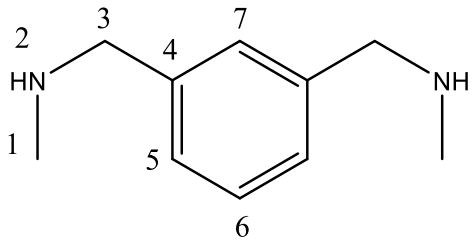

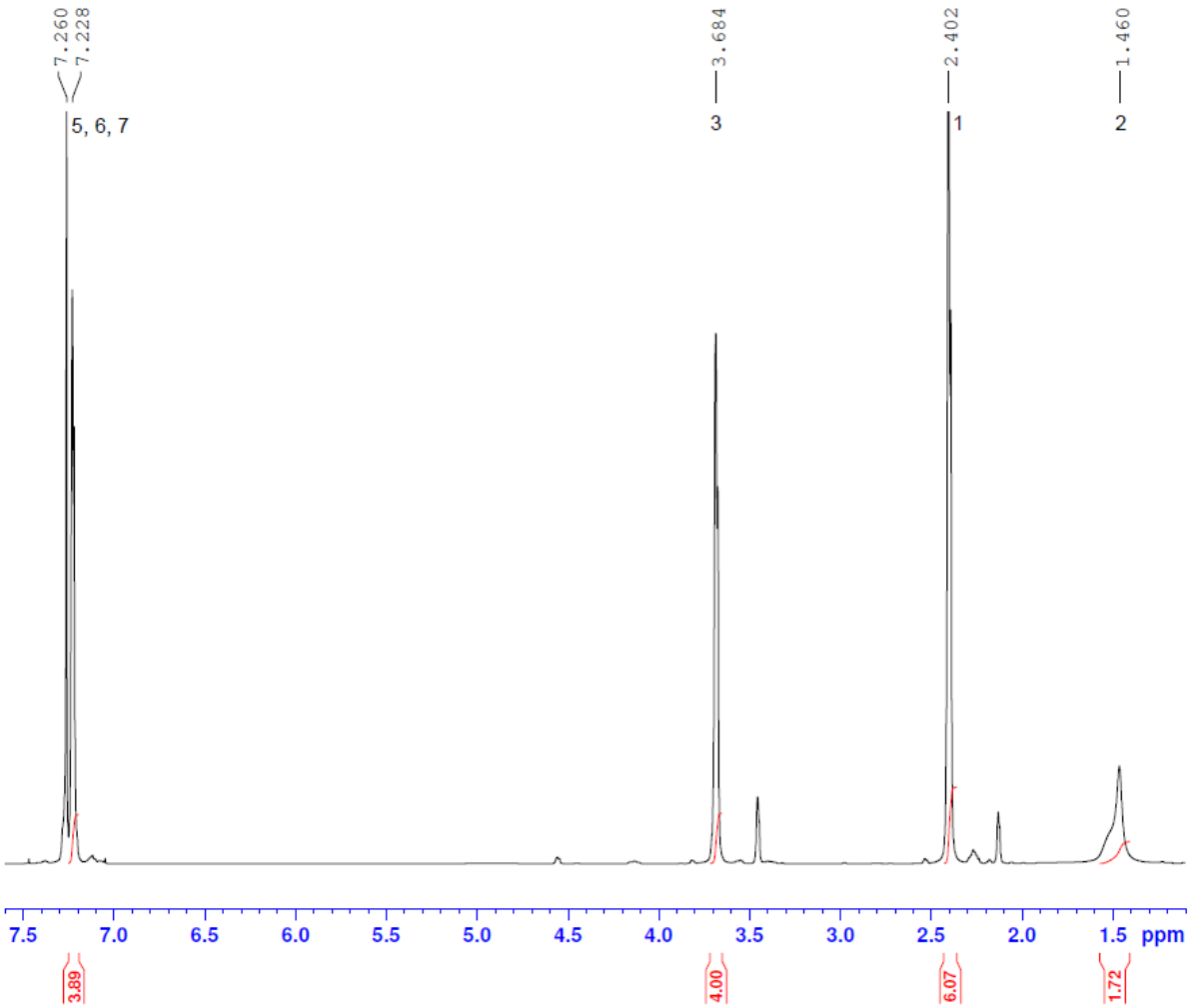

D1.8 ^{1}H NMR of 3b

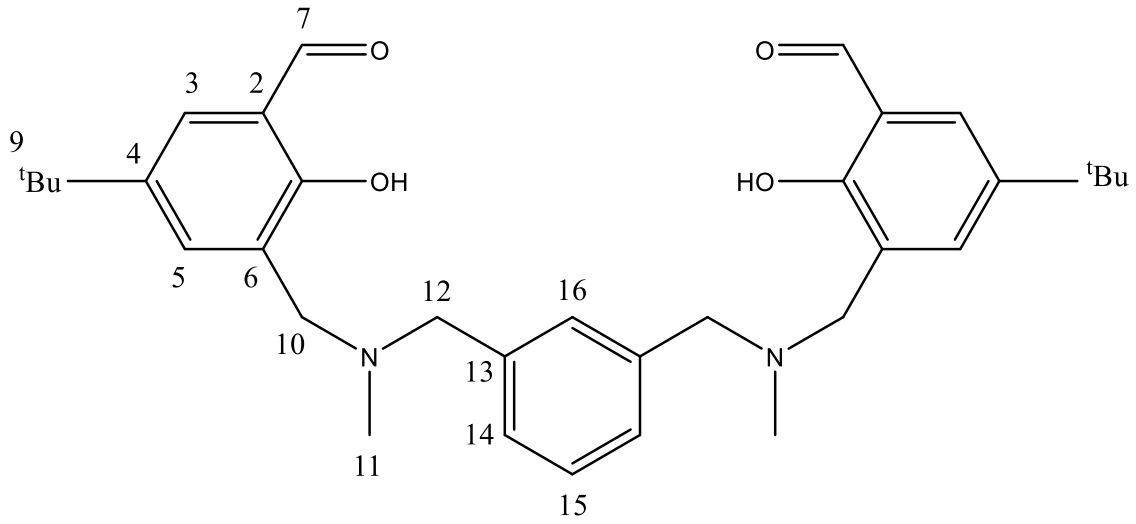

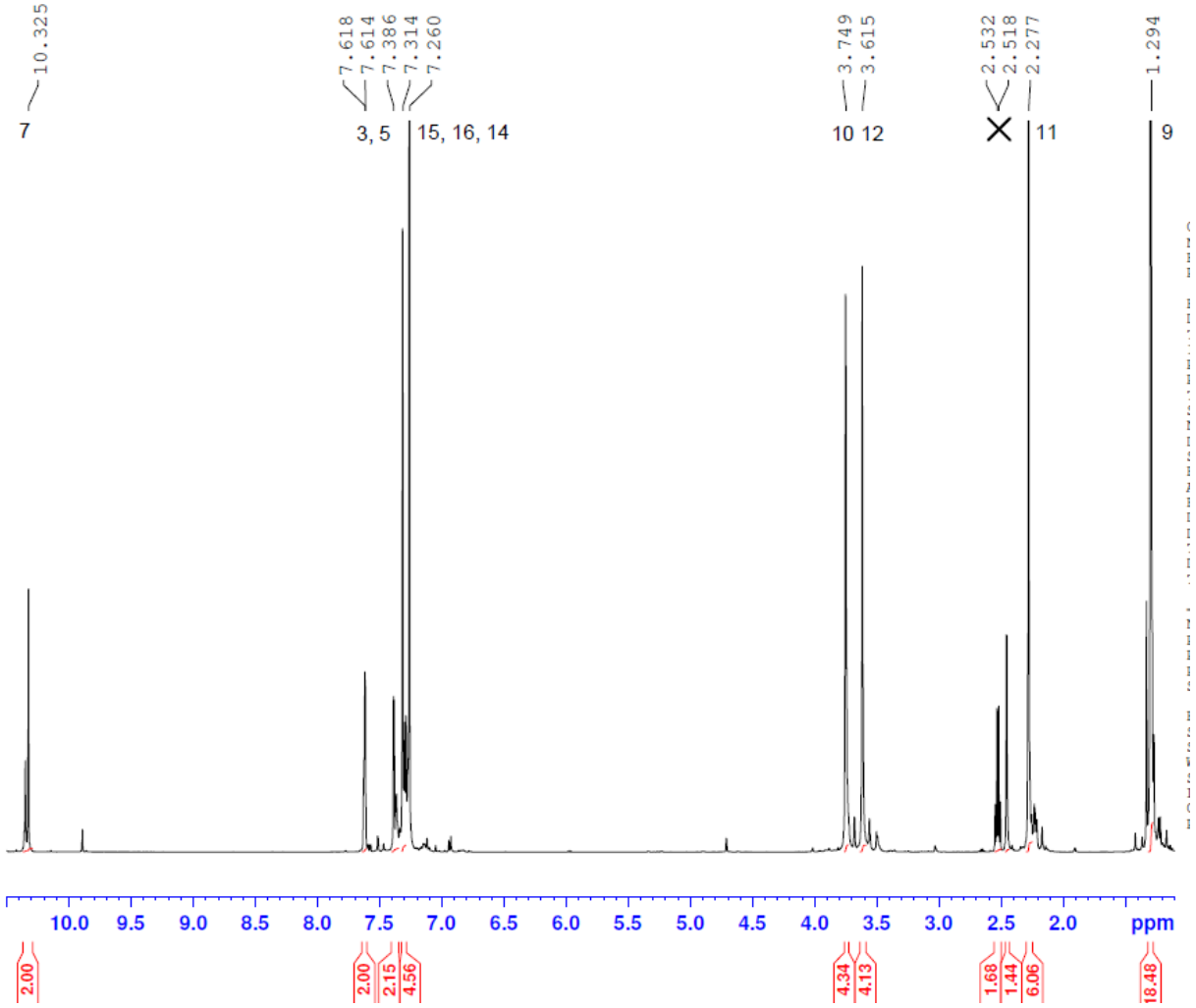

D1.9 ^{1}H NMR of L3

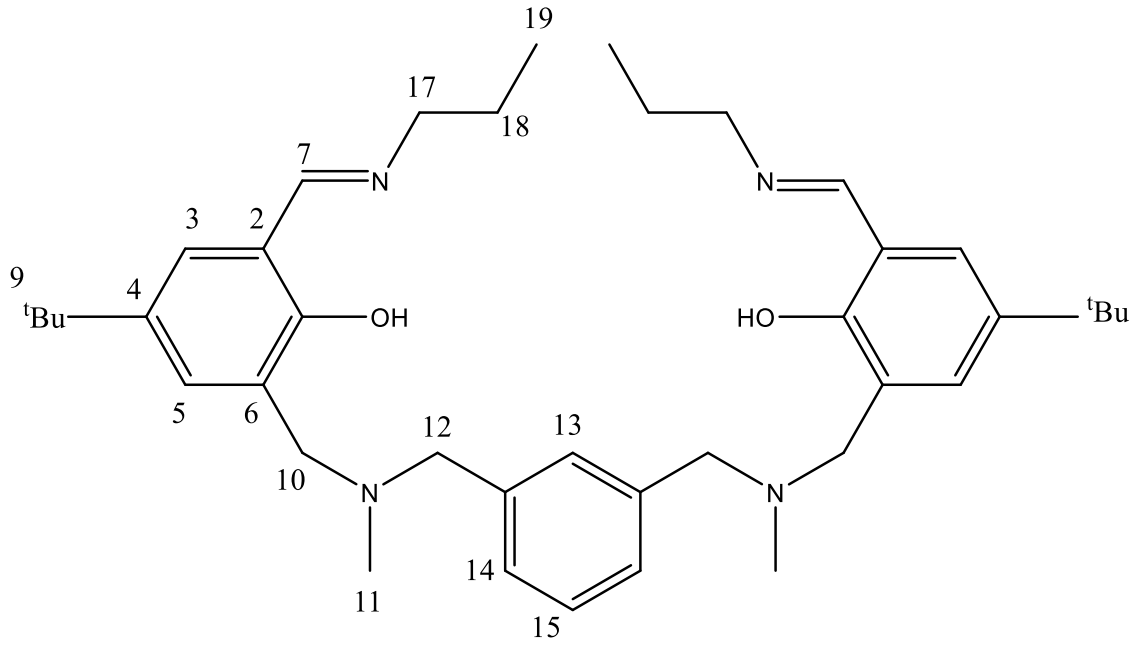

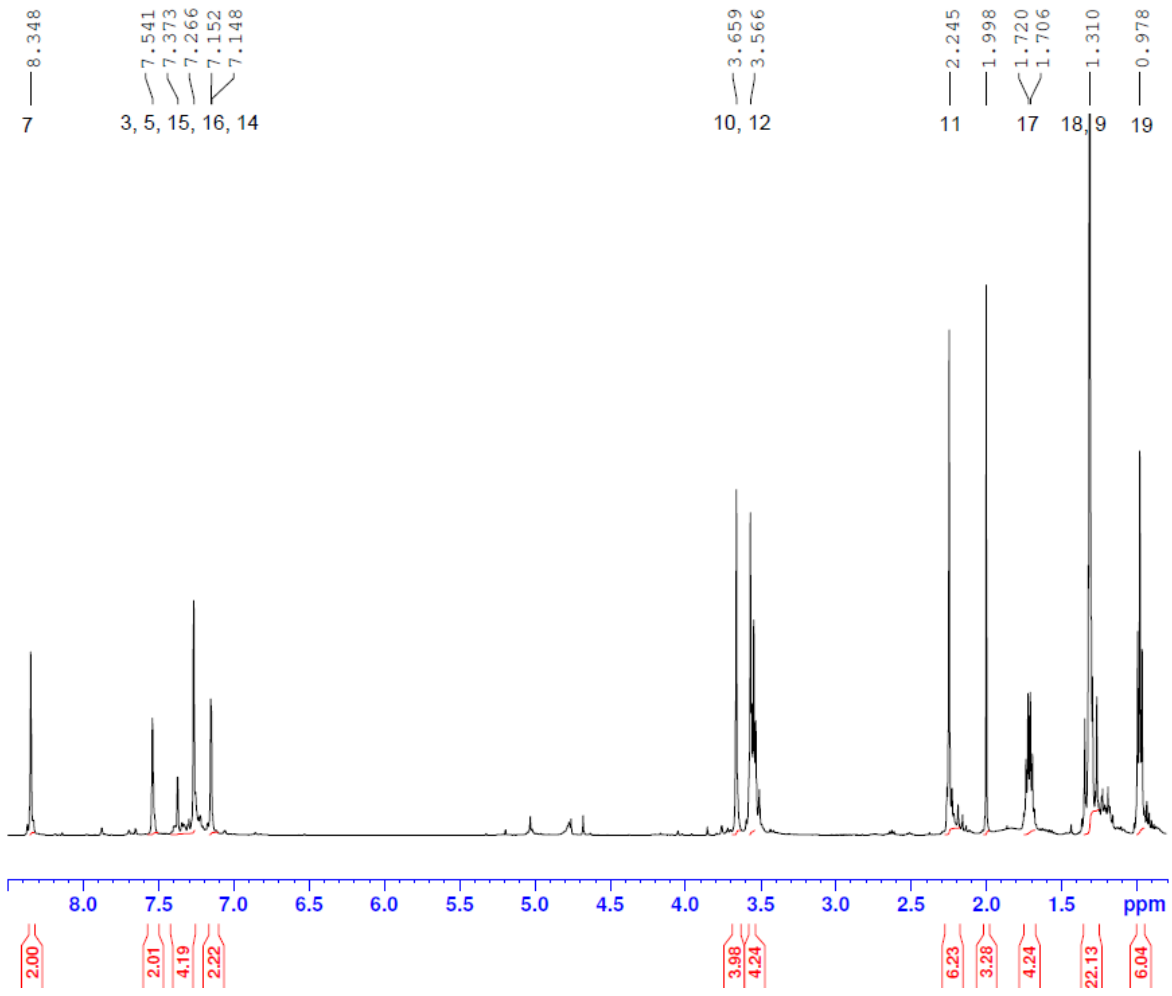

D1.10 ^{1}H NMR of L4

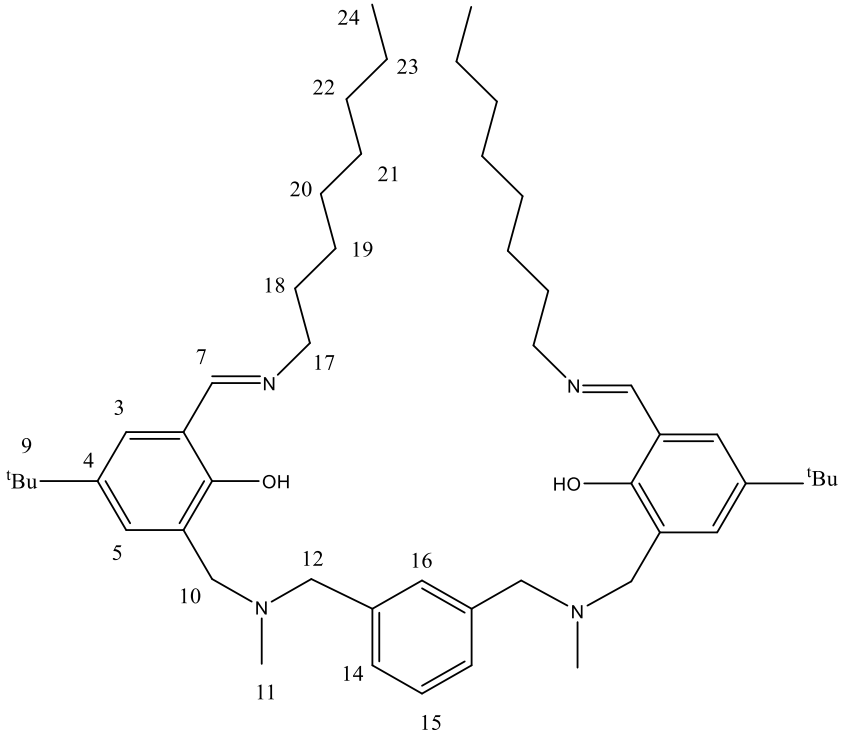

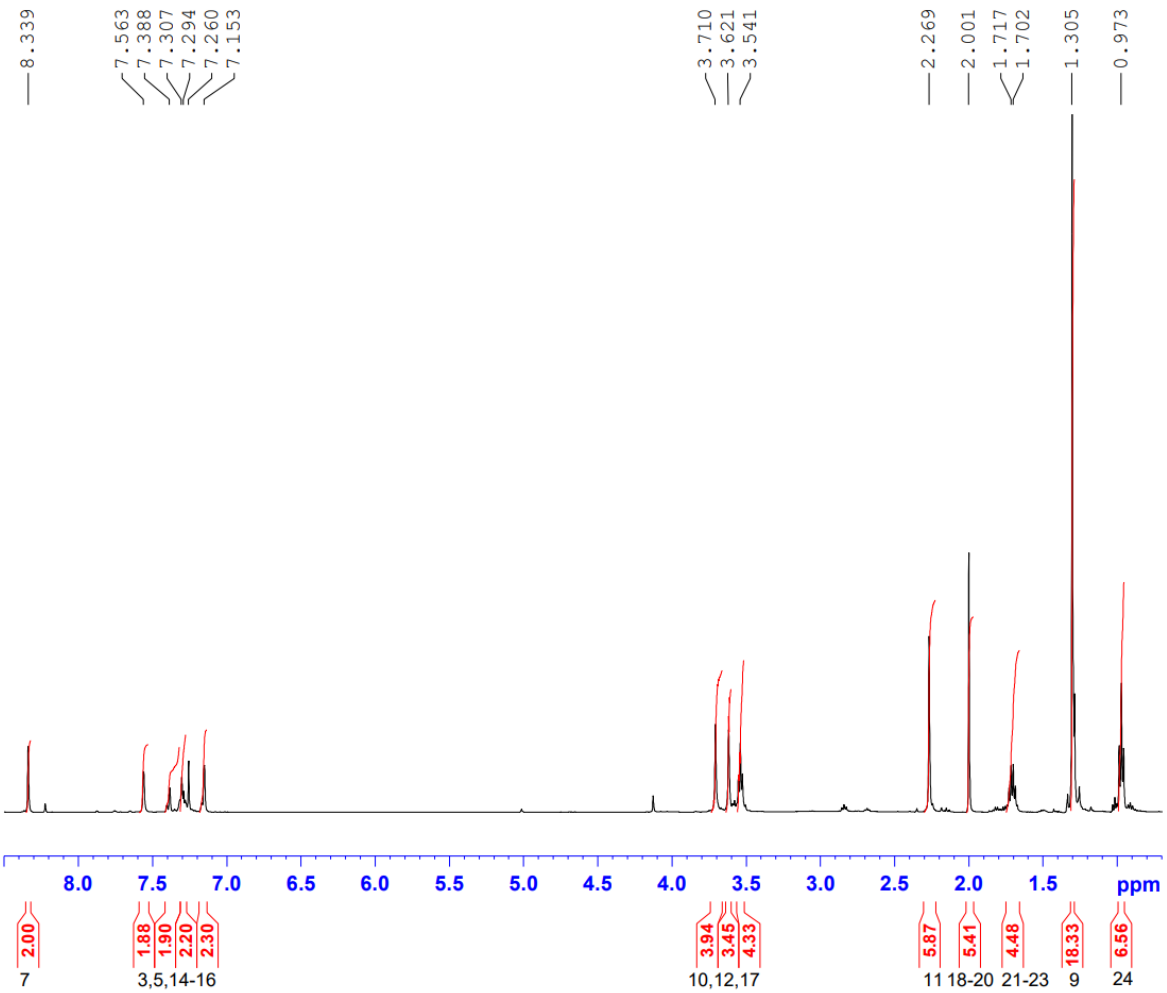

D1.11 ^{1}H NMR of P2a

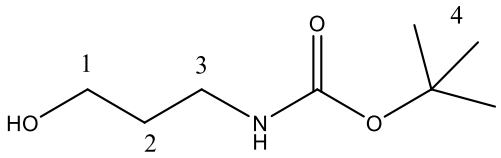

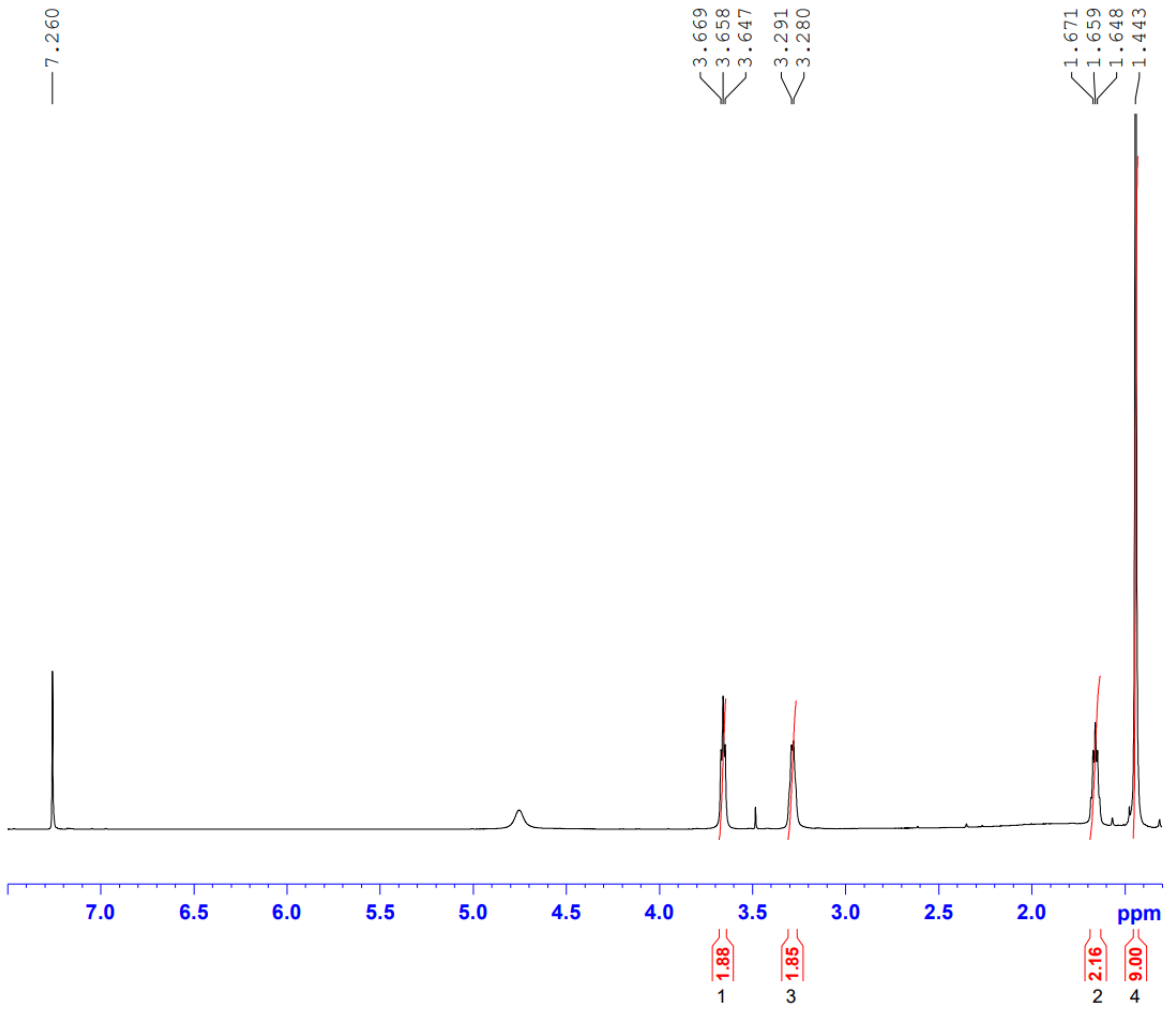

D1.12 ^{1}H NMR of P2b

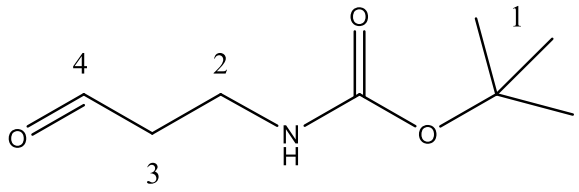

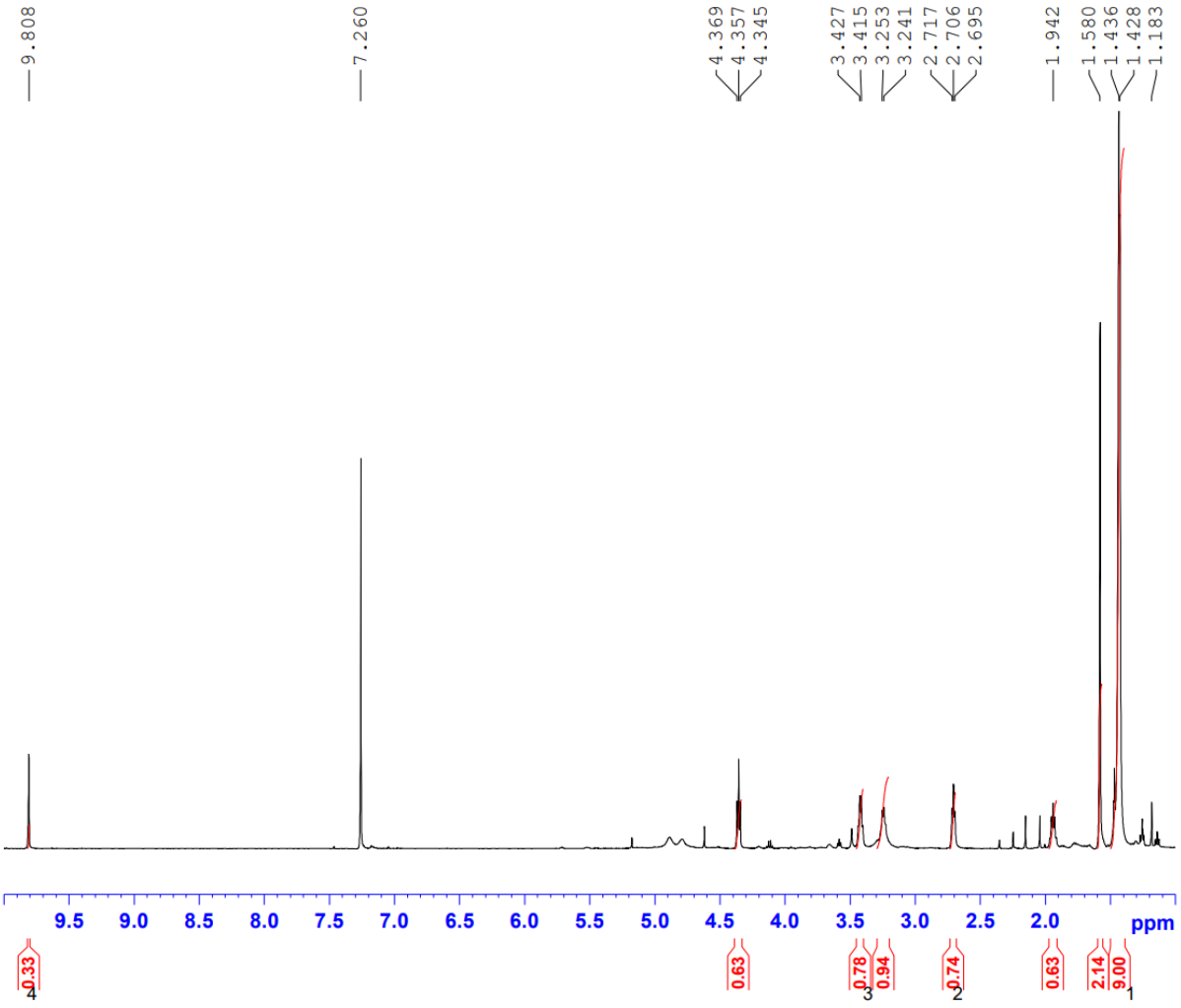

D1.13 ^{1}H NMR of P2c

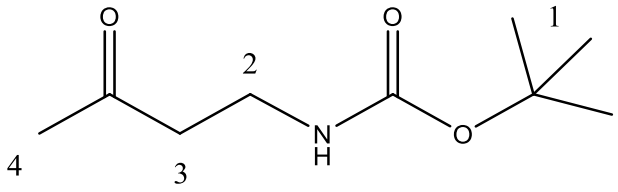

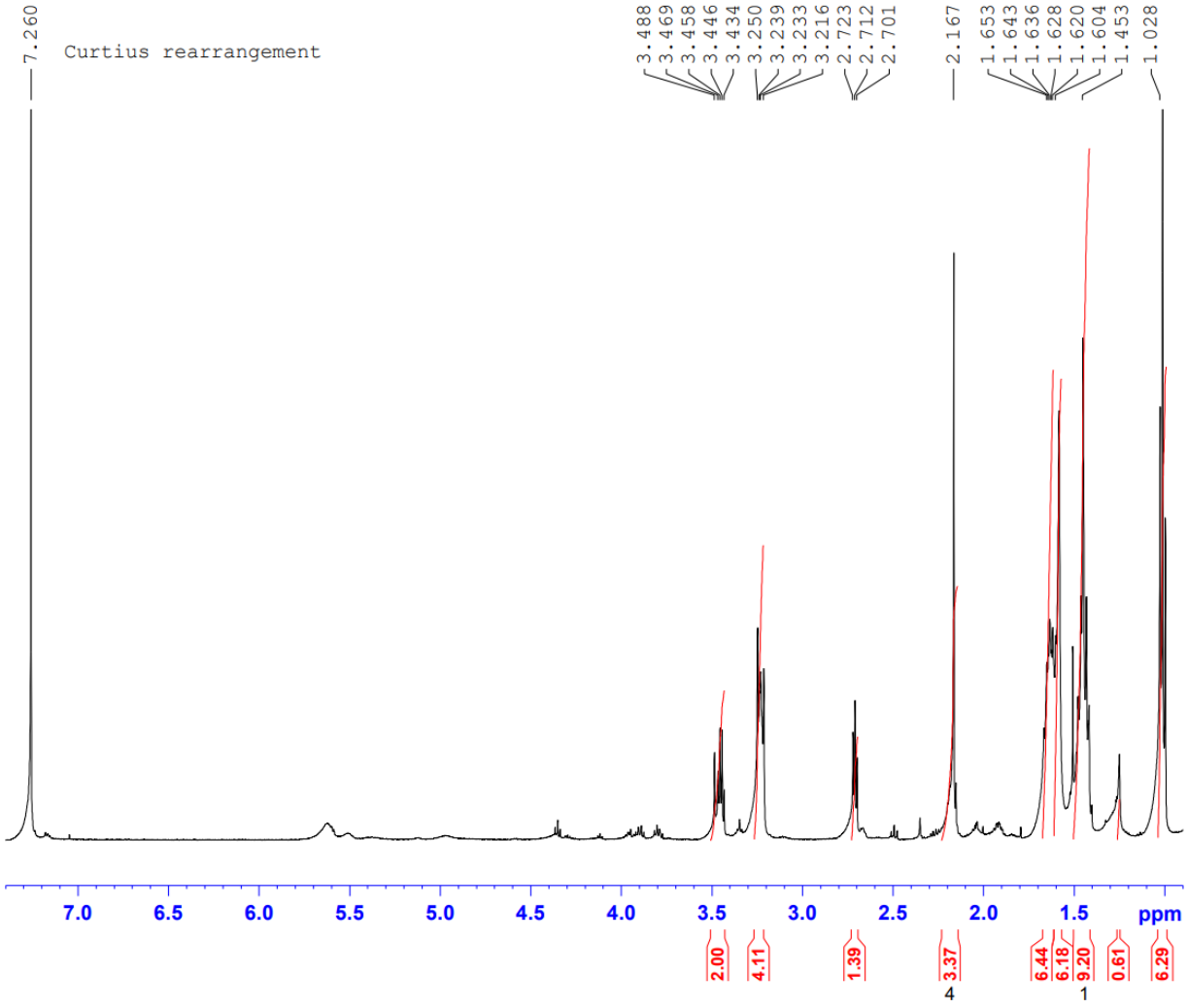

D1.14 ^{1}H NMR of P3a

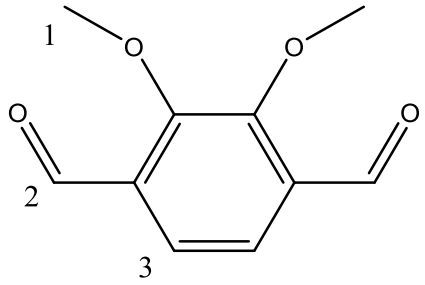

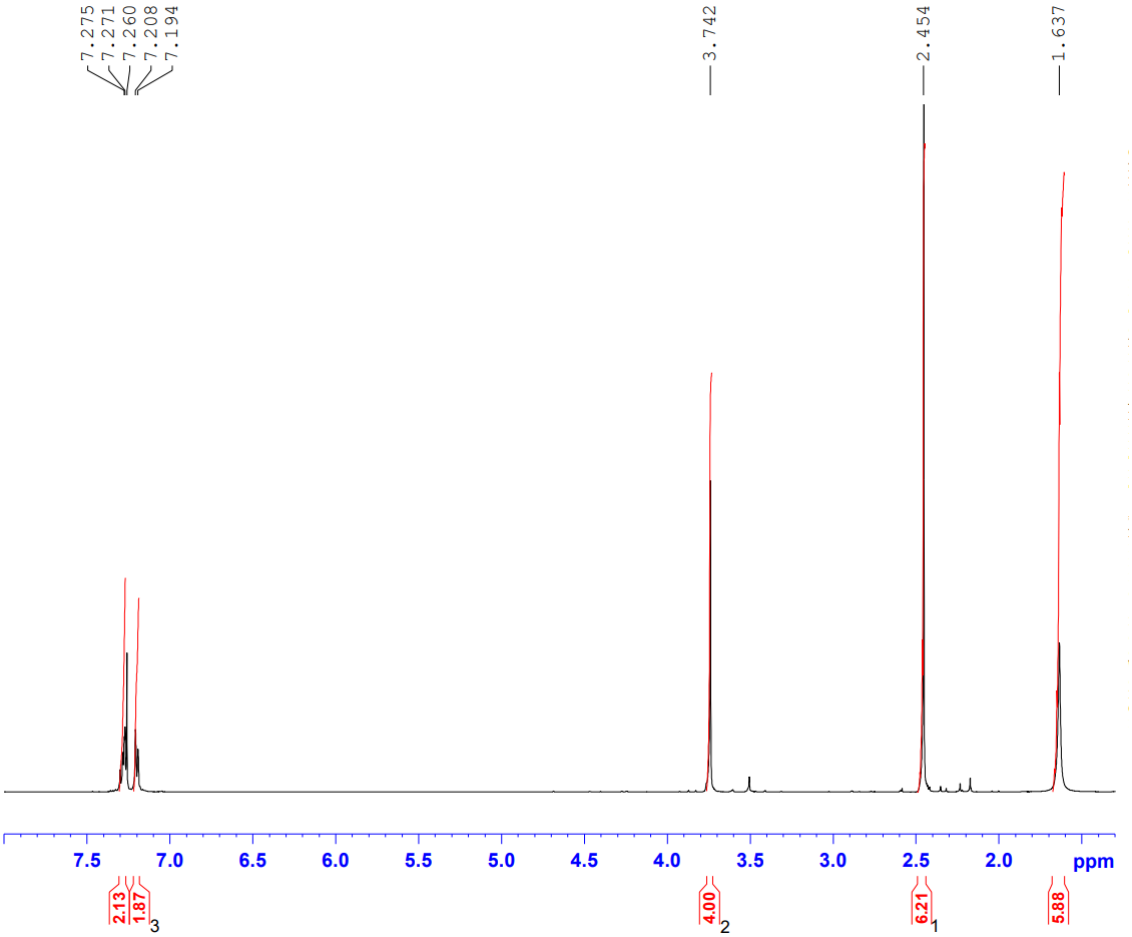

E1.0 IR Spectra of Ligands and Complexes

E1.1 IR Spectra of L1

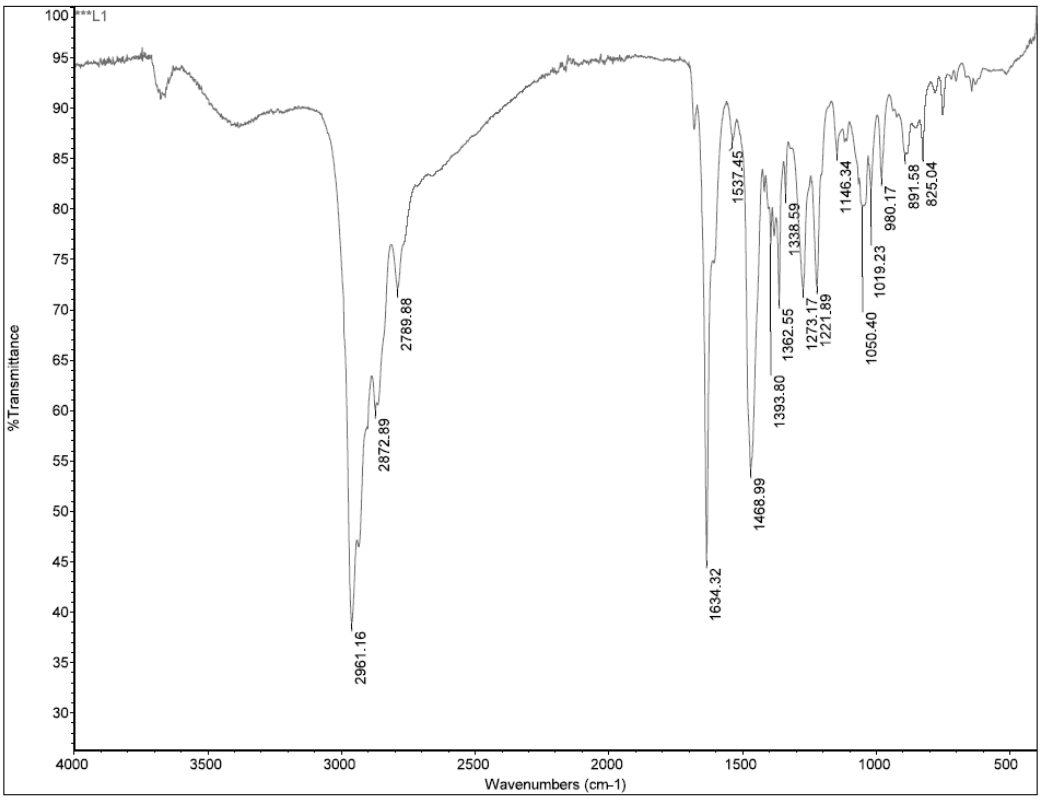

E1.2 IR Spectra of L2

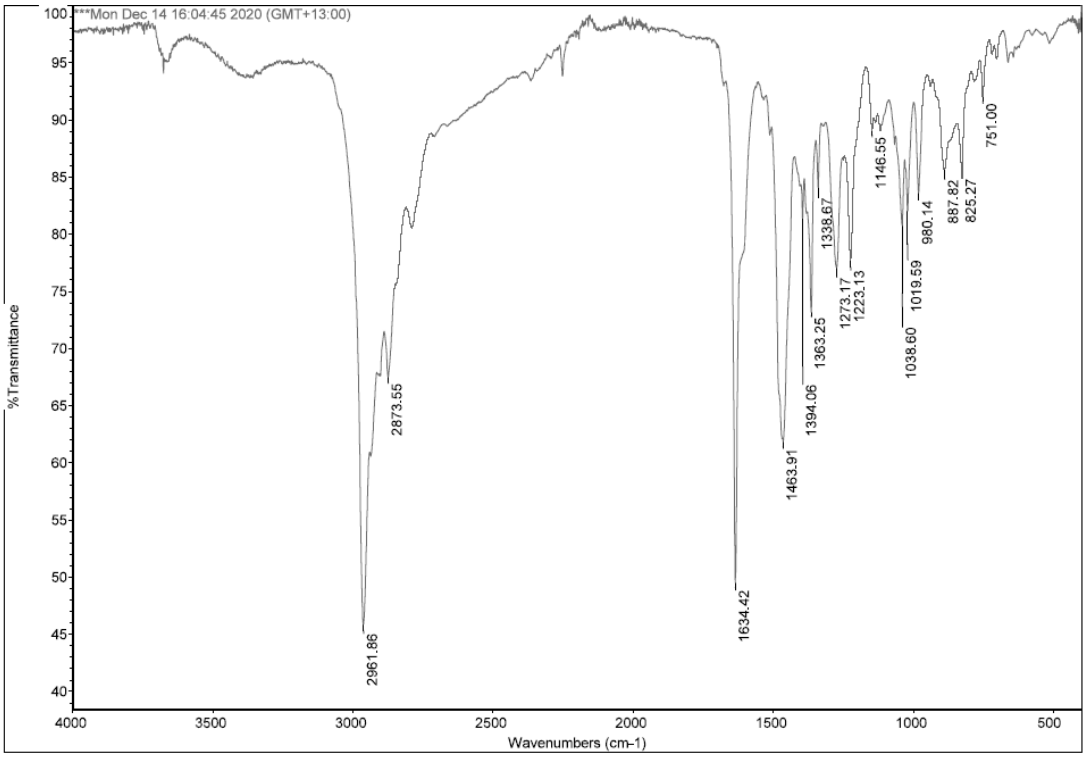

E1.3 IR Spectra of L3

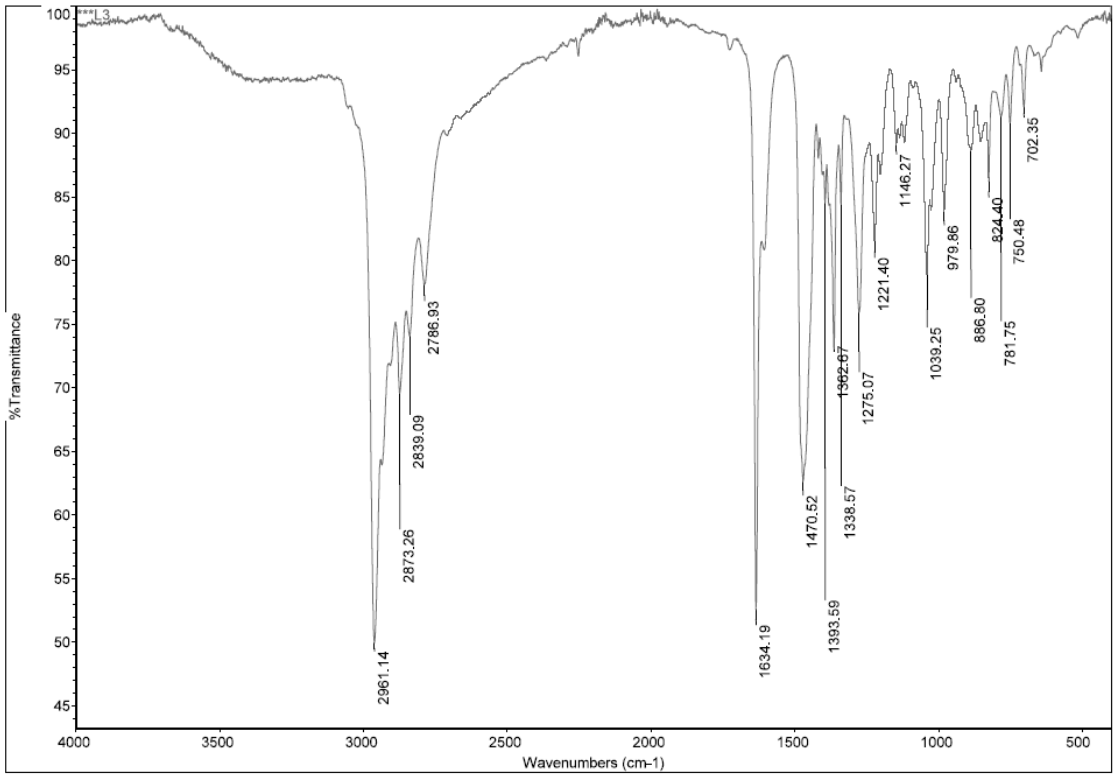

E1.4 IR Spectra of C1

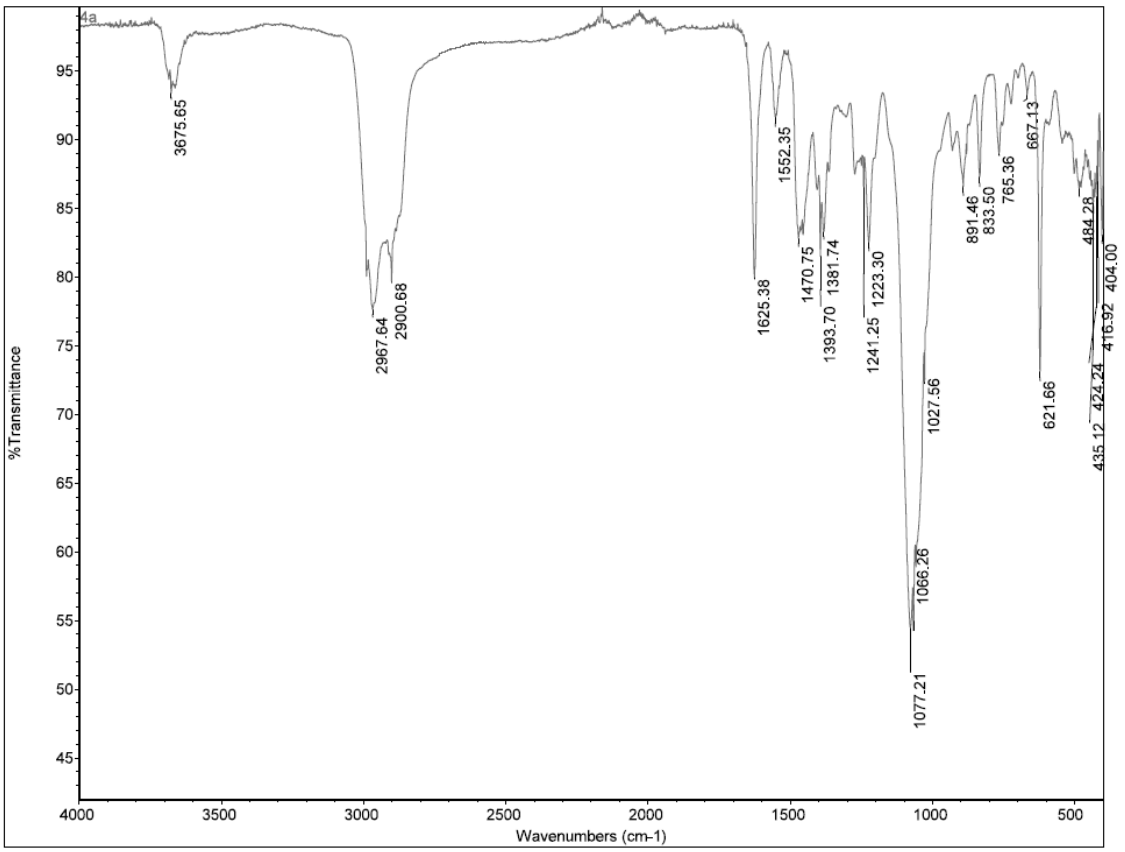

E1.5 IR Spectra of C2

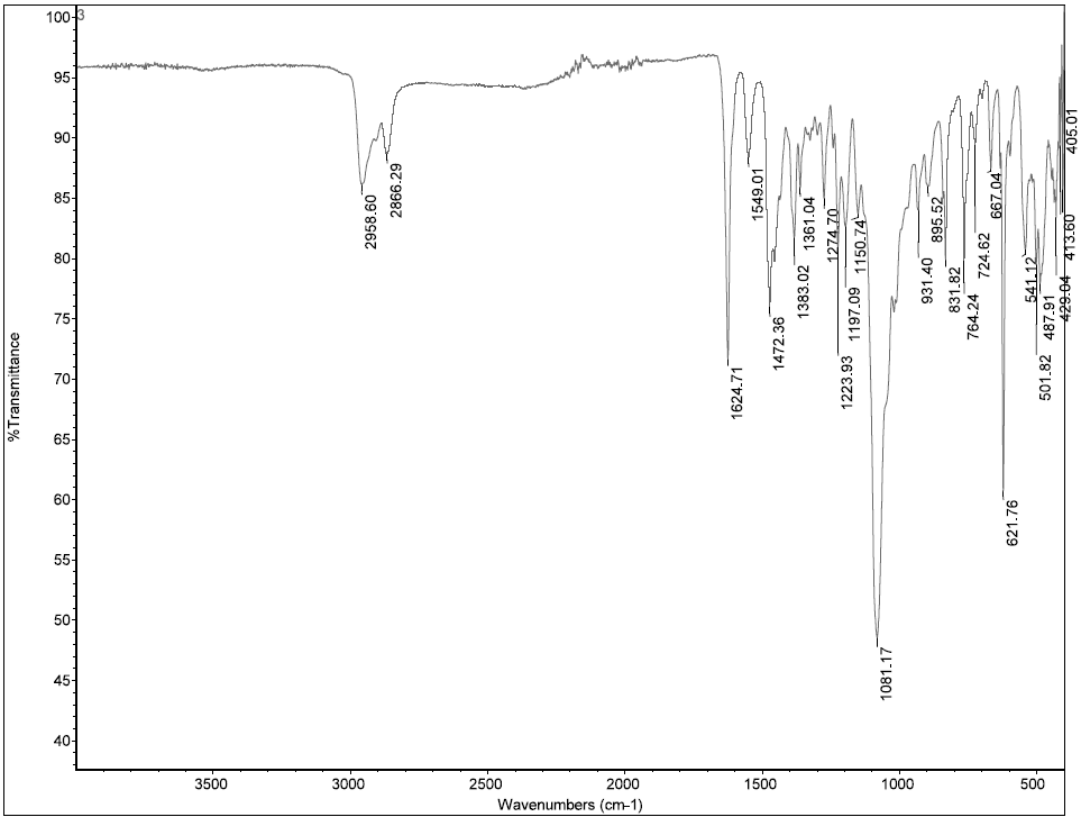

E1.6 IR Spectra of C3

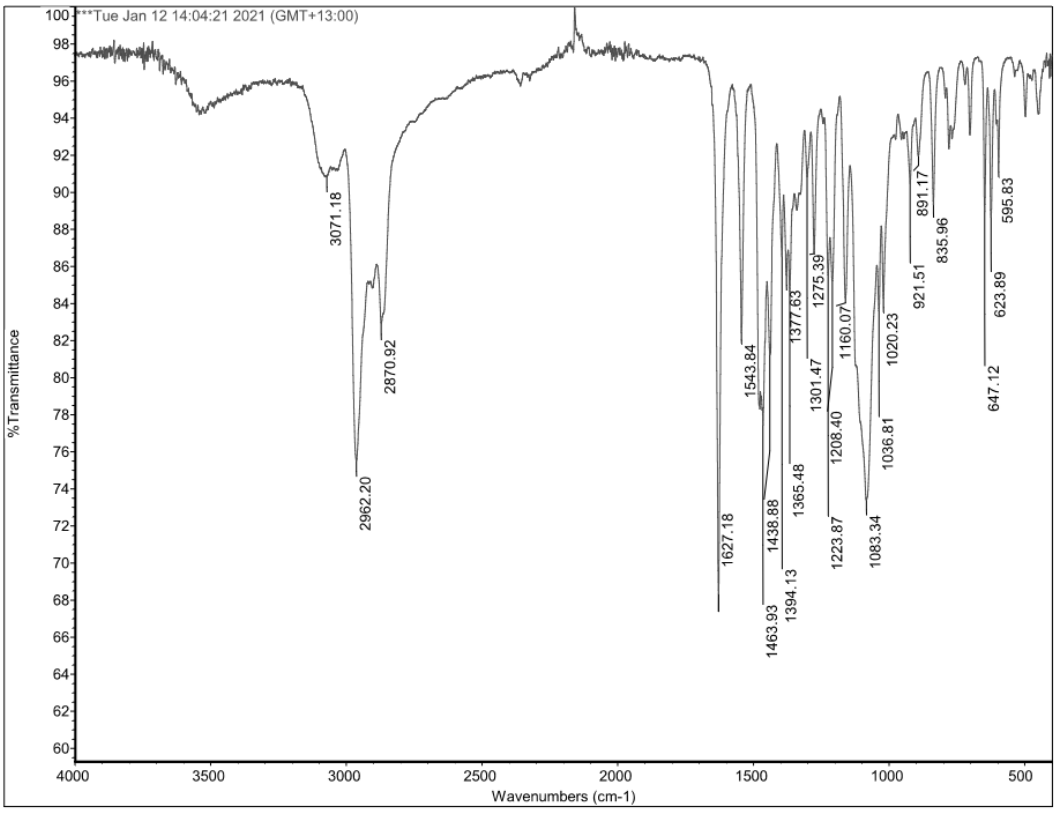

E1.7 IR Spectra of C4

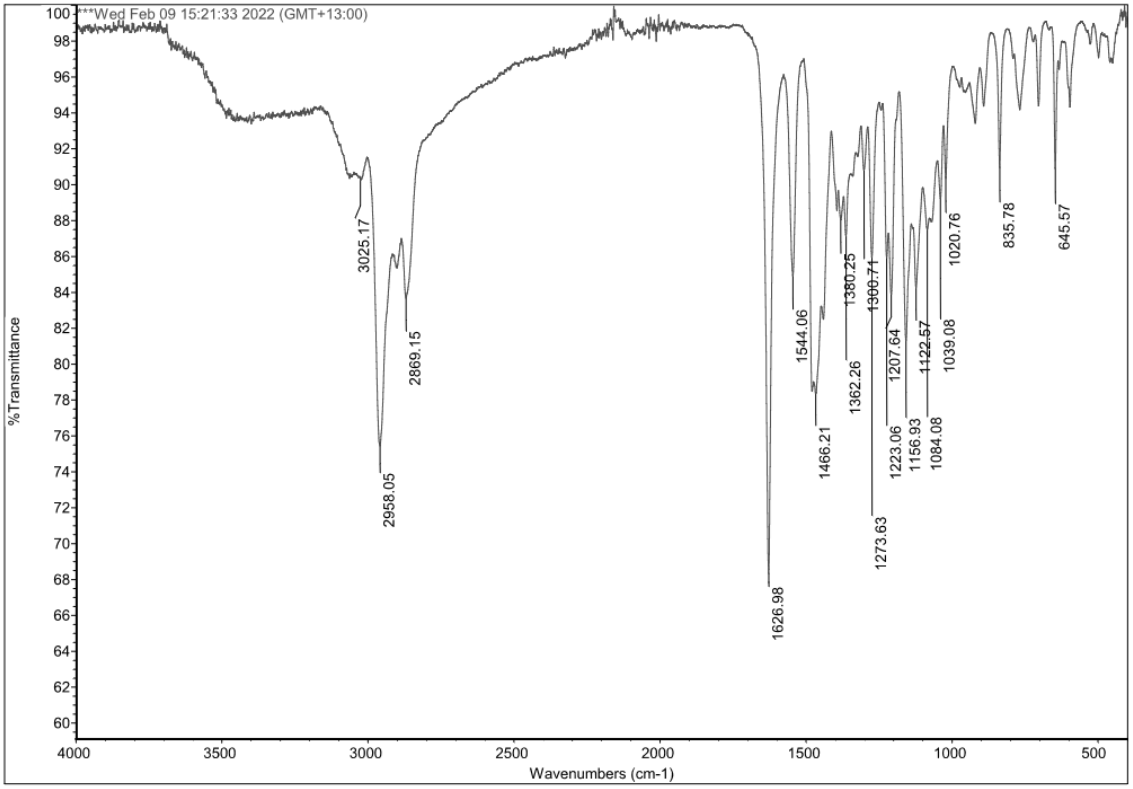

F1.0 Mass Spectrometry of Ligands and Complexes

F1.1 Mass spectrometry Spectrum for L1

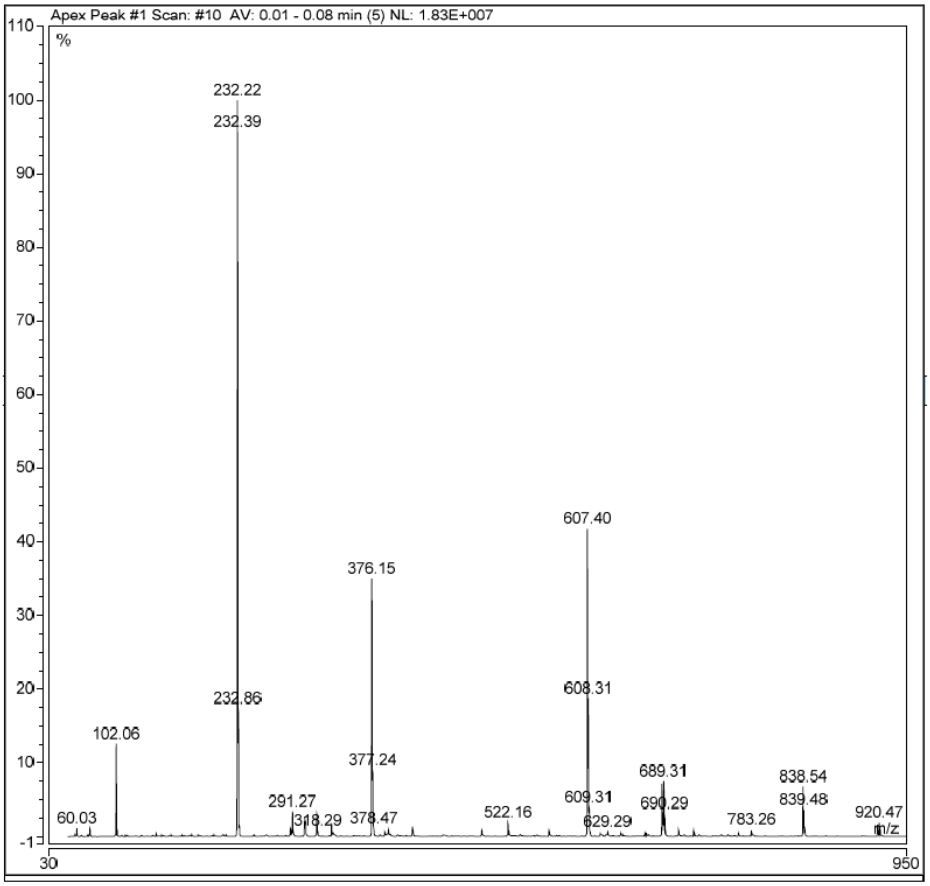

F1.2 Mass spectrometry Spectrum for L2

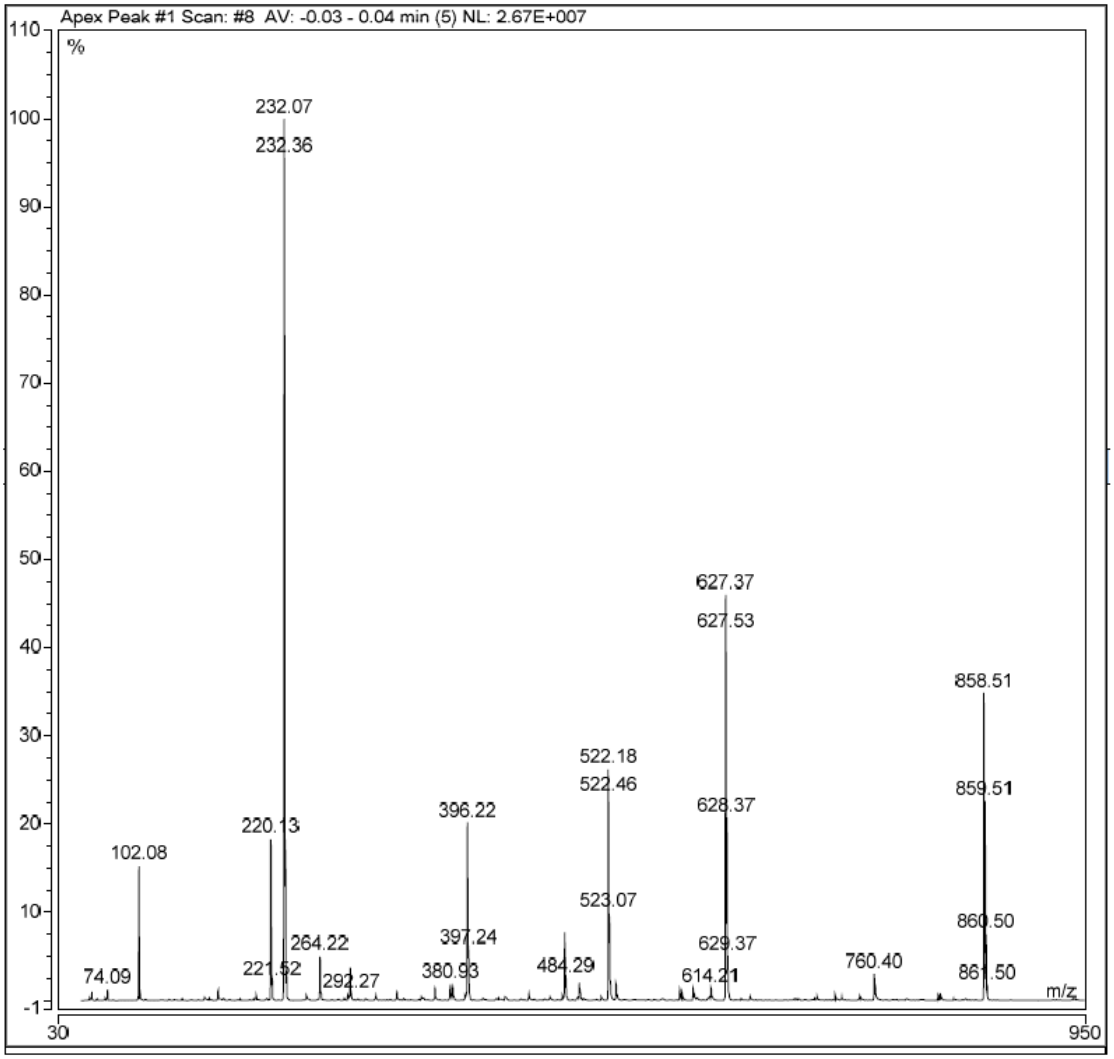

F1.3 Mass spectrometry Spectrum for L3

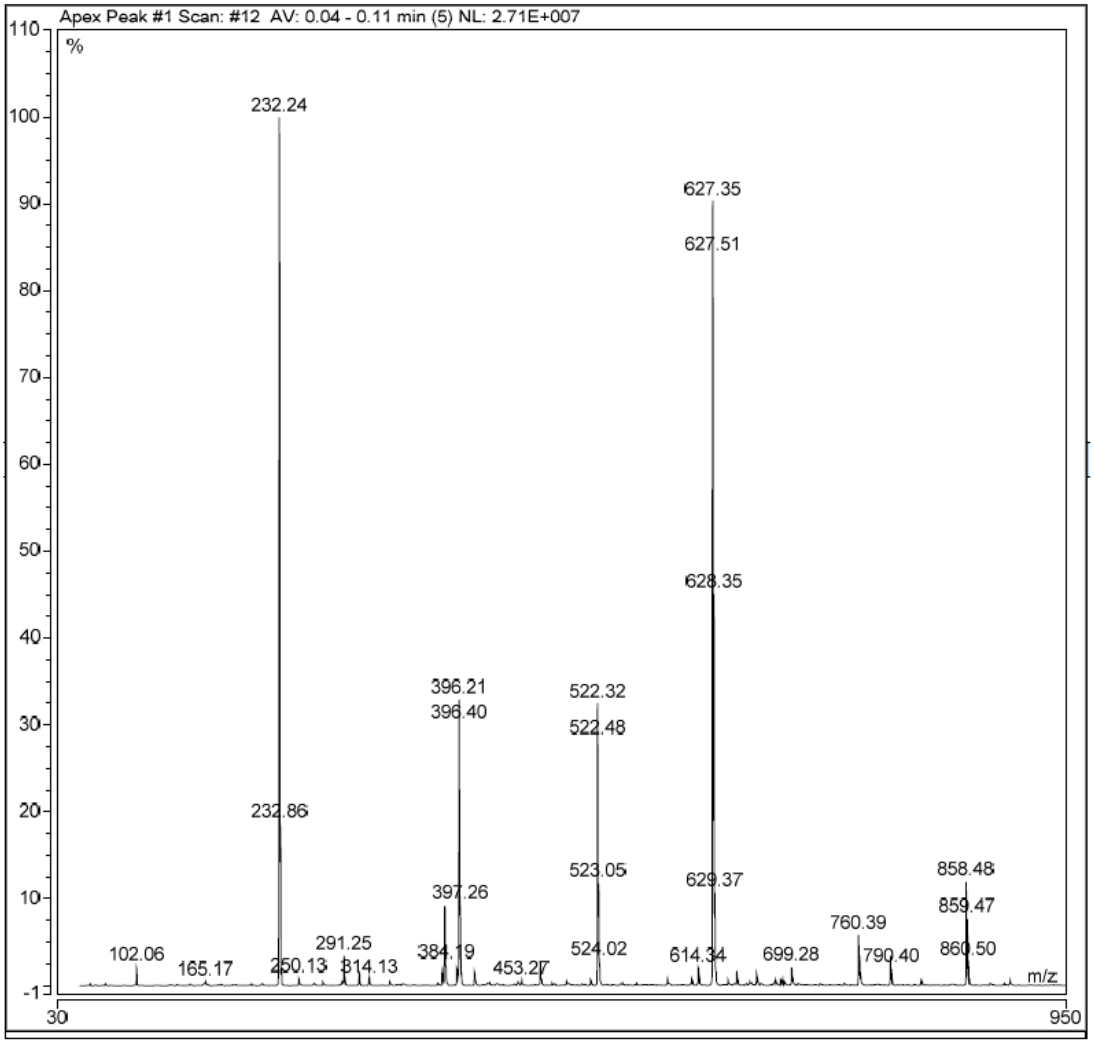

F1.4 Mass Spectrometry Spectrum for C1

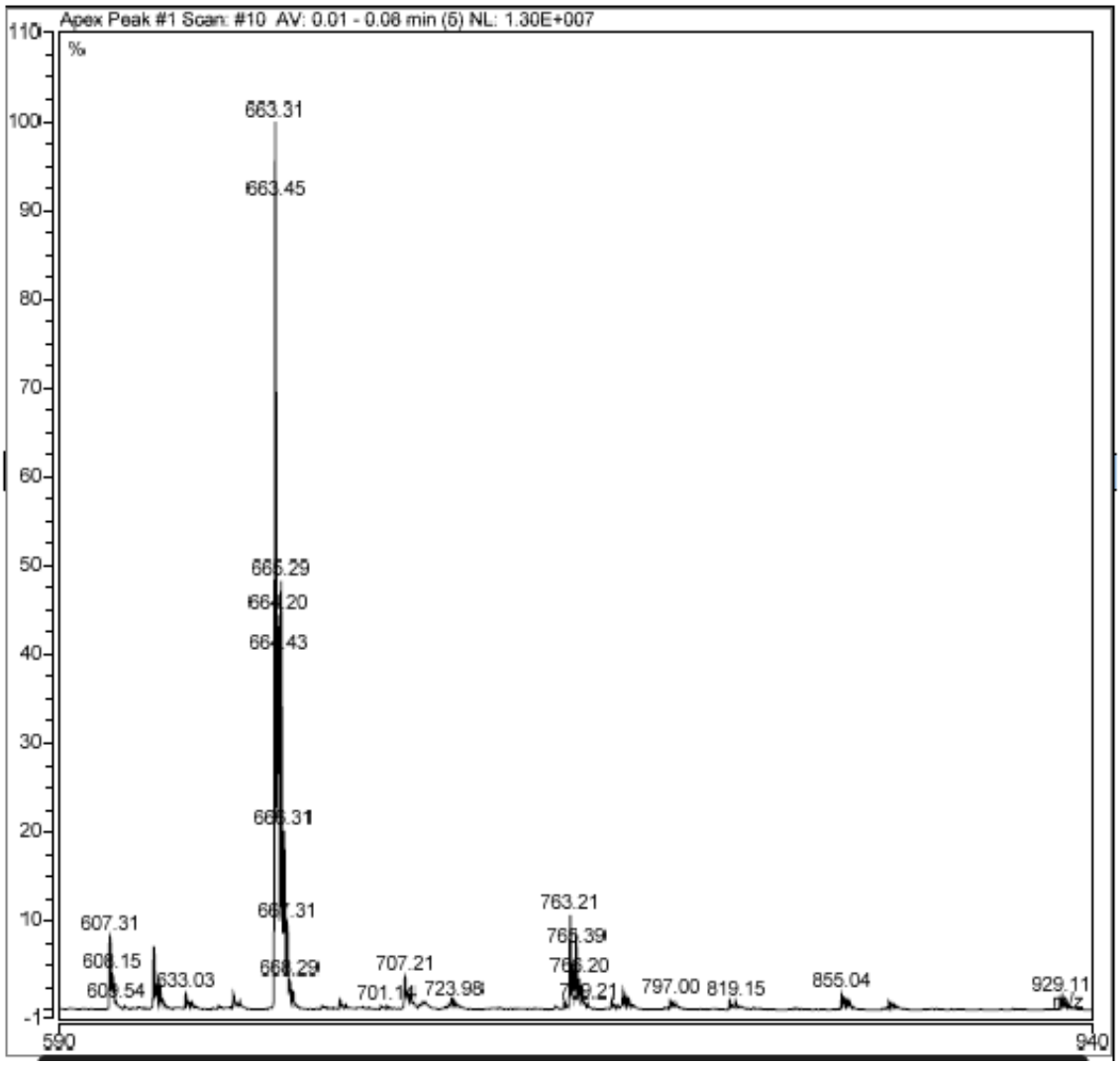

F1.5 Mass Spectrometry Spectrum for C2

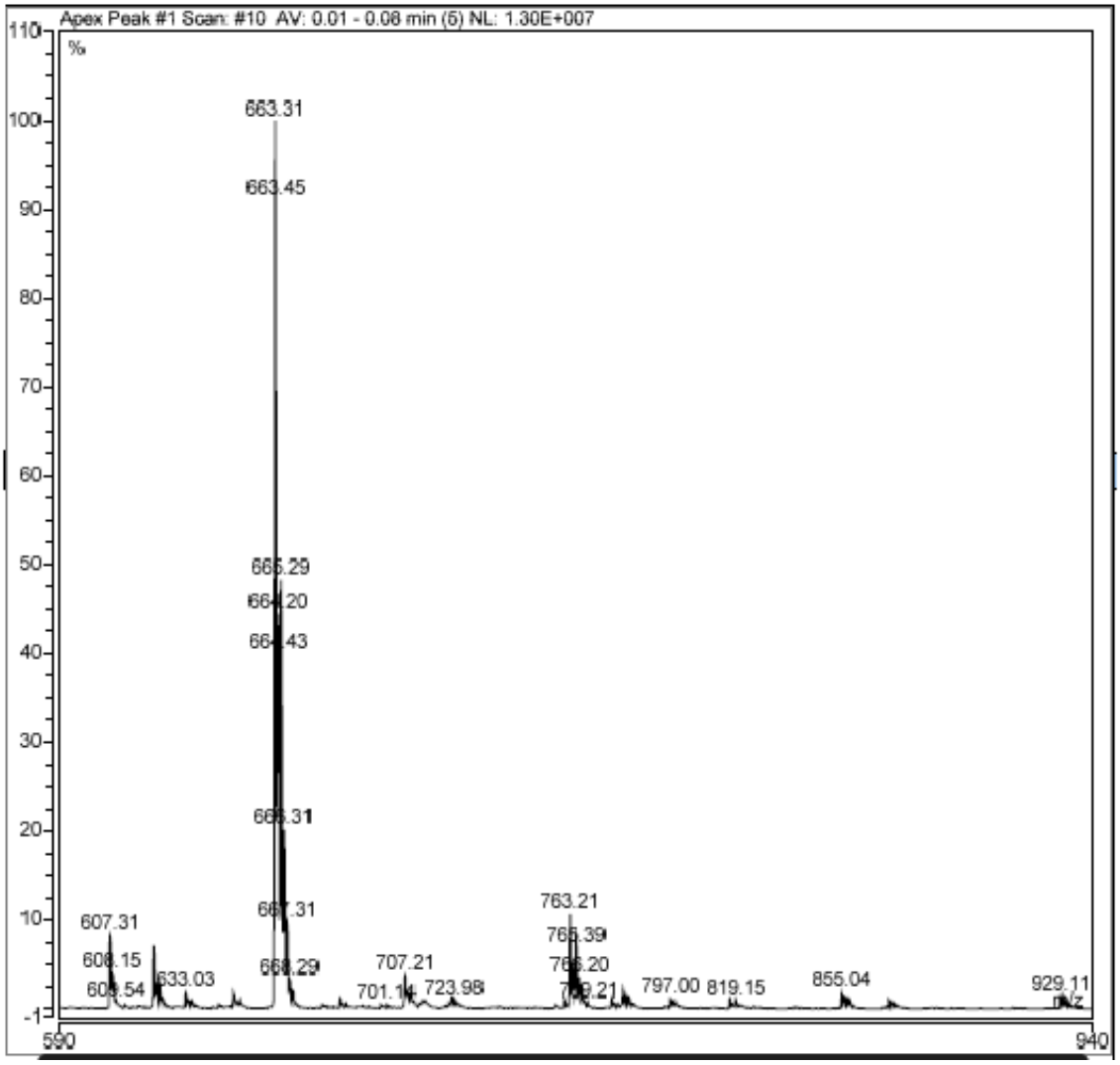

F1.6 Mass Spectrometry Spectrum for C3

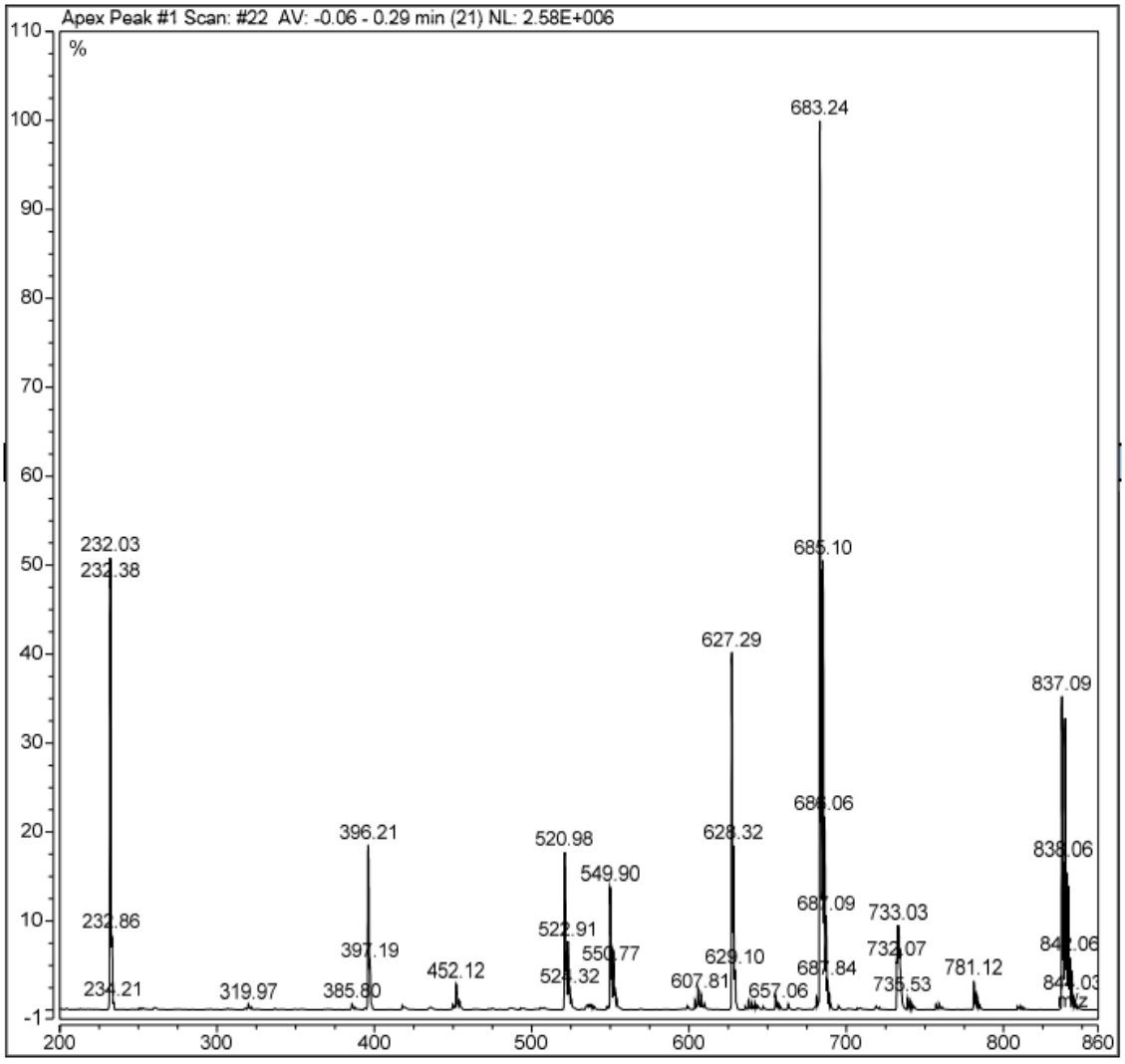

F1.7 Mass Spectrometry Spectrum for C4

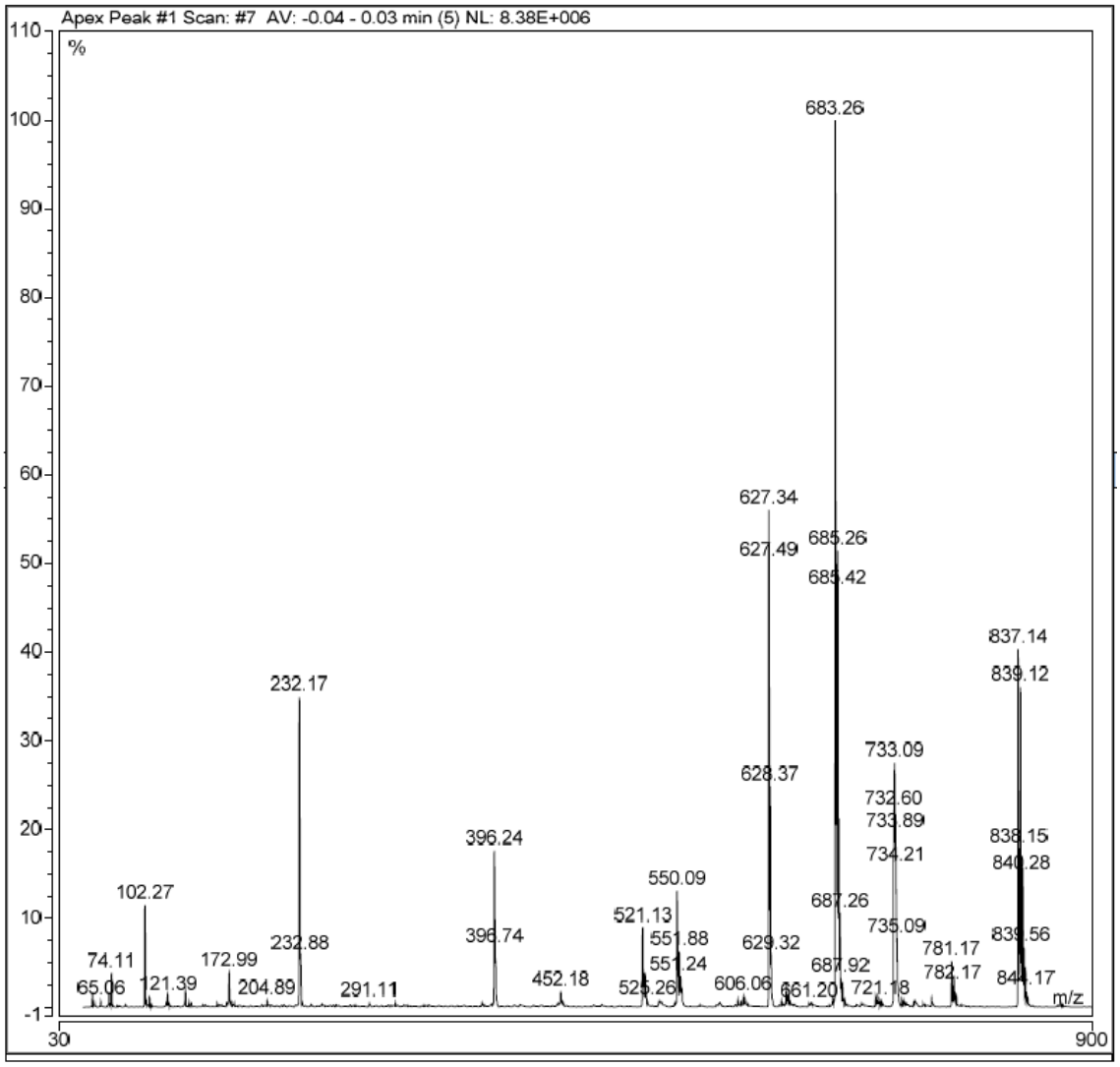

G1.0 UV-Vis Spectroscopy of Ligands and Complexes

G1.1 UV-Vis Spectrum of L1.

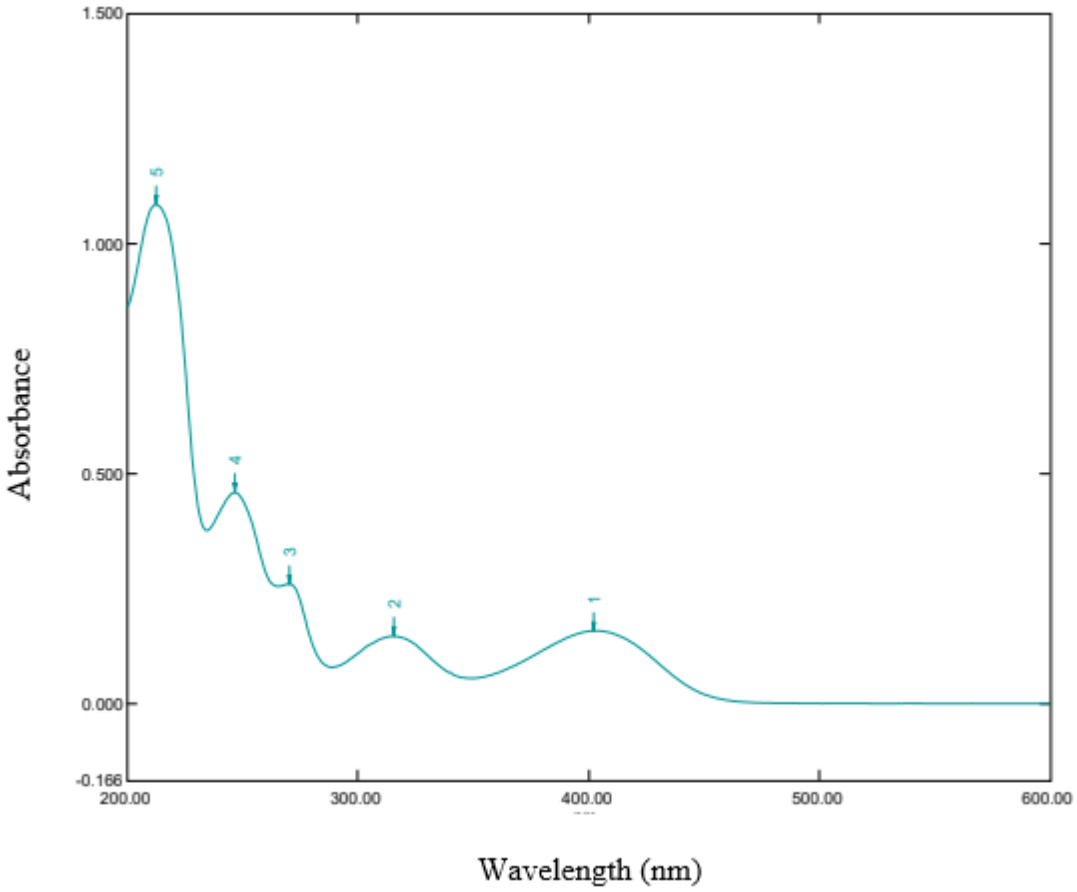

No.	Wavelength (nm)	Absorbance	Path length (cm)	Concentration (1x 10^{-6} M)	ε molar coefficient ($M^{-1}cm^{-1}$)
1	402.50	0.158	1	56.7	2,787
2	315.50	0.146	1	56.7	2,575
3	270.00	0.259	1	56.7	4,568
4	246.50	0.458	1	56.7	8,078
5	212.50	1.086	1	56.7	19,153

G1.2 UV-Vis Spectrum of L2.

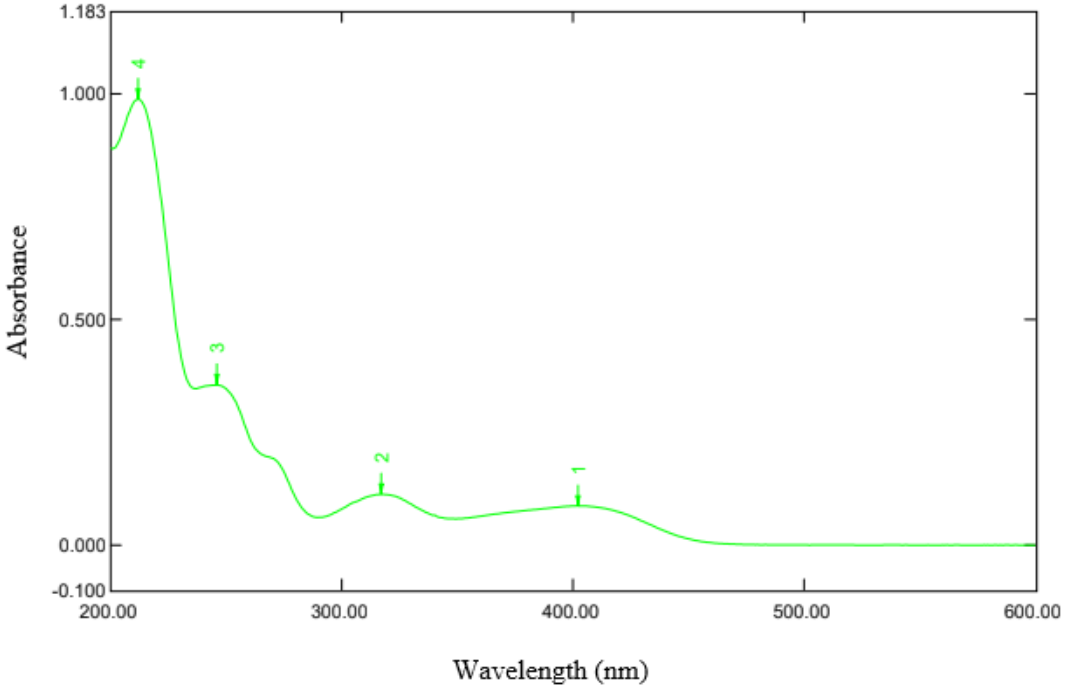

No.	Absorbance	Wavelength (nm)	Path length (cm)	Concentration ($1x\ 10^{-6}$ M)	ε molar coefficient ($M^{-1}cm^{-1}$)
1	402.00	0.086	1	43.7	1,968
2	317.00	0.112	1	43.7	2,563
3	246.00	0.355	1	43.7	8,124
4	212.00	0.989	1	43.7	22,632

G1.3 UV-Vis Spectrum of L3.

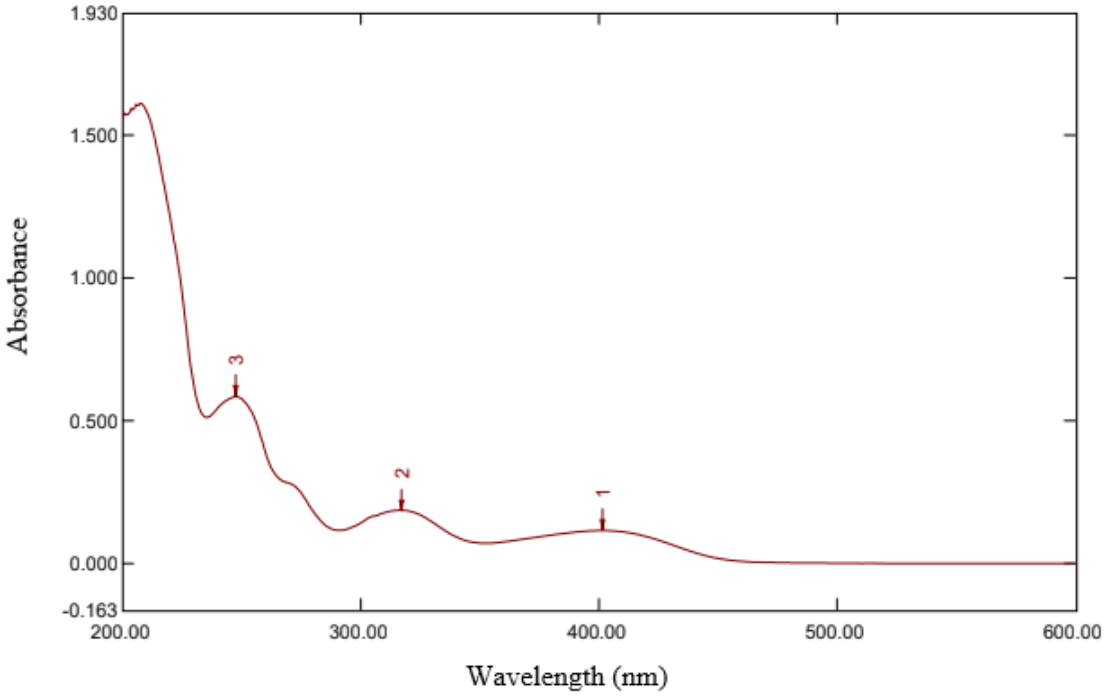

No.	Wavelength (nm)	Absorbance	Path length (cm)	Concentration ($1x\ 10^{-6}$ M)	ε molar coefficient ($M^{-1}cm^{-1}$)
1	401.50	0.115	1	42.7	2,693
2	317.00	0.186	1	42.7	4,356
3	247.50	0.585	1	42.7	13,700

G1.4 UV-Vis Spectrum of C1.

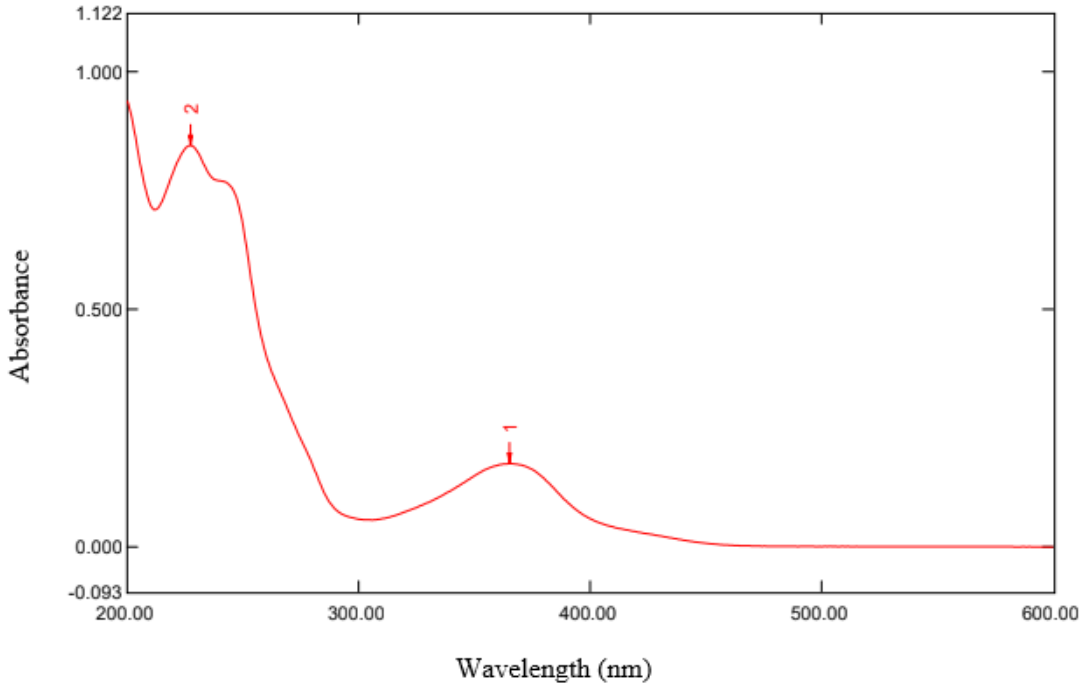

No.	Wavelength (nm)	Absorbance	Path length (cm)	Concentration ($1x\ 10^{-6}$ M)	ε molar coefficient ($M^{-1}cm^{-1}$)
1	365.50	0.176	1	8.77	20,068
2	227.50	0.845	1	8.77	96,351

G1.5 UV-Vis Spectrum of C2.

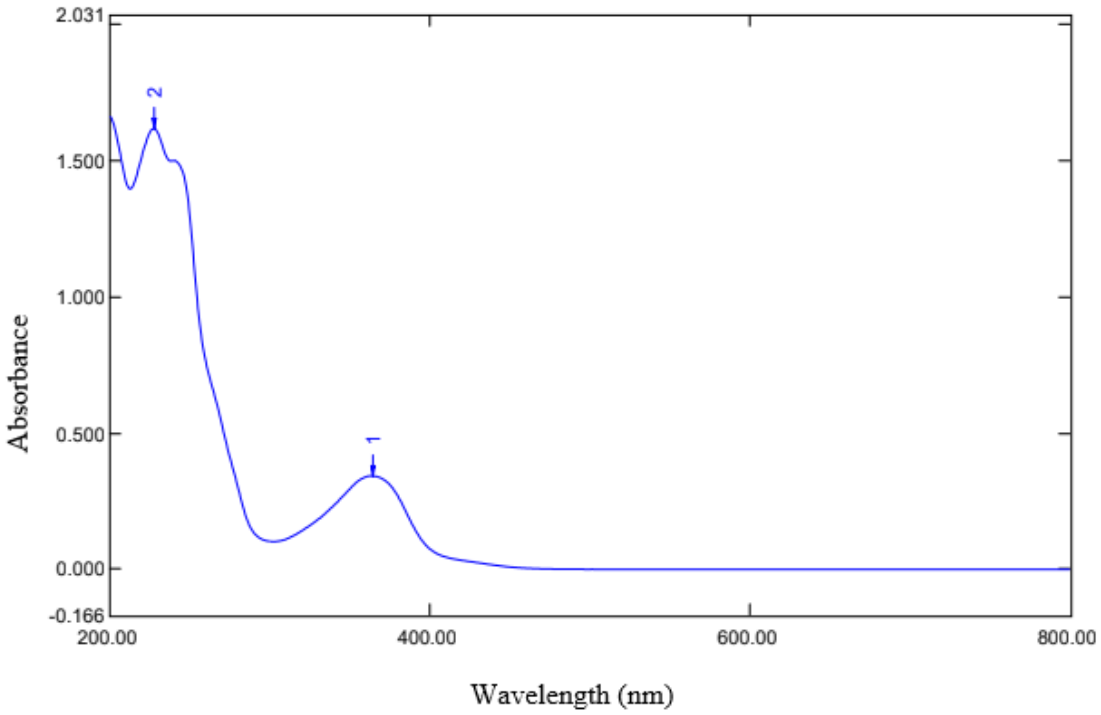

No.	Wavelength (nm)	Absorbance	Path length (cm)	Concentration ($1x\ 10^{-6}$ M)	ε molar coefficient ($M^{-1}cm^{-1}$)
1	364.00	0.343	1	29.6	11,572
2	227.50	1.618	1	29.6	54,588

G1.6 UV-Vis Spectrum of C3.

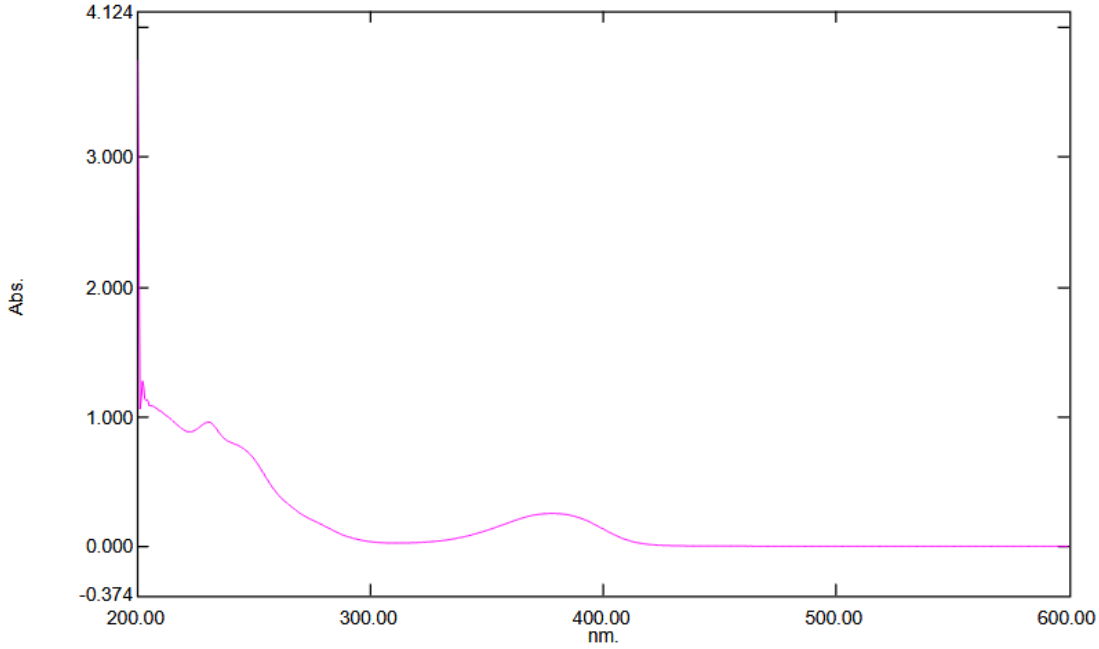

No.	Wavelength (nm)	Absorbance	Path length (cm)	Concentration ($1x\ 10^{-6}$ M)	ε molar coefficient ($M^{-1}cm^{-1}$)
1	378.00	0.253	1	505	501
2	230.50	0.958	1	505	1897

G1.7 UV-Vis Spectrum of C4.

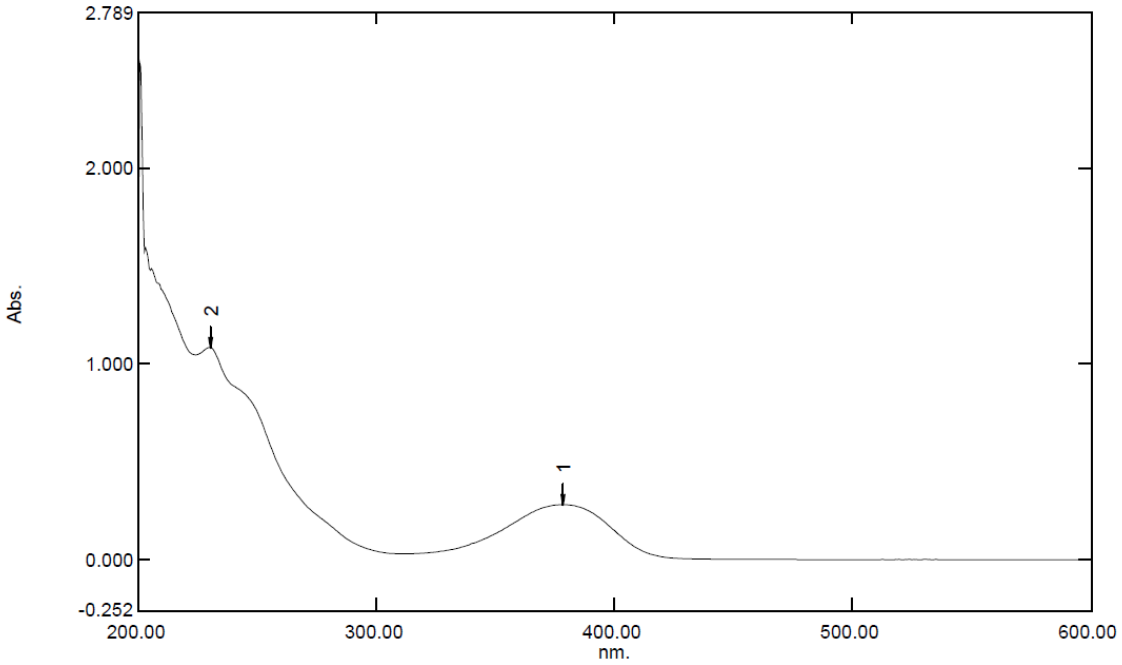

No.	Wavelength (nm)	Absorbance	Path length (cm)	Concentration ($1x\ 10^{-6}$ M)	ε molar coefficient ($M^{-1}cm^{-1}$)
1	378.50	0.262	1	43.8	5,982
2	230.00	1.083	1	43.8	24,726

H1.0 Conductivity of Complexes.

	MeOH cndct. (µS cm^{-1})	**Conc. (mol mL^{-1})**	**Cndct. (µS cm^{-1})**	**Molar cndct. (ʌ) (S cm^2 mol^{-1})**
C1 $[BF_4 \subset Ni_2(L1)_3](BF_4)_3$	2.55	5.63E-8	17.0	257
C2 $[ClO_4 \subset Ni_2(L1)_3](ClO_4)_3$	2.55	6.28E-8	10.9	133
C3 $[SO_4 \subset Ni_2(L3)_2][Ni(SO_4)_2(EtOH)_4]$	2.50	1.18E-8	3.70	102
C4 $[ClO_4 \subset Ni_2(L3)_2](ClO_4)_2$	2.55	3.88E-7	160	406

I1.0 CHN Analysis of C2.

	%C	%H	%N
Expected values	58.62	8.03	7.20
Error range 0.3%	58.32-92	7.73-8.33	6.90-7.50
Run 1 of C2	56.53	8.87	5.11
Run 2 of C2	54.25	8.25	4.96

I1.1 CHN Analysis of C4.

	%C	%H	%N
Expected values	57.55	7.00	6.71
Error range ± 0.3%	57.25-85	6.70-7.30	6.41-7.01
Run of C4	57.87	7.08	6.19